

-6 138 607 68

U.O.V.S. BIBLIOTEK

01

ab T

HIERDIE EKSEMPLAAR MAG ONDER
GEEN OMSTANDIGHEDE UIT DIE
BIBLIOTEK VERWYDER WORD NIE

University Free State

34300000461321
Universiteit Vrystaat

Characterisation and Substitution Kinetics of Chromium(III)-
and Cobalt(III)nitrilotriacetato complexes

A thesis submitted to meet the requirements for the degree of

Philosophiae Doctor

in the

Department of Chemistry

Faculty of Natural and Agricultural Sciences

at the

University of the Free State

by

Hendrik Gideon Visser

Promotors

Prof. W. Purcell

Prof. S.S. Basson

November 2000

Dankbetuigings

Hiermee wens ek my opregte dank en waardering te betuig aan:

*"Die Ewige God, Skepper van die hele aarde, Hy word nie moeg nie..." – Jes. 40:28.
Dankie dat U nie vir my moeg word nie, en dankie vir die mense om my.*

*My vrou, Karin, vir haar volgehoue liefde en aanmoediging gedurende hierdie studie.
Jou entoesiasme vir die lewe is my inspirasie.*

My seuntjie, Henré. Net omdat jy Pappa se seuntjie is.

*My ouers, Hentie en Monica Visser, vir al die opofferings, belangstelling, aanmoediging
en bystand. Woorde is nie genoeg nie.*

My familie en skoonouers, vir die belangstelling en aanmoediging.

My promotor en vriend, Walter, vir die geduld en vriendskap.

My taal- en teksversorger, Ebeth, sonder wie hierdie tesis nie leesbaar sou wees nie.

Die personeel en studente "oppie Knoppie" vir hul bydrae en toegewings.

Hierdie proefskrif word aan my ouers opgedra as 'n geringe blyk van waardering.

Deon Visser

Table of contents

List of abbreviations	v
List of figures	vi
List of tables	ix
List of schemes	xi
Chapter 1	
Aim of the Study	1
1.1 Introduction	1
1.1.1 Chromium and cobalt chemistry – where it started	1
1.1.2 The significance of M-nta complexes as biological models – focus on wool dyeing	3
1.2 Aim of this study	4
Chapter 2	
Literature overview	6
2.1 Introduction	6
2.2 Synthesis, characterisation and reactions of cobalt(III)- and chromium(III)- nitrilotriacetato complexes	6
2.2.1 Synthesis and characterisation	6
2.2.2 Reactions of cobalt(III)- and chromium(III)-nta and similar complexes	16
2.3 Conclusion	26
Chapter 3	
Synthesis and identification of different complexes	28
3.1 Introduction	28
3.2 Apparatus and Chemicals	29
3.3 Synthesis	30

Table of contents

3.3.1	$\text{Cs}_2[\text{Co}(\text{nta})(\mu\text{-OH})]_2 \cdot 4\text{H}_2\text{O}$	30
3.3.2	$\text{Cs}_2[\text{Co}(\text{nta})(\text{CO}_3)] \cdot \text{H}_2\text{O}$	30
3.3.3	$\text{K}_2[\text{Co}(\text{nta})(\text{ox})] \cdot x\text{H}_2\text{O}$	31
3.3.4	$\text{Ba}[\text{Co}(\text{nta})(\text{l-leu})]_2 \cdot x\text{H}_2\text{O}$	31
3.3.5	$\text{Cs}[\text{Co}(\text{nta})(\text{l-val})] \cdot x\text{H}_2\text{O}$	31
3.3.6	$[\text{Co}(\text{nta})(\text{N,N-Et}_2\text{en})]$	32
3.3.7	$[\text{Co}(\text{nta})(\text{N-Eten})]$	32
3.3.8	$[\text{Co}(\text{nta})(\text{dmap})_2] \cdot 6\text{H}_2\text{O}$	33
3.3.9	$(\text{NEt}_4)_2[\text{Co}(\text{nta})(\text{NCS})_2] \cdot x\text{H}_2\text{O}$	33
3.3.10	$\text{Cs}_2[\text{Cr}(\text{nta})(\mu\text{-OH})]_2 \cdot 4\text{H}_2\text{O}$ ($I4_1/a$) – (I)	33
3.3.11	$\text{Cs}_2[\text{Cr}(\text{nta})(\mu\text{-OH})]_2 \cdot 4\text{H}_2\text{O}$ ($P2_1/c$) – (II)	34
3.4	Results and Discussion	34
3.4.1	UV/VIS spectral studies	34
3.4.1.1	Effect of pH on different Co(III)-nta species in solution	34
3.4.1.2	Substitution reactions of $[\text{Co}(\text{nta})(\mu\text{-OH})]_2^{2-}$	36
3.4.1.3	Reactions of $[\text{Co}(\text{nta})(\text{CO}_3)]^{2-}$	36
3.4.1.4	Effect of pH on different Cr(III)-nta species in solution	37
3.4.2	^1H NMR spectra of Co(III)-nta complexes	39
3.5	Conclusion	44

Chapter 4

X-ray crystallography

	45	
4.1	Introduction	45
4.2	Experimental	46
4.3	Crystal structures of Cr(III)-nta complexes	46
4.3.1	Crystal structures of $\text{Cs}_2[\text{Cr}(\text{nta})(\mu\text{-OH})]_2 \cdot 4\text{H}_2\text{O}$ in ($I4_1/a$) = (I) and ($P2_1/c$) = (II)	46
4.3.2	Conclusion	54
4.4	Crystal structures of Co(III)-nta complexes	60
4.4.1	Crystal structure of $\text{Cs}_2[\text{Co}(\text{nta})(\mu\text{-OH})]_2 \cdot 4\text{H}_2\text{O}$	60
4.4.1.1	Comparison of the strain in $\text{Cs}_2[\text{Co}(\text{nta})(\mu\text{-OH})]_2 \cdot 4\text{H}_2\text{O}$ with the isomorphic chromium structure (I in Paragraph 4.3)	66
4.4.2	Crystal structure of $\text{Cs}_2[\text{Co}(\text{nta})(\text{CO}_3)] \cdot \text{H}_2\text{O}$	67

Table of contents

4.4.3 Crystal structure of [Co(nta)(N,N-Et ₂ en)]	73
4.5 Conclusion	78
 Chapter 5	
Kinetic study of the reactions of <i>cis</i>-[Co(nta)(H₂O)₂]	81
5.1 Introduction	81
5.2 Experimental Procedures	82
5.3 Results and Discussion	83
5.3.1 Influence of H ⁺ ions on the Co(III)-nta system	83
5.3.1.1 pH dependance of [Co(nta)(μ-OH)] ₂ ²⁻	83
5.3.1.2 pH dependence of [Co(nta)(H ₂ O) ₂]	85
5.3.1.3 Reaction of [Co(nta)(H ₂ O) ₂] with H ⁺ ions	87
5.3.1.4 Summary of results for pH dependance of Co(III)-nta system	90
5.3.2 Substitution reactions of [Co(nta)(H ₂ O) ₂] with NCS ⁻ ions	93
5.3.2.1. Substitution reactions between [Co(nta)(H ₂ O) ₂] and NCS ⁻ ions	93
 Chapter 6	
Kinetic study of the reactions of [Co(nta)(μ-OH)]₂²⁻	102
6.1 Introduction	102
6.2 Experimental Procedures	103
6.3 Results and Discussion	103
6.3.1 Reactions between [Co(nta)(μ-OH)] ₂ ²⁻ and monodentate ligands in basic medium	103
6.3.1.1. Reaction between [Co(nta)(μ-OH)] ₂ ²⁻ and dimethylaminopyridine (dmap)	103
6.3.1.2. Reaction between [Co(nta)(μ-OH)] ₂ ²⁻ and pyridine (py)	113
6.3.2 Reactions between [Co(nta)(μ-OH)] ₂ ²⁻ and bidentate ligands (LL') in basic medium	117
6.3.2.1 Reaction between [Co(nta)(μ-OH)] ₂ ²⁻ and bidentate ligands (ethylenediamine (en) and N,N-diethyl-ethylenediamine (N,N-Et ₂ en))	117

Table of contents

6.4	Conclusion	123
Chapter 7		
Critical evaluation		125
Supplementary data		127
Section I		
A	Crystal data for $\text{Cs}_2[\text{Cr}(\text{nta})(\mu\text{-OH})_2]\cdot 4\text{H}_2\text{O}$ (I)	127
B	Crystal data for $\text{Cs}_2[\text{Cr}(\text{nta})(\mu\text{-OH})_2]\cdot 4\text{H}_2\text{O}$ (II)	132
C	Crystal data for $\text{Cs}_2[\text{Co}(\text{nta})(\mu\text{-OH})_2]\cdot 4\text{H}_2\text{O}$	137
D	Crystal data for $\text{Cs}_2[\text{Co}(\text{nta})\text{CO}_3]\cdot \text{H}_2\text{O}$	143
E	Crystal data for $[\text{Co}(\text{nta})(\text{N,N-Et}_2\text{en})]$	150
Section II		
A	Kinetic data for Chapter 5	155
B	Kinetic data for Chapter 6	159
Bibliography		164
Abstract		169
Opsomming		172

List of abbreviations

acac	= pentane-2,4-dione
DBC	= 3,5-di-tert-butylcatecholate
dmap	= dimethylaminopyridine
EBT	= Eriochrome Black T
edda	= ethylenediaminediacetic acid
edta	= ethylenediaminetetra-acetate
en	= ethylenediamine
GTF	= glucose tolerance factor
H ₂ vi	= dihydrogenviolurate
im	= imidazole
IR	= infrared
k _{obs}	= observed rate constant
<i>l</i> -ala	= <i>l</i> -alanine
lda	= (S)-leucine-N,N-diacetate
leu	= leucin
<i>l</i> -gly	= <i>l</i> -glycine
<i>N,N</i> -Et ₂ en	= <i>N,N</i> -diethylethylenediamine
<i>N</i> -Eten	= <i>N</i> -ethylethylenediamine
NMR	= nuclear magnetic resonance
nta	= nitrilotriacetic acid
pd	= 1,3-propanediamine
pda	= (S)-phenylalanine-N,N-diacetate
phen	= <i>o</i> -phenanthroline
TPPS	= <i>meso</i> -tetra(<i>p</i> -sulphonatophenyl)porphyrine
trda	= trimethylenediaminetetra-acetate
tren	= 2,2',2''-triaminotriethylamine
val	= valine

List of figures

Chapter 1

- Figure 1.1. Nitritotriacetato cation. 3

Chapter 2

- Figure 2.1. Isomers prepared by Mori *et al.* 7
- Figure 2.2. Glycinato rings in M(III)-nta complexes. 8
- Figure 2.3. $K[Co(nta)(H_2O)] \cdot 2H_2O$ as isolated by Battaglia *et al.* 10
- Figure 2.4. Illustration of R and G acetato rings for different Co(III) complexes. 15
- Figure 2.5. Different intermediates and final product in CO_2 uptake reactions. 24

Chapter 3

- Figure 3.1. UV/VIS spectra of different Co(III)-nta species in solution. 35
- Figure 3.2. Spectral change of $[Co(nta)(CO_3)]^{2-}$ on addition of *N,N*-ethylenediamine. 37
- Figure 3.3. UV/VIS spectra of different Cr(III)-nta species in solution. 38
- Figure 3.4. Glycinato rings in M(III)-nta complexes (M = Cr/Co). 40
- Figure 3.5. 1H NMR spectrum for $[Co(nta)(N,N-Et_2en)]$. 41
- Figure 3.6. 1H NMR spectrum for $[Co(nta)(N-Eten)]$. 42

Chapter 4

- Figure 4.1. Numbering scheme of the $[Cr(nta)(\mu-OH)]_2^{2-}$ anion. 47
- Figure 4.2. Arrangement of oxygen atoms around Cs^+ in I and II. 51
- Figure 4.3. Close-up view of the interaction of I with Cs^+ cations. 52
- Figure 4.4. Close-up view of the interaction of II with Cs^+ cations. 52
- Figure 4.5. Perspective view of the unit cell of I along the b axis. 53
- Figure 4.6. Perspective view of the unit cell of II along the c axis. 53
- Figure 4.7. Perspective drawing of $[Co(nta)(\mu-OH)]_2^{2-}$. 62
- Figure 4.8. Arrangement of oxygen atoms around Cs^+ in $Cs_2[Co(nta)(\mu-OH)]_2 \cdot 4H_2O$. 64

List of figures

Figure 4.9. Packing of Cs ⁺ cations around [Co(nta)(μ-OH)] ₂ ²⁻ .	65
Figure 4.10. Projection of Cs ₂ [Co(nta)(μ-OH)] ₂ ·4H ₂ O along the b axis.	65
Figure 4.11. Perspective drawing of [Co(nta)(CO ₃)] ₂ ²⁻ .	68
Figure 4.12. Projection of Cs ₂ [Co(nta)(CO ₃) ₃]·H ₂ O along the b axis.	71
Figure 4.13. Arrangement of oxygen atoms around Cs ⁺ in Cs ₂ [Co(nta)(CO ₃) ₃]·H ₂ O.	71
Figure 4.14. Interaction of Cs ⁺ cations with [Co(nta)(CO ₃)] ₂ ²⁻ .	72
Figure 4.15. Perspective drawing of [Co(nta)(N,N-Et ₂ en)].	74
Figure 4.16. Projection of [Co(nta)(N,N-Et ₂ en)] along the a axis.	77
 Chapter 5	
Figure 5.1. Plot of A (λ = 320 nm) vs. pH for the [Co(nta)(μ-OH)] ₂ ²⁻ system, 25.0 °C, μ = 1 M (NaClO ₄), [dimer] = 2 × 10 ⁻³ M.	85
Figure 5.2. Plot of A (λ = 400 nm) vs. pH for [Co(nta)(H ₂ O) ₂] (2 × 10 ⁻³ M), 25.0 °C, μ = 1 M (NaClO ₄).	86
Figure 5.3. Plot of k _{obs} vs. [H ⁺] at different temperatures, μ = 1 M (NaClO ₄), λ = 550 nm, [dimer] = 1 × 10 ⁻² M.	88
Figure 5.4. UV/VIS spectral change for the reaction between [Co(nta)(H ₂ O) ₂] and NCS ⁻ ions.	93
Figure 5.5. Plot of k _{obs} vs. [NCS ⁻] for first reaction at different temperatures, μ = 1.0 M (NaClO ₄), λ = 400 nm, [Co(nta)(H ₂ O) ₂] = 4 × 10 ⁻³ M.	96
Figure 5.6. Plot of k _{obs} vs. [NCS ⁻] for second reaction at different temperatures, μ = 1.0 M (NaClO ₄), λ = 400 nm, [Co(nta)(H ₂ O) ₂] = 4 × 10 ⁻³ M.	97
Figure 5.7. Plot of k _{obs} vs. pH for the first reaction between [Co(nta)(H ₂ O) ₂] and NCS ⁻ ions. μ = 1.0 M (NaClO ₄), λ = 400 nm, [NCS ⁻] = 1.25 × 10 ⁻² M.	98
Figure 5.8. Plot of k _{obs} vs. [NCS ⁻] for the first reaction at pH = 7.00, 25.0 °C, μ = 1.0 M (NaClO ₄), λ = 400 nm.	98

Chapter 6

- Figure 6.1.** Intermediate formed during the reaction between $[\text{Co}(\text{en})_2(\mu\text{-OH})]_2^{4+}$ and CO_2 . 105
- Figure 6.2.** Plot of k_{obs} vs. $[\text{dmap}]$ for the reaction between $[\text{Co}(\text{nta})(\mu\text{-OH})]_2^{2-}$ and dmap at different pH levels, $25.0\text{ }^\circ\text{C}$, $\mu = 1\text{ M}$ (NaClO_4), $\lambda = 390\text{ nm}$, $[\text{dimer}] = 1.5 \times 10^{-3}\text{ M}$. 110
- Figure 6.3.** Plot of k_{obs} vs. pOH for the reaction between $[\text{Co}(\text{nta})(\mu\text{-OH})]_2^{2-}$ and dmap at $25.0\text{ }^\circ\text{C}$, $\mu = 1.0\text{ M}$ (NaClO_4), $\lambda = 390\text{ nm}$, $[\text{dimer}] = 1.5 \times 10^{-3}\text{ M}$. 111
- Figure 6.4.** Plot of k_{obs} vs. $[\text{dmap}]$ for the reaction between $[\text{Co}(\text{nta})(\mu\text{-OH})]_2^{2-}$ and py at different temperatures, $\text{pH} = 10.5$, $\mu = 0.5\text{ M}$ (NaClO_4), $\lambda = 390\text{ nm}$, $[\text{dimer}] = 1.5 \times 10^{-3}\text{ M}$. 113
- Figure 6.5.** Plot of k_{obs} vs. pOH for the reaction between $[\text{Co}(\text{nta})(\mu\text{-OH})]_2^{2-}$ and py , $\mu = 0.5\text{ M}$ (NaClO_4), $\lambda = 410\text{ nm}$, $[\text{dimer}] = 1.5 \times 10^{-3}\text{ M}$ and $25.0\text{ }^\circ\text{C}$. 115
- Figure 6.6.** Plot of k_{obs} vs. $[\text{py}]$ for the reaction between $[\text{Co}(\text{nta})(\mu\text{-OH})]_2^{2-}$ and py at different pH levels, $\mu = 0.5\text{ M}$ (NaClO_4), $\lambda = 410\text{ nm}$, $[\text{dimer}] = 1.5 \times 10^{-3}\text{ M}$ and $25.0\text{ }^\circ\text{C}$. 115
- Figure 6.7.** Plot of k_{obs} vs. pOH for the reaction between $[\text{Co}(\text{nta})(\mu\text{-OH})]_2^{2-}$ and en at $25.0\text{ }^\circ\text{C}$, $\mu = 0.2\text{ M}$ (NaClO_4), $\lambda = 325\text{ nm}$, $[\text{dimer}] = 1.5 \times 10^{-4}\text{ M}$. 119
- Figure 6.8.** Plot of k_{obs} vs. pOH for the reaction between $[\text{Co}(\text{nta})(\mu\text{-OH})]_2^{2-}$ and $N,N\text{-Et}_2\text{en}$ at $25.0\text{ }^\circ\text{C}$, $\mu = 0.2\text{ M}$ (NaClO_4), $\lambda = 325\text{ nm}$, $[\text{dimer}] = 1.5 \times 10^{-4}\text{ M}$. 120
- Figure 6.9.** Plot of k_{obs} vs. $[\text{en}]$ for the reaction between $[\text{Co}(\text{nta})(\mu\text{-OH})]_2^{2-}$ and en at different pH levels, $25.0\text{ }^\circ\text{C}$, $\mu = 0.2\text{ M}$ (NaClO_4), $\lambda = 325\text{ nm}$, $[\text{dimer}] = 1.5 \times 10^{-4}\text{ M}$. 120
- Figure 6.10.** Plot of k_{obs} vs. $[N,N\text{-Et}_2\text{en}]$ for the reaction between $[\text{Co}(\text{nta})(\mu\text{-OH})]_2^{2-}$ and $N,N\text{-Et}_2\text{en}$ at different pH levels, $25.0\text{ }^\circ\text{C}$, $\mu = 0.2\text{ M}$ (NaClO_4), $\lambda = 325\text{ nm}$, $[\text{dimer}] = 1.5 \times 10^{-4}\text{ M}$. 121

List of tables

Chapter 2

Table 2.1.	Co-N bond lengths, O-Co-O and O-Co-N angles for different cobalt(III)-nta complexes.	10
------------	--	----

Chapter 3

Table 3.1.	Summary of important IR and UV/VIS data for the prepared complexes.	39
Table 3.2.	Summary of ^1H NMR data for nta protons in symmetrical Co(III)-nta complexes.	43
Table 3.3.	Summary of ^1H NMR data for nta protons in non-symmetrical Co(III)-nta complexes.	43

Chapter 4

Table 4.1.	Crystal data and structure refinement for $\text{Cs}_2[\text{Cr}(\text{nta})(\mu\text{-OH})]_2 \cdot 4\text{H}_2\text{O}$.	48
Table 4.2.	Selected bond lengths for $\text{Cs}_2[\text{Cr}(\text{nta})(\mu\text{-OH})]_2 \cdot 4\text{H}_2\text{O}$.	49
Table 4.3.	Selected bond angles for $\text{Cs}_2[\text{Cr}(\text{nta})(\mu\text{-OH})]_2 \cdot 4\text{H}_2\text{O}$.	49
Table 4.4.	Sums of endocyclic angles, out-of-plane distances of N and Cr from CCOO plane and selected torsion angles for the different glycinato rings in I and II.	50
Table 4.5.	Comparison of ring strain in different Cr(III)-nta complexes.	55
Table 4.6.	Important bond angles for different Cr(III)-nta complexes.	56
Table 4.7.	Bond distances of different Cr(III)-nta complexes.	57
Table 4.8.	Crystal data and structure refinement for $\text{Cs}_2[\text{Co}(\text{nta})(\mu\text{-OH})]_2 \cdot 4\text{H}_2\text{O}$.	60
Table 4.9.	Selected bond lengths for $\text{Cs}_2[\text{Co}(\text{nta})(\mu\text{-OH})]_2 \cdot 4\text{H}_2\text{O}$.	61
Table 4.10.	Selected bond angles for $\text{Cs}_2[\text{Co}(\text{nta})(\mu\text{-OH})]_2 \cdot 4\text{H}_2\text{O}$.	61
Table 4.11.	Endocyclic angles, out-of-plane distances of N and Co from CCOO plane and torsion angles for $\text{Cs}_2[\text{Co}(\text{nta})(\mu\text{-OH})]_2 \cdot 4\text{H}_2\text{O}$.	63
Table 4.12.	Selected structural data for $[\text{Co}(\text{nta})(\mu\text{-OH})]_2^{2-}/[\text{Cr}(\text{nta})(\mu\text{-OH})]_2^{2-}$.	66

List of tables

Table 4.13.	Crystal data and structure refinement for $\text{Cs}_2[\text{Co}(\text{nta})(\text{CO}_3)] \cdot \text{H}_2\text{O}$.	67
Table 4.14.	Selected bond lengths for $\text{Cs}_2[\text{Co}(\text{nta})(\text{CO}_3)] \cdot \text{H}_2\text{O}$.	68
Table 4.15.	Selected bond angles for $\text{Cs}_2[\text{Co}(\text{nta})(\text{CO}_3)] \cdot \text{H}_2\text{O}$.	69
Table 4.16.	Endocyclic angles, out-of-plane distances of N and Co from CCOO plane and torsion angles for $\text{Cs}_2[\text{Co}(\text{nta})(\text{CO}_3)] \cdot \text{H}_2\text{O}$.	70
Table 4.17.	Crystal data and structure refinement [$\text{Co}(\text{nta})(\text{N},\text{N}\text{-Et}_2\text{en})$].	73
Table 4.18.	Selected bond lengths for [$\text{Co}(\text{nta})(\text{N},\text{N}\text{-Et}_2\text{en})$].	74
Table 4.19.	Selected bond angles for [$\text{Co}(\text{nta})(\text{N},\text{N}\text{-Et}_2\text{en})$].	75
Table 4.20.	Endocyclic angles, out-of-plane distances of N and Co from CCOO plane and torsion angles for [$\text{Co}(\text{nta})(\text{N},\text{N}\text{-Et}_2\text{en})$].	76
Table 4.21.	Selected features of different Co(III)-nta complexes	79

Chapter 5

Table 5.1.	Observed rate constants for the reaction between [$\text{Co}(\text{nta})(\text{H}_2\text{O})_2$] and different acids and anions, 25.0 °C	87
Table 5.2.	Summary of the rate constants and activation parameters for the reaction between [$\text{Co}(\text{nta})(\text{H}_2\text{O})_2$] and H^+ ions.	90
Table 5.3.	Summary of the rate constants and activation parameters for the reaction between [$\text{Co}(\text{nta})(\text{H}_2\text{O})_2$] and NCS^- ions.	99

Chapter 6

Table 6.1.	Summary of the rate constants for the reaction between [$\text{Co}(\text{nta})(\mu\text{-OH})_2$] ²⁻ and different monodentate ligands at 25.0 °C.	116
Table 6.2.	Summary of the rate constants for the reaction between [$\text{Co}(\text{nta})(\mu\text{-OH})_2$] ²⁻ and LL' at 25.0 °C.	121
Table 6.3.	Summary of the rate constants for the reaction between [$\text{Co}(\text{nta})(\mu\text{-OH})_2$] ²⁻ and L/LL' at 25.0 °C.	123

List of schemes

Chapter 2

- Scheme 2.1.** Formation of intermediate Cr(III)-nta species in acidic solution. 12
- Scheme 2.2.** Hydrolysis of $[\text{Cr}(\text{nta})(\text{Im})_2]$ according to Bocarsley *et al.* 13
- Scheme 2.3.** Reaction scheme for the reaction of $[\text{Cr}(\text{nta})(\text{H}_2\text{O})_2]$ with Eriochrome Black T, EBT. 17
- Scheme 2.4.** Formation of $[\text{Cr}(\eta^3\text{-nta})(\text{H}_2\text{O})_3]^+$. 18
- Scheme 2.5.** Acidic cleavage of $[\text{Co}(\text{NH}_3)(\text{OH})]_2^{4+}$. 20
- Scheme 2.6.** Acidic cleavage of a di- μ -hydroxo cobalt(III) complex. 21
- Scheme 2.7.** Acidic cleavage of $[\text{Co}(\text{nta})(\mu\text{-OH})]_2^{2-}$. 22
- Scheme 2.8.** Decarboxylation reactions of bidentate cationic carbonato tetramine complexes of cobalt(III). 25

Chapter 3

- Scheme 3.1.** Synthesis and reactions of $[\text{Co}(\text{nta})(\mu\text{-OH})]_2^{2-}$. 28

Chapter 4

- Scheme 4.1.** Complexes of Co(III)-nta. 45

Chapter 5

- Scheme 5.1.** Formation and reactions of $[\text{Co}(\text{nta})(\text{H}_2\text{O})_2]$. 82
- Scheme 5.1.1.** pH dependance of $[\text{Co}(\text{nta})(\mu\text{-OH})]_2^{2-}$. 83
- Scheme 5.1.2.** pH dependance of $[\text{Co}(\text{nta})(\text{H}_2\text{O})_2]$. 85
- Scheme 5.1.3.** Reaction of $[\text{Co}(\text{nta})(\text{H}_2\text{O})_2]$ with H^+ ions. 87
- Scheme 5.2.** Proposed mechanism for the reaction of $[\text{Co}(\text{nta})(\text{H}_2\text{O})_2]$ with H^+ ions. 89
- Scheme 5.3.** Influence of H^+ ions on the Co(III)-nta system. 90
- Scheme 5.4.** Behaviour of the Co(III)-nta system in acidic medium according to Meloon and Harris. 91

List of schemes

Scheme 5.5.	Reactions of $[\text{Co}(\text{nta})(\text{H}_2\text{O})_2]/[\text{Co}(\text{nta})(\text{H}_2\text{O})(\text{OH})]^-$ with NCS^- ions.	94
 Chapter 6		
Scheme 6.1.	Reactions of $[\text{Co}(\text{nta})(\mu\text{-OH})_2]^{2-}$.	102
Scheme 6.2.	Reaction scheme for the reaction between $[\text{Co}(\text{nta})(\mu\text{-OH})_2]^{2-}$ and dmap.	105
Scheme 6.3.	Mechanism II for the reaction between $[\text{Co}(\text{nta})(\mu\text{-OH})_2]^{2-}$ and dmap.	108
Scheme 6.4.	Mechanism III for the reaction between $[\text{Co}(\text{nta})(\mu\text{-OH})_2]^{2-}$ and dmap.	109
Scheme 6.5.	Reaction scheme for the reaction between $[\text{Co}(\text{nta})(\mu\text{-OH})_2]^{2-}$ and py.	114
Scheme 6.6.	Reaction scheme for the reaction between $[\text{Co}(\text{nta})(\mu\text{-OH})_2]^{2-}$ and LL'.	118

1

Aim of the Study

1.1 Introduction

1.1.1 *Chromium and cobalt chemistry – where it started*

Chromium was first isolated and identified in 1798 by the French chemist, Vauquelin. He named it chromium, derived from the Greek word *chroma*, meaning colour, because of the wide variety of brilliant colours displayed by its compounds. It is of no wonder then that one of the first applications of chromium was in the dyeing industry. One of the most important applications of chromium, namely its use as an alloying element, was developed during the nineteenth century. Its first application was in 1874 with the building of the famous East Bridge across the Mississippi. Today, the applications of chromium compounds are too numerous to mention, from uses in ceramics, electronics, catalysts, dyes and corrosion inhibitors to uses as fungicides in the agricultural industry (Westbrook, 1979:54 and Hartford, 1979:82).

The history of cobalt spans much further back than that of chromium. It was used as a colouring agent by the Egyptians as far back as 2000 BC. The cobalt amines were first discovered by Werner in the early twentieth century and form the basis for the formulation of the coordination theory in inorganic chemistry. The uses of cobalt compounds are just as widespread as for chromium. Cobalt compounds are used as catalysts, pigments, electroplaters, it also has uses in ceramics, as dryers for paints and varnishes, high temperature alloys and also in radiology (Planinsek & Newkirk, 1979:481 and Morral, 1979:495).

Chromium and cobalt salts and complexes are most commonly used in dyestuffs for polyamide fibres and leather because of their kinetic inertness and the stability of their complexes towards acid. The importance of such metal complexes stems principally from their very high light-fastness, attributed to the protection of the azo group of the dye by the metal against attack by, for example, singlet oxygen (Gordon & Gregory, 1983).

The substitution reactions of octahedral complexes of chromium(III) and especially cobalt(III) have been under investigation for many years. The reasons for this are that a great variety of these complexes can easily be prepared and the substitution reactions of these complexes are slow enough to be followed by conventional means (Purcell & Kotz, 1985:710). Hence it is not surprising that one finds so many publications and review articles on the substitution reactions of these metal complexes (Hay, 1984:1 and Moore, 1984).

1.1.2 *The significance of M-nta complexes as biological models – focus on wool dyeing*

Complexes of Cr(III) and Co(III) with ligands that simulate binding sites on protein chains have many applications and are of significant scientific value. According to Cooper *et al.* (1984:23) the glucose tolerance factor (GTF), a fraction isolated from brewer's yeast, which displays biological activity in a number of assay systems, may have an important role to play in glucose metabolism. This has led to several studies on this subject (Toepfer, *et al.*, 1977:162, Mertz, 1975:129 and Haylock *et al.*, 1983:105). Other examples include the construction of molecular recognition models for enzyme-substrate complex formation through weak non-covalent interactions (Jitsukawa *et al.* 1994:249), as well as many biomedical applications like the removal of toxic metal ions from the human body by chelating agents like penicillamine (Helis *et al.*, 1976:3309 and Santos *et al.*, 1992:1687).

Our interest in cobalt(III)- and chromium(III)-amino acid complexes date back as far as 1991, when a project for Textech was undertaken to investigate the mechanism of the wool dyeing process with Eriochrome Black T (Visser, 1992). The wool dyeing process is costly and the mechanism of the interaction between the dye, wool and chromium is not well understood.

The method most widely used for the dyeing of wool fibre is the afterchrome method (Welham, 1986:126). It is postulated that the dye penetrates the wool fibre where it is held by ionic and other intermolecular forces (Dobozy, 1973:36). Cr(VI) is then added to the dye bath where it is reduced to Cr(III). The final product is believed to be a stable wool-Cr(III)-dye complex. One of the biggest problems of this method of dyeing is the high levels of Cr(VI) which is found in the effluents of dye houses. It is a well known fact

Introduction

that Cr(VI) is highly carcinogenic and causes a lot of damage to the environment (Connet & Wetterhahn, 1983:93). The penetration of the lesser toxic Cr(III) ions into wool fibre is much slower than for the Cr(VI) ions (Hartley, 1969:66) which makes the use of it in the wool dyeing industry less economical.

Another method that is used is the application of 1:1 or 1:2 metal:azo complexes to cellulosic fibres, but its uses are more restricted (Puper, 1962:322).

Our aim with the initial study was to synthesise chromium(III)-complexes that would act as biological models for the complexes formed between wool, chromium and the dye and to investigate the substitution reactions of these complexes with different ligands and dyes like Eriochrome Black T (Visser, 1992). The idea was also to synthesise Cr(III) complexes that would react faster than normal in order to find possible substitutes for Cr(VI) in the dyeing process. The selected model complex was a nitrilotriacetato complex of Cr(III) which was first prepared by Mori *et al.* (1958:940).

The bonding modes of nitrilotriacetic acid (nta) (see Figure 1.1) have been of interest for many years. This tripod type ligand functions as a tetradentate ligand in most metal chelation compounds and its structure is well characterised in both its zwitterionic and chelated forms (Skrzypczak-Jankun & Smith, 1994:1097, Whitlow, S.H., 1972:1914 and Okamoto *et al.*, 1992:1025).

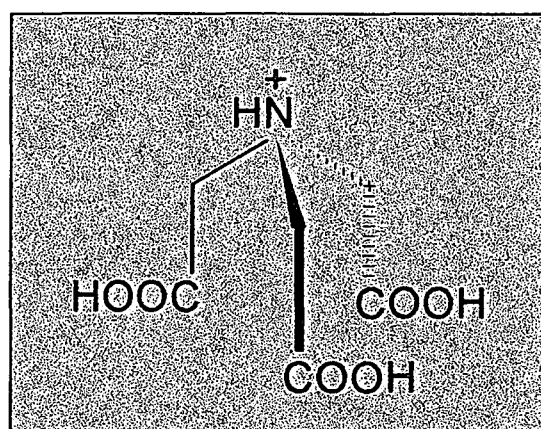


Figure 1.1. Nitrilotriacetato cation.

Substitution reactions at chromium(III)- and cobalt(III) centers are normally slow, but the rate of substitution can be significantly enhanced by having porphyrin, Schiff-base chelates or edta and related ligands (such as nta) in the metal coordination sphere

(Leipoldt & Meyer, 1987:1361 and Beswick *et al.*, 1996:991). It is believed that these ligands donate extra electron density to the inert central metal(III), thereby changing its properties to react more like the labile metal(II) ion.

The above factor, as well as the fact that fully coordinated nta leaves two *cis* positions available on the metal centre, makes this kind of complex very suitable to use as a biological model (Visser *et al.*, 1994:1051, Bhattacharyya & Banerjee, 1997:849, Jitsukawa *et al.*, 1994:249 and Bocarsley & Barton, 1992:2827).

1.2 Aim of this study

A lot of the pieces to the puzzle of metal(III)-nta complexes were still not explained on completion of the project for Textech (Visser, 1992). The aqueous chemistry of Cr(III) complexes with azo dyes is laden with challenges. Cr(III) is known to form many insoluble hydroxide compounds (Ley & Ficken, 1912:377), much more so than Co(III). Furthermore, many of these dyes can also act as chelating agents, thereby complicating kinetic and synthetic studies even more (Visser, 1992).

Most importantly our early studies also revealed that the identification of chromium(III)- and cobalt(III)-nta complexes were not sufficient (Visser *et al.*, 1994:1051). The starting Cr(III)-nta complex as well as the final products in two different kinetic studies could not be isolated and identified up to that point (Visser *et al.*, 1994:1051 and Hualin & Xu, 1990:137). This makes the determination of the intimate mechanism of these reactions very difficult.

From this discussion it should be clear that there is a lot of uncertainty regarding the synthesis, characterisation and reactions of Co(III)- and Cr(III)-nta complexes. Therefore we decided to do an in depth investigation of the Co(III)- and Cr(III)-nta systems.

The aim of this study was to:

- a) synthesise suitable Cr(III)- and Co(III)-nta complexes that can be used as biological models in future studies,
- b) develop alternative routes for the synthesis of Cr(III)- and Co(III)-nta complexes,

Introduction

- c) characterisation of these complexes with especially single-crystal X-ray crystallography and ^1H NMR so that it could be used as starting material in kinetic studies,
- d) investigate the ring strain in these complexes and the possible chemical effects it may have and
- e) to determine the mechanism of the substitution reactions of Co(III)-nta complexes with different ligands at different pH levels by means of a kinetic study and isolation and characterisation of the final products in these reactions.

2

Literature overview

2.1 Introduction

It was decided to focus the main part of the literature study on the synthesis and characterisation of cobalt(III)- and chromium(III) complexes with tripod-type ligands like nitrilotriacetic acid (see Figure 1.1) and the substitution reactions of these complexes with various ligands. Another part of the study will include an investigation of the mechanism of bridge cleavage reactions of di- μ -hydroxo bridged dimeric cobalt(III) complexes. The decarboxylation reactions of $[\text{Co}(\text{nta})(\text{CO}_3)]^{2-}$ and other similar complexes were also studied.

2.2 Synthesis, characterisation and reactions of cobalt(III)- and chromium(III)-nitrilotriacetato complexes

2.2.1 *Synthesis and characterisation*

Cobalt

Mori and co-workers (1958:940) were the first to prepare and identify different cobalt(III)-nitrilotriacetato complexes. According to their study two monomeric hydroxo-aqua cobalt(III)-nta isomers, the α - and β -complexes as well as a dimeric μ -hydroxo bridged species ($\text{K}_2[\text{Co}(\text{nta})(\text{OH})]_2 \cdot 3\text{H}_2\text{O}$) which they called a 'diol complex', could be isolated (Figure 2.1).

The α -isomer was isolated by neutralising nta with potassium bicarbonate, adding $\text{CoCl}_2 \cdot 6\text{H}_2\text{O}$ and H_2O_2 to this solution and then allowing the crystals to separate. The crystals were filtered and washed with ethanol and ether. The β -isomer was prepared by acidifying the filtrate obtained after isolation of the α -isomer with acetic acid, adding a large amount of ethanol and allowing the solution to stand overnight in a refrigerator.

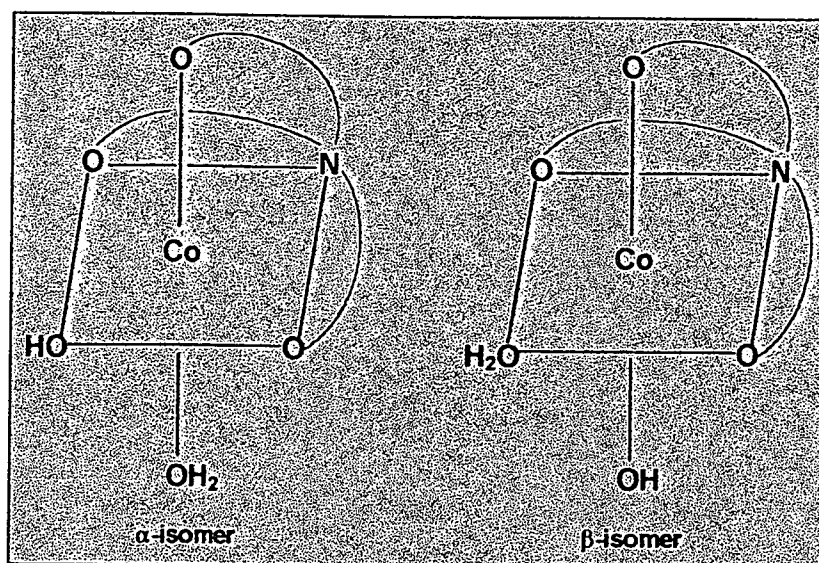


Figure 2.1. Isomers prepared by Mori *et al.* (1958:940).

The dimeric complex was isolated by acidifying and boiling the above-mentioned filtrate on a water-bath until the solution turned pink. On cooling a pink precipitate was collected. All the complexes were characterised by chemical analysis, thermal decomposition, coagulation studies and spectroscopic measurements.

Mori and his co-workers had difficulty to explain several observed abnormalities. Close inspection of the chemical analysis data revealed that the chemical composition of the three complexes is almost identical. They were also unable to explain the thermal decomposition and spectrochemical data with confidence.

The uncertainty around the structure of the complexes prepared by Mori and his co-workers was first addressed by Smith and Sawyer (1968:923) who did a ^1H NMR study on 1:1 and 1:2 cobalt(III)- and rhodium(III)-nta complexes. They observed different ^1H NMR spectra for the α - and β -forms of the Co(III)-nta complex at pH 6.

Both the spectra displayed an AB pattern of two doublets and a singlet, but at different chemical shifts. The two doublets were assigned to the non-equivalent, coupled protons in the two coplanar, five-membered, equatorial rings (G rings in Figure 2.2) and the singlet to the acetate CH_2 protons in the third ring (R ring).

Smith and Sawyer reasoned that the α - and β -isomers would be expected to interconvert rapidly in solution at pH 6 because of proton exchange and are expected to

have the same spectrum. The difference in spectra suggested the existence of a different Co(III)-nta species, possibly an oxo- or hydroxo-bridged dimer, which will have a spectrum different from that of the α - and/or β -isomers.

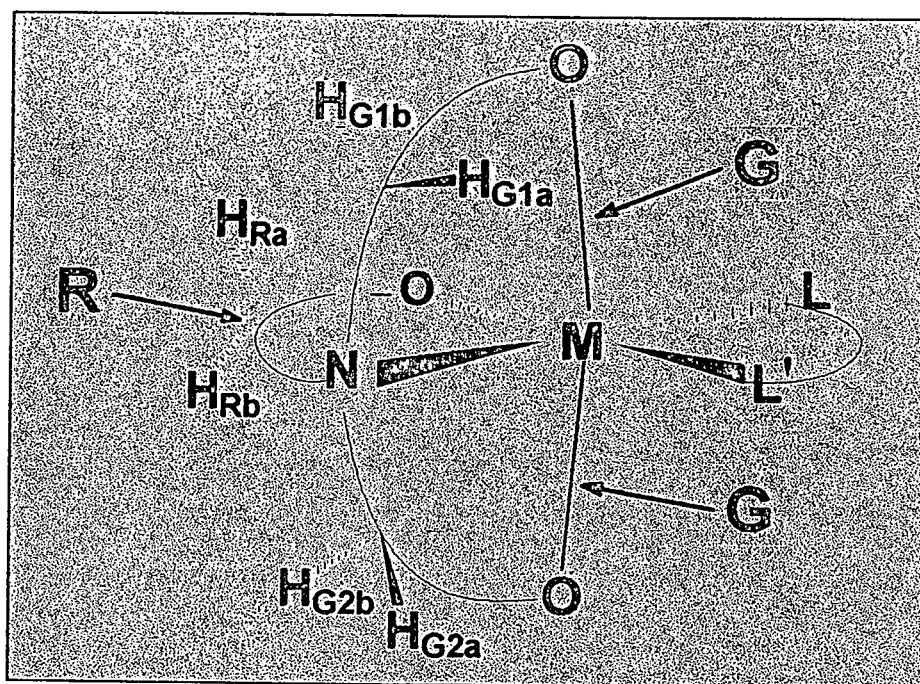


Figure 2.2. Glycinato rings in M(III)-nta complexes (M = Co/Cr).

Another important observation was that the ^1H NMR spectra of the α - and β -forms at pH 0.5 were identical. They attributed this to the formation of a diaquo Co(III)-nta species and also concluded that the α -isomer as according to Mori *et al.* (1958:940) is actually the dimeric form because of its lower field AB proton positions which would result from deshielding associated with the magnetic anisotropy of the metal-oxo or -hydroxo region.

Smith and Sawyer (1968:923) further noted that the IR spectra for the α - and β -forms were also different to each other. The α -form had COO-Co stretching at 1674 and 1615 cm^{-1} compared to 1634 cm^{-1} for the β -form. No COOH stretching was observed, thereby confirming tetradentate coordination of nta.

Koike and co-workers (1969:1583) continued the ^1H NMR study of Co(III)-nta complexes by investigating the spectra of $[\text{Co}(\text{nta})(\text{gly})]^-$ and $[\text{Co}(\text{nta})(l\text{-ala})]^-$. The spectrum of $[\text{Co}(\text{nta})(\text{gly})]^-$ was very similar to that found for the Co(III)-nta complexes studied by Smith & Sawyer (1968:923). These spectra consisted of two doublets in a

Literature overview

simple AB pattern and a singlet. The singlet integrates for two protons. The AB pattern with centers at 4.41 and 3.99 ppm obtained for $[\text{Co}(\text{nta})(\text{gly})]^-$ was assigned to the non-equivalent, coupled G ring protons, H_{G1b} , H_{G1a} and H_{G2a} , H_{G2b} , in Figure 2.2. The AB pattern is a result of the fact that H_{G1a} and H_{G2a} are equivalent to each other and couples with H_{G1b} and H_{G2b} respectively. The singlet at 4.12 ppm was assigned to the equivalent acetate protons of the R ring.

The spectra of $[\text{Co}(\text{nta})(\text{l-ala})]^-$ and $[\text{Co}(\text{nta})(\text{gly})]^-$ resembled each other, even though a more complex spectrum might have been expected for the *l*-alinato complex because all the acetate protons of nta have different chemical environments.

Thacker and Higginson (1975:704) confirmed most of the results of the previous studies. They added that their preparations of the β -form always contained cobalt(II) and that the 'diol complex' that Mori prepared is in fact a bis(nta) complex, $\text{K}[\text{Co}(\text{Hnta})_2] \cdot 2\text{H}_2\text{O}$ (Hnta represents the mono-pronated triply bonded form of nta).

Thacker and Higginson (1975:704) and later Meloon and Harris (1977:434) obtained the *cis*-aqua complex, $[\text{Co}(\text{nta})(\text{H}_2\text{O})_2]$, by acidifying the dimer or hydroxo-aqua complex, but reported that there were still difficulties to purify the starting material. $[\text{Co}(\text{nta})(\text{H}_2\text{O})_2]$ can also be obtained by acidifying $[\text{Co}(\text{nta})(\text{CO}_3)]^{2-}$ (Dasgupta & Harris, 1974:1275). This *cis*-aqua complex is obviously very suitable for kinetic studies (refer to Section 2.2.2).

The first crystal structure of a cobalt-nta complex that was published was that of a distorted octahedral cobalt(II) species, $\text{K}[\text{Co}(\text{nta})(\text{H}_2\text{O})] \cdot 2\text{H}_2\text{O}$ (Battaglia *et al.*, 1975:1160). The coordination sphere around the Co(II) centre was occupied by one tetradentate bonded nta ligand, a water molecule and the carboxylic oxygen of an adjacent anion (Figure 2.3).

Since the isolation of $\text{K}[\text{Co}(\text{nta})(\text{H}_2\text{O})] \cdot 2\text{H}_2\text{O}$ a few other cobalt(III)-nta complexes have been characterised by X-ray crystallography (see Table 2.1 for selected bond lengths and angles). It is important to note that up to this point in time nobody has yet been able to isolate single crystals for X-ray analysis of the complexes prepared by Mori's method (1958:940) or for cobalt(III)-nta complexes with monodentate ligands in the two available coordination positions.

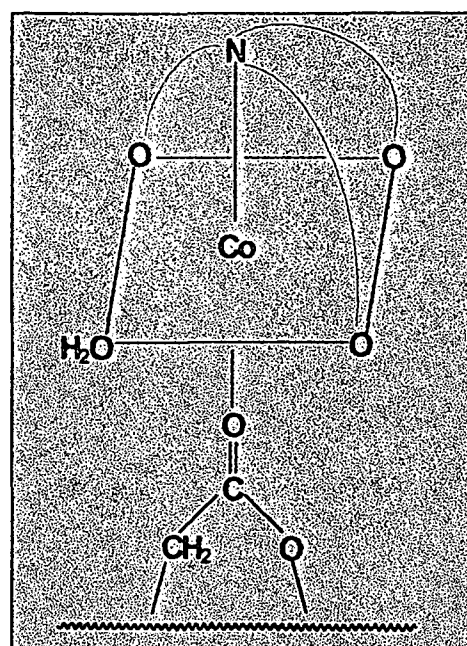


Figure 2.3. $K[Co(NTA)(H_2O)] \cdot 2H_2O$ as isolated by Battaglia *et al.* (1975:1160).

Table 2.1. Co-N bond lengths, O-Co-O and O-Co-N angles for different cobalt(III)-nta complexes*.

Complex	Co-N (Å)	O-Co-O (°)	O-Co-N (°)	Reference
$K[Co(H_2vi)(NTA)] \cdot 2H_2O$	1.942(7)	172.8(3)	86.3(3)	Almazán <i>et al.</i> , (1990:2565)
$[Co(NTA)(pd)] \cdot H_2O$	1.962(3)	170.5(1)	86.8(1)	Swaminathan & Sinha, (1989:566)
$[Co(NTA)(en)] \cdot H_2O$	1.946(3)	172.6(1)	87.6(1)	Gladkikh <i>et al.</i> , (1992:1231)
$Ba[Co(NTA)(gly)]ClO_4 \cdot 3H_2O$	1.928(8)	172.5(3)	89.3(3)	Gladkikh <i>et al.</i> , (1992:908)

* Co-N bond refers to bonding between Co and N of nta, O-Co-O refers to angle between *trans*-O atoms of the nta moiety, O-Co-N refers to the angle between the atoms in the same plane as the other chelating ligand e.g. en/pd etc.

Chromium

Compared to cobalt(III) even less structural and synthetic work were published on chromium(III)-nta complexes. Uehara and co-workers (1967:2317) were the first to prepare different chromium(III)-nta complexes. Crystals of two distinctly different colours were isolated. Both these complexes had the same absorption spectra in solution. The structure of the complex in solution was assumed to be $[Cr(\eta^3\text{-nta})(OH)(H_2O)_2]^-$, where the nta ligand is coordinated through its three carboxylates. They based their assignment primarily on the maximum of the first

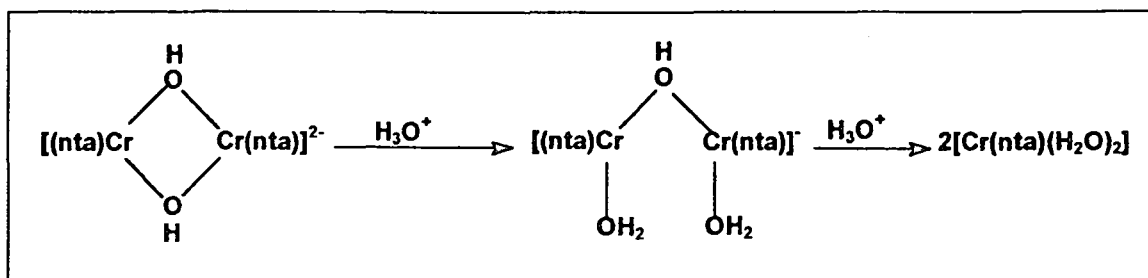
Literature overview

electronic absorption band, which is at considerably lower energy (585 nm) than that typically observed for mononuclear CrNO_5 -type complexes.

Koine *et al.* (1986:2835) used ^2H NMR to investigate the solution behaviour of Cr(III) complexes with nta by firstly blocking the *cis* sites with bidentate ligands to inhibit dimerisation. They observed three peaks with equivalent intensity, which is consistent with a structure where nta functions as a tetradentate ligand. Another important part of their experiment was the investigation of the solution properties of the complexes prepared by Uehara *et al.* (1967:2317). The ^2H NMR spectrum of the complex in solution was consistent with fully coordinated nta and not with tridentate coordination as first postulated by Uehara *et al.* This was further confirmed by obtaining the $^2\text{H}_2\text{O}$ solution IR spectrum as a function of pH. The carbonyl region was invariant with pH, consistent with full coordination of nta.

Another important aspect of the above-mentioned study is that the first absorption maximum of the starting complex is 28 nm lower in energy than that for $[\text{Cr}(\text{nta})(\text{H}_2\text{O})_2]$. Similar results was found for *sym,cis*- $[\text{Cr}(\text{edda})(\text{OH})]_2$ and *sym,cis*- $[\text{Cr}(\text{edda})(\text{H}_2\text{O})_2]^+$ where a shift of 23 nm was observed (Srdanov *et al.*, 1980:37 and Radanovic, 1984:159) when moving from the dimer to the monomeric species. This moved Koine *et al.* to propose that the complexes that Uehara and co-workers (1967:2317) prepared was actually a dimeric species, $[\text{Cr}(\text{nta})(\text{OH})]_2^{2-}$. There are two isomers possible for this bis(μ -hydroxo)-nta complex, but only one species was observed in solution.

Koine and co-workers also observed a change in spectrum when moving from pH 7.1 to 3.5. At pH 4.6 a third species was observed, but they did not have enough information to characterise the intermediate. It was postulated that it could be either a mono- μ -hydroxo species or a hydroxo-aqua bridged intermediate that exists at pH 4.6 (Scheme 2.1).



Scheme 2.1. Formation of intermediate Cr(III)-nta species in acidic solution (Koine *et al.*, 1986:2835).

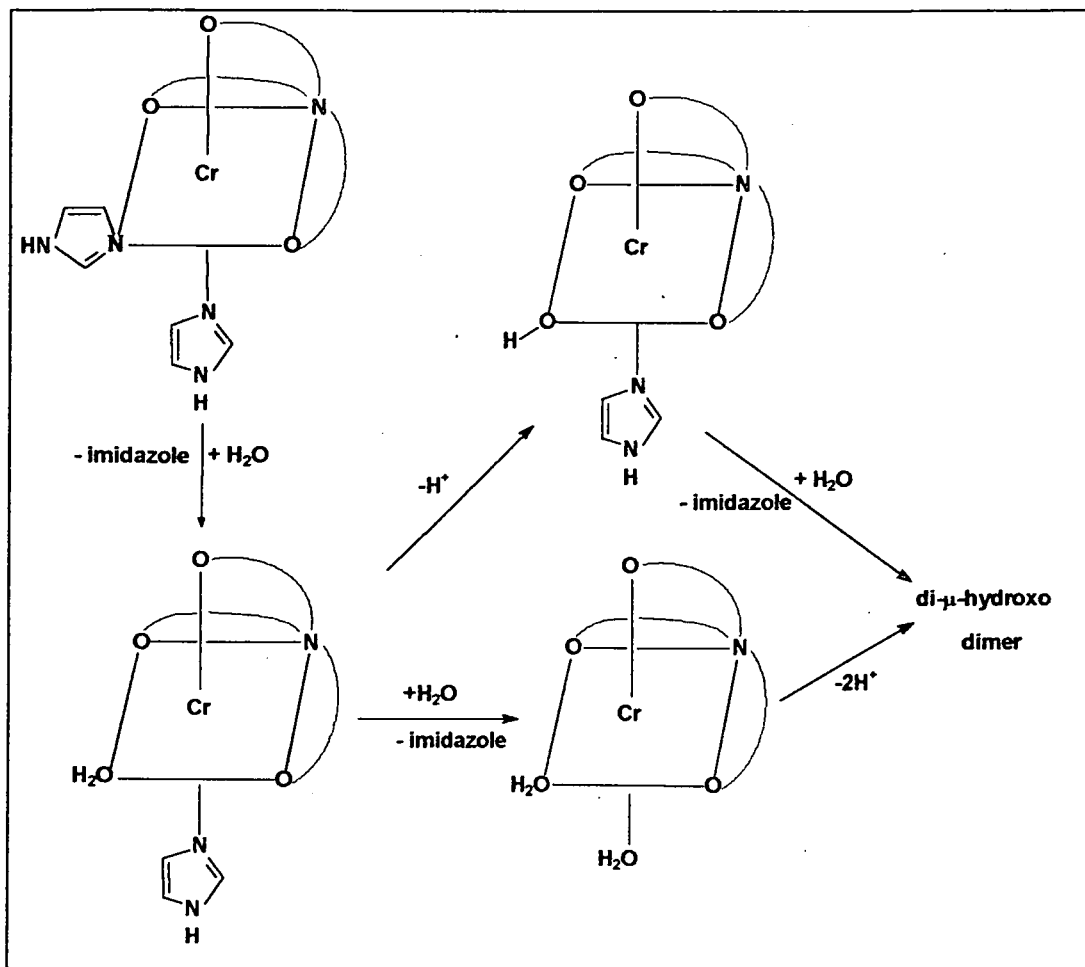
The isolation of chromium(III)-nta complexes where the available *cis* positions are occupied by monodentate ligands seems to be as difficult as for cobalt(III)-complexes. Bocarsley *et al.* (1990:4898) prepared several chromium(III)-nta derivatives. The crystal structures of $[\text{Cr}((\text{S})\text{-ida})(\text{Im})_2]$ and $[\text{Cr}((\text{S})\text{-pda})(\text{Im})_2]$ were determined and are the only data in the literature where the *cis* positions of a Cr(III) complex with a nta derivative are occupied by monodentate ligands.

$[\text{Cr}(\text{nta})(\text{Im})_2]$ was also prepared and characterised by elemental analysis, but it was observed that the chromium-monodentate ligand bond slowly hydrolysed to form the familiar di-aqua complex. The first order rate constants for this reaction were recorded as $5.9 \times 10^{-5} \text{ s}^{-1}$ (pH 6) and $8.0 \times 10^{-5} \text{ s}^{-1}$ (pH 7).

The UV/VIS spectra obtained for the hydrolysis of $[\text{Cr}(\text{nta})(\text{Im})_2]$ showed that the reaction appears to be of the form $\text{A} \rightarrow \text{B} \rightarrow \text{C}$. It was confirmed with ^2H NMR that it is the *trans*-amine-imidazole that aquates first to form an intermediate thought to be $[\text{Cr}(\text{nta})(\text{Im})(\text{H}_2\text{O})]$ (Scheme 2.2). It was explained that *trans*-amine-imidazole should be more labile because of *cis*-labilisation of the carboxylate donors of nta. The *trans*-amine-imidazole should also be affected by the three *cis*-carboxylate donors compared to the other imidazole that will only be affected by two *cis*-carboxylates. The *cis*-carboxylate labilisation effect has been previously observed in group 6 d^6 metal complexes (Atwood & Brown, 1976:3160).

Apart from the structures mentioned in the previous paragraphs the only other crystal structure studies of Cr(III)-nta complexes were done by Green *et al.* (1990:87) who isolated an interesting dimeric chromium(III)-nta complex with a μ -acetato-O,O- μ -hydroxo bridge and Fujihara *et al.* (1995:1813) who prepared and

characterised several hetero- and homo-metallic dihydroxo-bridged complexes of cobalt(III)- and chromium(III)-nta.



Scheme 2.2. Hydrolysis of $[\text{Cr}(\text{nta})(\text{Im})_2]$ according to Bocarsley *et al.* (1990:4898).

Other metal(III)-nta complexes

The tetradentate bonding mode of nta in most metal complexes was further confirmed by Okamoto *et al.* (1992:1025) who reported the crystal structure of a seven-coordinate triaqua(nitrilotriacetato)vanadium(III) tetrahydrate complex. White *et al.* (1984:8312) characterised a Fe(III)-nta complex, $[\text{Fe}(\text{nta})(\text{DBC})]^{2-}$, with the 3,5-di-*tert*-butylcatecholato anion (DBC^{2-}) acting as a bidentate ligand and showed that this complex is reactive towards dioxygen.

Ring strain in metal(III)-nta complexes

The strain in the acetate-metal rings of complexes containing polyamino polycarboxylate ligands like edta^- , trdta^- and of course nta brought about very interesting, yet conflicting studies. Weakliem and Hoard (1959:549) observed that the two coplanar carboxylate-containing, five-membered, equatorial rings (denoted G, or girdling rings) exhibit substantially more strain than the out-of-plane rings (termed R, or relaxed rings) for $[\text{Co(III)(edta)}]^-$. It was suggested that the sum of the bond angles of the rings could be used to determine ring strain. The ideal value for the sum of the bond angles is 538.4° , which would allow the rings to be nearly planar.

The primary reason for the strain in the G rings is thought to be the angular strain about the coordinated nitrogen atoms. Each ring attempts to impose its own stereochemical requirements on the nitrogen atom, which is also constrained to approximately tetrahedral geometry. The results are not only angle and bond abnormalities in the G rings but also significant distortions of the nitrogen tetrahedra.

A similar study on $[\text{Co(trdta)}]^-$ (Nagao *et al.* 1972:1852) also found that the R rings are lesser strained than the G rings. The least squares calculations of the deviations of the non-bonded carboxylate atoms from the Co-N-O-C-C planes showed that the R ring was nearly planar. Furthermore, the Co-O_R distance was slightly shorter than the Co-O_G bonding distance (1.861 Å compared to 1.904 Å). It was postulated that these results suggest that the G ring is more strained than the R ring.

A study of Halloran and co-workers (1975:1762) on $[\text{Co(edda)(pn)}]^+$ complexes (Figure 2.4) further supported the results of the previous two studies although it was observed that the total strain was more evenly distributed over the entire chelate in this case.

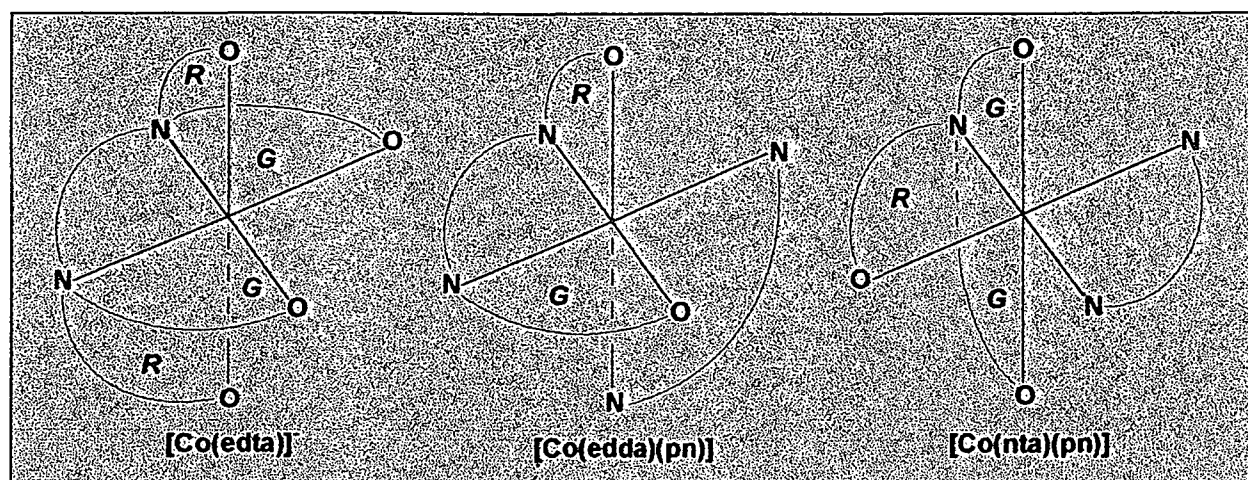


Figure 2.4. Illustration of R and G acetato rings for different Co(III) complexes.

A structural study of the penta-coordinated edta complex of the larger Ni(II) cation, $[\text{Ni}(\text{edta})(\text{H}_2\text{O})]$, (Smith & Hoard, 1959:556) in which one of the G ring arms fail to coordinate, demonstrated that ring strain can influence chemical behaviour in this type of complexes. It was found that the glycinato rings of the isomer that was isolated had less strain than the glycinato rings in hexadentate $[\text{Co}(\text{edta})]^-$.

The effect of the strain in glycinato rings on chemical behaviour was further illustrated by isotopic exchange studies on $[\text{Co}(\text{edta})]^-$. Sudmeier and Occupati (1968:2524) as well as Terril and Reilly (1966:1988) showed that the α -carbon protons of the R rings of $[\text{Co}(\text{edta})]^-$ exhibit a much more rapid rate of exchange in comparison with G ring protons. It was concluded that the strained nature of the G rings prevents the attainment of an enolate intermediate needed for proton exchange.

A structural study (Bocarsley *et al.*, 1990:4894) of two complexes with derivatives of nta, $[\text{Cr}(\text{pda})(\text{im})_2]$ and $[\text{Cr}(\text{lda})(\text{im})_2]$, measured the strain in the glycinato rings by comparing the ring torsion angles (O-C-CH₂-N), the angles subtended by the atoms on the mutually perpendicular axes of the octahedron and the octahedral angles about the Cr(III) centres. It was found that the observed angles followed the anticipated order of ring strain. Furthermore, the substituted G rings were more strained than its unsubstituted counterparts in each case.

The ring strain in Co(III)-nta complexes have also been investigated. The study of Swaminathan and co-workers (1989:566) on $[\text{Co}(\text{nta})(\text{pd})]\cdot\text{H}_2\text{O}$ indicated that the R

rings were more strained than the G ring. Unfortunately they misunderstood the method first used by Weakliem & Hoard (1959:549) to distinguish between the glycinato rings. Tetra-coordinated nta has two co-planar glycinato rings (G rings) and one R ring (see Figure 2.4 for correct representation of G and R rings in nta complexes). Therefore it can be concluded that the same sequence for strain is found for nta complexes with G rings being more strained than R rings.

The reasons for the strain in the glycinato rings of Co(III)-nta complexes have not yet been fully explained. Gladkikh *et al.* (1989:566 and 1989:549) observed that the Co octahedra in $[\text{Co}(\text{nta})(\text{en})]\cdot\text{H}_2\text{O}$ and $[\text{Co}(\text{nta})(\text{gly})]^-$ were significantly distorted and that the endocyclic angles of the G rings were much less than the ideal 538.4° . They concluded that it was due to the participation of the unbonded carboxylate oxygen atoms in the formation of intermolecular hydrogen bonds. No mention was made of the angular distortion around the nta nitrogen.

2.2.2 Reactions of cobalt(III)- and chromium(III)-nta and similar complexes

Anation reactions

The fact that nta acts as a tetradentate ligand means that the coordination sphere in an octahedral geometry can be completed by two ligands *cis* with respect to each other. It has already been postulated (refer to Paragraph 2.2.1) that *cis*-aquacobalt(III)- and chromium(III)-nta complexes can be obtained by merely acidifying either the μ -hydroxo dimeric species or the carbonato species.

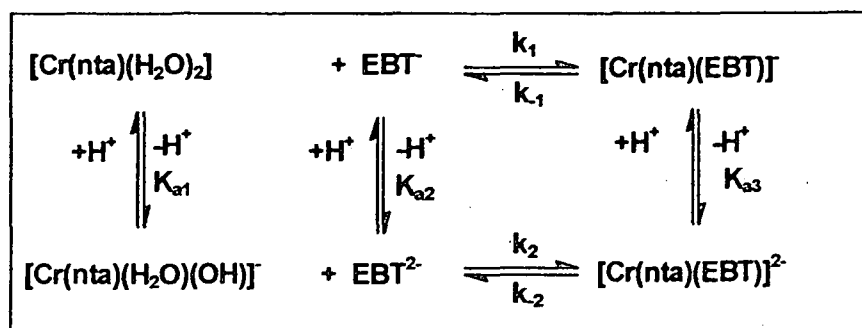
The mechanism of the substitution reactions of Cr(III)- and Co(III)-nta complexes is complicated as will be indicated in the following paragraphs.

The kinetics of the formation and dissociation of $[\text{Cr}(\text{nta})(\text{acac})]^-$ (acac = pentane-2,4-dione) have been investigated, but the complexity of the rate law prevented a full understanding of the mechanism (Bhattacharyya & Banerjee, 1997:4217).

Two kinetic studies investigated the reaction of $[\text{Cr}(\text{nta})(\text{H}_2\text{O})_2]/[\text{Cr}(\text{nta})(\text{H}_2\text{O})(\text{OH})]^-$ with different synthetic dyes, Solochrome Yellow 2G (Hualin & Xu, 1990:137) and

Literature overview

Eriochrome Black T (Visser *et al.*, 1994:1051). The second study also included the reaction with thiocyanate and H^+ ions. Both these studies were complicated by the fact that the dyes have very large extinction coefficients so that the reactions were rather performed with the [metal] in excess. The reaction scheme for the second study is represented in Scheme 2.3.



Scheme 2.3. Reaction scheme for the reaction of $[\text{Cr}(\text{nta})(\text{H}_2\text{O})_2]$ with Eriochrome Black T, EBT.

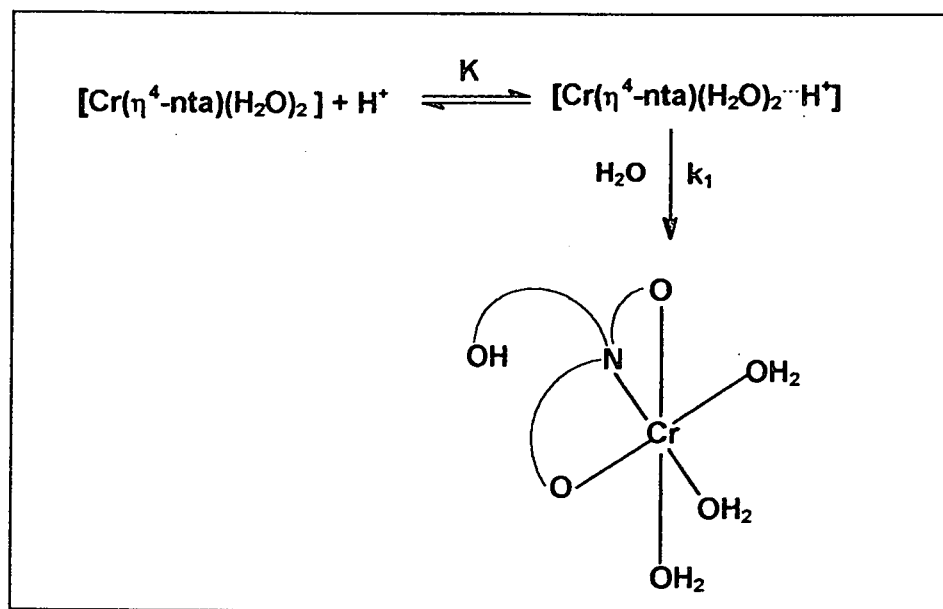
In Scheme 2.3 EBT⁻ is Eriochrome Black T, K_{a1} , K_{a2} and K_{a3} are acid dissociation constants while k_1 , k_2 , k_{-1} and k_{-2} are rate constants. The study of Visser *et al.* (1994:1051) was further complicated by the fact that EBT⁻ has an acid dissociation constant of 6.3 (Vogel, 1989), close to that of $[\text{Cr}(\text{nta})(\text{H}_2\text{O})(\text{OH})]^-$ which has a pK_a value of 5.47. It was also reported in this study that the formation of precipitates at pH 6 and higher complicated the understanding of the mechanism even further.

It was possible however to deduct some information from these studies. The reaction between $[\text{Cr}(\text{nta})(\text{H}_2\text{O})_2]$ and EBT⁻ is about 16 times faster ($9.5 \times 10^{-2} \text{ M}^{-1}\text{s}^{-1}$ at 30 °C) than the corresponding reaction with NCS⁻ ($5.8 \times 10^{-3} \text{ M}^{-1}\text{s}^{-1}$ at 25 °C). This was attributed to the chelation effect of the EBT⁻ ligand during the reaction. Hualin & Xu proposed a different mechanism for the reaction of $[\text{Cr}(\text{nta})(\text{H}_2\text{O})_2]$ with Solochrome Yellow 2G. They suggested a two-step mechanism (ion pair formation) that involved a rapid formation of the monodentate coordinated dye intermediate, followed by the rate-determining ring-closure. The value for the ring-closure step of the reaction of $[\text{Cr}(\text{nta})(\text{H}_2\text{O})_2]$ with this dye was determined as $2.3 \times 10^{-2} \text{ s}^{-1}$.

Both studies found that the electron donating ability of nta improved the reactivity of the chromium(III) complex by several orders of magnitude. The second-order rate constant ($5.8 \times 10^{-3} \text{ M}^{-1} \text{ s}^{-1}$) for the reaction of $[\text{Cr}(\text{nta})(\text{H}_2\text{O})_2]$ with NCS⁻ compares well with the k_1 value of $4.7 \times 10^{-3} \text{ M}^{-1} \text{ s}^{-1}$ which was obtained for the reaction between

$[\text{Cr}(\text{TPPS})(\text{H}_2\text{O})_2]^{3-}$ and NCS^- (Ashley *et al.*, 1980:1608). Porphyrins like TPPS are known to enhance the rate of substitution of inert metal(III) complexes by several orders of magnitude. The main reason for this is believed to be the electron donating ability of the porphyrin, which increases the electron density on the central metal ion, making it react more like the labile metal(II) species.

The reaction of $[\text{Cr}(\text{nta})(\text{H}_2\text{O})_2]$ with H^+ ions (Visser *et al.*, 1994:1051) was also investigated. It was proposed that the mechanism for the reaction involved the formation of an ion pair. Protonation of one of the carboxylate groups of the nta then occurs, which results in the dissociation of this bond to give the aquated tridentate nta complex, $[\text{Cr}(\eta^3\text{-nta})(\text{H}_2\text{O})_3]^+$. A possible reaction scheme is presented in Scheme 2.4.



Scheme 2.4. Formation of $[\text{Cr}(\eta^3\text{-nta})(\text{H}_2\text{O})_3]^+$.

The only available literature on the anation reactions of *cis*- $[\text{Co}(\text{nta})(\text{H}_2\text{O})_2]$ is a study by Thacker and Higginson (1975:704). They studied the redox and substitution reactions of *cis*- $[\text{Co}(\text{nta})(\text{H}_2\text{O})_2]$ with various ligands. They found that only NCS^- ions did not show redox properties in the pH region they investigated (pH = 3 - 5). Unfortunately their experimental results were not very good due to, among other things, interference of the buffer solutions used.

The labilisation effect of nta is further proved by other studies on similar types of ligands. There are a few papers available in the literature on the anation and aquation

Literature overview

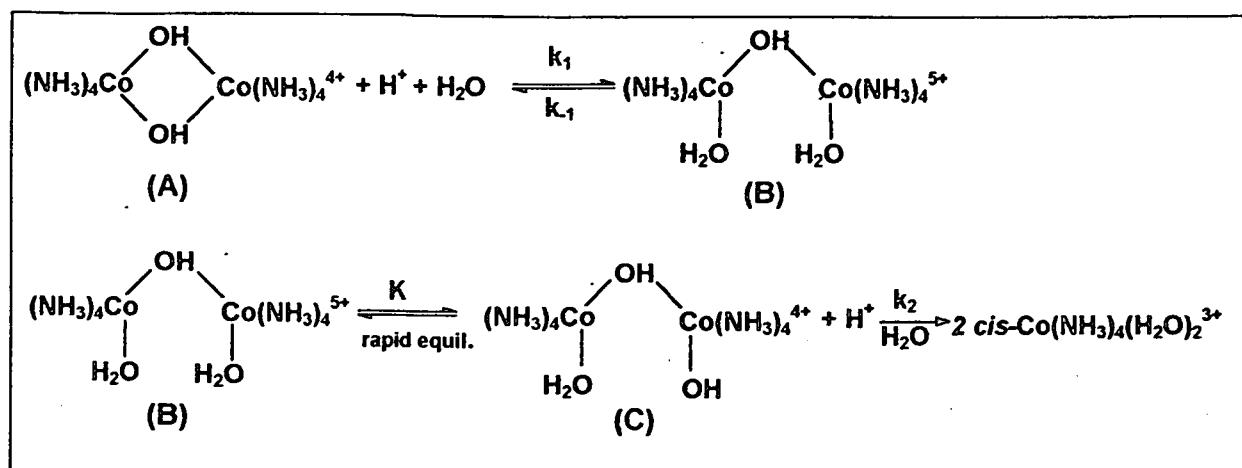
reactions of *cis*-[Co(edda)(X₂)] complexes (X = Cl⁻, H₂O) (Weyh *et al.*, 1973:2374; 1976:2298 and Garnett & Watts, 1974:307). There are also a few reports on the substitution reactions of mono-aqua complexes of chromium(III) where the other five coordination positions are occupied by five-coordinate, edta-type ligands (Ogino *et al.*, 1975:2093 and Sulfab *et al.*, 1976:2388). All these studies prove that these type of ligands (multidentate N, O donors) labilise the metal centre and enhance the rate of substitution by several orders of magnitude.

Bridge cleavage reactions – hydrogen ions

Sykes and Weil (1970) wrote a comprehensive review on the acidic bridge cleavage reactions of binuclear cobalt complexes. Bridging ligands can vary from peroxy, amido, superoxy, phosphato, nitrito, halido, acetato to hydroxo ligands.

It has been suggested that complexes of cobalt and aminopolycarboxylic acids like nta and edta do not appear to combine with O₂ to form peroxy- or superoxy- bridged species. The reason given is that these ligands contain too many oxygenic groups attached to the cobalt, which reduce the readiness with which these complexes form stable adducts with molecular oxygen (Fallab, 1967:496). On the other hand, there are countless examples of hydroxo-bridged species of cobalt complexes.

The stability of di- and tri- μ -hydroxo complexes in aqueous solutions is very much dependent on the hydrogen-ion concentration. Hoffman and Taube (1968:903) studied the kinetics of the reaction of hydrogen ions with [Co(NH₃)₄(μ -OH)]₂⁴⁺. The assigned rate law is shown in Equation 2.1 and the reaction scheme is shown in Scheme 2.5. The value of k_1 was determined as $1.2 \times 10^{-3} \text{ M}^{-1} \text{ s}^{-1}$ at 25.0 °C and $\mu = 1.0 \text{ M}$.



Scheme 2.5. Acidic cleavage of $[\text{Co}(\text{NH}_3)_4(\text{OH})]_2^{4+}$.

$$R = \frac{k_2 k_1 K [\text{H}^+]}{k_2 K + k_{-1}} \quad (2.1)$$

Lee Hin-Fat and Higginson (1971:2589) investigated the hydroxo bridge cleavage of $[\text{Co}(\text{C}_2\text{O}_4)_2(\text{OH})]_2^{4-}$ at pH 3.5 - 4.5. They also found a first-order $[\text{H}^+]$ dependence for this reaction.

The acid-assisted cleavage of the di- μ -hydroxo bridges in $[\text{Co}(\text{en})_2(\text{OH})]_2^{4+}$ was also studied (El-Awady & Hugus, 1971:1415 and DeMaine & Hunt, 1971:2106). The study of Demaine and Hunt suggested the same mechanism as the one proposed for $[\text{Co}(\text{NH}_3)_4(\mu\text{-OH})]_2^{4+}$ (Scheme 2.5).

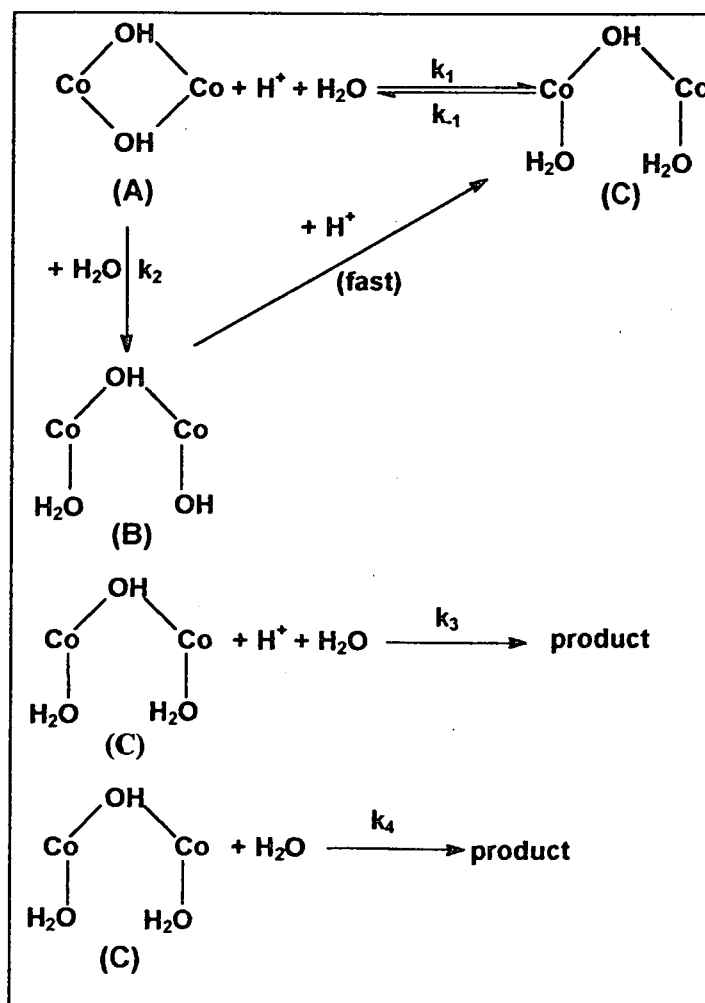
The study of El-Awady and Hugus (1971:1415) proposed two possible mechanisms for this reaction. Both mechanisms included the formation of a single hydroxo-bridged dimeric species as an intermediate. One of the proposed mechanisms involves the protonation of the dimer and the intermediate in a fast reversible step. The second mechanism is very similar to that proposed by Hoffman and Taube (1968:903) (Scheme 2.5). The rate law included a $[\text{H}^+]^2$ dependence in the numerator, which the other studies did not.

Sykes and co-workers (1972:2565) provided a possible solution for the differences in the observed $[\text{H}^+]$ dependence in the above mentioned studies. The rate laws for the acid cleavage of μ -hydroxo-cobalt(III) complexes sometimes involve an acid-

Literature overview

independent term and invariably show an acid dependence for the reaction which varies from simple first-order to a combination of first- and second-order terms. Complexes with a single hydroxo bridge yield a linear dependence between the observed rate constant and the hydrogen ion concentration. Any deviation from such dependence in di- μ -hydroxo bridged complexes must be a function of the second hydroxo bridge. The mechanism that they predicted is shown in Scheme 2.6.

It can be seen from Scheme 2.6 that a k_2 pathway was ignored. The reason given for this is that the intermediate, (B) in this scheme, can partially rotate and form hydrogen bonds with another intermediate complex or the dimer, especially through the OH⁻ ligand. It was further concluded that k_2 will only make a contribution at very small [H⁺] values.



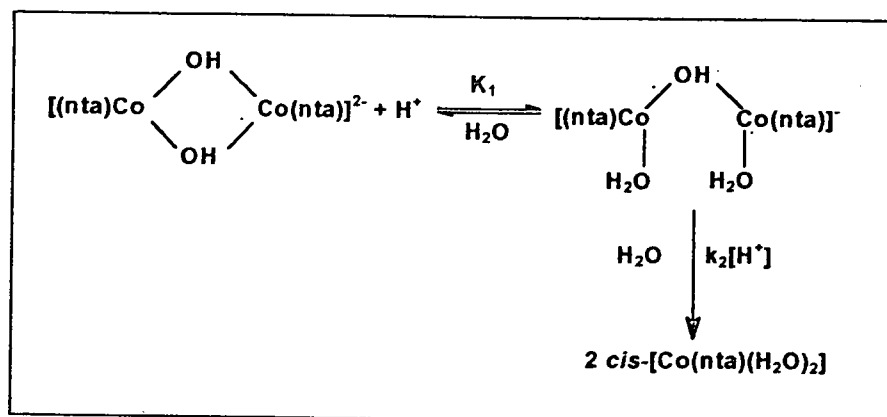
Scheme 2.6. Acidic cleavage of a di- μ -hydroxo cobalt(III) complex.

The pseudo-first-order rate constant, k_{obs} , is given in Equation 2.2.

$$k_{\text{obs}} = \frac{k_2 k_4 + (k_2 k_3 + k_1 k_4)[\text{H}^+] + k_1 k_3 [\text{H}^+]^2}{k_{-1} + k_4 + k_3 [\text{H}^+]} \quad (2.2)$$

The acidic cleavage of the hydroxo bridges of $[\text{Co}(\text{nta})(\mu\text{-OH})]_2^{2-}$ have been investigated by other workers (Thacker & Higginson, 1975:704 and Meloon & Harris, 1977:434). Both these studies observed a fast initial reaction followed by a second slower reaction upon allowing $[\text{Co}(\text{nta})(\mu\text{-OH})]_2^{2-}$ to stand in moderately acidic solutions for 20 – 30 minutes. It was observed that aqueous solutions of $[\text{Co}(\text{nta})(\mu\text{-OH})]_2^{2-}$ did not show any evidence of normal acidic or basic properties when titrated rapidly with dilute acid and back-titrated with base.

It was postulated that these two reactions involved the formation of a mono-hydroxobridged species which dissociates to form *cis*- $[\text{Co}(\text{nta})(\text{H}_2\text{O})_2]$ in the second, slower step (Scheme 2.7).



Scheme 2.7. Acidic cleavage of $[\text{Co}(\text{nta})(\mu\text{-OH})]_2^{2-}$.

The rate law that was proposed for this reaction is illustrated in Equation 2.3.

$$k_{\text{obs}} = \frac{k_2 K [\text{H}^+]^2}{1 + K [\text{H}^+]} \quad (2.3)$$

The values for K and k_2 at 25 °C in Equation 2.3 were determined as 43(3) M^{-1} and 17(1) $\text{M}^{-1} \text{s}^{-1}$ respectively (Meloon & Harris, 1977:434).

Literature overview

Thacker and Higginson also calculated the acid dissociation constant ($pK_a = 6.71(1)$) for the formation of $cis-[Co(nta)(H_2O)(OH)]^-$ from $cis-[Co(nta)(H_2O)_2]$. It was mentioned that $cis-[Co(nta)(H_2O)(OH)]^-$ was not very stable in solution.

Koine *et al.* (1986:2835) showed with 2H NMR that an intermediate species is formed upon acidification of $[Cr_2(nta)_2(OH)_2]^{2-}$. They concluded that the intermediate might also be a mono-hydroxo bridged species. Other observers also support this assumption (Toftlund & Springborg, 1976:1017 and Grant & Hamm, 1958:4166).

The study of the kinetics of the acid cleavage of $[(phen)_2Cr(\mu-OH)]_2^{4+}$ (Wolcott & Hunt, 1968:755) showed different mechanistic results than the previously mentioned studies. It was proposed that proton-transfer reactions in aqueous solutions are far too rapid for the acid dependence of the cleavage rate to be explained in terms of a rate-determining addition of a proton to the dimer. They suggested that the first-order dependence of the cleavage rate on $[H^+]$ is due to a rapid acid-base reaction preceding the rate determining step and involving the addition of a proton to the dimer.

It can be seen from the previous paragraphs that one can readily derive an expression corresponding to any of the observed mechanisms for related cobalt(III) complexes by making the appropriate assumptions concerning the magnitude of the various constants and that different workers suggest different types of mechanisms for bridge cleavage reactions. There is also very little literature available on these kinds of reactions, making the investigation of these reactions very interesting.

Bridge cleavage reactions – hydroxide ions

Very little work has been done on bridge cleavage reactions of di- μ -hydroxo bridged cobalt(III) and chromium(III) complexes. El-Awady and Hugus (1971:1415) investigated the reaction between $[Co(en)_2(OH)]_2^{4+}$ and OH^- ions and predicted a mechanism similar to those discussed for the acidic cleavage of this complex. It was also mentioned that they were not very satisfied with their experimental data.

Sadler and Dasgupta (1987:3254 and 1987:185) investigated the carbon dioxide uptake of different tri- μ -hydroxo bridged cobalt(III) complexes. They observed that OH^- ions first split one of the hydroxo bridges, forming the intermediate (A) in Figure 2.5. One of the non-bridging hydroxide ions in intermediate (A) reacts with CO_2 in the rate

determining step to form intermediate (B) which quickly undergoes ring-closure to form the final product, (C).

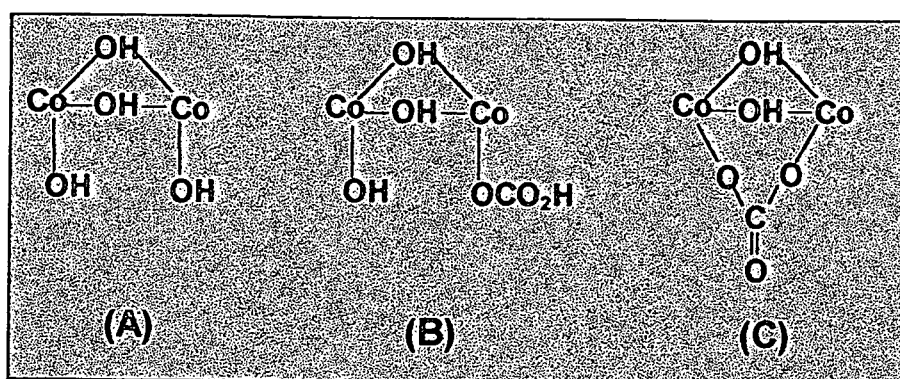


Figure 2.5. Different intermediates and final product in CO₂ uptake reactions.

Decarboxylation reactions of bidentate carbonato cobalt(III)-nta and other complexes

The general mechanism of decarboxylation reactions of bidentate carbonato cobalt(III) complexes has been well investigated (Dasgupta & Harris, 1974:1275, Garnett & Watts, 1974:313 and Van Eldik *et al.*, 1983:149). These carbonato complexes undergo aquation *via* a mechanism consisting of ring opening of the chelated carbonato group catalysed both by water (k_2 pathway in Scheme 2.8) and hydronium ion (k_1 pathway in Scheme 2.8). This is followed by rapid decarboxylation of the monodentate intermediate.

The corresponding rate law for the above reaction at pH = 2 and higher is given by Equation 2.4.

$$k_{obs} = k_2 + k_1[H^+] \tag{2.4}$$

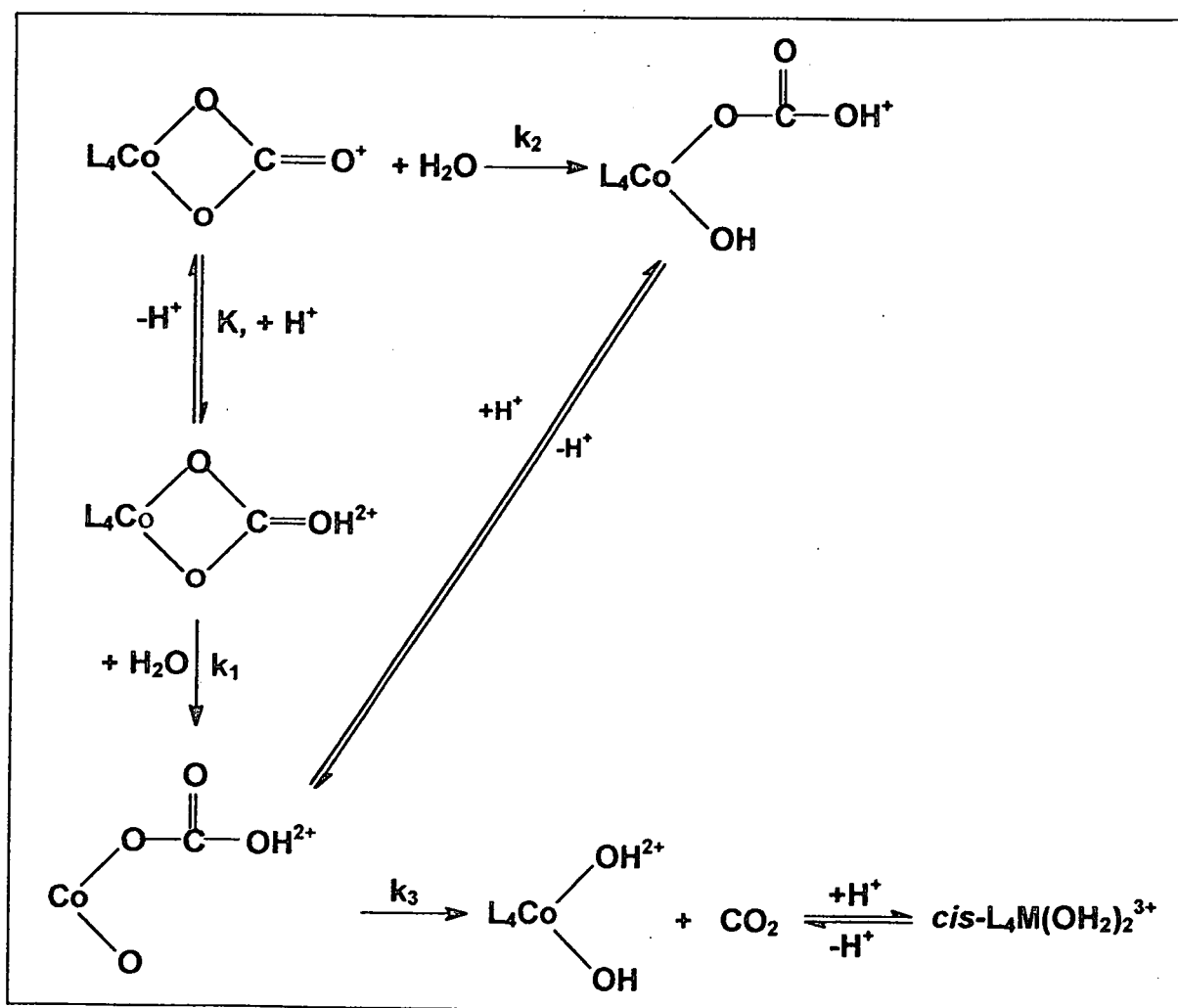
Under conditions where the $[H^+]$ is very high, the contribution of the water catalysed pathway to the rate of the reaction becomes small enough to be omitted from the rate law. The rate law for acid-catalysed aquation of bidentate carbonato complexes then becomes,

$$k_{obs} = \frac{k_1 K [H^+]}{1 + K_1 [H^+]} \tag{2.5}$$

which in general simplifies to Equation 2.6 since K_1 is usually very small.

$$k_{\text{obs}} = k_1 K [\text{H}^+] \quad (2.6)$$

It was found for a number of systems (Dasgupta & Harris, 1971:91; 1974:1275, Van Eldik *et al.*, 1975:2573 and Harris & Hyde, 1978:1892) that a limiting value for k_{obs} is reached at high $[\text{H}^+]$. This was attributed to the situation where the ring opening rate ($k_1 K_1 [\text{H}^+]$) had been increased to such an extent that decarboxylation (k_3), which is independent of $[\text{H}^+]$, became rate determining.



Scheme 2.8. Decarboxylation reactions of bidentate cationic carbonato tetramine complexes of cobalt(III).

Dasgupta and Harris (1974:1275) investigated the aquation of $[\text{Co}(\text{nta})(\text{CO}_3)]^{2-}$ and found that the acid-catalysed path dominates the aquation rate at pH levels below 2. At higher pH the water catalysed path contributes significantly so that k_{obs} becomes the sum of two rate constants (refer to Equation 2.4). At 25 °C the water-catalysed rate

constant, k_2 , for the ring opening of $[\text{Co}(\text{nta})(\text{CO}_3)]^{2-}$ was calculated as $3.0(8) \times 10^{-3} \text{ s}^{-1}$, compared to $41.9(8) \text{ M}^{-1}\text{s}^{-1}$ for the rate constant of the acid catalysed ring opening reaction, k_1 . The rate constant for the decarboxylation reaction, k_3 , was calculated as $57(3) \text{ s}^{-1}$ at 25°C .

A comparison of the above data with that found for $[\text{Co}(\text{tren})(\text{CO}_3)]^+$ (Dasgupta & Harris, 1971:91) showed that the acid catalysed pathway, k_1 , for $[\text{Co}(\text{nta})(\text{CO}_3)]^{2-}$ is about 20 times faster and that the water catalysed path, k_2 , is about 10 times faster than for $[\text{Co}(\text{tren})(\text{CO}_3)]^+$. The reason for this is that the negatively charged nta complex will interact more favourably with the positively charged hydronium ion than $[\text{Co}(\text{tren})(\text{CO}_3)]^+$.

The rate of decarboxylation, k_3 , of $[\text{Co}(\text{nta})(\text{CO}_3)]^{2-}$ is also almost 50 times faster than what was found for the corresponding penta-amine complex (Palmer & Harris, 1974:965) and in the same order for $[\text{Co}(\text{edda})(\text{CO}_3)]$ (calculated as $83 \text{ M}^{-1}\text{s}^{-1}$), further supporting the assumption that negatively charged carbonato complexes will interact more favourably with hydronium ions (Van Eldik *et al.*, 1975:2573). Furthermore, it is proposed that the electron donating ability of ligands like nta and edda, decreases the positive charge on the central metal atom, thereby increasing the basicity of the bonded oxygen of the carboxylate. This increased basicity facilitates H bonding which will in turn weaken the $\text{C}-\text{O}_{\text{bonded}}$ bond.

2.3 Conclusion

It can be seen from this chapter that there are many questions surrounding the chemistry of cobalt(III)- and chromium(III)-nta complexes. The isolation and characterisation of new nta complexes by way of especially NMR and X-ray crystallography will bring more light to the understanding of the strain in these complexes. Although several kinetic studies have been undertaken, very few have been able to isolate starting complexes, intermediates or final products. The isolation of the above mentioned complexes will provide a lot of information on the mechanism of the substitution reactions of these complexes. The mechanism of bridge-cleavage reactions at higher pH are also not well understood, while the decarboxylation studies of

Literature overview

$[\text{Co}(\text{nta})(\text{CO}_3)]^{2-}$ have been well investigated. Lastly, it was shown that nta complexes have significant relevance as biological model complexes and that further studies on these complexes could provide important information on the behaviour of living systems in the presence of transition metals.

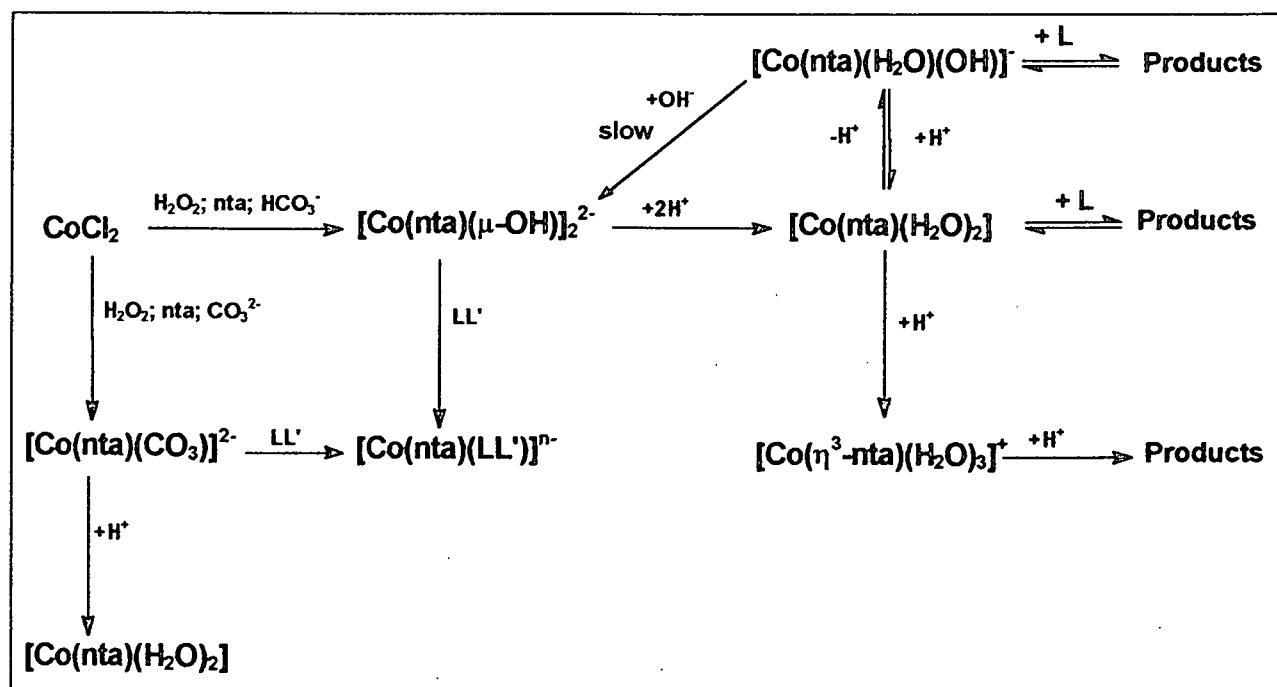
3

Synthesis and identification of different complexes

3.1 Introduction

It has been shown in the previous chapters that the syntheses and identification of cobalt(III)- and chromium(III)-nta complexes have not yet been conclusively documented. The identification of starting complexes and final products in kinetic studies is vital to the determination of the mechanism of these reactions. This chapter deals mainly with the synthesis of different Co(III)- and Cr(III)-nta complexes. The characterisation of these complexes with IR-, UV/VIS- and ^1H NMR spectroscopy is also discussed in this chapter while the identification with X-ray crystallography will be discussed in detail in the next chapter.

Scheme 3.1 provides an illustration of the complex cobalt(III)-nta system in solution which was investigated in this study.



Scheme 3.1. Synthesis and reactions of $[\text{Co}(\text{nta})(\mu\text{-OH})]_2^{2-}$.

It is important to note that LL' in Scheme 3.1 represents both different monodentate ligands like pyridine and dimethylaminopyridine as well as bidentate ligands like ethylenediamine.

Most of the previous studies on nta complexes (Chapter 2) relied heavily on identification with IR and UV/VIS. The identification of this type of complexes by IR is complicated. It has been shown that the oxygen atoms of the carboxyl groups which are not bonded to the metal are hydrogen-bonded, either to the amino group of the neighbouring molecule, or to the water of crystallisation, or weakly bonded to the metal of a neighbouring complex (Nakamoto, 1963:206). Therefore the COO stretching frequencies of nta complexes and related compounds are affected by coordination as well as by intermolecular interaction. According to previous studies COO groups have peaks at 1650-1620 cm^{-1} when coordinated to metals such as Cr(III) and Co(III), (Bush & Bailar, 1953:4574 and 1956:716).

^1H NMR data can also provide important structural information, especially by investigating the signals of the acetate ring protons of nta (refer to Paragraph 2.2.1). This chapter includes very interesting results with regards to this subject.

Previous workers found it difficult to prepare and identify cobalt(III)-nta complexes from the complexes prepared by Mori *et al.* (1958:940). It was therefore our aim to also find a new synthetic route for preparing Co(III)-nta complexes. This has been achieved with the synthesis of $[\text{Co}(\text{nta})(\text{CO}_3)]^{2-}$ in a pure form (Paragraph 4.4.2), which has been used as starting material in some cases.

3.2 Apparatus and Chemicals

Unless otherwise stated, all reagents were of reagent grade. UV/VIS measurements were performed on a Cary 50 (Conc) and a GBC UV/VIS 916 spectrophotometer equipped with constant temperature cell holders (accuracy within 0.1 $^{\circ}\text{C}$), while infrared spectra were recorded on a Hitachi 270-50 instrument in KBr discs in the range 4000 – 250 cm^{-1} (s = strong; sh = shoulder, w = weak). Elemental analysis was done by the Canadian Microanalytical Service Ltd. ^1H NMR spectra were recorded on a 300 MHz

Bruker spectrometer (s = singlet, d = doublet, m = multiplet, t = triplet).

3.3 Synthesis

3.3.1 $\text{Cs}_2[\text{Co}(\text{nta})(\mu\text{-OH})]_2 \cdot 4\text{H}_2\text{O}$ (Visser et al., 1997:2851)

The $\text{Cs}_2[\text{Co}(\text{nta})(\mu\text{-OH})]_2 \cdot 4\text{H}_2\text{O}$ complex was prepared similar to the method described by Mori *et al.* (1958:940) for the preparation of $\alpha\text{-K}[\text{Co}(\text{nta})(\text{H}_2\text{O})(\text{OH})] \cdot 2\text{H}_2\text{O}$. $\text{CoCl}_2 \cdot 6\text{H}_2\text{O}$ (5 g, 21 mmol) and nitrilotriacetic acid (4 g, 21 mmol) was added to a KHCO_3 solution (25 cm³, 2.5 M). H_2O_2 (1 cm³, 30 %) was added to this solution and the mixture was placed on an ice bath. After ca 5 h a blue precipitate separated out. The precipitate was filtered and washed several times with cold water. The product was then redissolved in hot water after which an excess of CsCl was added. The blue/purple $\text{Cs}_2[\text{Co}(\text{nta})(\mu\text{-OH})]_2 \cdot 4\text{H}_2\text{O}$ crystals, suitable for X-ray data collection, were obtained after 24 h (Chapter 4, Paragraph 4.4.1).

IR ($\nu_{\text{COO-Co}}(\text{cm}^{-1})$): 1644 (sh), 1618 (s).

UV/VIS: λ_{max} , 216 (sh), 303 (w), 226 nm, ϵ_{226} , $1.55 \times 10^4 \text{ M}^{-1} \text{ cm}^{-1}$, 406 nm, ϵ_{406} , 302(3) $\text{M}^{-1} \text{ cm}^{-1}$, 547 nm, ϵ_{547} , 191(4) $\text{M}^{-1} \text{ cm}^{-1}$.

¹H NMR (D_2O): ¹H NMR (D_2O): δ 3.82 (2H d. J 16.6 Hz), 3.91 (2H s.), 4.52 (2H d. J 16.6 Hz).

3.3.2 $\text{Cs}_2[\text{Co}(\text{nta})(\text{CO}_3)] \cdot \text{H}_2\text{O}$ (Visser et al., 2000b)

Nitrilotriacetic acid (4 g) was dissolved in 30 cm³ of H_2O by adding Cs_2CO_3 until all the acid was dissolved. $\text{CoCl}_2 \cdot 6\text{H}_2\text{O}$ (5 g) was dissolved in a minimum of H_2O and added to the nta solution. 30 % H_2O_2 (1 cm³) was added and the pH of the solution was adjusted to 7 with Cs_2CO_3 . The mixture was placed on an ice bath and purple crystals, suitable for X-ray diffraction data collection, were obtained after ca 24 hours (Paragraph 4.4.2).

IR ($\nu_{\text{COO-Co}}(\text{cm}^{-1})$): 1620 (s).

UV/VIS: λ_{max} , 215 nm, ϵ_{215} , $4.78 \times 10^4 \text{ M}^{-1} \text{ cm}^{-1}$, 294 nm (sh), 384 nm, ϵ_{384} , 178(4) $\text{M}^{-1} \text{ cm}^{-1}$, 565 nm, ϵ_{565} , 135(3) $\text{M}^{-1} \text{ cm}^{-1}$.

¹H NMR (D_2O): δ 3.99 (2H s.), 4.06 (2H d. J 16.7 Hz.), 4.42 (2H d. J 16.7 Hz.).

3.3.3 $K_2[Co(nta)(ox)].xH_2O$

Crystals of $Cs_2[Co(nta)(CO_3)].H_2O$ (0.5 g) were dissolved in water (20 cm³) and an equimolar amount of $K_2C_2O_4$ was added to the solution. The mixture was placed on a water bath for two hours after which the reddish violet solution was cooled. About 15 ml of ethanol was added to precipitate the product. The IR spectrum indicated the presence of H_2O in the crystal lattice (reason for $.xH_2O$) but the number of water molecules per mole was not determined experimentally.

IR ($\nu_{COO-Co}(cm^{-1})$): 1623 (s).

UV/VIS: λ_{max} , 235 nm, ϵ_{235} , $2.22(4) \times 10^4 M^{-1} cm^{-1}$, 384 nm, ϵ_{384} , $190(4) M^{-1} cm^{-1}$, 554 nm, ϵ_{554} , $197(5) M^{-1} cm^{-1}$.

¹H NMR (D_2O): δ 3.88 (2H d. J 16.7 Hz.), 4.02 (2H s.), 4.42 (2H d. J 16.7 Hz.).

3.3.4 $Ba[Co(nta)(l-leu)]_2.xH_2O$ (Visser et al., 2000b)

Crystals of $Cs_2[Co(nta)(CO_3)].H_2O$ (0.5 g) were dissolved in water (20 cm³) and an equimolar amount of *l*-leucin was added to the solution. The mixture was placed on a water bath for two hours after which the reddish solution was dried under vacuum. The product was redissolved in water (20 cm³) and the required amount $BaCl_2$ was added to the solution. After several days, red crystals separated out. Unfortunately these crystals were multiply twinned and not suitable for X-ray data collection. Also, due to impurities (possibly Co(II) residues) ¹H NMR spectra could not be obtained for identification purposes. The IR spectrum indicated the presence of H_2O in the crystal lattice (reason for $.xH_2O$) but the number of water molecules per mole was not determined experimentally.

IR ($\nu_{COO-Co}(cm^{-1})$): 1632(s).

UV/VIS: λ_{max} , 370 nm, ϵ_{370} , $166(3) M^{-1} cm^{-1}$, 525 nm, ϵ_{525} , $185(3) M^{-1} cm^{-1}$.

3.3.5 $Cs[Co(nta)(l-val)].xH_2O$ (Visser et al., 2000b)

Crystals of $Cs_2[Co(nta)(CO_3)].H_2O$ (0.5 g) were dissolved in water (20 cm³) and an equimolar amount of *l*-valine was added to the solution. The mixture was placed on a water bath for two hours after which the reddish solution was dried under vacuum. The red powder was redissolved in a minimum amount of water and left to stand. The

crystals obtained were not suitable for X-ray diffraction data collection. The IR spectrum indicated the presence of H₂O in the crystal lattice (reason for $\cdot x\text{H}_2\text{O}$) but the number of water molecules per mole was not determined experimentally.

IR ($\nu_{\text{COO-Co}}(\text{cm}^{-1})$): 1638(s).

UV/VIS: λ_{max} , 374 nm, ϵ_{374} , 178(5) M⁻¹ cm⁻¹, 519 nm, ϵ_{519} , 195(5) M⁻¹ cm⁻¹.

¹H NMR (D₂O): δ 0.64 (3H d. J 6.67 Hz), 1.10 (3H d. J 6.67 Hz.), 1.97-2.10 (2H m.), 4.02-4.10 (4H m.), 4.37 (1H d. J 5.55 Hz), 4.42 (1H d. J 5.55 Hz).

3.3.6 [Co(nta)(N,N-Et₂en)] (Visser et al., 2000a)

Cs₂[Co(nta)(μ -OH)]₂·4H₂O (0.5 g) was dissolved in water (30 cm³) and an equimolar amount of *N,N*-diethylethylenediamine was added in a dropwise manner. The pH of the solution was adjusted to 10.5 with concentrated HCl and the mixture was allowed to react on a water bath at 70 °C. After ca 20 minutes the colour of the solution changed from deep purple to red. The solution was dried under vacuum, the solid was redissolved in water (15 cm³) and allowed to stand. Red needle-like crystals, suitable for X-ray diffraction data collection, crystallised overnight. The same result was achieved by using Cs₂[Co(nta)(CO₃)]·H₂O as starting material (Paragraph 4.4.3).

IR ($\nu_{\text{COO-Co}}(\text{cm}^{-1})$): 1617(s).

UV/VIS: λ_{max} 232.1 nm (sh), 539.0 nm, $\epsilon_{539.0}$, 73.6(4) × 10¹ M⁻¹ cm⁻¹.

¹H NMR (D₂O): δ 1.06 (6H t. J 9.4 Hz.), 2.38-2.49 (2H m.), 2.54 (2H t. J 9.4 Hz.), 2.70 (2H t. J 9.4 Hz.), 3.24 (2H m.), 3.87 (2H d. J 16.7 Hz.), 3.99 (2H s.), 4.15 (2H d. J 16.7 Hz).

3.3.7 [Co(nta)(N-Eten)] (Visser et al., 2000a)

Crystals of [Co(nta)(N-Eten)] was prepared in the exact same manner as [Co(nta)(N,N-Et₂en)]. Unfortunately the red crystals obtained were not suitable for X-ray diffraction data collection.

IR ($\nu_{\text{COO-Co}}(\text{cm}^{-1})$): 1623 (s).

UV/VIS: λ_{max} 227.0 nm, $\epsilon_{227.0}$, 3.98(6) × 10³ M⁻¹ cm⁻¹, 539.9 nm, $\epsilon_{539.9}$, 63.0(7) M⁻¹ cm⁻¹,

¹H NMR (D₂O): δ 1.29 (3H t. J 8.3 Hz.), 2.21-2.30 (1H m.), 2.43-2.76 (3H m.), 2.94-3.01 (1H m.), 3.20-3.33 (1H m.), 3.97-4.08 (4H m.), 4.19 (1H d. J 16.7 Hz), 4.29 (1H d. J 16.7 Hz).

3.3.8 [Co(nta)(dmap)₂].6H₂O (Visser et al., 2000a)

Crystals of [Co(nta)(dmap)₂] (dmap = dimethylaminopyridine) were prepared similar to the method used for the synthesis of [Co(nta)(N,N-Et₂en)]. Unfortunately the red crystals obtained were excessively twinned and therefore not suitable for X-ray diffraction data collection.

[Co(nta)(dmap)₂].6H₂O (Found: Co, 9.2; N, 12.12 calcd.: Co, 9.46; N, 12.23 %)

IR ($\nu_{\text{COO-Co}}$ (cm⁻¹)): 1616 (s).

UV/VIS: λ_{max} 209.9 nm (sh), 272.1 nm, $\epsilon_{272.1}$, 6.31(4) × 10³ M⁻¹ cm⁻¹, 514.9 nm, $\epsilon_{514.9}$, 79.4(3) M⁻¹ cm⁻¹.

¹H NMR (D₂O): δ 2.89 (6H s.), 2.95 (6H s.), 4.02 (2H d. *J* 16.0 Hz.), 4.14 (2H d. *J* 16.0 Hz.), 4.21 (2H s.), 6.55 (2H d. *J* 8.0 Hz.), 6.65 (2H d. *J* 8.0 Hz.), 7.09 (2H d. *J* 7.0 Hz), 7.62 (2H d. *J* 7.0 Hz).

3.3.9 (NEt₄)₂[Co(nta)(NCS)₂].xH₂O

Cs₂[Co(nta)(μ -OH)]₂.4H₂O (0.075 g) was dissolved in water (10 cm³) and the pH of the solution was adjusted to 2.0. The correct amount of thiocyanate was added and the solution was stirred on a waterbath for 10 minutes after which an excess of Et₄NCl (tetraethylammonium chloride) was added. A blue precipitate formed immediately and was filtered off and dried in vacuum.

IR ($\nu_{\text{COO-Co}}$ (cm⁻¹)): 1635 (s).

IR ($\nu_{\text{NCS-Co}}$ (cm⁻¹)): 2064 (s).

UV/VIS: λ_{max} , 340.0 nm, ϵ_{340} , 160(6) M⁻¹ cm⁻¹; λ_{max} , 565.0 nm, $\epsilon_{565.0}$, 65(6) M⁻¹ cm⁻¹.

3.3.10 Cs₂[Cr(nta)(μ -OH)]₂.4H₂O (I_{4/a}) – (I) (Visser et al., 1999:2795)

The method proposed by Uehara *et al.* (1967:2317) did not give satisfactory results as a mixture of reaction products were isolated. Therefore it was decided to use a slight variation to their method for the preparation of (I). Cr(OH)₃ was prepared by dissolving 10 g chromium alum in 30 cm³ of H₂O and adding 3 cm³ of NH₃ (25 % m/m) in a dropwise manner. The blue-green precipitate was separated from the solution on a centrifuge. Nitrilotriacetic acid (4 g) and the freshly prepared Cr(OH)₃ was added together in 60 cm³ of H₂O and the mixed solution was evaporated to almost dryness on

a water bath. The residue was dissolved in 30 cm³ of warm H₂O and filtered. The pH of the purple filtrate was adjusted with solid Cs₂CO₃ to 5.5 and allowed to stand for several days. The crystals that formed after several days were recrystallised in H₂O. Dark purple prisms suitable for X-ray structure determination (Paragraph 4.3.1) were obtained after several days.

IR ($\nu_{\text{COO-Co}}(\text{cm}^{-1})$): 1635 (s).

UV/VIS: λ_{max} , 409.1 nm, $\epsilon_{409.1}$, 187(8) M⁻¹ cm⁻¹; λ_{max} , 584.0 nm, $\epsilon_{584.0}$, 150(6) M⁻¹ cm⁻¹.

3.3.11 Cs₂[Cr(nta)(μ -OH)]₂.4H₂O (P2₁/c) – (II) (Visser *et al.*, 1999:2795)

The complex was prepared in the same way as (I) except that the pH of the final solution was adjusted to 7 instead of 5.5 as before. Dark purple cube-like crystals, suitable for X-ray structure determination, were obtained after several days. The IR and UV/VIS spectra of this complex are exactly similar to those of (I).

3.4 Results and Discussion

3.4.1 UV/VIS spectral studies

3.4.1.1 Effect of pH on different Co(III)-nta species in solution (Visser *et al.* 1997:2851)

The Cs₂[Co(nta)(μ -OH)]₂.4H₂O crystals were dissolved in water and the UV/VIS spectrum was recorded (216 (sh), 226 (s) and 303 (w)). These results are identical to the complex described by Mori *et al.* (1958:940) as α -[Co(nta)(H₂O)(OH)]⁻. Close inspection of Mori's work reveals that results from a chemical analysis of different Co-nta complexes (α -[Co(nta)(H₂O)(OH)]⁻, β -[Co(nta)(H₂O)(OH)]⁻ and [Co(nta)(μ -OH)]₂²⁻) were almost identical, thereby raising more uncertainty around their findings.

Cs₂[Co(nta)(μ -OH)]₂.4H₂O crystals were dissolved in water (pH ca 6) and the UV/VIS spectrum recorded in order to get a better understanding of the structure of the complexes first prepared by Mori *et al.* (1958:940). NaHCO₃ was added to the solution (pH ca 7) and again the spectrum was recorded. No change in absorption maxima at

Synthesis

226 and 303 nm was observed. A fresh solution of this complex was again prepared and its spectrum recorded, (1) in Figure 3.1. A few drops of 1.0 M HCl were added to this solution (pH ca 1) and the spectrum immediately changed with the disappearance of the peak at 303 nm (2). The [Cl⁻] was low (refer also to Table 5.1, Paragraph 5.3.1.2) so that possibility that the newly formed species could be an aqua-chloro-Co(III) complex is excluded with confidence. The addition of base to this solution (pH ca 7) resulted in the immediate change of the spectrum with an absorption maximum at 236 nm (3). After addition of acid to this solution (pH ca 1) the spectrum changed back to the original spectrum at low pH (2). These results clearly point to a stable [Co(nta)(μ-OH)]₂²⁻ complex in slightly alkaline solution, which when protonated, immediately forms the *cis*-di-aqua complex. Addition of base forms the aquahydroxo complex. This protonation reaction is reversible, see Equation 3.1. It was also observed that the aquahydroxo complex changed back to the dimer at pH 6 – 7 upon standing for several days.

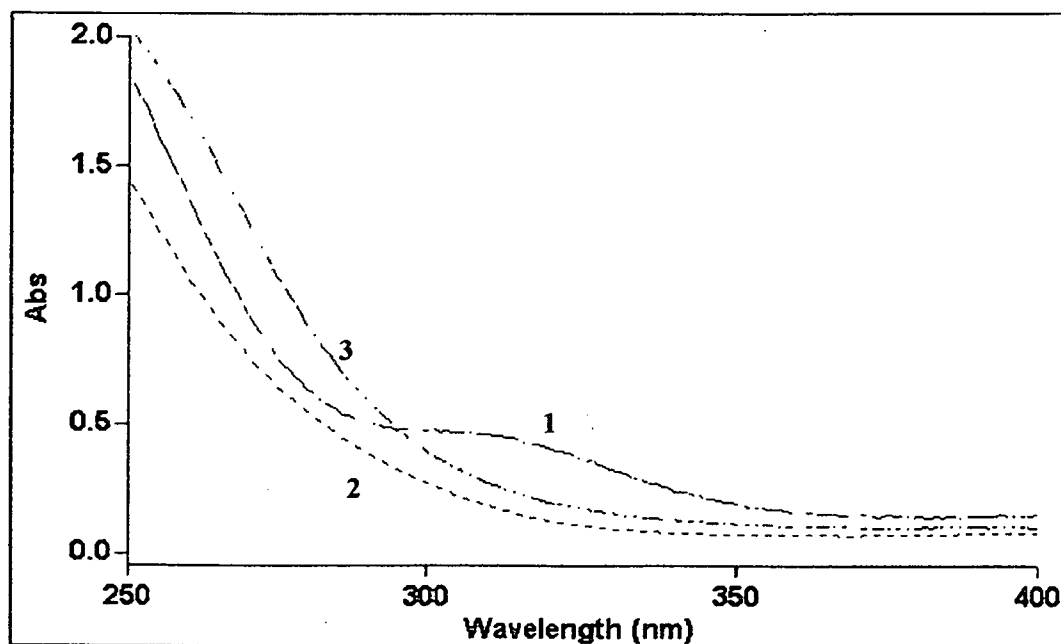
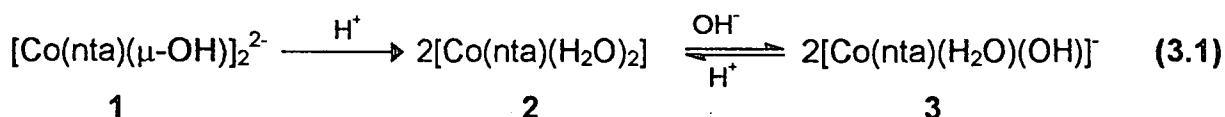


Figure 3.1. UV/VIS spectra of different Co(III)-nta species in solution.

1 [Co(nta)(μ-OH)]₂²⁻, pH 5 - 7; 2 [Co(nta)(H₂O)₂], pH~1; 3 [Co(nta)(H₂O)(OH)]⁻, pH 5 - 7.

These results together with the crystallographic results presented in the next chapter confirm the results of Smith and Sawyer (1968:923) who observed that

" α -[Co(nta)(H₂O)(OH)]²⁻" is possibly a dimer (see paragraph 2.2.1) at pH 6, which forms a diaqua Co(III)-nta species at low pH.

3.4.1.2 Substitution reactions of [Co(nta)(μ -OH)]₂²⁻

Very little is known about the mechanism of the substitution (bridge cleavage) reactions of dimeric complexes at pH > 7 (Paragraph 2.2.2). It was observed that [Co(nta)(μ -OH)]₂²⁻ reacts with different ligands (e.g. pyridine, ethylenediamine etc.) at high pH to give similar products to that isolated for the reactions of [Co(nta)(CO₃)]²⁻ with these ligands (Scheme 3.1). These reactions will be discussed in detail in Chapter 6.

3.4.1.3 Reactions of [Co(nta)(CO₃)]²⁻ (Visser et al., 2000b)

The UV/VIS spectrum (1) of an aqueous solution of Cs₂[Co(nta)(CO₃)]·H₂O was recorded. The complex gives an absorption maximum at 570 nm. The addition of *N,N*-diethylethylenediamine results in the shift of the absorption maximum to 540 nm, (Figure 3.2). Two isosbestic points are also observed at 482 and 561 nm respectively. The absorption maximum correlates well with the absorption maximum of [Co(nta)(*N,N*-Et₂en)] (539 nm) that was obtained for the reaction between [Co(nta)(μ -OH)]₂²⁻ and *N,N*-diethylethylenediamine (Paragraph 3.3.6).

The ¹H NMR data for the product isolated for the reaction of [Co(nta)(CO₃)]²⁻ with *N,N*-diethylethylenediamine is similar to the product isolated for the reaction between *N,N*-diethylethylenediamine and [Co(nta)(μ -OH)]₂²⁻. These results indicate that [Co(nta)(CO₃)]²⁻ can successfully be used as starting material in the synthesis of different Co(III)-nta complexes.

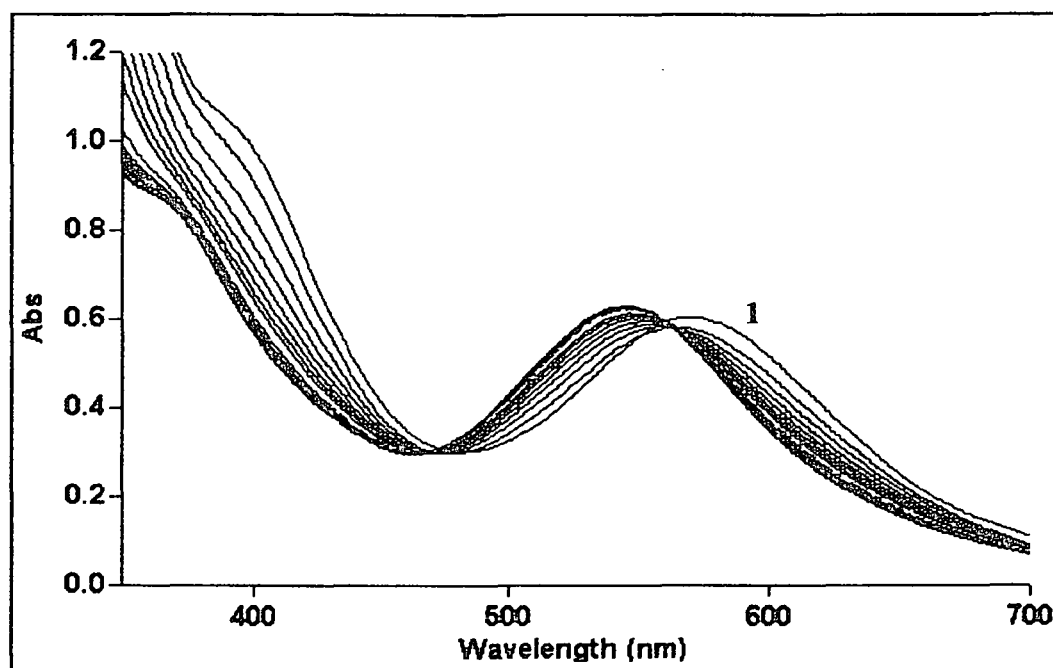


Figure 3.2. Spectral change of $[\text{Co}(\text{нта})(\text{CO}_3)]^{2-}$ (1) on addition of *N,N*-diethylethylenediamine.

3.4.1.4 Effect of pH on different Cr(III)-нта species in solution (Visser *et al.*, 1999:2795)

The crystals of the complexes prepared in 3.3.10 and 3.3.11 (I and II) were dissolved in H_2O and the UV/VIS spectra were recorded. The spectra of both complexes are exactly the same in solution with absorption maxima at 409.1 and 584.0 nm (Figure 3.3). This agrees well with the values of 409 and 585 nm obtained by Koine *et al.* (1986:2835) for $[\text{Cr}(\text{нта})(\mu\text{-OH})]_2^{2-}$ and 408 and 585 nm for the complexes that were isolated by Uehara *et al.* (1967:2317). The IR spectra of both I and II are identical and consistent with that found by Uehara for $\text{NH}_4[\text{Cr}(\text{OH})(\text{нта})(\text{H}_2\text{O})] \cdot 2\text{H}_2\text{O}$ and $\text{NH}_4[\text{Cr}(\text{OH})(\text{нта})(\text{H}_2\text{O})_2] \cdot 3\text{H}_2\text{O}$ (COO-Cr stretching $1658 - 1613 \text{ cm}^{-1}$).

$\text{Cs}_2[\text{Cr}(\text{нта})(\mu\text{-OH})]_2 \cdot 4\text{H}_2\text{O}$ crystals were dissolved in water (pH ca 6) and the UV/VIS spectrum recorded. NaHCO_3 was added to the solution (pH ca 7) and the spectrum was recorded. No change in absorption maxima was observed. A fresh $\text{Cs}_2[\text{Cr}(\text{нта})(\mu\text{-OH})]_2 \cdot 4\text{H}_2\text{O}$ solution ($5.9 \times 10^{-3} \text{ M}$) was prepared and the UV/VIS spectrum was recorded, (1) in Figure 3.3. Spectrum 2 in Figure 3.3 was recorded in acidic solution ($5.9 \times 10^{-3} \text{ M}$ dimer in 0.1 M HClO_4). The addition of base (solid NaHCO_3) to the solution in (2) resulted in an immediate change to spectrum (3). Addition of acid to this solution resulted in the same spectrum as recorded in (2).

These results clearly point to a stable $[\text{Cr}(\text{nta})(\mu\text{-OH})]_2^{2-}$ complex in slightly alkaline solution, but when protonated, immediately forms the *cis*-diaqua complex, which by addition of base forms the aquahydroxo complex. This reaction is reversible. The rapid change of spectrum with the addition of HClO_4 to the dimer in solution can only be attributed to the protonation of the hydroxo groups in $[\text{Cr}(\text{nta})(\mu\text{-OH})]_2^{2-}$. These results are summarised by the following reaction and is in accordance with that found for $[\text{Co}(\text{nta})(\mu\text{-OH})]_2^{2-}$ (Paragraph 3.4.1.1)

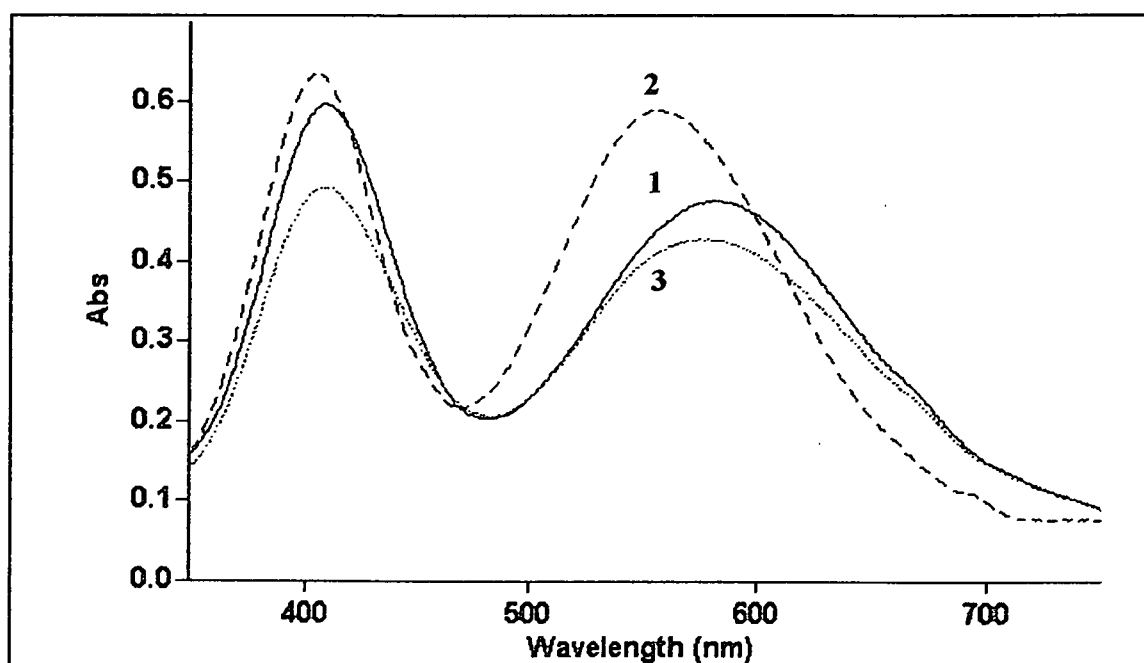
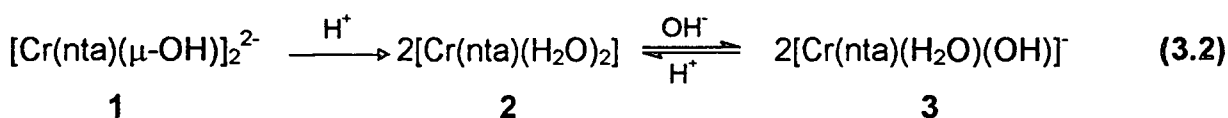


Figure 3.3. UV/VIS spectra of different Cr(III)-nta species in solution.

1 $[\text{Cr}(\text{nta})(\mu\text{-OH})]_2^{2-}$, pH 5 - 7; 2 $[\text{Cr}(\text{nta})(\text{H}_2\text{O})_2]$, pH ~ 1; 3 $[\text{Cr}(\text{nta})(\text{H}_2\text{O})(\text{OH})]^-$, pH 5-7.

These results are also in accordance with the ^2H NMR and other experiments that Koine *et al.* (1986:2835) performed. They also attributed the observed changes in UV/VIS and ^2H NMR spectra to acidic cleavage of the dihydroxo bridged species.

The spectroscopic results, together with the crystallographic results presented in the next chapter, lead to the assumption that the different crystals prepared by Uehara *et al.* (1967:2317) are in fact not different, but possibly a $[\text{Cr}(\text{nta})(\mu\text{-OH})]_2^{2-}$ species that crystallises in two space groups of the tetragonal and monoclinic crystal systems.

Synthesis

All the important IR and UV/VIS data are represented in Table 3.1.

Table 3.1. Summary of important IR and UV/VIS data for the prepared complexes.

	$\nu_{\text{COO-Co}}$ (cm^{-1})	λ_{max} (ϵ) (nm) ($M^{-1} \text{cm}^{-1}$)		
$\text{Cs}_2[\text{Co}(\text{nta})(\mu\text{-OH})]_2 \cdot 4\text{H}_2\text{O}$	1644 (sh) 1618 (s)	226 (1.55×10^4)	406 (302)	547 (191)
$\text{Cs}_2[\text{Co}(\text{nta})(\text{CO}_3)] \cdot \text{H}_2\text{O}$	1620 (s)	215 (4.78×10^4)	384 (178)	565 (135)
$\text{K}_2[\text{Co}(\text{nta})(\text{ox})] \cdot x\text{H}_2\text{O}$	1623 (s)	235 (2.22×10^4)	384 (190)	554 (197)
$\text{Ba}[\text{Co}(\text{nta})(\text{I-leu})]_2 \cdot x\text{H}_2\text{O}$	1632 (s)		370 (166)	525 (185)
$\text{Cs}[\text{Co}(\text{nta})(\text{I-val})] \cdot x\text{H}_2\text{O}$	1638 (s)		374 (178)	519 (195)
$[\text{Co}(\text{nta})(\text{N,N-Et}_2\text{en})]$	1617 (s)	232.1 (sh)		506.0 (316)
$[\text{Co}(\text{nta})(\text{N,N-Eten})]$	1623 (s)	227.0 (3.98×10^5)		539.9 (63)
$[\text{Co}(\text{nta})(\text{dmap})_2]$	1616 (s)	272.1 (6.31×10^5)		514.9 (79)
$[\text{Co}(\text{nta})(\text{H}_2\text{O})_2]$		227 (1.55×10^4)		
$[\text{Co}(\text{nta})(\text{H}_2\text{O})(\text{OH})]$		236 (1.70×10^4)		
$\text{Cs}_2[\text{Cr}_2(\text{nta})_2(\mu\text{-OH})_2] \cdot 4\text{H}_2\text{O}$	1635 (s)		409.1 (187)	584.0 (150)
$[\text{Cr}(\text{nta})(\text{H}_2\text{O})_2]$			406.0 (103)	558.1 (96)
$[\text{Cr}_2(\text{nta})(\text{H}_2\text{O})(\text{OH})]$			409.1 (84)	574.0 (79)

3.4.2 ^1H NMR spectra of Co(III)-nta complexes

It was mentioned in earlier paragraphs that IR spectra of Co(III)-nta complexes do not provide conclusive evidence with regards to its structure or characterisation. The identification of $[\text{Co}(\text{nta})(\text{gly})]$ and $[\text{Co}(\text{nta})(\text{I-ala})]$ with ^1H NMR by Koine *et al.* (1969:1583) provided new possibilities to the identification and structure of these complexes.

The protons of a specific G ring of nta (H_{G1a} and H_{G1b} in Figure 3.4) are non-equivalent if $\text{R}' = \text{R}''$, while protons of the two different G rings (e.g. H_{G2a} and H_{G1a} in Figure 3.4) are equivalent under the same conditions for R' and R'' . This results in two doublets with an AB pattern with centers between 3.9 and 4.5 ppm (Figure 3.5). A singlet in the same region is assigned to the equivalent protons of the remaining acetate ring (R ring) which is co-planar with the bidentate or other ligands. Complexes in which all the ring protons of nta are non-equivalent ($\text{R}' \neq \text{R}''$) will exhibit totally different spectra than the

above.

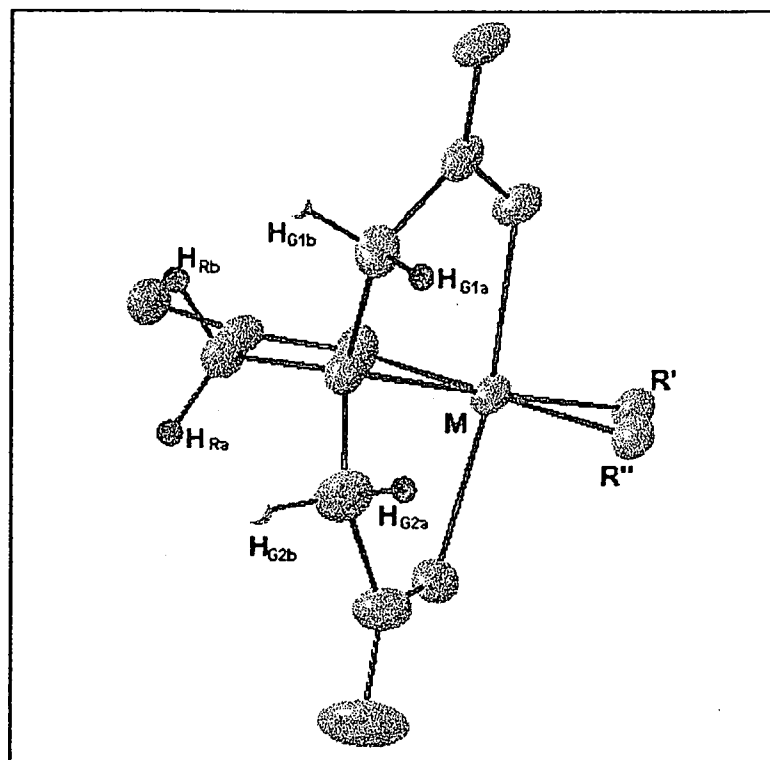
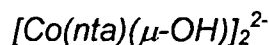


Figure 3.4. Glycinato rings in M(III)-nta complexes (M = Cr/Co).



The ^1H NMR spectrum obtained for $[\text{Co}(\text{nta})(\mu\text{-OH})]_2^{2-}$ is identical with that found by Smith and Sawyer (1968:923) for " α - $[\text{Co}(\text{nta})(\text{H}_2\text{O})(\text{OH})]^{-1}$ ". It consists of one simple AB pattern and a singlet, with relative intensities of 2:1 (refer to Paragraph 2.2.1). Smith and Sawyer found that the AB pattern of " α - $[\text{Co}(\text{nta})(\text{H}_2\text{O})(\text{OH})]^{-1}$ " shifts upfield upon acidification of the complex to pH 0.5 to form $[\text{Co}(\text{nta})(\text{H}_2\text{O})_2]$. It was proposed that this " α - $[\text{Co}(\text{nta})(\text{H}_2\text{O})(\text{OH})]^{-1}$ " complex is more likely a dimeric form of Co(III)-nta with either hydroxo or oxo bridges because its lower field AB proton positions would result from deshielding associated with the magnetic anisotropy of the metal-oxo or metal-hydroxo region.

The crystallographic study of $[\text{Co}(\text{nta})(\mu\text{-OH})]_2^{2-}$ in the next chapter as well as the UVVIS spectral study in the previous paragraphs finally confirms the structure of the α -complex prepared by Mori *et al.* (1958:940) as $[\text{Co}(\text{nta})(\mu\text{-OH})]_2^{2-}$.

[Co(nta)(dmap)₂], [Co(nta)(N-Eten)] and [Co(nta)(N,N-Eten)]

The ¹H NMR. spectra provide very interesting results for the identification of Co(III)-nta complexes. The spectra of [Co(nta)(N,N-Et₂en)] (Figure 3.5) and [Co(nta)(dmap)₂] are basically the same as for [Co(nta)(gly)]⁻ and [Co(nta)(μ-OH)]₂²⁻ in that the AB patterns are repeated for all the mentioned complexes. The only difference in these spectra is that the chemical shifts of these patterns vary slightly, Table 3.2.

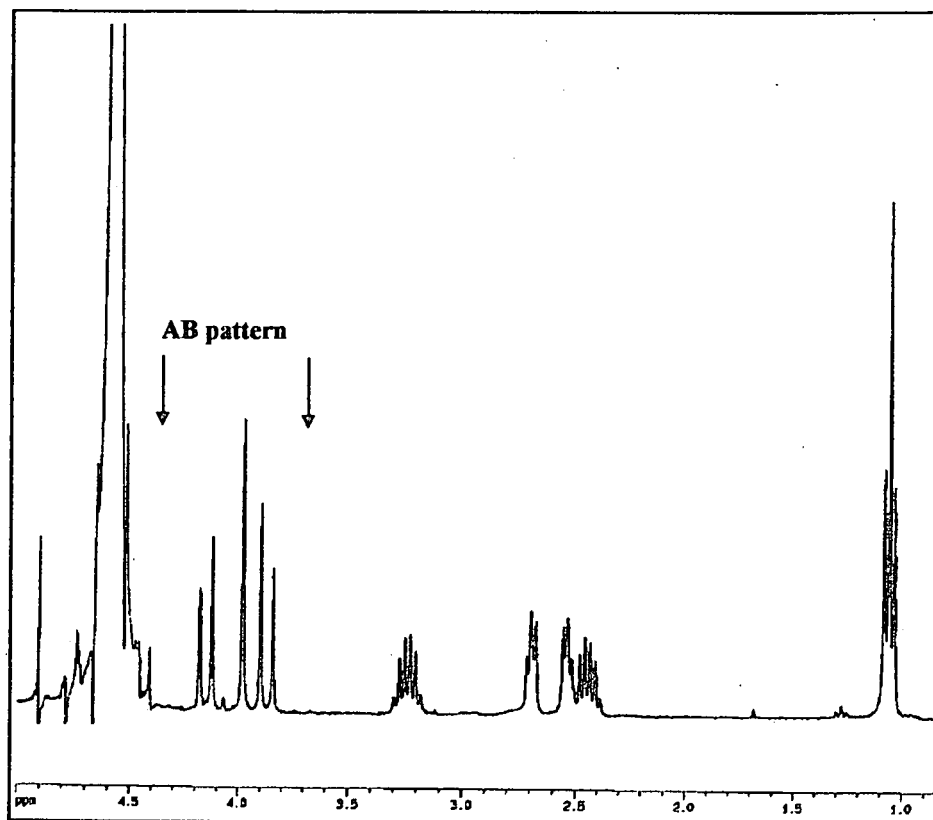


Figure 3.5. ¹H NMR spectrum for [Co(nta)(N,N-Et₂en)].

The two doublets at 3.87 and 4.15 ppm (AB pattern) for the spectrum of [Co(nta)(N,N-Et₂en)] are assigned to the non-equivalent, coupled acetate protons, H_{G1a}, H_{G1b}, H_{G2a}, H_{G2b}, of the two G rings of nta and the singlet at 3.99 ppm is assigned to the R ring protons (Figure 3.4). The AB pattern is not repeated for the spectrum of [Co(nta)(N-Eten)] (Figure 3.6 and Table 3.3). All six the nta protons are non-equivalent as explained earlier, leading to two distinguishable doublets and a multiplet in the 3.9 – 4.4 ppm region. Both the doublets integrate for one proton each as expected for non-equivalent protons. The spectrum of [Co(nta)(dmap)₂] also confirms the presence of two dmap molecules, thereby supporting the chemical analysis data.

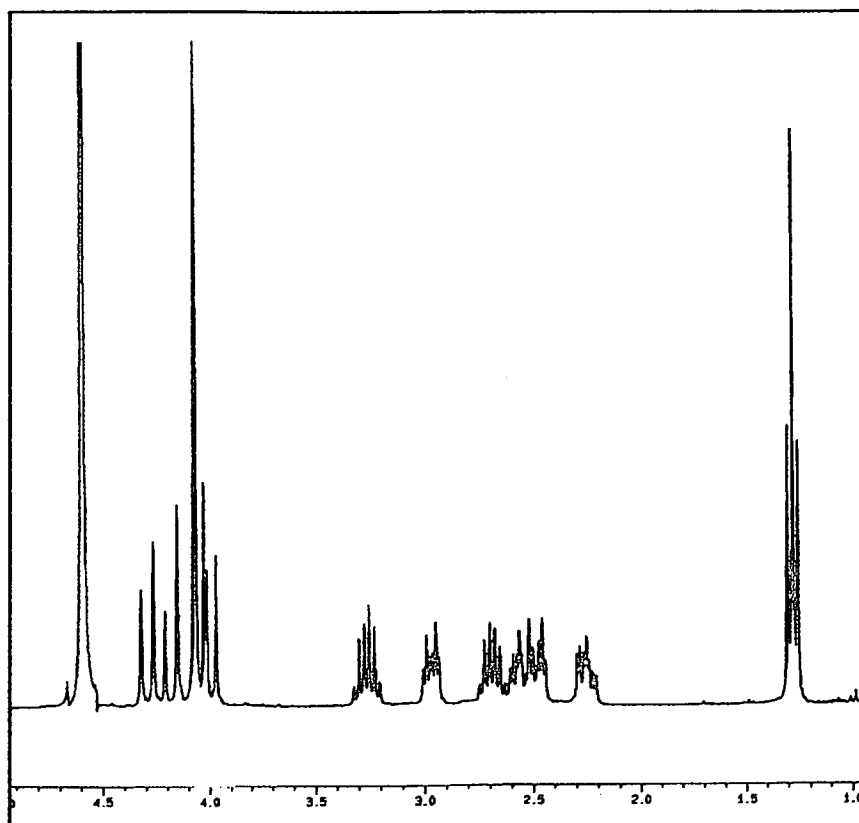


Figure 3.6. ^1H NMR spectrum for $[\text{Co}(\text{nta})(N\text{-Eten})]$.

It is not possible to distinguish from the ^1H NMR spectrum of $[\text{Co}(\text{nta})(N\text{-Eten})]$ whether the substituted nitrogen of *N*-Eten is *trans* or *cis* to the nitrogen of nta as the acetate protons of nta would be non-equivalent for both cases. The substituted nitrogen $[\text{Co}(\text{nta})(N,N\text{-Et}_2\text{en})]$ is *trans* to the nitrogen of nta (see structural data). This is not surprising since the ethyl groups would cause much more steric hindrance on the G rings with the substituted nitrogen in the *cis* position than in the *trans* position. We conclude that it is highly likely that it would be the same for $[\text{Co}(\text{nta})(N\text{-Eten})]$.

$[\text{Co}(\text{nta})(\text{CO}_3)]^{2-}$ and $[\text{Co}(\text{nta})(\text{ox})]^{2-}$

The ^1H NMR spectra for $[\text{Co}(\text{nta})(\text{CO}_3)]^{2-}$ and $[\text{Co}(\text{nta})(\text{ox})]^{2-}$ exhibit the same AB pattern as for the other complexes with equivalent H_{Ga} and H_{Gb} protons (Figure 3.4). Both have doublets at 4.42 ppm while the singlets are almost at the same positions, 3.99 compared to 4.02 ppm. The only real difference in the two spectra is with the doublets at higher field where the $[\text{Co}(\text{nta})(\text{ox})]^{2-}$ doublet is at 3.88 ppm compared to 4.06 ppm for $[\text{Co}(\text{nta})(\text{CO}_3)]^{2-}$ and 3.82 for $[\text{Co}(\text{nta})(\mu\text{-OH})_2]^{2-}$. The reason for this small shift can be contributed to the change in chemical environment that H_{G1a} and H_{G2a} experience when R' and R'' is varied.

Synthesis

[Co(nta)(l-val)]

This spectrum is understandably very similar to that of [Co(nta)(N-Eten)] because the H_{Ga} and H_{Gb} protons are also not equivalent in this case (Table 3.3). The rest of the peaks are also consistent with coordinated valine. Once again we have good reason to believe that the nitrogen of valine is *trans* to the nta nitrogen due to possible lesser steric hindrance.

Table 3.2. Summary of ¹H NMR data for nta protons in symmetrical* Co(III)-nta complexes.

	Chemical shift (number of protons, multiplicity)		
	(ppm)		
	G ring protons		R ring protons
Cs₂[Co(nta)(μ-OH)]₂·4H₂O	3.82 (2H, d.)	4.52 (2H, d.)	3.91 (2H, s.)
Cs₂[Co(nta)(CO₃)]·H₂O	4.06 (2H, d.)	4.42 (2H, d.)	3.99 (2H, s.)
K₂[Co(nta)(ox)]·xH₂O	3.88 (2H, d.)	4.42 (2H, d.)	4.02 (2H, s.)
[Co(nta)(N,N-Et₂en)]	3.87 (2H, d.)	4.15 (2H, d.)	3.99 (2H, s.)
[Co(nta)(dmap)₂]	4.02 (2H, d.)	4.14 (2H, d.)	4.21 (2H, s.)

* Refers to R' = R" (Figure 3.3)

Table 3.3. Summary of ¹H NMR data for nta protons in non-symmetrical* Co(III)-nta complexes.

	Chemical shift (number of protons, multiplicity)		
	(ppm)		
Cs[Co(nta)(l-val)]·xH₂O	4.02-4.10 (4H, m.)	4.37 (1H, d.)	4.42 (1H, d.)
[Co(nta)(N-Eten)]	3.97-4.08 (4H, m.)	4.19 (1H, d.)	4.29 (1H, d.)

* Refers to R' ≠ R" (Figure 3.3)

3.5 Conclusion

All the ^1H NMR, UV/VIS and IR data for the synthesised complexes are represented in Table 3.1. It can be seen from this that ^1H NMR studies provide a much better synthetic identification tool for identifying Co(III)-nta complexes than IR due to especially the fact that a simple AB pattern is observed for complexes with equivalent G ring protons as opposed to complexes with inequivalent G ring protons. The UV/VIS studies on the Co(III)-nta and Cr(III)-nta complexes first prepared by Mori *et al.* (1958:940) and Uehara *et al.* (1967:2317) together with the crystallographical studies in the next chapter finally clears all the doubt surrounding the structures of these complexes.

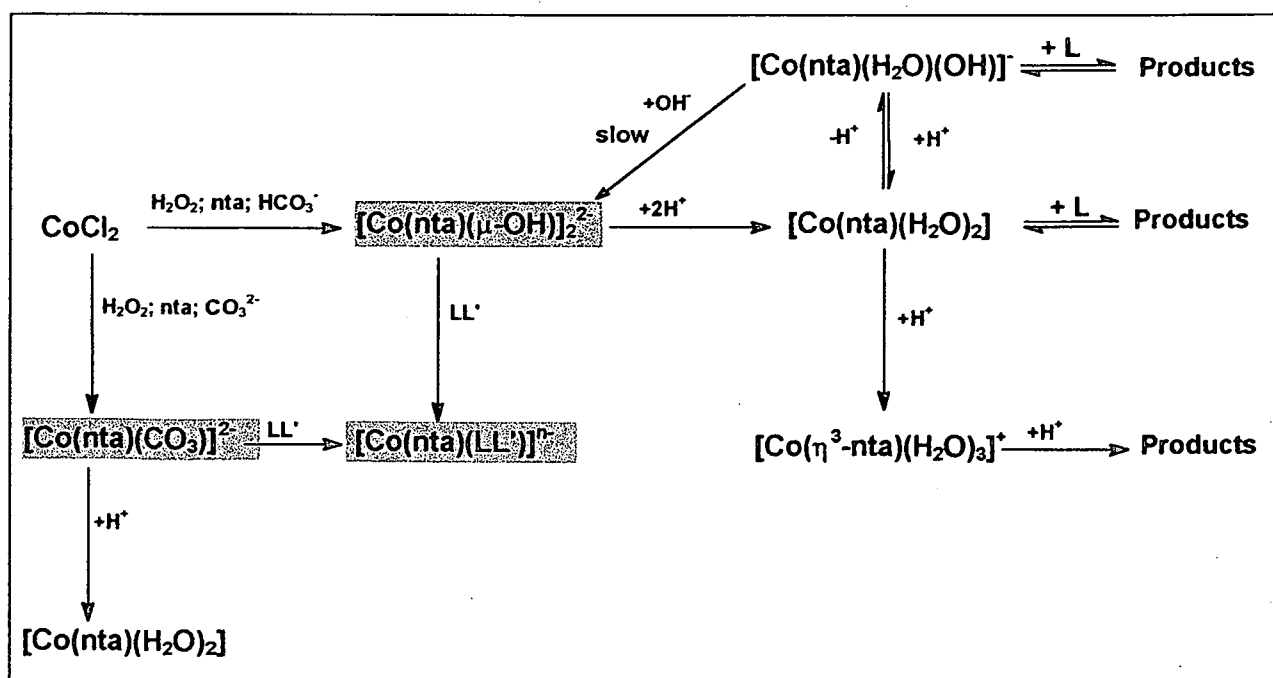
It has also been shown that $\text{Cs}_2[\text{Co}(\text{nta})(\text{CO}_3)] \cdot \text{H}_2\text{O}$ can easily be prepared and that this complex can be used very effectively as starting material for the preparation of different Co(III)-nta complexes.

4

X-ray crystallography

4.1 Introduction

There are very few examples of structures of Co(III)- or Cr(III)-nta complexes available in the literature (see Chapter 2). Furthermore, the structures of the Co(III)-nta and Cr(III)-nta complexes first prepared by Mori *et al.* (1958:940) and Uehara *et al.* (1967:2317) have not been solved up to this stage, even though these complexes have been used as starting material in several synthetic and kinetic studies. This chapter deals with three new Co(III)-nta crystal structures (highlighted in Scheme 4.1) including the complex that Mori *et al.* first prepared. Two structures of a Cr(III)-nta complex crystallising in different space groups that Uehara *et al.* first prepared are also described in this chapter. The strain in the glycinato rings of coordinated nta is also investigated in the following paragraphs.



Scheme 4.1. Complexes of Co(III)-nta (shaded box = Co(III) complexes identified by X-ray crystallography).

4.2 Experimental

Unless specified otherwise the following experimental information is the same for all the structures. The density of the compounds was determined by flotation in an iodomethane/benzene mixture. Lorentz, polarisation and absorption corrections were applied to all the data sets. The structures were solved with the heavy atom method and all the other atoms were located and their positions refined by successive Fourier calculations. The hydrogen atom positions were calculated riding on the adjacent carbon, nitrogen and oxygen atoms ($d(\text{C-H}) = 0.93$ and $d(\text{N-H}) = 0.86 \text{ \AA}$) using an overall isotropic thermal parameter. Atomic scattering factors were obtained from Cromer and Mann (1968:321). The SHELXS86 (Sheldrick, 1986), SHELXL93 (Sheldrick, 1993) and SHELXL97 (Sheldrick, 1997) programs were used for all the calculations. The molecular graphics were calculated with the Diamond 2.1a program (Brandenburg & Berndt, 1998).

4.3 Crystal structures of Cr(III)-nta complexes

4.3.1 Crystal structures of $\text{Cs}_2[\text{Cr}(\text{nta})(\mu\text{-OH})]_2 \cdot 4\text{H}_2\text{O}$ in $(I4_1/a) = (I)$ and $(P2_1/c) = (II)$ (Visser et al., 1999:2795)

A summary of the general crystal data and refinement parameters for I and II is given in Table 4.1. A final difference Fourier for both structures showed no sign of disorder or residual peaks. The most relevant bond lengths and angles for both structures are reported in Tables 4.2 and 4.3. The numbering scheme of the $[\text{Cr}(\text{nta})(\mu\text{-OH})]_2^{2-}$ anion for both structures is shown in the perspective drawing in Figure 4.1.

The two chromium atoms are octahedrally surrounded by a nitrogen atom and three carboxylate oxygen atoms of the nta ligand plus the two bridging hydroxo oxygen atoms. The nta ligand forms three glycinate rings around the central metal ion (Paragraphs 2.2.1 and 3.4.2). According to Weakliem and Hoard (1959:549), these rings can be classified into one R ring, Cr-N1-C6-C5-O6, and two G rings, Cr-N1-C2-C1-O2 (G2 ring) and Cr-N1-C3-C4-O4 (G1 ring).

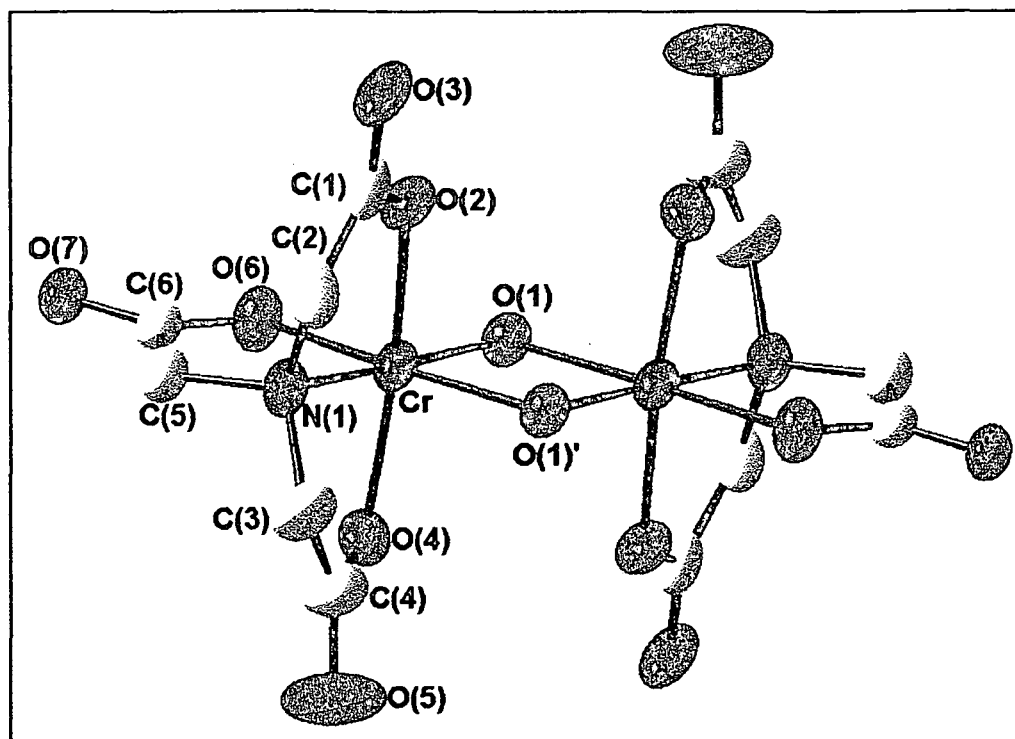


Figure 4.1. Numbering scheme of the $[\text{Cr}(\text{nta})(\mu\text{-OH})]_2^{2-}$ anion.

The Cr-OH bond distances for I are slightly shorter than in II (1.942(7) and 1.961(6) Å vs. 1.987(2) and 1.991(1) Å). The Cr-OH-Cr angle for I is 98.5(3)° compared to 97.9(1)° for II. The Cr-N bond length is 2.048(9) Å for I, and 2.061(3) Å for II. The Cr-O bond distances vary between 1.965(7) and 1.970(8) Å for I and between 1.954(2) and 1.988(2) Å for II.

The different bond lengths in $[\text{Cr}(\text{nta})(\mu\text{-OH})]_2^{2-}$ correspond well with those in $[\text{Cr}(\text{nta})(\mu\text{-OH})(\mu\text{-acetato-O,O})\text{Cr}(\text{nta})]^{2-}$ in which the Cr-N, Cr-OH and Cr-O bonds lengths were 2.060(5), 1.936(4) and 1.982(4) Å respectively (Green *et al.*, 1990:87). The M-OH-M bond angles are identical for the two complexes (98.5(3) and 98.2(2) °) while the OH-M-OH bond angles are 81.5(3) and 81.8(2) Å respectively. The rest of the N-C, C-C and C-O bond distances of the nta ligand are all considered normal and agree well with those found in $[\text{Ca}(\text{nta})] \cdot 2\text{H}_2\text{O}$ and Hnta (Hnta = nitrilotriacetic acid) (Skrzypczak-Jankun *et al.*, 1994:1097 and Whitlow, 1972:1914).

CHAPTER 4

Table 4.1. Crystal data and structure refinement for $\text{Cs}_2[\text{Cr}(\text{nta})(\mu\text{-OH})_2]\cdot 4\text{H}_2\text{O}$.

	I	II
Empirical formula	$\text{C}_{12}\text{H}_{22}\text{Cr}_2\text{Cs}_2\text{N}_2\text{O}_{18}$	$\text{C}_{12}\text{H}_{22}\text{Cr}_2\text{Cs}_2\text{N}_2\text{O}_{18}$
Formula weight	852.14	852.14
Temperature (K)	293(2)	293(2)
Wavelength (Å)	0.71073	0.71073
Diffractometer	Enraf-Nonius CAD4	Smart CCD
Crystal system	Tetragonal	Monoclinic
Space group	$I4_1/a$	$P2_1/c$
Unit cell dimensions	$a = 19.987(3)\text{Å}$ $b = 19.987(3)\text{Å}$ $c = 12.357(2)\text{Å}$ $\alpha = 90^\circ$ $\beta = 90^\circ$ $\gamma = 90^\circ$	$a = 10.5437(5)\text{Å}$ $b = 12.4022(3)\text{Å}$ $c = 10.4780(6)\text{Å}$ $\alpha = 90^\circ$ $\beta = 113.4900(10)^\circ$ $\gamma = 90^\circ$
Volume (Å ³)	4936.4(13)	1256.61(11)
Z	8	4
Density (calculated) (mg/m ³)	2.293	2.252
Absorption coefficient (mm ⁻¹)	3.873	3.803
F(000)	3280	820
Crystal size	0.35x0.35x0.26mm	0.30x0.36x0.30mm
Theta range for data collection (°)	1.94 to 24.92	2.11 to 28.30
Index ranges	$0 \leq h \leq 23$ $0 \leq k \leq 23$ $0 \leq l \leq 14$	$-9 \leq h \leq 13$ $-16 \leq k \leq 16$ $-13 \leq l \leq 9$
Reflections collected	1242	7909
Independent reflections	1170 [R(int)=0.0236]	2892 [R(int)=0.0283]
Refinement method	Full-matrix least-squares on F^2	Full-matrix least-squares on F^2
Data/restraints/parameters	1170/0/164	2892/0/164
Goodness-of-fit on F^2	1.064	1.009
Final R indices [$I > 2\sigma(I)$]	$R_1 = 0.0490$ $wR_2 = 0.1226$	$R_1 = 0.0354$ $wR_2 = 0.0946$
R indices (all data)	$R_1 = 0.0490$ $wR_2 = 0.1226$	$R_1 = 0.0391$ $wR_2 = 0.0946$
Largest diff. peak and hole (Å ⁻³)	1.045 and -1.298	0.759 and -1.690

X-ray Crystallography

Table 4.2. Selected bond lengths (Å) for $\text{Cs}_2[\text{Cr}(\text{nta})(\mu\text{-OH})_2]\cdot 4\text{H}_2\text{O}$.

	I	II		I	II
Cr-O(1)	1.942(7)	1.987(2)	Cr-N(1)	2.048(9)	2.061(3)
Cr-O(6)	1.965(7)	1.954(2)	N(1)-C(3)	1.48(2)	1.481(4)
Cr-O(2)	1.966(8)	1.985(2)	N(1)-C(2)	1.497(14)	1.482(4)
Cr-O(4)	1.970(8)	1.988(2)	N(1)-C(5)	1.492(12)	1.498(4)
Cr-O(1)'	1.961(6)	1.991(2)			

Table 4.3. Selected bond angles ($^\circ$) for $\text{Cs}_2[\text{Cr}(\text{nta})(\mu\text{-OH})_2]\cdot 4\text{H}_2\text{O}$.

	I	II		I	II
O(1)-Cr-O(6)	95.5(3)	94.62(10)	O(1)'-Cr-O(4)	87.6(3)	90.43(10)
O(1)-Cr-O(2)	95.2(3)	101.80(10)	O(1)-Cr-N(1)	178.1(3)	176.01(11)
O(6)-Cr-O(2)	90.0(3)	88.69(11)	O(6)-Cr-N(1)	85.0(3)	84.50(11)
O(1)-Cr-O(1)'	81.5(3)	82.08(10)	O(2)-Cr-N(1)	82.9(3)	82.09(10)
O(6)-Cr-O(1)'	177.0(3)	176.52(10)	O(1)'-Cr-N(1)	98.0(3)	98.87(10)
O(2)-Cr-O(1)'	90.4(3)	90.87(10)	O(4)-Cr-N(1)	81.7(4)	81.59(11)
O(1)-Cr-O(4)	100.1(3)	94.54(10)	C(3)-N(1)-C(2)	114.2(9)	114.3(3)
O(6)-Cr-O(4)	92.9(3)	90.96(11)	C(3)-N(1)-C(5)	110.9(9)	111.1(3)
O(2)-Cr-O(4)	164.1(3)	163.63(10)	C(2)-N(1)-C(5)	112.1(8)	112.1(3)
O(1)'-Cr-O(4)	87.6(3)	90.43(10)	Cr-O(1)-Cr'	98.5(3)	97.92(10)

The angular distortion around Cr from the ideal octahedral geometry is significant in both structures. Most of the N-Cr-OH and O-Cr-OH angles deviate from 90° and range between $81.5(3)$ and $98.0(3)^\circ$ for I and between $82.08(10)$ and $98.87(10)^\circ$ for II. The *trans*-N(1)-Cr-O(1) and O(1)'-Cr-O(6) angles of the two structures also differ somewhat with $178.1(3)$ and $177.0(3)^\circ$ respectively for I versus $176.01(11)$ and $176.62(10)^\circ$ for II. The O(4)-Cr-O(2) angles deviate significantly from the ideal 180° with $164.1(3)$ for I and $163.63(10)^\circ$ for II.

The strain in the two complexes may be expressed by the deviation from planarity of the three glycinato rings. Weakliem and Hoard (1959:549) pointed out that an unstrained glycinato ring should be planar and that the sum of the endocyclic angles should be 538.4° . The sums of the endocyclic angles for the different glycinato rings of I and II are presented in Table 4.4. The angles vary between 526.7 and 538.9° for I and between

CHAPTER 4

524.2 and 539.6 ° for II. The ring strain decrease for both structures in the order G1 > G2 > R. The lesser strain in the in-plane R rings is repeated in all the known structures of Co(III)- and Cr(III)-nta complexes.

Table 4.4. Sums of endocyclic angles, out-of-plane distances of N and Cr from CCOO plane and selected torsion angles for the different glycinato rings in I and II.

	I			II		
	G1	G2	R	G1	G2	R
Endocyclic angles (°)	526.7	533.4	538.9	524.2	531.0	539.6
N distance from CCOO* plane (Å)	-0.36(2)	-0.31(2)	-0.23(2)	0.705(6)	0.439(6)	-0.019(6)
Cr distance from CCOO plane (Å)	0.41(2)	0.21(2)	-0.09(9)	0.067(6)	-0.125(5)	0.130(5)
Torsion Angles (°)						
N-Cr-O-C	-25.5(9)	15.8(7)	-2.8(8)	16.8(3)	-16.3(2)	5.9(3)
O-Cr-N-C	32.2(7)	-21.9(7)	7.6(7)	31.9(2)	-25.6(2)	5.6(2)
Cr-N-C-C	-33(1)	25(1)	-11(1)	-41.1(3)	-25.6(2)	-4.8(3)
Cr-O-C-C	12(1)	-4(1)	-3.1(1)	3.6(4)	2.2(4)	-4.5(4)
N-C-C-O	15(1)	16(1)	10(1)	31.6(4)	20.3(4)	0.6(5)

* CCOO plane = two carbons, one carboxylate oxygen and the metal bonded oxygen atom in a specific plane.

The angular strain around the nitrogen atom of nta can be demonstrated by the non-planarity of the G rings, see Table 4.4. Deviations of N from the CCOO planes vary between 0.23(3) and 0.36(2) Å for I and between 0.019(6) and 0.705(6) Å for II. Similarly the out-of plane distances of chromium was calculated to be between 0.09(9) and 0.41(2) Å for I and between 0.067(6) and 0.130(5) Å for II. The deviation of N and Cr from the planes in I decrease in the order G1 > G2 > R. The same trend is observed in II for N distances from the plane, but not for the Cr distances. The main reason for this is possibly that the nitrogen atom is more displaced from the CCOO plane (0.705(6) Å) in the G1 ring. This forces the Cr atom into the G1 plane and out of the R plane (Cr distance from R plane is surprisingly long, 0.130(5) Å).

The different torsion angles for the glycinato rings are also presented in Table 4.4. These angles further illustrate the non-planarity of the G rings and also the distortion of the nitrogen tetrahedron. It is especially the O-Cr-N-C and Cr-N-C-C angles in the G

rings that deviate significantly from planarity. The O-Cr-N-C angles vary between 7.6(7) and 32.2(7) ° for I and between 5.6(2) and 31.9(2) ° for II. The Cr-N-C-C angles vary between 11(1) and 33(1) ° for I and between 4.8(3) and 41.1(3) ° for II. The torsion angles decrease in the same order as observed before namely, G1 > G2 > R.

The Cs⁺ to oxygen interatomic distances vary between 3.057(8) and 3.379(8) Å for I and between 3.117(3) and 3.386(3) Å for II. The Cs⁺ interacts with eight oxygen atoms in both cases, but there are substantial differences in the mode of interaction for the two structures. The geometry of the arrangement of Cs⁺ and oxygen atoms in I is in the form of a twisted dodecahedron, see Figure 4.2a. One Cs⁺ interacts with three oxygen atoms of a specific dimeric unit; namely a bridging oxygen O(1) and two ring oxygen atoms O(2) and O(6). The dodecahedron is completed by two carboxylate oxygen atoms, O(7), in two different dimeric units and three water molecules. This arrangement suggests that the Cs⁺ cations play the role of a link between the dimeric units and joins them in dimer – Cs – dimer "chains".

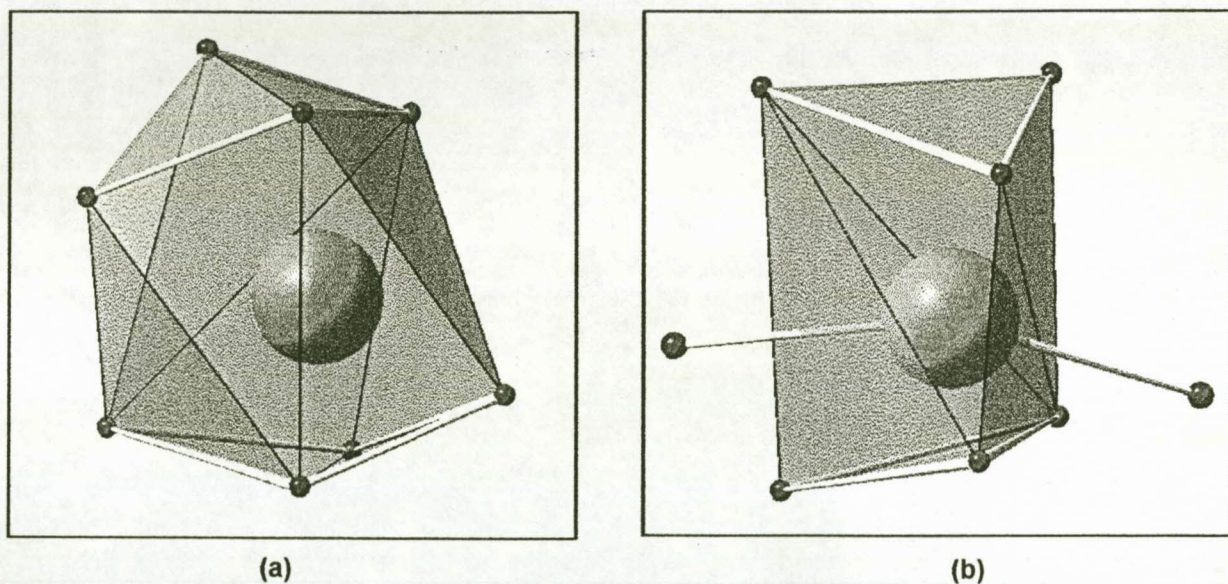


Figure 4.2. Arrangement of oxygen atoms around Cs⁺ in I (4.2a) and II (4.2b).

The geometry around Cs⁺ in II is more in the form of a distorted bicapped trigonal prism, Figure 4.2b. The polyhedron is made up as follows: the oxygen atoms of the G1 ring of a specific complex, O(2) and O(3); the oxygen atoms of the G2 ring that are in the opposite nta ligand of the same dimer, O(4) and O(5); two carboxylate oxygen atoms of two different dimeric units, O(7) and O(3), and two water molecules. This arrangement

means that each O(3) atom of the G2 ring interacts with two different Cs⁺ cations and that the cations once again form links between the different complexes.

The interaction of the dimer molecules in I and II with Cs⁺ cations is illustrated in Figures 4.3 and 4.4 respectively. The polyhedra around the cations are drawn in for a better view of this interaction.

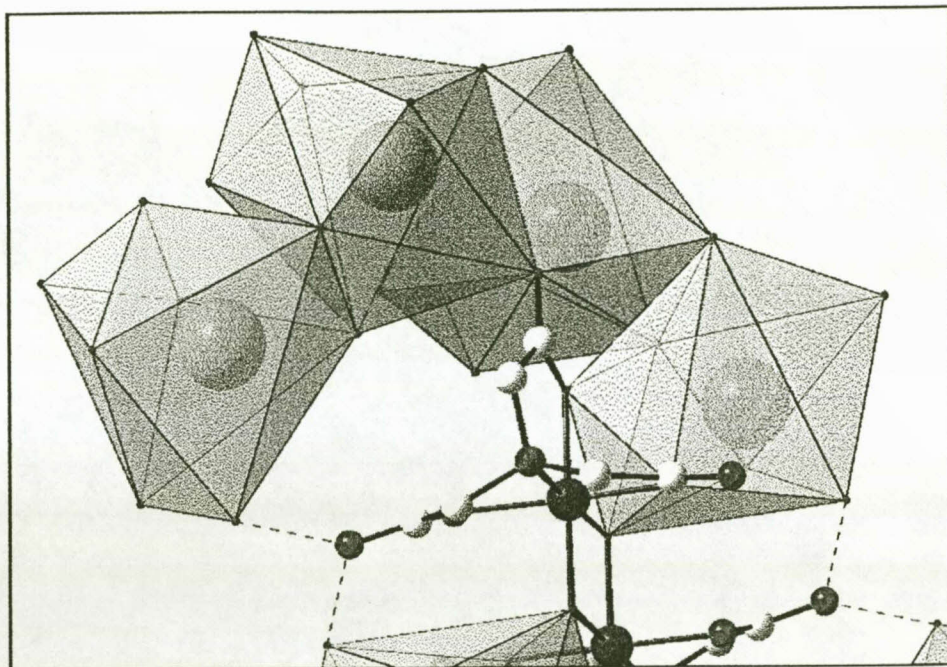


Figure 4.3. Close-up view of the interaction of I with Cs⁺ cations.

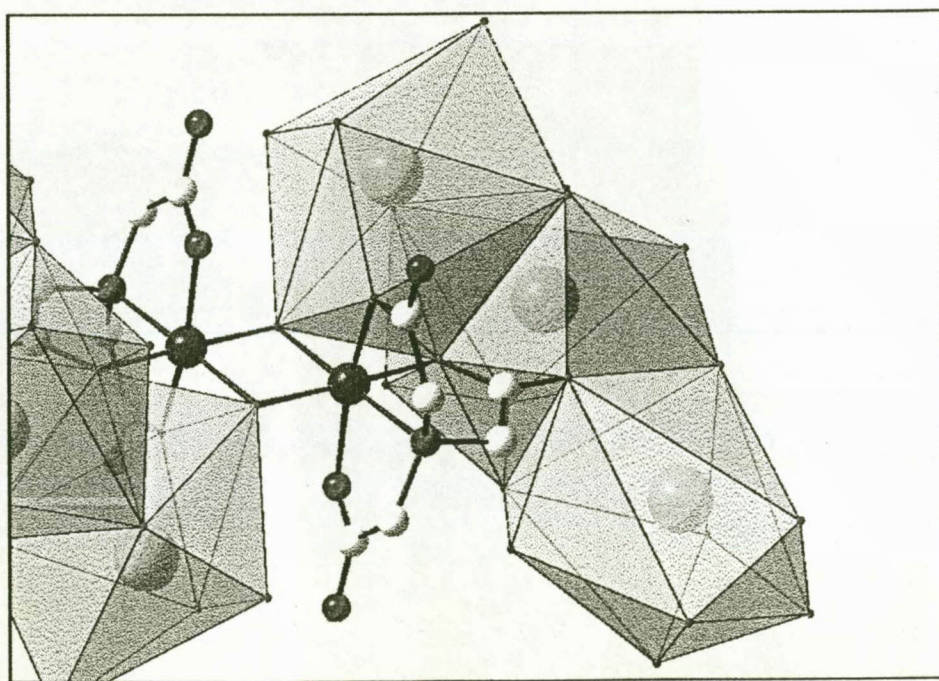


Figure 4.4. Close-up view of the interaction of II with Cs⁺ cations.

X-ray Crystallography

A projection of **I** along the *b* axis is shown in Figure 4.5. Interesting features of the packing of the complex anions are that they lie in layers parallel and diagonal to the *a* axis. A cavity (5.3 x 4.8 Å) is created in the middle of the unit cell. The carboxylate oxygens (O(5)) of the G1 chelate rings are protruding into the cavity and form hydrogen bonds with the nearby water molecules. Oxygen-oxygen contact distances are 2.918(6) and 2.912(5) Å respectively.

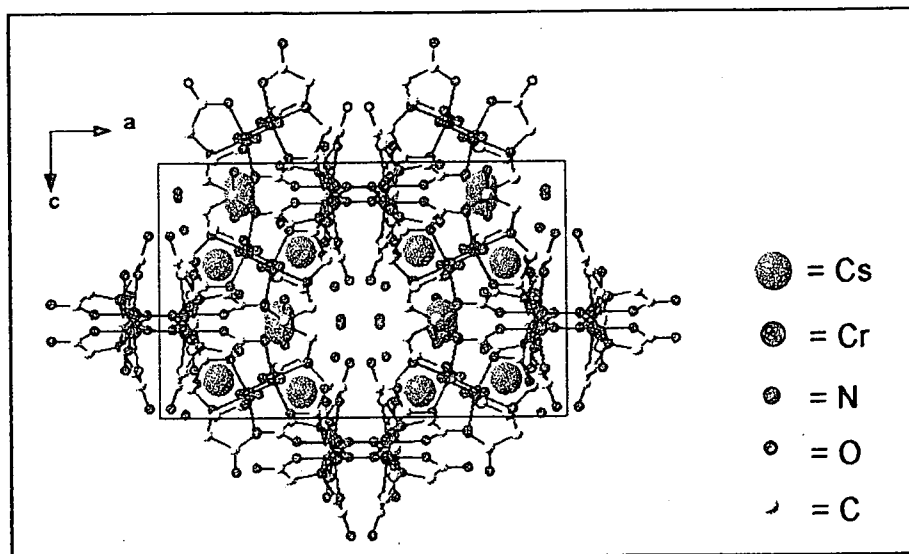


Figure 4.5. Perspective view of the unit cell of **I** along the *b* axis. H atoms are omitted for clarity.

A projection of **II** along the *c* axis is shown in Figure 4.6.

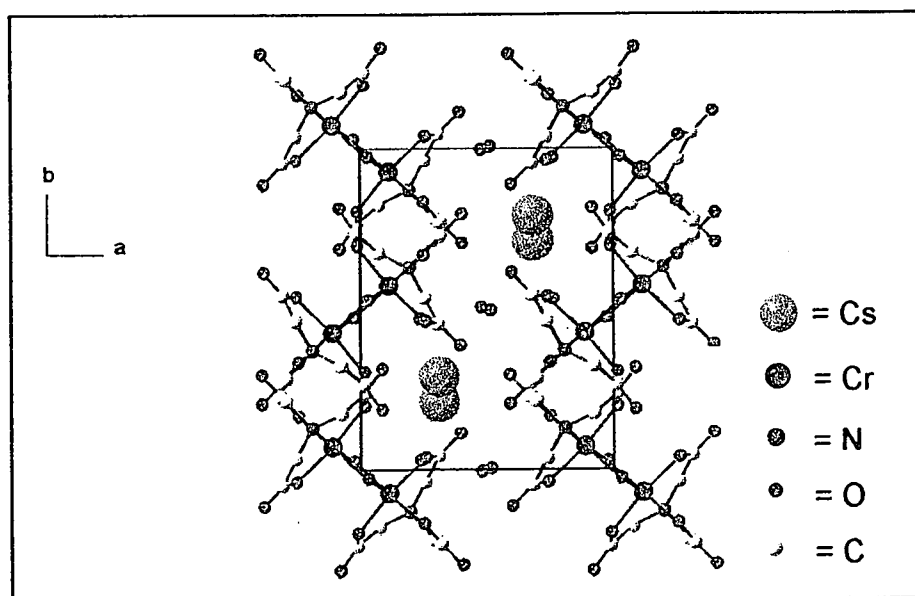


Figure 4.6. Perspective view of the unit cell of **II** along the *c* axis. H atoms are omitted for clarity.

The complex anions in Figure 4.6 are packed in layers that stretch diagonally across the a-b plane with the Cs⁺ cations filling in between the layers. Quite strong hydrogen bonding is observed for the bridging oxygen with a water molecule (O - O contact distance is 2.868(7) Å) and also between the R ring carboxylate oxygen and a water molecule (O - O contact distance is 2.850(6) Å).

4.3.2 Conclusion

The crystal structure determinations of I and II together with the information obtained in Chapter 3 is a final confirmation that the complexes first prepared by Uehara *et al.* (1967:2317) was in fact [Cr(nta)(μ-OH)]₂²⁻ and not a monomeric form of Cr(III)-nta as first postulated.

The strain in the different glycinato rings of nta in I and II differ substantially, even though the molecular formulas are exactly the same, Table 4.4. It seems that structure II experiences higher strain in its G rings than I. The average of the sum of the endocyclic angles of II is 527,6 compared to 530,5 ° in I. It is also evident from Table 4.4 that the N atom of nta in II is further away from the CCOO plane for both the G rings, indicating higher strain in these rings.

The above evidence suggests that inter-molecular forces also contribute to the strain in these complexes. Specific differences in the way that each dimer interacts with Cs⁺ cations should be highlighted. In I the bridging oxygen atoms each interact with a cation while there is no such interaction in II. The O(1)-Cr-O(2) angle in I is almost 7 ° smaller than in II, see Table 4.3. This might be linked to the interaction of Cs⁺ with O(1), O(2) and O(6) in I, causing the O-M-O angle to be smaller.

The interaction of the Cs⁺ cations with G ring oxygens in II is also more pronounced than in I, probably causing more strain in II. In II there are five interactions between G ring oxygen atoms and Cs⁺ ions while there is only one such interaction in I.

In order to investigate the above more carefully the structural data of I and II are compared to other available data in the literature (refer to Table 4.5). From this it is evident that all the complexes experience more strain in its G rings than R rings.

X-ray Crystallography

Table 4.5. Comparison of ring strain in different Cr(III)-nta complexes.

	G_{av}^a (°)	$C_G-N-C_G^b$ (°)	$Cr-N-C-C_{av}^c$ (°)	$O-Cr-N-C_{av}^d$ (°)	Reference
$[Cr(nta)(\mu-OH)]_2^{2-}$ (I)	530.1	114.2	29.0	27.1	This study
$[Cr(nta)(\mu-OH)]_2^{2-}$ (II)	527.5	114.3	33.5	28.8	This study
$Cr(nta)(\mu-OH)(acetate-O,O)Cr(nta)]^{2-}$ ^e	532.6	115.1	29.97	27.63	Green <i>et al.</i> (1990:87)
	529.7	114.6	31.35	27.32	
$[Cr(nta)(\mu-OH)_2Cr(phen)_2]^+$ ^f	530.1	114.1	31.9	28.4	Fujihara <i>et al.</i> (1995:1813)
$[Cr(nta)(\mu-OH)_2Cr(tn)_2]^+$ ^g	528.6	114.8	33.6	27.7	<i>ibid.</i>

^a average of the endocyclic angles in the G rings

^b angle formed between nitrogen of nta and the two closest G ring carbons

^c average of G ring Cr-N-C-C torsion angles

^d average of G ring O-Cr-N-C torsion angles

^e this complex has two nta moieties

^f phen = 1,10-phenanthroline

^g propane-1,3-diamine

It is important to note that two of the complexes in Table 4.5, namely $[Cr(nta)(\mu-OH)_2Cr(tn)_2]^+$ and $[Cr(nta)(\mu-OH)_2Cr(phen)_2]^+$, are cations so that there could be no interaction of dimer oxygens with cations as for I and II. It is also important to note that the hydrogen bonding observed in these two cationic dimers is comparable to the other complexes. This means that these complexes should have lesser strain in all the rings if inter-atomic forces are the main reason for strain in these type of complexes.

The average of the endocyclic angles of the G rings in II and $[Cr(nta)(\mu-OH)_2Cr(tn)_2]^+$ are much lower than the angles in I and $[Cr(nta)(\mu-OH)_2Cr(phen)_2]^+$. Furthermore, the Cr-N-C-C torsion angles listed for II and $[Cr(nta)(\mu-OH)_2Cr(tn)_2]^+$ are higher than what was observed for I and $[Cr(nta)(\mu-OH)_2Cr(phen)_2]^+$. This indicates that the strain in I and $[Cr(nta)(\mu-OH)_2Cr(phen)_2]^+$ are in the same order and that the strain in the other two complexes are also more or less equal.

Green *et al.* (1990:1813) performed a ²H NMR study on $[Cr(nta)(\mu-OH)_2Cr(tn)_2]^+$, $[Cr(nta)(\mu-OH)_2Cr(phen)_2]^+$ and several other complexes. They found that the proton signals for the G ring protons were equivalent for all the complexes except for

CHAPTER 4

$[\text{Cr}(\text{nta})(\mu\text{-OH})_2\text{Cr}(\text{phen})_2]^+$. Two G ring signals of equivalent intensity was observed. Their conclusion was that some of the oxygen atoms of the G rings in this complex formed hydrogen bonding with hydrogen atoms of the phen ligands and that these interactions were not of the same strength as was observed from the structural data. These van der Waals contact interactions probably freeze the inequivalent G ring conformations in solution so that two signals are observed.

This last study, together with the fact that the strain in I and II differ substantially proves that inter-atomic forces play a role in the strain of the different glycinato rings, although it could not be the main reason for the strain in the different rings of these complexes. Inter-molecular forces can not explain the fact that the R rings are almost completely unstrained in all the complexes studied.

Tables 4.6 and 4.7 present a comparison of important bond angles and distances of different Cr(III)-nta complexes.

Table 4.6. Important bond angles for different Cr(III)-nta complexes.

	Cr-O-Cr ^a (°)	O-Cr-O ^b (°)	N-Cr-O _R ^c (°)	N-Cr-O _G ^d (°)	O _G -Cr-O _G ^e (°)
$[\text{Cr}(\text{nta})(\mu\text{-OH})]_2^{2-}$ (I)	98.5(3)	81.5(3)	85.0(3)	82.3(3)	164.1(3)
$[\text{Cr}(\text{nta})(\mu\text{-OH})]_2^{2-}$ (II)	97.9(1)	82.1(1)	84.5(1)	81.8(2)	163.6(1)
$[\text{Cr}(\text{nta})(\mu\text{-OH})_2\text{Cr}(\text{phen})_2]^+$ ^f	99.6(4)	80.5(4)	85.3(4)	82.1(4)	162.8(4)
$[\text{Cr}(\text{nta})(\mu\text{-OH})_2\text{Cr}(\text{tn})_2]^+$ ^g	99.5(9)	80.1(1)	84.9(1)	81.4(1)	163.8(1)
Average	98.8(4)	80.8(6)	84.9(2)	81.9(2)	163.6(3)

^a Average of Cr-O-Cr bite angle

^b Average of O-Cr-O angle

^c N-Cr-O bite angle of R ring

^d average of N-Cr-O bite angles of G rings

^e O-Cr-O angle of G ring oxygens and Cr

^f Fujihara *et al.* (1995:1813)

^g Fujihara *et al.* (1995:1813)

It is evident from Tables 4.6 and 4.7 that the comparative geometry and bonding distances around Cr are basically the same within experimental error for all the different complexes. This evidence leads one to believe that the difference in strain between R and G rings should be ascribed to electronic effects rather than packing effects and that

X-ray Crystallography

the difference in strain between G rings of the same complex is possibly due to packing effects.

Table 4.7. Bond distances of different Cr(III)-nta complexes.

	Cr-O _R ^a (Å)	Cr-O _G ^b (Å)	Cr-O _{cis} ^c (Å)	Cr-O _{trans} ^d (Å)	Cr-N _{nta} ^e (Å)
[Cr(nta)(μ-OH)] ₂ ²⁻ (I)	1.965(7)	1.968(8)	1.961(6)	1.942(7)	2.048(9)
[Cr(nta)(μ-OH)] ₂ ²⁻ (II)	1.954(2)	1.986(2)	1.991(2)	1.987(2)	2.061(3)
[Cr(nta)(μ-OH) ₂ Cr(phen) ₂] ^{+f}	1.94(1)	1.974(8)	1.92(1)	1.92(1)	2.05(1)
[Cr(nta)(μ-OH) ₂ Cr(tn) ₂] ^{+g}	1.951(2)	1.951(8)	1.976(2)	1.921(3)	2.052(3)
Average	1.953(5)	1.97(4)	1.965(9)	1.94(2)	2.053(2)

^a Bond between Cr and R ring oxygen of nta

^b Average of bonds between Cr and G ring oxygens of nta

^c Bond between Cr and bridging oxygen *cis* to N of nta

^d Bond between Cr and bridging oxygen *trans* to N of nta

^e Bond between Cr and N of nta

^f Fujihara *et al.* (1995:1813)

^g Fujihara *et al.* (1995:1813)

Some very important bond information in Tables 4.6 and 4.7 must be highlighted. The average of the Cr-O_G bonding distances for individual molecules are longer than Cr-O_R distances in all cases. The difference in the overall averages (1.953(5) compared to 1.97(4) Å) is substantial, although statistically not meaningful.

Another important difference is observed for the R ring and G ring bite angles. Once again the G ring bite angles in a specific molecule is substantially smaller than R ring bite angles. This is observed for all the complexes studied thus far (average of 84.9(3)° in R rings compared to 81.9(3)° for the G rings).

From the data in Tables 4.6 and 4.7 we can interpret the bonding pattern of Cr(III)-nta complexes as displaying shorter equatorial bonds and two longer axial bonds. This elongation of the axial bonds was also found for other μ-hydroxo-bridged Cr(III) complexes (Veal *et al.*, 1973:343 and references therein). Pronounced *quasi-tetragonal/Jahn-Teller* distortion of *d⁴*, *d⁷* and especially *d⁹* species like Cu(II) in octahedral environment is well established (Barnes *et al.*, 1970:904; Lewis *et al.*, 1972:2216 and Purcell & Kotz, 1985:553). The basis of this distortion lies in the

stabilisation of the $d_{x^2-y^2}$ orbitals and destabilisation of d_{z^2} orbitals, thereby creating better overlap of metal and ligand bonding orbitals in the equatorial position and elongation of axial bonds. The overall result is stabilisation of the molecule in question.

Keeping all the above and the fact that Cr(III) is a d^3 and not a d^4 species in mind, the following explanation for the specific geometry in Cr(III)-nta complexes is attempted:

- 1) Nitritotriacetic acid is an electron-rich species and it has been shown that coordination of this ligand to inert metal centres like Cr(III) greatly enhance the reactivity of these complexes (Visser *et al.*, 1994:1051). The reason for this is that the electron density is donated to the Cr(III) metal centre, making it react more like the labile Cr(II) species. It has also been shown by Veal *et al.* (1973:343) that the bridging oxygen atoms in μ -hydroxo bridged chromium(III) dimers also donated electron density to the metal.
- 2) The extra electron density on the metal centre gives it more of a Cr(II), d^4 character.
- 3) This leads to stabilisation of the metal $d_{x^2-y^2}$ orbitals and destabilisation of the d_{z^2} orbitals and thus shorter equatorial and longer axial bonds. This effect will not be as pronounced as for Cu(II) complexes because electron-rich Cr(III) will still retain some of its d^3 character.
- 4) Stabilisation of the $d_{x^2-y^2}$ orbitals will lead to better overlap with the nta R chelate ring as can be seen by the shorter Cr-O_R bonds and larger N-Cr-O_R bite angles (Tables 4.6 and 4.7). The better overlap also means the R ring remains planar.
- 5) The destabilisation of the d_{z^2} orbital means weaker overlap with ligand orbitals. This, plus the fact that each G ring attempts to impose its own stereochemical requirements on the nitrogen atom, which is also constrained to approximately tetrahedral geometry forces longer Cr-O_G bonds and smaller N-Cr-O_G bite angles. The resulting compromised structure contains not only angle and bond length abnormalities in the G rings, but also significant distortions of the nitrogen tetrahedra, specifically between the C_{G1}-N(1)-C_{G2} angles. The opened C(3)-N(1)-C(2) angles are 114.2(9) ° for I and 114.3(3) ° for II. The angles

for $[\text{Cr}(\text{nta})(\mu\text{-OH})_2\text{Cr}(\text{phen})_2]^+$ and $[\text{Cr}(\text{nta})(\mu\text{-OH})_2\text{Cr}(\text{phen})_2]^+$ were also larger than 114° (Fujihara *et al.*, 1995:1813). The angle for $[\text{Cr}(\text{nta})(\text{OH})(\text{acetate-O,O})\text{Cr}(\text{nta})]^{2-}$ was recorded as $115.1(6)^\circ$. This is higher than what was found for $[\text{Ca.HN}^+(\text{CH}_2\text{COO}^-)_3].2\text{H}_2\text{O}$ (C-N-C angles were between 110.3 and 112.9°) and Hnta (angles were between $112.3(1)$ and $113.6(1)^\circ$), indicating higher ring strain in the dimers (Skrzypczak-Jankun *et al.*, 1994:1097 and Whitlow, 1972:1914).

- 6) The difference in strain on the G rings of a specific molecule/ion can be contributed to intermolecular forces. The data from I and II suggests that cations affect ring strain in the G rings of those two structures (Table 4.5 and preceding text). In the other structures listed in Table 4.5 most of the observed intermolecular interaction is between G ring oxygens and cations or hydrogen bonding between G ring oxygens and water molecules. The ^2H NMR study of Green *et al.* (1990:1813) that found that the G rings of $[\text{Cr}(\text{nta})(\mu\text{-OH})_2\text{Cr}(\text{phen})_2]^+$ had different strain, even in solution, further supports this assumption.

Therefore, we conclude that the planarity of the R rings in Cr(III)-nta complexes is probably due to stabilisation of the $d_{x^2-y^2}$ orbitals, causing better overlap in the equatorial positions. The non-planarity of G rings is attributed to destabilisation of d_{z^2} orbitals, causing longer bonds in the axial positions. This fact, together with the angular strain on the nta nitrogen cause the G rings to deviate from planarity. Lastly, we conclude that the difference in strain of different G rings is due to intermolecular forces.

4.4 Crystal structures of Co(III)-nta complexes

4.4.1 Crystal structure of $Cs_2[Co(nta)(\mu-OH)]_2 \cdot 4H_2O$ (Visser et al., 1997:2851)

A summary of the general crystal data and refinement parameters for $Cs_2[Co(nta)(\mu-OH)]_2 \cdot 4H_2O$ is presented in Table 4.8. A final difference Fourier showed no sign of disorder or residual peaks. This structure is isomorphic to I in Paragraph 4.3.1.

Table 4.8. Crystal data and structure refinement of $Cs_2[Co(nta)(\mu-OH)]_2 \cdot 4H_2O$.

Empirical formula	$C_6H_{11}CoCsNO_9$	
Formula weight	433.00	
Temperature	293(2) K	
Wavelength	0.71073 Å	
Diffractometer	Enraf-Nonius CAD4	
Crystal system	Orthorhombic	
Space group	I4 ₁ /a	
Unit cell dimensions	a = 19.640(2) Å	$\alpha = 90^\circ$
	b = 19.640(2) Å	$\beta = 90^\circ$
	c = 12.581(2) Å	$\gamma = 90^\circ$
Volume	4852.9(10) Å ³	
Z	16	
Density (calculated)	2.371 Mg/m ³	
Absorption coefficient	4.411 mm ⁻¹	
F(000)	3328	
Crystal size	0.30 x 0.30 x 0.22 mm	
Theta range for data collection	1.92 to 24.97°	
Index ranges	0 ≤ h ≤ 23, -15 ≤ k ≤ 16, 0 ≤ l ≤ 14	
Reflections collected	1246	
Independent reflections	1246 [R(int) = 0.0000]	
Refinement method	Full-matrix least-squares on F ²	
Data / restraints / parameters	1244 / 0 / 164	
Goodness-of-fit on F ²	0.839	
Final R indices [I > 2σ(I)]	R1 = 0.0322, wR2 = 0.0854	
R indices (all data)	R1 = 0.0325, wR2 = 0.0879	
Absolute structure parameter	10(10)	
Largest diff. peak and hole	1.195 and -1.034 e. Å ⁻³	

X-ray Crystallography

The most relevant bond lengths and angles for for $\text{Cs}_2[\text{Co}(\text{nta})(\mu\text{-OH})]_2 \cdot 4\text{H}_2\text{O}$ are reported in Tables 4.9 and 4.10.

Table 4.9. Selected bond lengths (Å) for $\text{Cs}_2[\text{Co}(\text{nta})(\mu\text{-OH})]_2 \cdot 4\text{H}_2\text{O}$.

Co-O(2)	1.892(5)	Co-N(1)	1.922(6)
Co-O(4)	1.893(6)	N(1)-C(5)	1.503(9)
Co-O(6)	1.902(5)	N(1)-C(3)	1.478(10)
Co-O(1)	1.899(5)	N(1)-C(2)	1.488(9)

Table 4.10. Selected bond angles (°) for $\text{Cs}_2[\text{Co}(\text{nta})(\mu\text{-OH})]_2 \cdot 4\text{H}_2\text{O}$.

O(2)-Co-O(4)	172.0(2)	O(2)-Co-O(6)	89.6(2)
O(4)-Co-O(6)	91.9(2)	O(4)-Co-O(1)	95.9(2)
O(2)-Co-O(1)	91.8(2)	O(4)-Co-N(1)	85.2(2)
O(6)-Co-O(1)	93.9(2)	O(1)-Co-N(1)	96.1(2)
O(2)-Co-N(1)	87.0(2)	O(4)-Co-Cs(1)	135.2(2)
O(6)-Co-N(1)	88.1(2)	Co'-O(1)-Co	98.2(2)
O(1)-Co-N(1)	177.6(2)	C(4)-O(4)-Co	111.7(5)
C(6)-O(6)-Co	114.9(5)	C(3)-N(1)-C(5)	110.3(6)
C(1)-O(2)-Co	113.5(5)	C(3)-N(1)-Co	103.9(4)
C(3)-N(1)-C(2)	115.7(6)	C(5)-N(1)-Co	107.2(4)
C(2)-N(1)-C(5)	112.3(6)	O(7)-C(6)-O(6)	125.4(7)
C(2)-N(1)-Co	106.6(5)	O(6)-C(6)-C(5)	116.1(6)
N(1)-C(5)-C(6)	112.1(6)	O(5)-C(4)-O(4)	124.4(8)
O(7)-C(6)-C(5)	118.6(7)	O(4)-C(4)-C(3)	116.7(7)
O(5)-C(4)-C(3)	118.9(8)	O(3)-C(1)-O(2)	122.2(8)
O(3)-C(1)-C(2)	120.7(7)	O(2)-C(1)-C(2)	117.0(7)
N(1)-C(2)-C(1)	109.9(6)	N(1)-C(3)-C(4)	107.8(6)

The numbering scheme of the $[\text{Co}(\text{nta})(\mu\text{-OH})]_2^{2-}$ anion is shown in the perspective drawing in Figure 4.7.

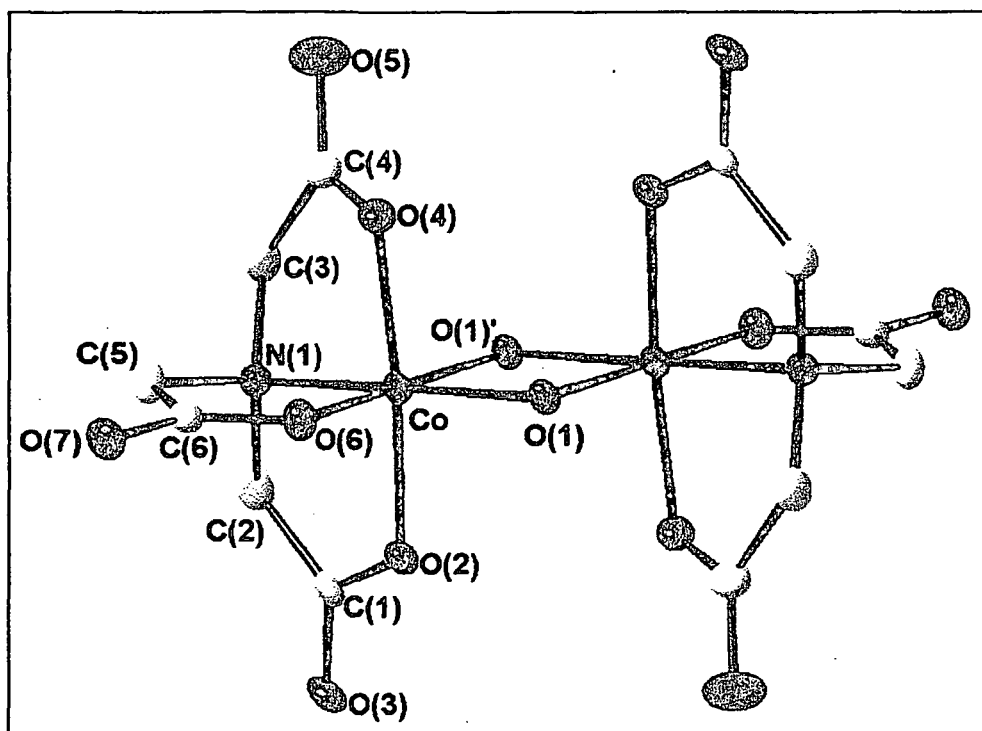


Figure 4.7. Perspective drawing of $[\text{Co}(\text{nta})(\mu\text{-OH})]_2^{2-}$.

The two cobalt atoms are octahedrally surrounded by a nitrogen atom and three carboxylate oxygen atoms of the nta ligand plus the two bridging hydroxo oxygen atoms. The nta ligand forms three glycinate rings around the central metal ion (Paragraphs 2.2.1 and 3.4.2). These rings can be classified into one R ring, Co-N1-C5-C6-O6, and two G rings, Co-N1-C2-C1-O2 (G2 ring) and Co-N1-C3-C4-O4 (G1 ring), according to Weakliem and Hoard (1959:549).

The angular distortion around Co from the ideal octahedral geometry is significant. Most of the N-Co-OH and O-Co-OH angles deviate from 90° and range between $87.0(2)$ and $96.1(2)^\circ$. The *trans*-N-Co-O and O-Co-O angles also deviate from 180° and range from $172.0(2)$ to $177.6(2)^\circ$.

The different bond lengths in $[\text{Co}(\text{nta})(\mu\text{-OH})]_2^{2-}$ correspond well with that found for $[\text{Co}(\text{nta})(\text{gly})]^-$ and $[\text{Co}(\text{nta})(\text{viol})]^-$ (Almazan *et al.*, 1990:2565 and Gladkikh *et al.*, 1992:908). They observed Co-N bond distances of $1.928(8)$ and $1.942(7)$ Å respectively and Co-O distances that varied between 1.884 and 1.902 Å. The Co-N bond distance for $[\text{Co}(\text{nta})(\mu\text{-OH})]_2^{2-}$ was determined as $1.922(6)$ Å and the Co-O

X-ray Crystallography

distances varied between 1.892(5) and 1.902(5) Å. The rest of the N-C, C-C and C-O bond distances of the nta ligand are all considered normal and agree well with those found in [Ca(nta)].2H₂O and Hnta (Skrzypczak-Jankun *et al.*, 1994:1097 and Whitlow, 1972:1914).

The Co-O-Co bond angle for [Co(nta)(μ-OH)]₂²⁻ is 98.2(2) ° while the OH-Co-OH bond angle is 81.8(2) °. This agrees well with the corresponding bond angles for I and II in Paragraph 4.3.1 where the respective angles were determined as 98.5(3), 97.9(1), 81.5(3) and 82.1(1) °.

The strain in the complex can once again be described by the deviation from planarity of the three glycinato rings of nta (Weakliem & Hoard, 1959:549), refer to Table 4.11. The sums of the endocyclic angles for the different glycinato rings of [Co(nta)(μ-OH)]₂²⁻ are 525.3, 533.1 (G rings) and 538.4 ° (R ring). The ring strain decrease in the order G1 > G2 > R.

Table 4.11. Endocyclic angles, out-of-plane distances of N and Co from CCOO planes and torsion angles for Cs₂[Co(nta)(μ-OH)]₂.4H₂O.

	G1	G2	R
Endocyclic angles (°)	525.3	533.1	538.4
N distance from CCOO* plane (Å)	-0.36(1)	-0.34(2)	-0.26(1)
Co distance from CCOO plane (Å)	0.44(1)	0.09(1)	-0.08(1)
Torsion Angles (°)			
N-Co-O-C	-27.8(5)	13.3(5)	-4.1(6)
Co-O-C-C	12.7(8)	-0.8(8)	-2.9(9)
N-C-C-O	-15.7(9)	-16.9(9)	-10.9(9)
Co-N-C-C	-34.4(7)	25.1(7)	-12.9(8)
O-Co-N-C	34.2(4)	-21.3(5)	9.4(5)

* CCOO plane = two carbons, one carboxylate oxygen and a bonded oxygen atom in a specific plane.

The angular strain around the nitrogen can be demonstrated by the non-planarity of the G rings (Table 4.11). Distances of N from the CCOO planes vary between 0.26(1) and 0.36(1) Å.

The different torsion angles for the glycinic rings are also presented in Table 4.11. These angles further illustrate the non-planarity of the G rings and also the distortion of the nitrogen tetrahedron. It is especially the O-Co-N-C and Co-N-C-C angles in the G rings that deviate significantly from planarity. The O-Co-N-C angles vary between $9.4(5)$ and $34.2(4)^\circ$ and the Co-N-C-C angles vary between $12.9(8)$ and $34.4(7)^\circ$. The torsion angles decrease in the same order as observed before namely, $G1 > G2 > R$.

The Cs^+ to oxygen interatomic distances vary between $3.008(6)$ and $3.504(5)$. The Cs^+ interacts with ten oxygen atoms in the form of a twisted bicapped square antiprism, see Figure 4.8. The Cs^+ cations play the role of a link between the dimeric units and join them in dimer – Cs – dimer "chains".

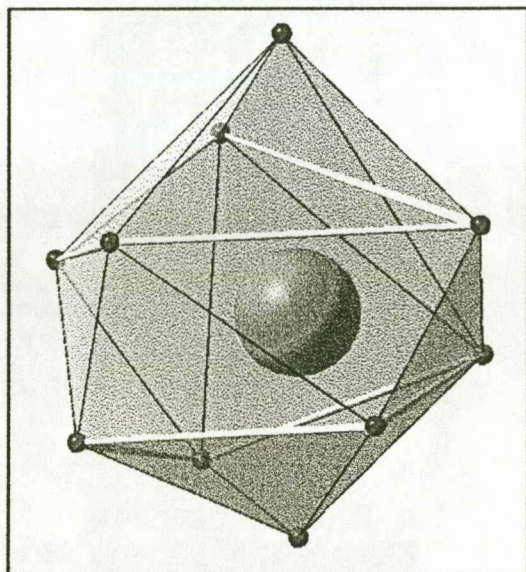


Figure 4.8. Arrangement of oxygen atoms around Cs^+ in $\text{Cs}_2[\text{Co}(\text{nta})(\mu\text{-OH})_2]\cdot 4\text{H}_2\text{O}$.

The packing of Cs^+ cations around the dimer ion is very similar to I, Figure 4.3, as expected. The mode of interaction between cations and oxygen atoms is also basically the same, only difference being that the cations in the cobalt structure are surrounded by ten oxygen atoms instead of eight.

The interaction of a dimer molecule with Cs^+ cations is illustrated in Figure 4.9. The polyhedra around the cations are drawn in for a better view of this interaction. This interaction is very similar to that found for I in Paragraph 4.3.

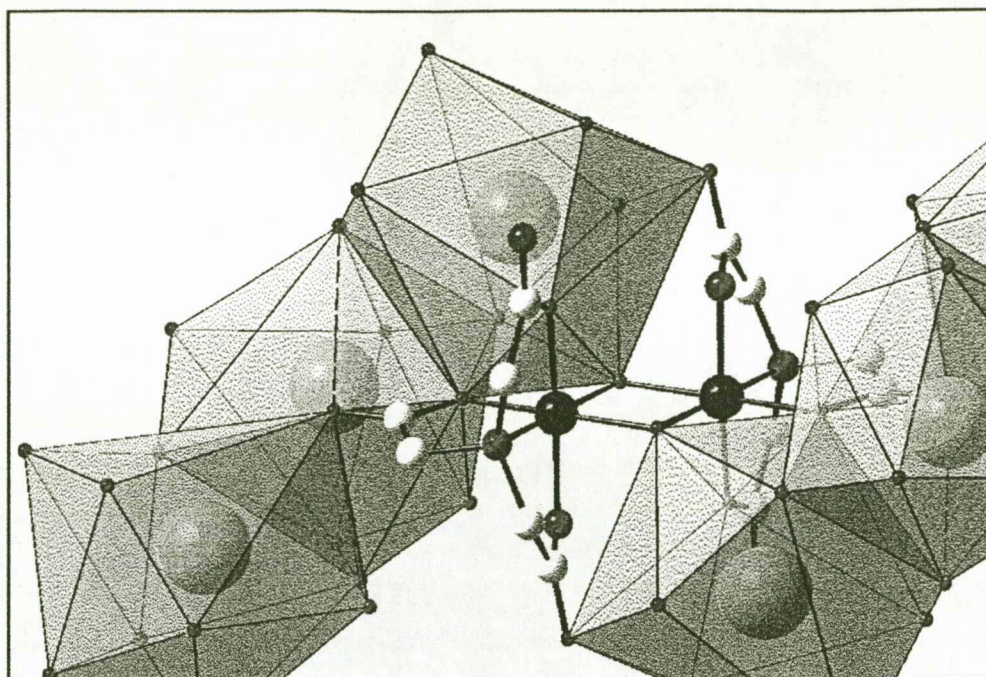


Figure 4.9. Packing of Cs⁺ cations around [Co(nta)(μ-OH)]₂²⁻.

A projection of [Co(nta)(μ-OH)]₂²⁻ along the b axis is shown in Figure 4.10. The complex anions lie in layers parallel and diagonal to the a axis. A cavity (5.4 x 4.8 Å) is created in the middle of the unit cell. The carboxylate oxygens (O(5)) of the G1 ring chelate rings are protruding into the cavity and form hydrogen bonds with the nearby water molecules. Oxygen-oxygen contact distances are 2.887(6) and 2.902(6) Å respectively, which correspond well with those of the isomorphous chromium structure (refer to Paragraph 4.3.1).

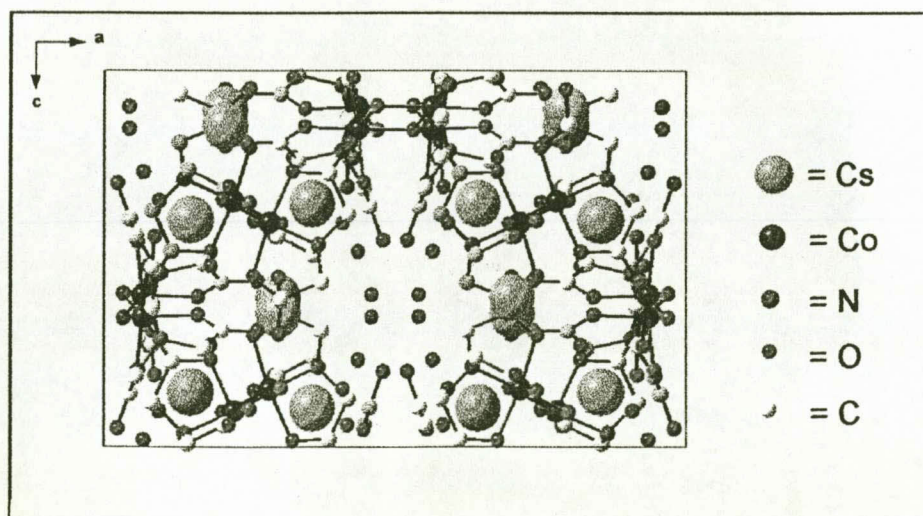


Figure 4.10. Projection of Cs₂[Co(nta)(μ-OH)]₂·4H₂O along the b axis.

4.4.1.1 Comparison of the strain in $Cs_2[Co(nta)(\mu-OH)]_2 \cdot 4H_2O$ with the isomorphous chromium structure (I in Paragraph 4.3)

Table 4.12 lists important structural data for the two complexes in question. It seems as if the strain in the two structures are more or less the same as expected. Significant differences are observed for the O_G-M-O_G bond angle of the cobalt structure which is almost 8° larger than for chromium. The nta bite angles are also significantly larger for the cobalt structure. The M-N and M-O bonding distances for these two structures are basically the same if one considers the fact that the ionic radii of low spin Co(III) metal centres are 0.07 Å smaller than Cr(III) centres (Shannon, 1976:751). The differences in bite angles and O-M-O angles can also be contributed to the difference in ionic radii.

Table 4.12. Selected structural data for $[Co(nta)(\mu-OH)]_2^{2-}$ and $[Cr(nta)(\mu-OH)]_2^{2-}$.

	$[Co(nta)(\mu-OH)]_2^{2-}$	$[Cr(nta)(\mu-OH)]_2^{2-}$
Average sum of G ring endocyclic angles ($^\circ$)	529.1	530.1
Average distances from $CCO_{G\text{-ring}}$ planes (Å)		
N	0.35	0.34
M (=Cr/Co)	0.26	0.31
Torsion Angles ($^\circ$)		
M-N-C-C (average of G rings)	29.8	29.0
O-M-N-C	27.8	27.1
Other bond angles ($^\circ$)		
O_G-M-O_G	172.0(2)	164.1(3)
C_G-N-C_G	115.7(6)	114.2(9)
M-OH-M	98.2(2)	98.5(3)
OH-M-OH	81.8(2)	81.5(3)
R ring bite angle ($^\circ$)	88.1(2)	85.0(3)
Average of G ring bite angles ($^\circ$)	86.1(1)	82.3(2)

4.4.2 Crystal structure of $\text{Cs}_2[\text{Co}(\text{nta})(\text{CO}_3)] \cdot \text{H}_2\text{O}$ (Visser et al., 2000b)

The crystallographic data are presented in Table 4.13.

Table 4.13. Crystal data and structure refinement for $\text{Cs}_2[\text{Co}(\text{nta})(\text{CO}_3)] \cdot \text{H}_2\text{O}$.

Empirical formula	$\text{C}_7\text{H}_7\text{CoCs}_2\text{NO}_{10}$
Formula weight	589.89
Temperature (K)	293(2)
Wavelength (Å)	0.71073
Diffractometer	Enraf-Nonius CAD4
Space group	$P2_1/c$
Unit cell dimensions	$a = 14.4646(7) \text{ \AA}, \alpha = 90^\circ$ $b = 7.7996(4) \text{ \AA}, \beta = 68.4220(10)^\circ$ $c = 13.5027(7) \text{ \AA}, \gamma = 90^\circ$
Volume (Å ³)	1416.59(12)
Z	4
Density (calculated) (Mg/m ³)	2.766
Absorption coefficient (mm ⁻¹)	6.325
F(000)	1092
Theta range for data collection (°)	1.51 to 28.26
Index ranges	$-8 \leq h \leq 19, -10 \leq k \leq 9, -17 \leq l \leq 17$
Reflections collected	8624
Independent reflections	3252 [R(int) = 0.0349]
Refinement method	Full-matrix least-squares on F ²
Data /restraints/parameters	3252/0/200
Goodness-of-fit on F ²	1.086
Final R indices [I > 2σ(I)]	$R_1 = 0.0249, wR_2 = 0.0609$
R indices (all data)	$R_1 = 0.0270, wR_2 = 0.0623$
Extinction coefficient	0.0258(5)
Largest diff. Peak and hole (e.Å ⁻³)	1.020 and -0.945

The numbering scheme of the molecule is shown in the perspective drawing in Figure 4.11.

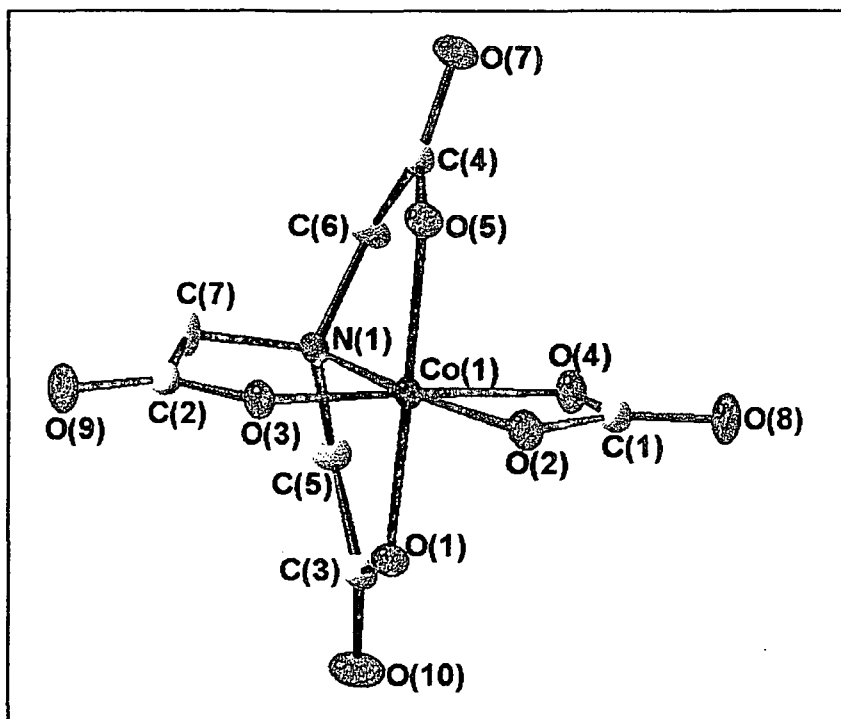


Figure 4.11. Perspective drawing of $[\text{Co}(\text{nta})(\text{CO}_3)]^{2-}$.

The most relevant bond distances and angles for the $\text{Cs}_2[\text{Co}(\text{nta})(\text{CO}_3)] \cdot \text{H}_2\text{O}$ molecule are reported in Tables 4.14 and 4.15.

Table 4.14. Selected bond lengths (Å) for $\text{Cs}_2[\text{Co}(\text{nta})(\text{CO}_3)] \cdot \text{H}_2\text{O}$.

Co-O(2)	1.908(2)	Co-N(1)	1.920(2)
Co-O(4)	1.889(2)	N(1)-C(5)	1.503(9)
Co-O(5)	1.902(2)	N(1)-C(3)	1.478(10)
Co-O(3)	1.901(2)	N(1)-C(2)	1.488(9)
Co-O(1)	1.897(2)		

X-ray Crystallography

Table 4.15. Selected bond angles ($^{\circ}$) for $\text{Cs}_2[\text{Co}(\text{nta})(\text{CO}_3)] \cdot \text{H}_2\text{O}$.

O(4)-Co(1)-O(1)	90.08(10)	O(5)-Co(1)-O(2)	91.98(9)
O(4)-Co(1)-O(3)	170.57(9)	O(4)-Co(1)-N(1)	100.91(9)
O(1)-Co(1)-O(3)	90.42(9)	O(1)-Co(1)-N(1)	87.99(10)
O(4)-Co(1)-O(5)	88.52(10)	O(3)-Co(1)-N(1)	88.52(9)
O(1)-Co(1)-O(5)	173.62(9)	O(5)-Co(1)-N(1)	86.17(10)
O(3)-Co(1)-O(5)	91.99(9)	O(2)-Co(1)-N(1)	170.26(9)
O(4)-Co(1)-O(2)	69.46(9)	C(5)-N(1)-C(7)	112.7(2)
O(1)-Co(1)-O(2)	93.36(9)	C(5)-N(1)-C(6)	114.3(2)
O(3)-Co(1)-O(2)	101.11(9)	C(7)-N(1)-C(6)	112.0(3)

The cobalt centre has a distorted octahedral geometry and is surrounded by three oxygen atoms and the nitrogen atom of the nta ligand (N(1), O(1), O(3) and O(5)) and the two oxygen atoms of the carbonato ligand, O(2) and O(4). The Co-N(1) bond distance is 1.920(2) Å while the Co-O_{nta} bond distances vary between 1.897(2) and 1.902(2) Å. The Co-O bond distances for the carbonato ligand are 1.889(2) and 1.908(2) Å. The rest of the N-C, C-C and C-O bond distances of the nta ligand are all considered normal and agree well with those found in $[\text{Ca}(\text{nta})] \cdot 2\text{H}_2\text{O}$ and Hnta (Skrzypczak-Jankun *et al.*, 1994:1097 and Whitlow, 1972:1914). The C-O bond distances of the carbonato ligand are 1.316(4), 1.312(4) and 1.233(4) Å and also agrees well with other bidentate cobalt(III)-carbonato complexes (Toriami & Saito, 1975:1247 and Bigoli *et al.*, 1980:1261).

The angular distortion around Co from the octahedral geometry is significant. The O-Co-O and N-Co-O angles deviate considerably from 90° and range between 69.46(9) and $100.91(9)^{\circ}$ while the O(1)-Co-O(5) angle is only $173.62(9)^{\circ}$. The O-Co-O bite angle of the carbonato ligand agrees well with other complexes (Toriami & Saito, 1975:1247 and Bigoli *et al.*, 1980:1261).

CHAPTER 4

The strain in the glycinato rings of nta is once again illustrated by its deviation from planarity (Weakliem & Hoard, 1959:549), refer to Table 4.16.

Table 4.16. Endocyclic angles, distances of N and Co from CCOO planes and torsion angles for $\text{Cs}_2[\text{Co}(\text{nta})(\text{CO}_3)] \cdot \text{H}_2\text{O}$.

	G1	G2	R
Endocyclic angles (°)	527.0(5)	532.3(6)	538.7(5)
N distance from CCOO* plane (Å)	-0.233(5)	-0.308(5)	-0.275(6)
Co distance from CCOO plane (Å)	0.520(4)	0.241(5)	-0.218(4)
Torsion Angles (°)			
N-Co-O-C	-28.5(2)	18.7(2)	1.9(2)
Co-O-C-C	15.8(3)	-6.5(3)	1.9(2)
N-C-C-O	10.9(4)	-14.3(4)	12.9(4)
Co-N-C-C	-30.7(3)	26.5(3)	-10.4(3)
O-Co-N-C	32.1(2)	-24.8(2)	5.1(2)

* CCOO plane = two carbons, one carboxylate oxygen and a bonded oxygen atom in a specific plane.

The sums of the endocyclic angles of the rings, the torsion angles and distances of Co and N from the CCOO planes are represented in Table 4.16. The endocyclic angles vary between 527.0(6) and 538.7(5) ° while the torsion angles and distances of Co and N from the CCOO planes also indicate lesser strain in the R ring. This observation is repeated in all known structures of Co(III)-nta complexes.

The nitrogen (nta) tetrahedron is significantly distorted from tetrahedral geometry with C-N-C angles varying between 112.0(3) and 114.3(2) °. This agrees well with those found for uncoordinated nta where C-N-C angles were between 112.3(1) and 113.6(1) °.

X-ray Crystallography

A projection of $\text{Cs}_2[\text{Co}(\text{nta})(\text{CO}_3)] \cdot \text{H}_2\text{O}$ along the *b* axis reveals that the complex molecules are packed in layers that stretch diagonally along the *ac* plane, Figure 4.12.

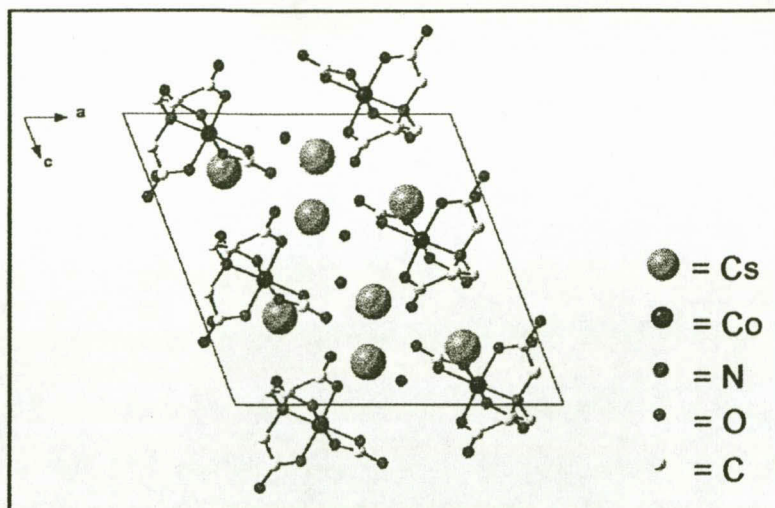


Figure 4.12. Projection of $\text{Cs}_2[\text{Co}(\text{nta})(\text{CO}_3)] \cdot \text{H}_2\text{O}$ along the *b* axis.

The geometry around $\text{Cs}(1)$ and $\text{Cs}(2)$ is in the form of bicapped trigonal prisms with Cs-O distances varying between 3.046(2) and 3.525(4) Å, Figure 4.13. One of the prisms is formed between $\text{Cs}(1)$ and O(1), O(2), O(3) of a specific Co-nta molecule and O(4), O(9), O(7) and O(10) from different molecules. A water molecule fills the other available position. The other prism is formed between $\text{Cs}(2)$ and O(7), O(3), O(5) of a specific Co-nta molecule; O(8) and O(2) from another molecule; two water molecules and O(8) from yet another molecule.

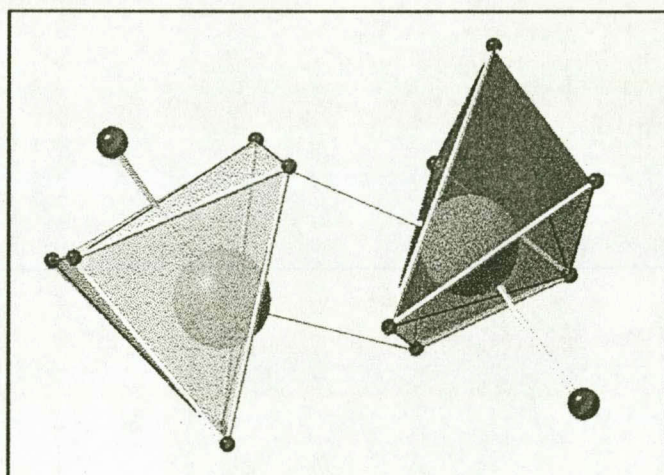


Figure 4.13. Arrangement of oxygen atoms around Cs^+ in $\text{Cs}_2[\text{Co}(\text{nta})(\text{CO}_3)] \cdot \text{H}_2\text{O}$.

The interaction of Cs^+ cations with the anion is extensive in this case, making it impossible to illustrate with different polyhedra as in the previous structures. The

interaction of the cations with R ring oxygen atoms seems to be substantial, possibly leading to the slight distortion of the R ring (Co and N is more than 0.2 Å from the CCOO plane). Figure 4.14 (a) and (b) illustrates the interaction of Cs^+ cations with $[\text{Co}(\text{nta})(\text{CO}_3)]^{2-}$.

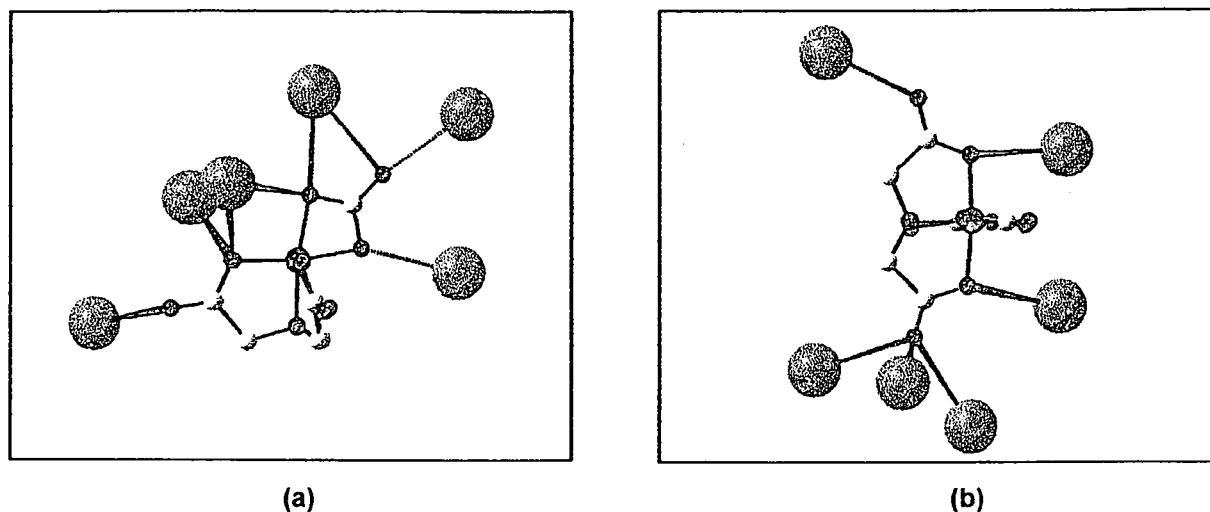


Figure 4.14. Interaction of Cs^+ cations with $[\text{Co}(\text{nta})(\text{CO}_3)]^{2-}$ (a) with R ring and carbonato ligand oxygen atoms and (b) with G ring oxygen atoms.

The only notable intermolecular interaction in terms of hydrogen bonding is observed between O(5) and the water molecule, Ow(1), where an O-O interatomic distance of 2.827(5) Å was recorded.

4.4.3 Crystal structure of [Co(nta)(N,N-Et₂en)] (Visser et al., 2000a)

The crystallographic data for [Co(nta)(N,N-Et₂en)] is listed in Table 4.17.

Table 4.17. Crystal data and structure refinement for [Co(nta)(N,N-Et₂en)].

Empirical formula	C ₁₂ H ₂₂ CoN ₃ O ₆
Formula weight	363.26
Temperature (K)	293(2)
Wavelength (Å)	0.71073
Diffractometer	CAD-4
Crystal system	Orthorhombic
Space group	Pbcm
Unit cell dimensions	a = 10.186(2) Å, α = 90° b = 13.105(3) Å, β = 90° c = 11.540(2) Å, γ = 90°
Volume (Å ³)	1540.4(5)
Z	4
Density (calculated) (Mg/m ³)	1.566
Absorption coefficient (mm ⁻¹)	1.147
F(000)	760
Crystal size (mm)	0.15x0.20x0.24
Theta range for data collection (°)	2.00 to 25.97
Index ranges	0 ≤ h ≤ 12, -16 ≤ k ≤ 0, 0 ≤ l ≤ 14
Reflections collected	1591
Independent reflections	1591 [R(int)=0.0000]
Refinement method	Full-matrix least-squares on F ²
Data /restraints/parameters	1590/0/143
Goodness-of-fit on F ²	1.227
Final R indices [I > 2σ(I)]	R ₁ =0.0309, wR ₂ =0.0637
R indices (all data)	R ₁ =0.0981, wR ₂ =0.1000
Largest diff. Peak and hole (e/Å ³)	1.135 and -0.906

The numbering scheme of the molecule is shown in the perspective drawing in Figure 4.15

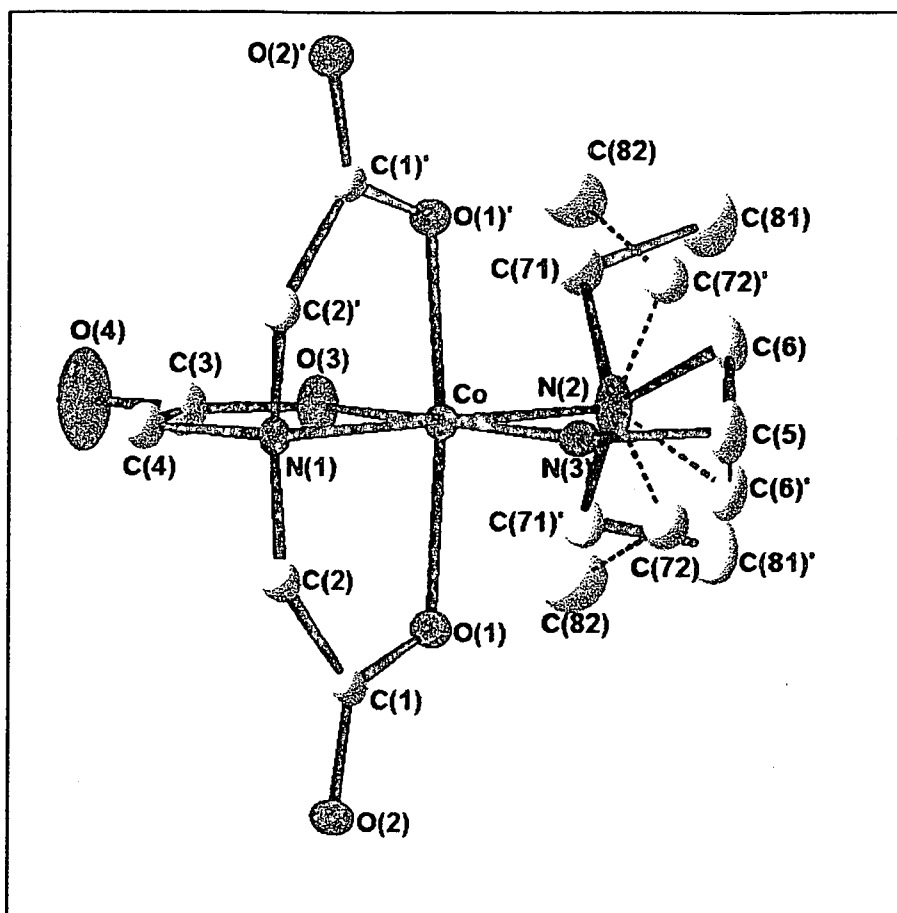


Figure 4.15. Perspective drawing of $[\text{Co}(\text{nta})(\text{N},\text{N}\text{-Et}_2\text{en})]$.

The most relevant bond distances and angles for the $[\text{Co}(\text{nta})(\text{N},\text{N}\text{-Et}_2\text{en})]$ molecule are reported in Tables 4.18 and 4.19.

Table 4.18. Selected bond lengths (\AA) for $[\text{Co}(\text{nta})(\text{N},\text{N}\text{-Et}_2\text{en})]$.

Co-O(3)	1.884(4)	N(3)-C(5)	1.472(7)
Co-O(1)	1.905(2)	N(1)-C(2)	1.475(4)
Co-N(1)	1.950(4)	N(1)-C(4)	1.505(6)
Co-N(3)	1.953(4)	N(2)-C(72)	1.348(9)
Co-N(2)	2.011(5)	N(2)-C(6)	1.553(8)
N(2)-C(71)	1.601(10)		

X-ray Crystallography

Table 4.19. Selected bond angles ($^{\circ}$) for [Co(nta)(*N,N*-Et₂en)].

O(3)-Co-O(1)	91.03(8)	N(1)-Co-N(3)	95.0(2)
O(3)-Co-N(1)	87.9(2)	O(3)-Co-N(2)	91.1(2)
O(1)-Co-N(1)	85.46(7)	O(1)-Co-N(2)	94.56(7)
O(3)-Co-N(3)	177.0(2)	N(1)-Co-N(2)	179.1(2)
O(1)-Co-N(3)	89.21(8)	N(3)-Co-N(2)	85.9(2)
C(2)-N(1)-C(4)	110.5(2)		

The R ring of nta, the nitrogen atoms of *N,N*-Et₂en and the cobalt centre lie in a mirror plane around which some disordered arrangements are observed. The ethyl substituents of *N,N*-Et₂en have a disorder arrangement with a 50% occupancy for the two carbon atoms. The carbon atom of the ethane chain, C(6), also has this disorder arrangement around the mirror plane. The distance of C(6) from the plane was calculated as 0.689(3) Å.

The cobalt centre has a distorted octahedral geometry and is surrounded by three oxygen atoms and the nitrogen atom of the nta ligand (N(1), O(1), O(1)' and O(3)) and the two nitrogen atoms of the ethylenediamine molecule, N(2) and N(3). The Co-N(1) bond distance is 1.950(2) Å while the two Co-O bond distances are 1.884(4) and 1.905(2) Å respectively. The Co-N(2) bond distance (*trans* to the nta-nitrogen) is 2.011(5) Å, significantly longer than the Co-N(3) bond distance of 1.953(4) Å which bonded *trans* to a carboxylate oxygen atom. The rest of the N-C, C-C and C-O bond distances of the nta ligand are all considered normal and agree well with those found in [Ca(nta)].2H₂O and Hnta (Skrzypczak-Jankun *et al.*, 1994:1097 and Whitlow, 1972:1914).

The angular distortion around Co from the octahedral geometry is significant. The O-Co-O, N-Co-N and N-Co-O angles deviate from 90° and range between 85.46(7) and 95.0(2)° while the O(1)-Co-O(1)' angle is only 170.6(2)°.

The sums of the endocyclic angles, the torsion angles and the distances of Co and N_{nta} from the CCOO planes of the G rings are presented in Table 4.20. The strain in nta complexes is expressed by the deviation from planarity of the acetate rings of nta (Weakliem & Hoard, 1959:549). The R ring in this structure lies on the mirror plane and is perfectly planar, therefore the torsion angles in this ring are all equal to zero. It can

be seen from Table 4.20 that the R ring is less strained than the G rings as with all the previous structures.

Table 4.20. Endocyclic angles, distances of N and Co from the G ring CCOO plane and torsion angles for [Co(nta)(N,N-Et₂en)].

	G1 = G2
Endocyclic angles (°)	530.3(3)
N distance from CCOO* plane (Å)	-0.508(7)
Co distance from CCOO plane (Å)	0.027(5)
Torsion Angles (°)	
N-Co-O-C	-15.5(30)
Co-O-C-C	-0.4(4)
N-C-C-O	22.7(5)
Co-N-C-C	-32.1(4)
O-Co-N-C	26.5(3)

* CCOO plane = two carbons, one carboxylate oxygen and a bonded oxygen atom in a specific plane.

The nitrogen (nta) tetrahedron is significantly distorted, especially the C(2)-N(1)-C(2)' angle of 116.8(4) ° which differs substantially from the tetrahedral geometry. This is more than what was found for uncoordinated nta where C-N-C angles were between 112.3(1) and 113.6(1) °. The other angles around the nitrogen tetrahedron in the title complex vary between 105.8(2) (C-N-Co) and 110.5(2) ° (C-N-C). The Co and N atoms are displaced on different sides of the CCOO planes of the G rings, with Co being 0.027(5) Å and N 0.508(7) Å from the plane in each case.

A projection of [Co(nta)(N,N-Et₂en)] along the a axis reveals that the complex molecules are stacked in layers that stretch vertically across the bc plane (Figure 4.16). No hydrogen bonding of note is observed.

A comparison between the bond distances of the title complex, [Co(nta)(en)] (Gladkikh *et al.*, 1992:980) and [Co(nta)(propen)] (propen = 1,3-propanediamine) (Swaminathan *et al.*, 1989:566) indicates that Co-N_{nta} distances are the same within experimental error. The Co-N_{nta} distance in the title complex is 1.950(4) compared to 1.946(3) for

[Co(nta)(en)] and 1.962(3) Å for [Co(nta)(propen)] respectively. The Co-O_{nta} bond distances of [Co(nta)(*N,N*-Et₂en)] and [Co(nta)(en)] are also similar and vary between 1.884(4) and 1.905(2) Å for [Co(nta)(*N,N*-Et₂en)] and between 1.892(3) and 1.896(3) Å for [Co(nta)(en)]. In contrast to the other complexes the difference in Co-O_{nta} bond distances of [Co(nta)(propen)] is substantial. The bond lengths vary between 1.857(3) Å and 1.947(3) Å.

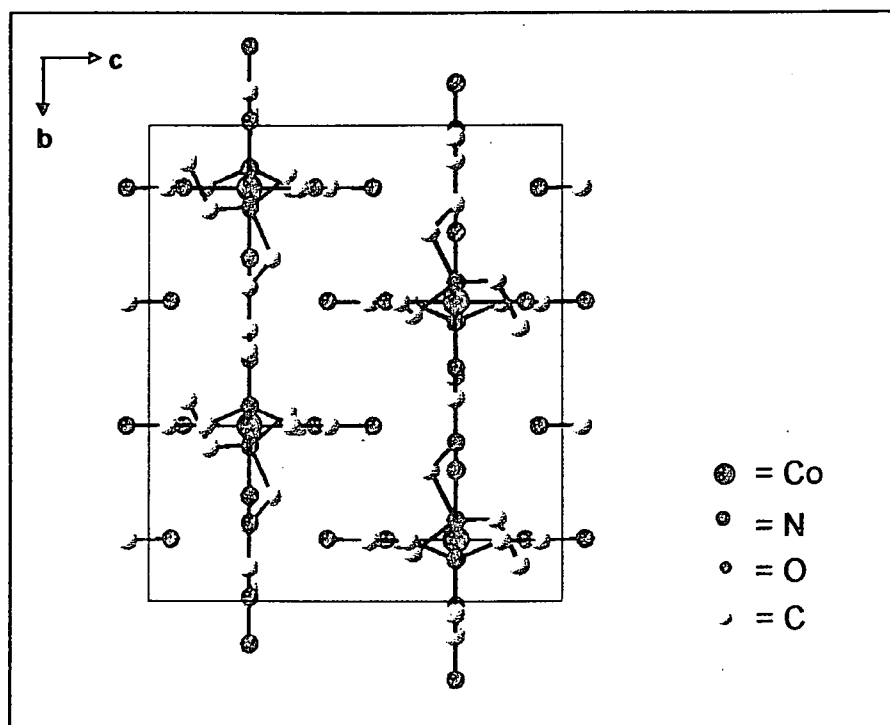


Figure 4.16. Projection of [Co(nta)(*N,N*-Et₂en)] along the *a* axis.

The Co-N bond *cis* to N_{nta} in [Co(nta)(*N,N*-Et₂en)] is 1.953(4) Å compared to 1.969(3) in [Co(nta)(en)] and 1.948(4) Å in [Co(nta)(propen)].

The Co-N bond length *trans* to N_{nta} in the title complex is significantly longer than in the other two complexes. The Co-N(2) bond in [Co(nta)(*N,N*-Et₂en)] is 2.011(5) Å compared to 1.941(3) for [Co(nta)(en)] and 1.940(3) Å for [Co(nta)(propen)]. This can possibly be attributed to steric repulsion between the glycinato rings of nta and the substituted nitrogen of *N,N*-Et₂en since the p*K*_a values of ethylenediamine and *N,N*-Et₂en are almost the same (9.96 and 10.02) (Meites, 1963), thereby ruling out huge differences in electronic factors. Furthermore the ring strain described by the sum of the endocyclic angles of the glycinato rings in these complexes is in the same order so that the longer Co-N bond distance in [Co(nta)(*N,N*-Et₂en)] cannot be attributed to extra strain in the molecule.

The glycinato rings in $[\text{Co}(\text{nta})(\text{N},\text{N}\text{-Et}_2\text{en})]$ are not lesser strained than the rings of anionic complexes where the presence of a cationic species might have an influence. The sums of the endocyclic angles of the glycinato rings of $[\text{Co}(\text{nta})(\mu\text{-OH})]_2^{2-}$ are 525.3, 533.1 and 538.4° respectively and compare very well with the title complex.

4.5 Conclusion

The Co(III)-nta and Cr(III)-nta complexes first prepared by Mori *et al.* (1958:940) and Uehara *et al.* (1967:2317) have not been characterised with X-ray crystallography before. $[\text{Co}(\text{nta})(\mu\text{-OH})]_2^{2-}$ and $[\text{Cr}(\text{nta})(\mu\text{-OH})]_2^{2-}$ have been isolated and characterised with X-ray crystallography for the first time. $[\text{Co}(\text{nta})(\text{CO}_3)]^{2-}$ has also been synthesised and characterised with X-ray crystallography (Chapter 3 and this chapter). It has also been shown that either $[\text{Co}(\text{nta})(\mu\text{-OH})]_2^{2-}$ or $[\text{Co}(\text{nta})(\text{CO}_3)]^{2-}$ can be used as starting material for the synthesis of many different Co(III)-nta complexes, of which $[\text{Co}(\text{nta})\text{N},\text{N}\text{-Et}_2\text{en}]$ is one example (Scheme 4.1).

A comparison of selected features of all the known structures of Co(III)-nta complexes is shown in Table 4.21. The following observations can be made.

- (1) The average strain in the G rings of all the structures is equal.
- (2) The R rings are almost perfectly planar in all the structures.
- (3) The R ring bite angles are slightly closer to 90 ° than the average of the G ring bite angles.
- (4) The angular strain experienced by the nitrogen of nta is most pronounced in the $\text{C}_G\text{-N-C}_G$ angles, which are almost similar for all complexes studied.
- (5) The Co-N_{nta} bond distances vary slightly, especially when moving from $[\text{Co}(\text{nta})(\mu\text{-OH})]_2^{2-}$ to $[\text{Co}(\text{nta})(\text{propen})]$ where a difference of 0.04 Å is observed.
- (6) The Co-O_{nta} bonding distances are the same within experimental error. This is different to what was found for Cr(III)-nta complexes where the Cr-O_{G ring} distances were slightly longer than the R ring Cr-O distances (Paragraph 4.3.2).
- (7) All the other bonding features of the different Co(III)-nta complexes are the same within experimental error, even though there are substantial differences in charge and therefore packing features as well as bidentate ligand ring sizes.

X-ray Crystallography

Table 4.21. Selected features of different Co(III)-nta complexes.

Complex	Reference	^a Co-N _{nta} (Å)	^b G _{end} (°)	^c G _{bite} (°)	^d R _{bite} (°)	^e O _G -Co-O _G (°)	^f C _G -N-C _G (°)
[Co(nta)(μ-OH)] ₂ ²⁻	This study	1.922(6)	529.0	86.1	88.1(2)	172.0(2)	115.7(6)
[Co(nta)(CO ₃)] ₂ ²⁻	This study	1.920(2)	529.0	87.3	88.52(9)	173.62(9)	114.3(2)
[Co(nta)(en)]	Gladkikh <i>et al.</i> (1992:1231)	1.946(3)	529.8	86.5	87.6(1)	172.6(1)	116.3(3)
[Co(nta)(gly)]	Gladkikh <i>et al.</i> (1992:908)	1.928(8)	531.3	86.4	89.3(3)	172.5(3)	115.6(7)
[Co(nta)(viol)]	Almazán <i>et al.</i> (1990:2565)	1.942(7)	529.9	86.5	89.4(3)	172.8(3)	115.3(7)
[Co(nta)(NN-Et ₂ en)]	This study	1.950(4)	530.3	85.5	87.9(2)	170.6(2)	116.8(4)
[Co(nta)(propen)]	Swaminathan & Sinha (1989:566)	1.962(2)	529.5	85.3	86.8(1)	170.5(1)	115.5(4)

^a Bonding distance of Co to nitrogen of nta

^b Average of the sums of the endocyclic angles of G rings

^c Average of N-O bite angles of G rings

^d R ring bite angles

^e Bonding angle of Co to G ring oxygen atoms

^f Bonding angle of N of nta to C atoms of G rings

It was suggested in Paragraph 4.3.2 that part of the reason for the planarity of the R rings in Cr(III)-nta complexes is due to a Jahn-Teller type of stabilisation of the metal dx^2-y^2 orbitals and destabilisation of the dz^2 orbitals. Cr(III) is a d^3 species, but the extra electron density donated by the nta ligand to the metal centre gives it more of a Cr(II) (d^4 species) character. This observation was well supported by the crystallographic data where the axial bond distances were seen to be longer than the equatorial bond distances.

The same observation is not made for the Co(III)-nta complexes. The axial and equatorial bond distances around the Co(III) centre are the same within experimental error. In spite of this we conclude that the reason for planar glycinato R rings and non-planar G rings in Co(III)-nta complexes are basically the same as for Cr(III)-nta complexes. The extra electron density donated to the Co(III) centre by the electron rich

nta ligand gives it more of a d^7 than d^6 character. This implies stabilisation of the metal dx^2-y^2 orbitals and destabilisation of the dz^2 orbitals which in turn means better overlap in the equatorial (R ring) position. The fact that the R ring bite angles are slightly closer to 90° than the average of the G ring bite angles (Table 4.20) support this theory to some degree.

It is obvious from this study that more evidence is required to explain with total conviction why the R rings in these complexes are not strained. Molecular modulations/calculations for example could give more information on this phenomenon, but unfortunately does not fall in the scope of this study. It is possible that the reason/s for unstrained R rings and strained G rings might be a combination of electronic (Jahn Teller type distortions) and thermodynamic effects.

5

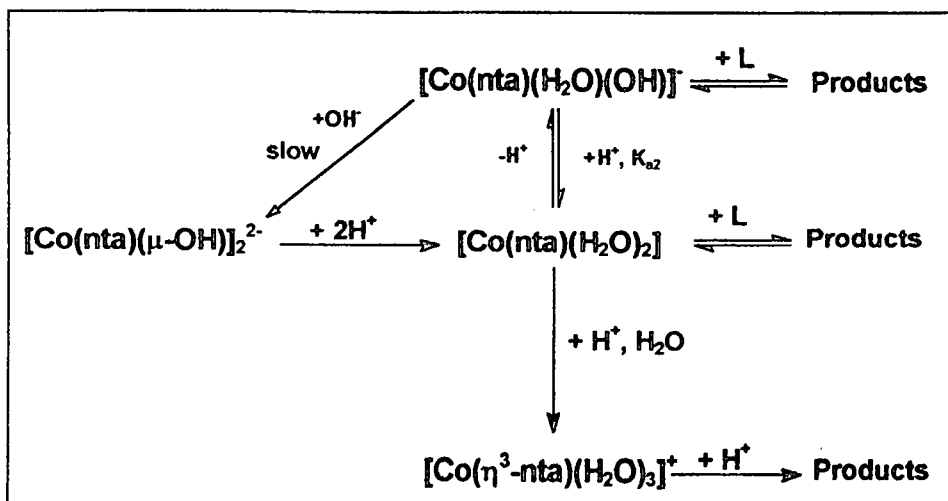
Kinetic study of the reactions of *cis*-[Co(nta)(H₂O)₂]

5.1 Introduction

The UV/VIS results reported earlier (Paragraph 3.4.1.1) clearly point to a stable [Co(nta)(μ-OH)]₂²⁻ complex (dimer) in slightly alkaline solution, which when protonated, immediately forms the *cis*-diaqua complex, [Co(nta)(H₂O)₂]. Addition of base to this di-aqua complex forms the aquahydroxo complex, [Co(nta)(H₂O)(OH)]⁻. This protonation reaction is reversible (refer to Equation 3.1). It was also observed that the aquahydroxo complex changed back to the dimer at pH 6 – 7 upon standing for several days.

The mechanism of the acidic bridge cleavage reactions of [Co(nta)(μ-OH)]₂²⁻ have been investigated by other groups (Thacker & Higginson, 1975:704 and Meloon & Harris, 1977:434) and have been discussed in detail in Chapter 2. Both these groups observed two reactions upon the addition of acid to [Co(nta)(μ-OH)]₂²⁻ and contributed this observation to the cleavage of the μ-hydroxo bridges. None of these workers included a detailed pH dependence study of [Co(nta)(μ-OH)]₂²⁻. This leaves some doubt on the influence of H⁺ ions on the behaviour of the Co(III)-nta system at low pH. The possibility of the protonation of the carboxylate groups of coordinated nta and subsequent ring-opening reactions as observed for the reaction of [Cr(nta)(H₂O)₂] with H⁺ ions, was also not investigated (Visser *et al.*, 1994:1051).

This chapter deals with the influence of H⁺ ions on the behaviour of the Co(III)-nta system in aqueous medium and with the substitution reactions of [Co(nta)(H₂O)₂] with NCS⁻ ions as well as H⁺ ions (Scheme 5.1). The first pH study involves the protonation properties of the [Co(nta)(μ-OH)]₂²⁻ dimer, while the second part of the chapter deals with the protonation/deprotonation of the [Co(nta)(H₂O)₂] complex and its subsequent reactions with acid. The last part of this chapter deals with the substitution reactions between [Co(nta)(H₂O)₂] and NCS⁻ ions.



Scheme 5.1. Formation and reactions of $[\text{Co(nta)(H}_2\text{O)}_2]$.

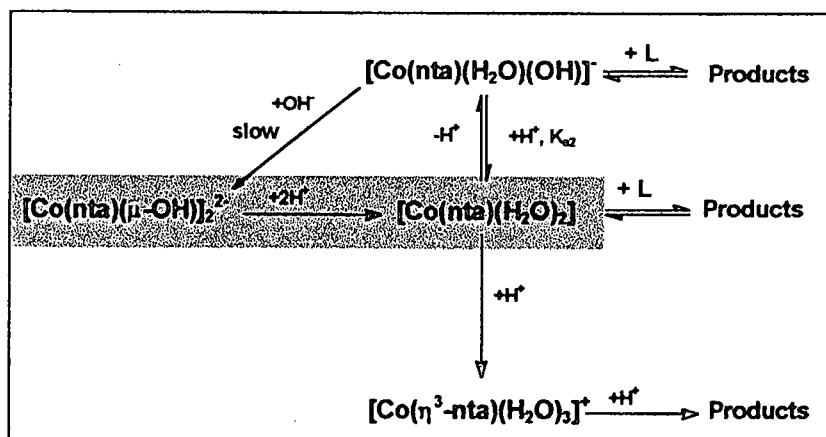
5.2 Experimental Procedures

All reagents and chemicals were of analytical grade and double distilled water was used in all experiments. All pH measurements were done on a Hannah model 8519 pH meter using standard buffer solutions for calibration. Kinetic measurements were done on a GBC 916 spectrophotometer. Temperature control of the reaction solutions was maintained to within ± 0.1 °C by means of a circulating water bath system. The Scientist (Micromath, 1990) program was used to fit the data to selected functions. All the kinetic runs were performed under pseudo first-order conditions with the ligand in excess in each case. The ionic strength of all the reaction solutions were kept constant by addition of NaClO_4 . Linear plots of $\log(A_\infty - A_t)$ vs time were obtained for at least two half-lives under all conditions. The solid lines in the figures represent computer least squares fits of data, while the experimentally determined values are represented by dots. Detailed tables of the experimental values are given in Appendix A.

5.3 Results and Discussion

5.3.1 Influence of H⁺ ions on the Co(III)-nta system

5.3.1.1 pH dependance of [Co(nta)(μ-OH)]₂²⁻



Scheme 5.1.1. pH dependance of [Co(nta)(μ-OH)]₂²⁻.

The pH dependance of [Co(nta)(μ-OH)]₂²⁻ was studied at room temperature between pH 2 and 6. In general, for protonation of diprotic species as defined by Equations 5.1 and 5.2, UV/VIS studies of the acid/base behaviour of diprotic complexes such as H₂A is given by Equation 5.3.



$$A_{\text{tot}} = \frac{A_a + A_h(K_{a1}/[\text{H}^+]) + A_o(K_{a1}K_{a2}/[\text{H}^+]^2)}{1 + (K_{a1}/[\text{H}^+]) + K_{a1}K_{a2}/[\text{H}^+]^2} \quad (5.3)$$

In Equation 5.3 A_{tot} is the absorbance at a specific [H⁺], A_a = absorbance of the H₂A species, A_o = absorbance of A²⁻, A_h = absorbance of HA⁻ and K_{a1} and K_{a2} the acid dissociation constants. Our results did not exhibit the expected diprotic behaviour for the protonation of [Co(nta)(μ-OH)]₂²⁻, leading to a simplified version of Equation 5.3 for

determining the acid dissociation constant of a monoprotic species, refer to Equations 5.4 and 5.5.



$$A = \frac{A_h + A_o(K_{a1}/[\text{H}^+])}{1 + (K_{a1}/[\text{H}^+])} \quad (5.5)$$

In Equation 5.5 A is the absorbance at a specific $[\text{H}^+]$, A_h = absorbance of the HB species, A_o = absorbance of B^- and K_{a1} the acid dissociation constant.

The acid dissociation constant of $[\text{Co}(\text{nta})(\mu\text{-OH})_2]^{2-}$ was determined spectrophotometrically at $\lambda = 320$ nm and 25.0 °C by adjusting the pH of a 2×10^{-3} M $[\text{Co}(\text{nta})(\mu\text{-OH})_2]^{2-}$ solution and immediately measuring the absorbance. This procedure was not followed below $\text{pH} \approx 2.0$ in order to avoid the reactions of $[\text{Co}(\text{nta})(\text{H}_2\text{O})_2]$ with H^+ ions (Paragraph 5.3.1.3). The results were fitted to Equation 5.5 and are illustrated in Figure 5.1. The $\text{p}K_a$ was determined as 3.09(3).

The change in absorbance occurs over 2 pH units, possibly indicating that both hydroxo groups are protonated at the same time, or that the two dissociation constants are very close to being equal. It is also possible that the change of absorbance for one of the protonation steps is very small, so that it can not be determined under the current experimental conditions.

It can be concluded from these results that the fast change in spectrum observed upon acidification of $[\text{Co}(\text{nta})(\mu\text{-OH})_2]^{2-}$ (refer to Figure 3.1) is in fact a protonation step or possibly even two steps and that the final complex that forms under these experimental conditions most probably is $[\text{Co}(\text{nta})(\text{H}_2\text{O})_2]$. Further discussion of this data is undertaken in Paragraph 5.3.1.3.

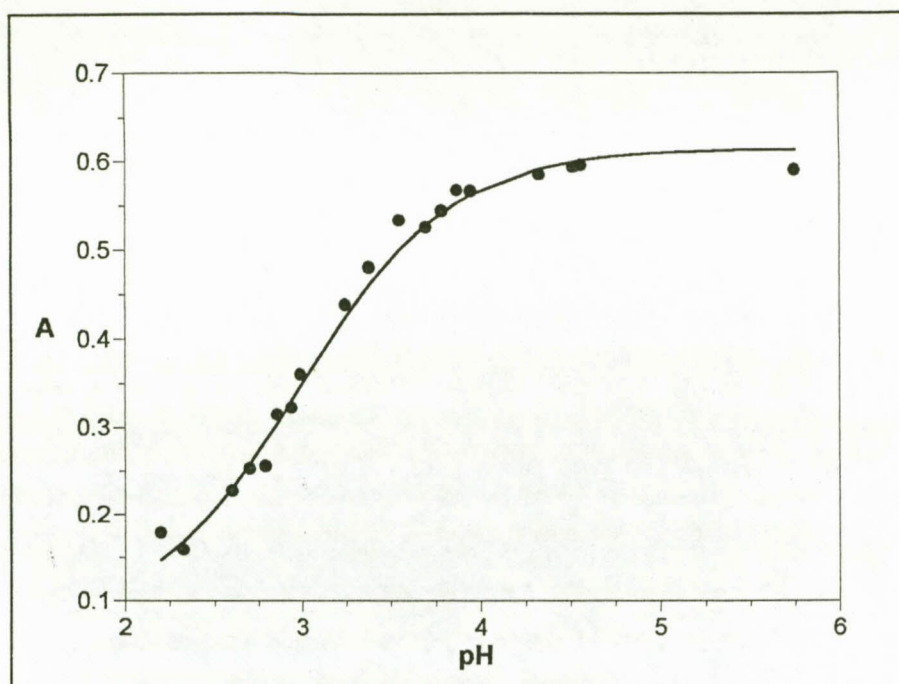
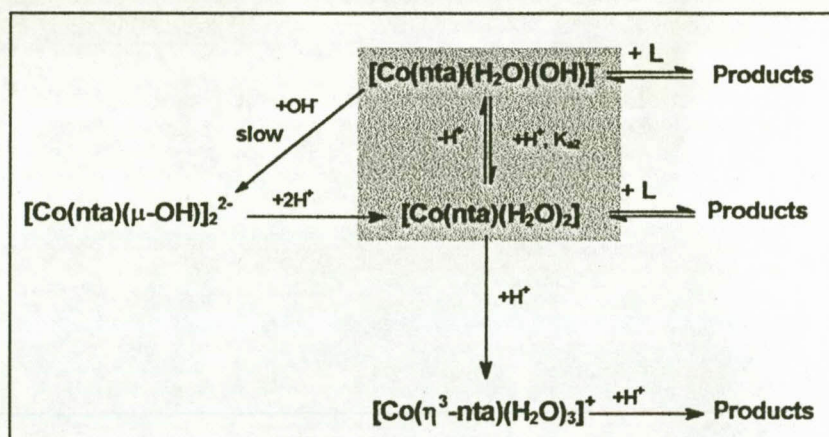


Figure 5.1. Plot of A ($\lambda = 320 \text{ nm}$) vs. pH for the $[\text{Co}(\text{nta})(\mu\text{-OH})_2]^{2-}$ system, $25.0 \text{ }^\circ\text{C}$, $\mu = 1.0 \text{ M}$ (NaClO_4), $[\text{dimer}] = 2 \times 10^{-3} \text{ M}$.

5.3.1.2 pH dependence of $[\text{Co}(\text{nta})(\text{H}_2\text{O})_2]$



Scheme 5.1.2. pH dependence of $[\text{Co}(\text{nta})(\text{H}_2\text{O})_2]$.

It was observed in Paragraph 3.4.1.1 that the aquahydroxo complex reverts back to the dimer at pH 6 – 7 upon standing for several days. Spectroscopic results indicated that this reaction becomes faster as the pH is increased. In order to avoid complication by competitive reactions, it was decided to keep the reaction conditions between pH 2 – 7.

The $[\text{Co}(\text{nta})(\text{H}_2\text{O})_2]$ complex was obtained by acidifying a $[\text{Co}(\text{nta})(\mu\text{-OH})]_2^{2-}$ solution to $\text{pH} = 2.0$ (HClO_4) and allowing it to stand for 30 minutes (also refer to Chapters 2 & 3). The acid dissociation constant of $[\text{Co}(\text{nta})(\text{H}_2\text{O})_2]$, K_{a2} , (Equation 5.6) was determined spectrophotometrically at $\lambda = 400$ nm and 25.0 °C by adjusting the pH of a $[\text{Co}(\text{nta})(\text{H}_2\text{O})_2]$ solution (8×10^{-3} M) and immediately measuring the absorbance. The results were fitted to Equation 5.5 and are illustrated in Figure 5.2.

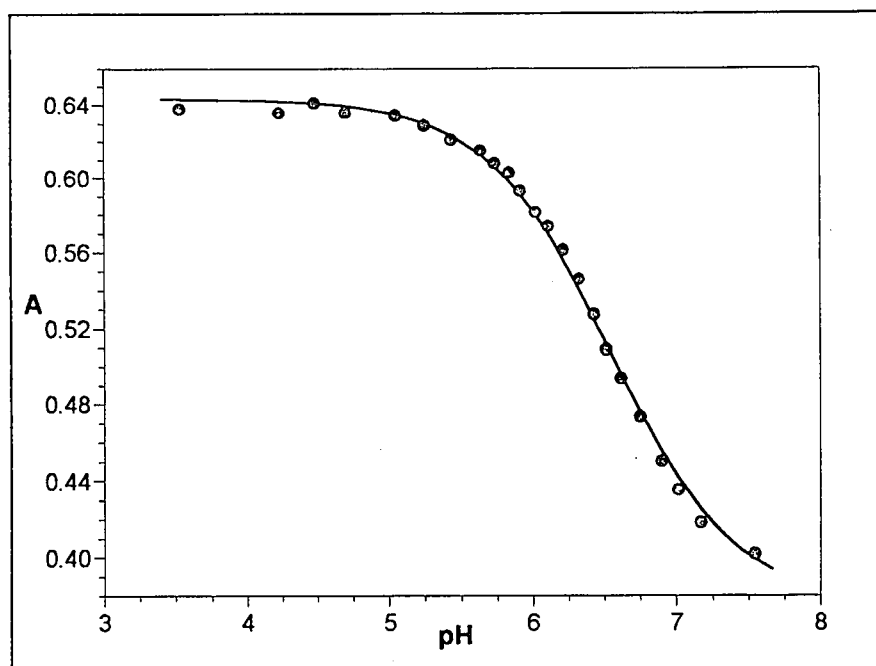
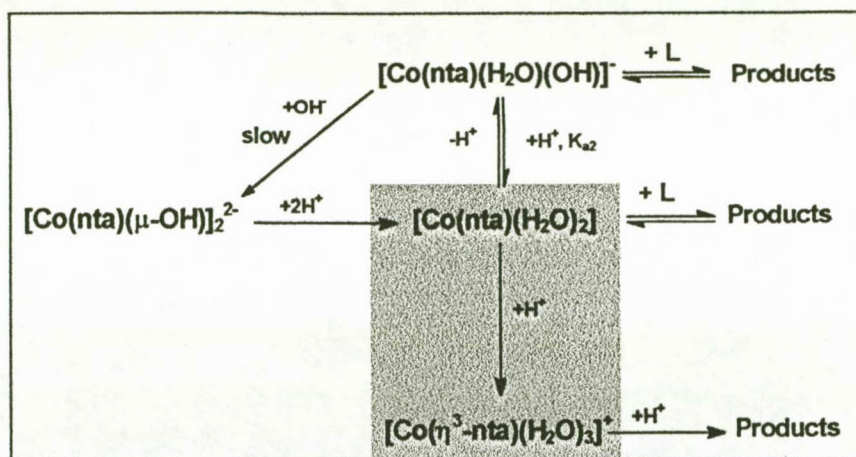


Figure 5.2. Plot of Abs ($\lambda = 400$ nm) vs. pH for $[\text{Co}(\text{nta})(\text{H}_2\text{O})_2]$ (2×10^{-3} M), 25.0 °C, $\mu = 1.0$ M (NaClO_4).

The value for $\text{p}K_{a2}$ was determined as 6.52(2). This compares well with the value of 6.71(1) determined by Thacker and Higginson (1975:704) for the " β -form" of Co(III)-nta used in their study. The value of $\text{p}K_{a2}$ is also higher than what was found for the similar acid dissociation equilibrium involving $[\text{Cr}(\text{nta})(\text{H}_2\text{O})_2]$, $\text{p}K_a = 5.43$ (Hualin and Xu, 1990:137).

5.3.1.3 Reaction of [Co(nta)(H₂O)₂] with H⁺ ions

 Scheme 5.1.3. Reaction of [Co(nta)(H₂O)₂] with H⁺ ions.

A slow change in spectrum was observed after lowering the pH of solutions of [Co(nta)(H₂O)₂] (pH < 1.0). This does not correspond to normal protonation reactions as was observed in Paragraph 3.4.1.1.

The possibility of substitution reactions with different ligands in solution at these pH values were eliminated by the study of the reactions between [Co(nta)(H₂O)₂] and strong acids with non-coordinating anions, see Table 5.1.

Table 5.1. Observed rate constants for the reaction between [Co(nta)(H₂O)₂] and different acids and anions, 25.0 °C.

Reactant	(10 ³)k _{obs} (s ⁻¹)
0.2 M HCl	9.79(4)
0.2 M HCl + 0.4 M NaCl	9.81(2)
0.2 M HClO ₄	9.83(3)
0.4 M HCl	19.3(4)

[Co(nta)(H₂O)₂] was obtained by acidifying solutions of the dimer to pH = 2.0. It can be seen from Table 5.1 that the observed rate constant remains the same within experimental error upon addition of different acids (HCl and HClO₄) to this solution and that this rate remains the same even upon addition of an excessive amount of Cl⁻. Furthermore, the increase in k_{obs} with increase in [H⁺] clearly indicate that the observed

reaction is in fact between $[\text{Co}(\text{nta})(\text{H}_2\text{O})_2]$ and H^+ ions. This same procedure was also followed previously for the reaction between $[\text{Cr}(\text{nta})(\text{H}_2\text{O})_2]$ and H^+ ions (Visser *et al.*, 1994:1051).

In order to identify the final products in this reaction, the dimer was dissolved in acidic solution ($\text{pH} = 1$) and allowed to stand for a few days. The resulting precipitate was isolated and the ^1H NMR spectrum was obtained. The spectrum showed no sign of coordinated nta, indicating that the observed reaction is possibly the stepwise dissociation of the tetradentate ligand.

A study of the reactions between $[\text{Co}(\text{nta})(\text{H}_2\text{O})_2]$ and H^+ ions at low pH and at different temperatures showed non-linear kinetics, see Figure 5.3. Keeping this in mind as well as the fact that nta dissociates from the metal in acidic solution, Scheme 5.2 is proposed for describing the observed kinetics.

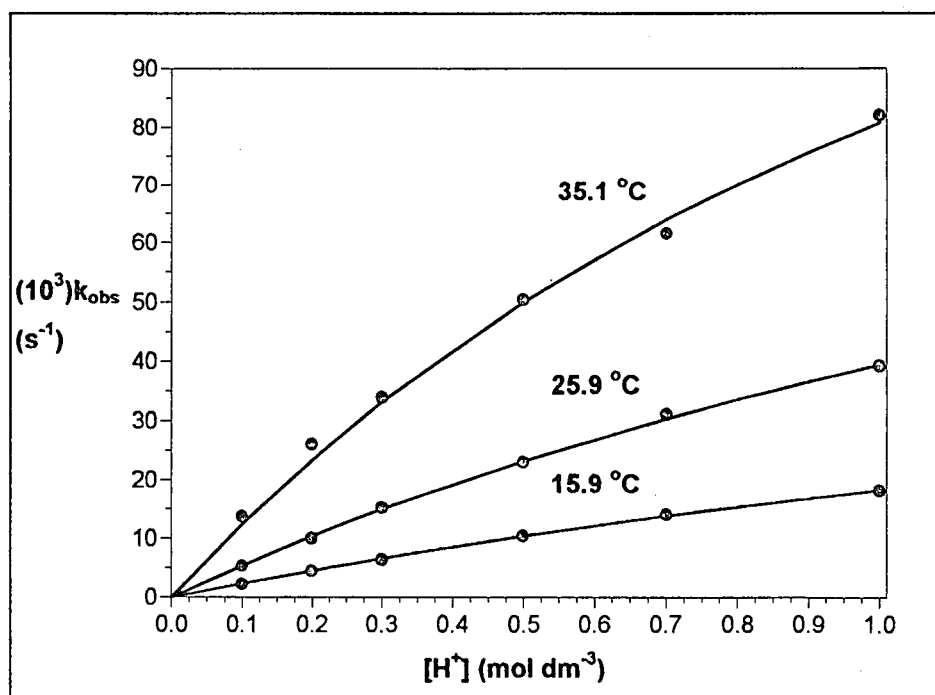
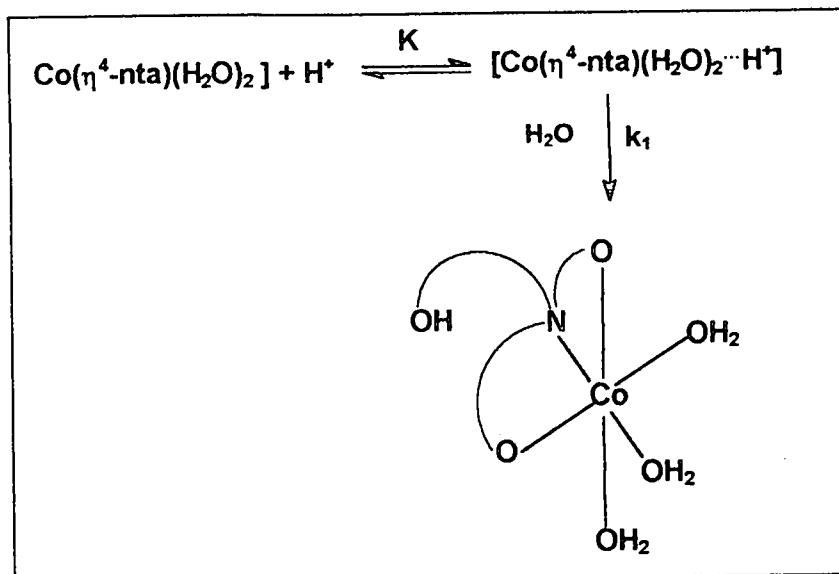


Figure 5.3. Plot of k_{obs} vs. $[\text{H}^+]$ at different temperatures, $\mu = 1.0 \text{ M}$ (NaClO_4), $\lambda = 550 \text{ nm}$, $[\text{dimer}] = 1 \times 10^{-2} \text{ M}$.

The formation of an ion associated species between $[\text{Co}(\text{nta})(\text{H}_2\text{O})_2]$ and H^+ ions upon addition of acid is postulated. This species dissociates in the rate determining step and is aquated to form the tridentate nta complex ion, $[\text{Co}(\eta^3\text{-nta})(\text{H}_2\text{O})_3]^+$.



Scheme 5.2. Proposed mechanism for the reaction of [Co(nta)(H₂O)₂] with H⁺ ions.

The total rate law according to Scheme 5.2 is given by Equation 5.7.

$$R = k_1[\text{Co}(\eta^4\text{-nta})(\text{H}_2\text{O})_2 \cdots \text{H}^+] \quad (5.7)$$

Using the steady-state approximation the observed rate law according to the above mechanism is as follows:

$$k_{\text{obs}} = \frac{k_1 K [\text{H}^+]}{1 + K [\text{H}^+]} \quad (5.8)$$

The results in Figure 5.3 were fitted to Equation 5.8. The calculated k_1 and K values, as well as the activation parameters (using the Eyring-Polanyi equation) are reported in Table 5.2.

CHAPTER 5

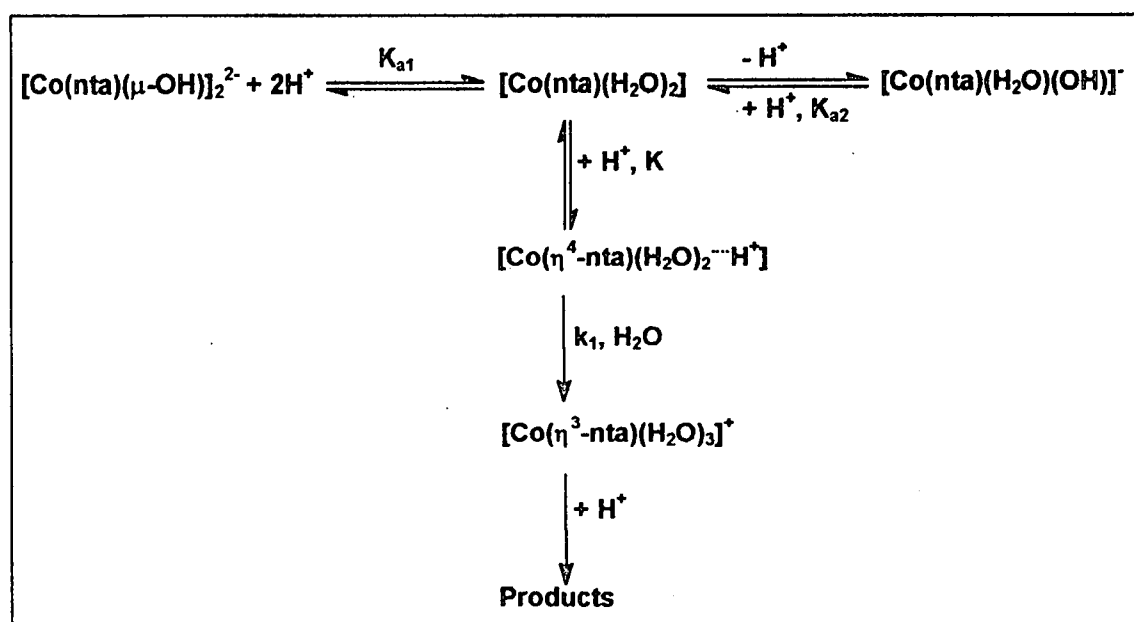
Table 5.2. Summary of the rate constants and activation parameters for the reaction between $[\text{Co}(\text{nta})(\text{H}_2\text{O})_2]$ and H^+ ions.

Temperature (°C)	15.9	25.9	35.1
k_1 (s^{-1})	0.077(6)	0.13(1)	0.21(1)
K (M^{-1})	0.31(3)	0.43(5)	0.6(1)
<hr/>			
ΔH^\ddagger (k_1) (kJ mol^{-1})		138(4)	
ΔS^\ddagger (k_1) ($\text{J mol}^{-1} \text{K}^{-1}$)		-26(2)	
$\text{p}K_{a1}$ (25.0 °C)		3.09(3)	
$\text{p}K_{a2}$ (25.0 °C)		6.52(2)	

The mechanism proposed here is similar to what was found for the reaction between $[\text{Cr}(\text{nta})(\text{H}_2\text{O})_2]$ and H^+ ions (Visser *et al.*, 1994:1051) and involves the formation of an ion pair. Protonation of one of the carboxylate groups of the nta ligand then occurs, which results in the dissociation of this bond to give the tridentate nta complex, $[\text{Co}(\eta^3\text{-nta})(\text{H}_2\text{O})_3]^+$.

5.3.1.4 Summary of results for pH dependance of Co(III)-nta system

From the previous paragraphs a more detailed representation of the behaviour of the Co(III)-nta system in acidic medium can be attempted:



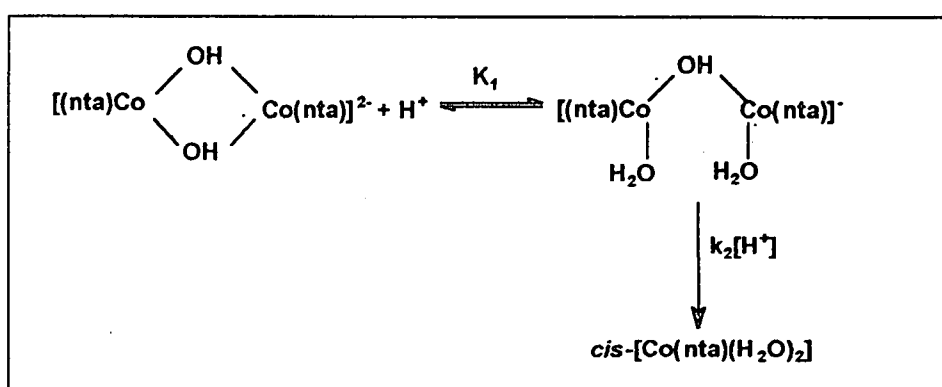
Scheme 5.3. Influence of H^+ ions on the Co(III)-nta system.

Kinetic study of the reactions of *cis*-[Co(nta)(H₂O)₂]

According to Scheme 5.3 [Co(nta)(μ-OH)]₂²⁻ is protonated upon addition of acid to form *cis*-[Co(nta)(H₂O)₂] (refer also to Paragraph 3.4.1.1). This complex can react further with H⁺ ions to form a tridentate Co(III)-nta complex which we propose dissociates stepwise until nta is no longer bonded to the metal.

Our results differ somewhat from those of Thacker and Higginson (1975:704) who investigated the reaction of the "β-form" of the Co(III)-nta complex first prepared by Mori *et al.* (1958:940) with H⁺ ions. They observed an initial fast reaction, followed by a slower reaction (more or less 100 times slower than the first) upon acidification of the starting solution. The second reaction was investigated in more detail with [H⁺] varying between 8.1 × 10⁻³ M (*k*_{obs} = 0.53 × 10⁻³ s⁻¹) and 0.324 M (*k*_{obs} = 4.9 × 10⁻² s⁻¹). These observed rate constants are more or less in the same order as the rate constants observed for the reaction of [Co(nta)(H₂O)₂] with H⁺ ions in this study (e.g. *k*_{obs} = 1.52(3) × 10⁻² s⁻¹ at [H⁺] = 0.3 M).

The study by Meloon and Harris (1977:435) focused on the faster reaction within the acid concentration range of 1.72 × 10⁻³ – 1.955 M. It was postulated that the two observed reactions appeared to have identical properties. This led to an explanation that the acid catalysed hydrolysis of [Co(nta)(μ-OH)]₂²⁻ probably takes place in two consecutive steps (refer to Scheme 5.4), one much more rapid than the other but both fitted by rate equations of the form of Equation 2.2.



Scheme 5.4. Behaviour of the Co(III)-nta solution in acidic medium according to Meloon and Harris (1977:435).

This type of stepwise bridge fission of di-μ-hydroxo complex ions has previously been observed for cationic species [Co(NH₃)₄(μ-OH)]₂⁴⁺ (Hoffman & Taube, 1968:903) and

$[\text{Co}(\text{en})_2(\mu\text{-OH})_2]^{4+}$ (DeMaine & Hunt, 1971:1415). A similar situation exists for triply bridged species like $[(\text{NH}_3)_3\text{Co}(\mu\text{-OH})_3\text{Co}(\text{NH}_3)_3]^{3+}$, except that there were no observable evidence of a singly bridged species (Linhardt & Siebert, 1969:24).

The only study of this kind on an anionic di- μ -hydroxo complex was done by Hin-Fat and Higginson (1971:2589) who investigated the reaction between $[\text{Co}(\text{C}_2\text{O}_4)_2(\mu\text{-OH})_2]^{4-}$ and H^+ ions, but unfortunately this study was complicated by the internal redox reaction between oxalate and cobalt(III).

In light of the previous paragraphs and the experimental evidence gained in this study, it seems that the second slower reaction first observed by Thacker and Higginson (1975:704) might possibly be the nta ring opening reaction described in Paragraph 5.3.1.3. This could especially be true if the uncertainty surrounding purity of the metal complex used by them is taken into consideration. Another supporting fact for this assumption is that the final product of the reaction between dimer and H^+ ions showed no evidence of coordinated nta, thereby providing more evidence for the ring-opening theory.

It is possible that the first reaction as observed by Meloon and Harris (1977:435) describes the breaking of both μ -hydroxo bridges of the dimer, followed by ring opening reactions of nta (this chapter). This seems more probable, especially as $[\text{Co}(\text{nta})(\mu\text{-OH})_2]^{2-}$ is an anionic species and one would expect that two consecutive reactions (breaking of μ -hydroxo bridges) of this complex with a cationic species like H^+ ions would probably be in the same order (Meloon and Harris observed a factor 100 orders of magnitude difference in rate between the first and second reactions).

The acid dissociation constant, K_{a1} in Scheme 5.3, is probably then an overall composite value that describes the whole process of obtaining the di-aquo species from $[\text{Co}(\text{nta})(\mu\text{-OH})_2]^{2-}$. The reaction between $[\text{Co}(\text{nta})(\text{H}_2\text{O})_2]$ and H^+ ions is about 10 times faster than the corresponding reaction (Visser *et al.*, 1994:1051) between $[\text{Cr}(\text{nta})(\text{H}_2\text{O})_2]$ and H^+ ions (0.13 s^{-1} at $25.9 \text{ }^\circ\text{C}$ vs. $1.27 \times 10^{-2} \text{ s}^{-1}$ at $25.1 \text{ }^\circ\text{C}$). This would be expected as it is well known that Co(III) complexes are more labile than Cr(III) complexes.

5.3.2 Substitution reactions of [Co(nta)(H₂O)₂] with NCS⁻ ions5.3.2.1. Substitution reactions between [Co(nta)(H₂O)₂] and NCS⁻ ions

Thacker and Higginson (1975:704) investigated the substitution reactions between [Co(nta)(H₂O)₂] and different incoming ligands, including thiocyanate ions, very briefly and concluded that only NCS⁻ ions did not reduce the metal centre. The range of incoming ligands were expanded to HCN, N₃⁻ and thiourea in this study, but unfortunately none of these ligands provided satisfactory results. HCN did not react with [Co(nta)(H₂O)₂] in the pH range 2 – 7, while the reactions between [Co(nta)(H₂O)₂] and N₃⁻ and thiourea were complicated by the reduction of the metal centre in each case.

The substitution reactions of [Co(nta)(H₂O)₂]/[Co(nta)(H₂O)(OH)]⁻ with NCS⁻ ions were studied at pH values between 2 and 7, see Figure 5.4.

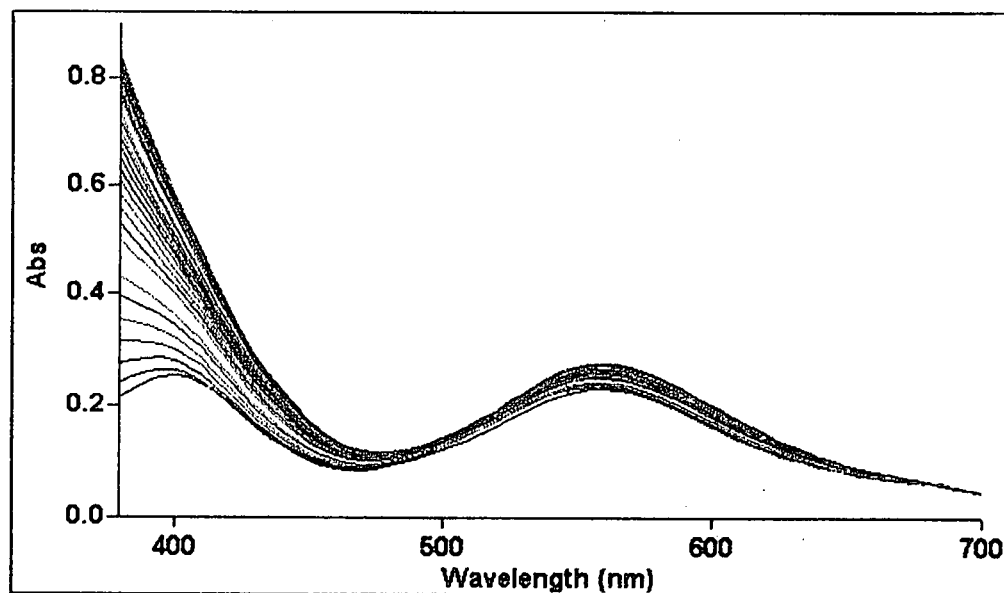
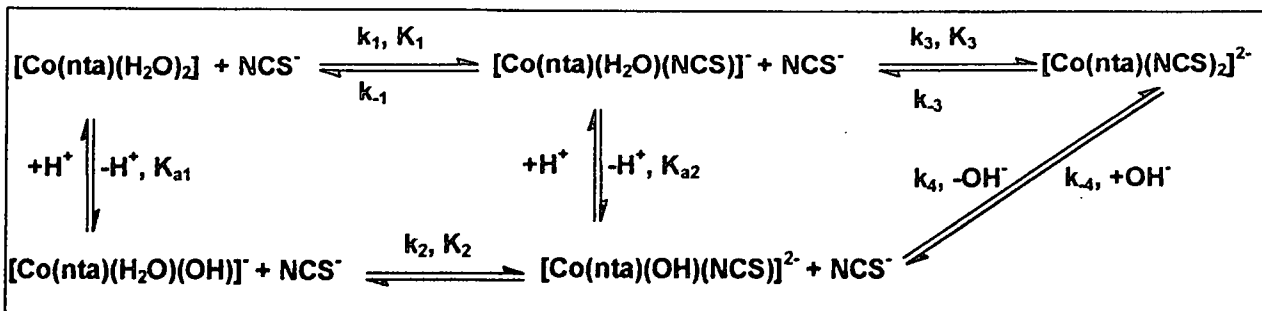


Figure 5.4. UV/VIS spectral change for the reaction between [Co(nta)(H₂O)₂] and NCS⁻ ions.

CHAPTER 5

At these pH values, where both Co(III) species can react with NCS⁻, the following reaction scheme is proposed:



Scheme 5.5. Reactions of [Co(nta)(H₂O)₂]/[Co(nta)(H₂O)(OH)]⁻ with NCS⁻ ions.

The final products in Scheme 5.5 was substantiated by the synthesis of [Co(nta)(NCS)₂]²⁻, refer to Chapter 3.

The total rate law according to Scheme 5.5 is given by Equation 5.9.

$$\begin{aligned}
 R = & k_1[\text{Co(nta)(H}_2\text{O)}_2][\text{NCS}^-] + k_2[\text{Co(nta)(H}_2\text{O)(OH)}][\text{NCS}^-] + k_3[\text{Co(nta)(H}_2\text{O)(NCS)}][\text{NCS}^-] \\
 & + k_4[\text{Co(nta)(OH)(NCS)}^{2-}][\text{NCS}^-] - k_{-1}[\text{Co(nta)(H}_2\text{O)(NCS)}^-] - k_{-2}[\text{Co(nta)(OH)(NCS)}^{2-}] \\
 & - k_{-3}[\text{Co(nta)(NCS)}_2^{2-}] - k_{-4}[\text{Co(nta)(NCS)}_2^{2-}][\text{OH}^-]
 \end{aligned} \tag{5.9}$$

The total Co(III) concentration, [Co]_{tot}, is indicated by Equation 5.10.

$$[\text{Co}]_{\text{tot}} = [\text{Co(nta)(H}_2\text{O)}_2] + [\text{Co(nta)(H}_2\text{O)(OH)}^-] \tag{5.10}$$

The total concentration of the Co(III)-monothiocyanato complex, [Co-NCS]_{tot}, is illustrated by Equation 5.11.

$$[\text{Co-NCS}]_{\text{tot}} = [\text{Co(nta)(H}_2\text{O)(NCS)}^-] + [\text{Co(nta)(OH)(NCS)}^{2-}] \tag{5.11}$$

The acid dissociation constants, K_{a1} and K_{a2}, are given in Equations 5.12 and 5.13 respectively.

$$K_{a1} = \frac{[\text{Co(nta)(H}_2\text{O)(OH)}^-][\text{H}^+]}{[\text{Co(nta)(H}_2\text{O)}_2]} \tag{5.12}$$

$$K_{a2} = \frac{[\text{Co(nta)(OH)(NCS)}^{2-}][\text{H}^+]}{[\text{Co(nta)(H}_2\text{O)(NCS)}^-]} \quad (5.13)$$

The observed rate, k_{obs} , can be derived from Equations 5.9 – 5.13.

$$k_{\text{obs}} = \frac{k_1[\text{H}^+] + k_2K_{a1}}{(K_{a1} + [\text{H}^+])} [\text{NCS}^-] + \frac{k_3[\text{H}^+] + k_4K_{a2}}{(K_{a2} + [\text{H}^+])} [\text{NCS}^-] + \frac{k_{-1}[\text{H}^+] + k_{-2}K_{a2}}{(K_{a2} + [\text{H}^+])} + k_{-3} + k_{-4}[\text{OH}^-] \quad (5.14)$$

In the pH range studied (2 – 7.5) $[\text{OH}^-]$ is very small so that the $k_{-4}[\text{OH}^-]$ term in Equation 5.13 becomes negligible. A provisional fit of the experimental data to Equation 5.13 (excluding the $k_{-4}[\text{OH}^-]$ factor) also gave a value for k_4 approaching zero. One would also expect the observed rate constant, k_{obs} , to decrease with increase in pH if the k_4 pathway does contribute to these reactions. This is not observed in this study as well as other reports (Ashley & Leipoldt, 1981:2326).

In order to further verify the last assumption the first reaction between dimer and NCS^- ions were allowed to go to completion at low pH after which the pH of the reaction solution was increased to ~ 6. The spectroscopic results did not indicate that hydroxide ions are substituted (k_4 pathway). In general the replacement of an OH^- ligand by any other ligand is not observed in complexes of this kind (Leipoldt *et al.*, 1993:241).

Taking the above into consideration Equation 5.15 can be derived.

$$k_{\text{obs}} = \frac{k_1[\text{H}^+] + k_2K_{a1}}{(K_{a1} + [\text{H}^+])} [\text{NCS}^-] + \frac{k_3[\text{H}^+]}{(K_{a2} + [\text{H}^+])} [\text{NCS}^-] + \frac{k_{-1}[\text{H}^+] + k_{-2}K_{a2}}{(K_{a2} + [\text{H}^+])} + k_{-3} \quad (5.15)$$

Initial calculations showed that $K_{a2} \approx 7.0$. This means that the values for K_{a1} and K_{a2} becomes negligible at pH 2.00 so that Equation 5.15 can be simplified to Equation 5.16.

$$k_{\text{obs}} = k_1[\text{NCS}] + k_{-1} + k_3[\text{NCS}] + k_{-3} \quad (5.16)$$

CHAPTER 5

The second substitution step (k_3 step in Scheme 5.5) is almost a factor 100 orders of magnitude slower than the first aqua substitution step (k_1 step) so that the rate equation for the formation of $[\text{Co}(\text{nta})(\text{H}_2\text{O})(\text{NCS})]^-$ and $[\text{Co}(\text{nta})(\text{NCS})_2]^{2-}$ in consecutive substitution steps but different time scales can be described by Equations 5.17 and 5.18 respectively.

$$k_{\text{obs}} = k_1[\text{NCS}^-] + k_{-1} \quad (5.17)$$

$$k_{\text{obs}} = k_3[\text{NCS}^-] + k_{-3} \quad (5.18)$$

Plots of k_{obs} vs $[\text{NCS}^-]$ for both reactions at pH = 2.00 and three different temperatures were linear (refer to Figures 5.5 and 5.6) and the k_1 , k_{-1} , k_3 and k_{-3} values were calculated, see Table 5.3.

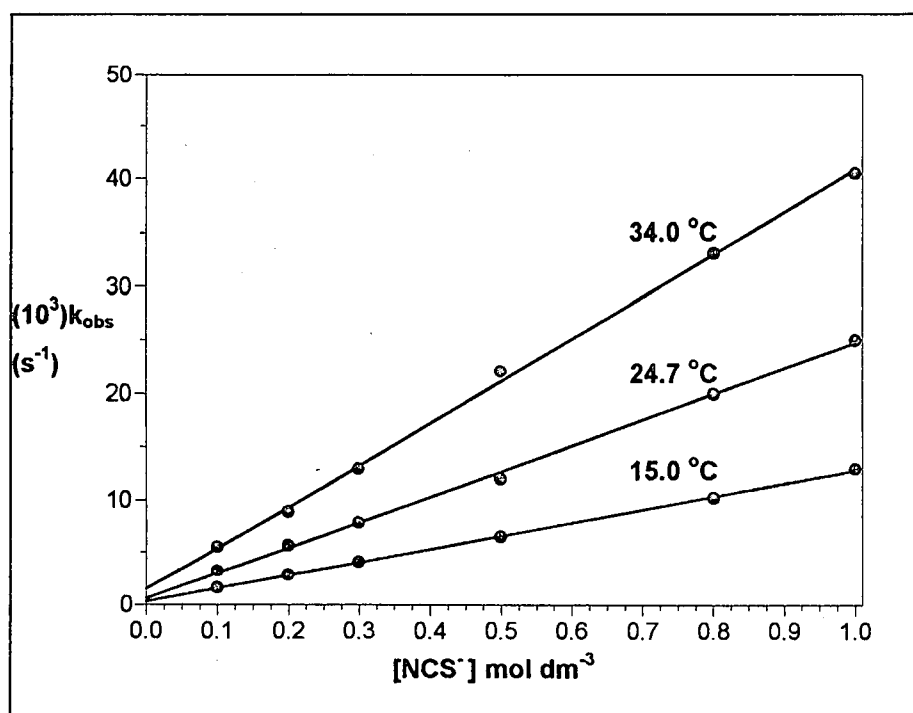


Figure 5.5. Plot of k_{obs} vs. $[\text{NCS}^-]$ for first reaction (k_1 step, Scheme 5.5) at different temperatures, $\mu = 1.0 \text{ M}$ (NaClO_4), $\lambda = 400 \text{ nm}$, $[\text{Co}(\text{nta})(\text{H}_2\text{O})_2] = 4 \times 10^{-3} \text{ M}$.

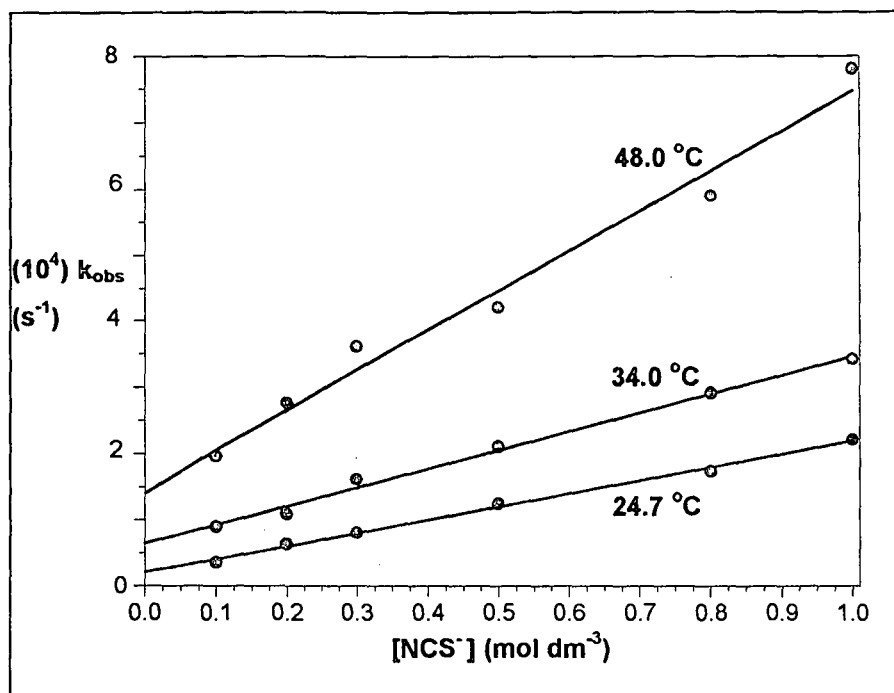


Figure 5.6. Plot of k_{obs} vs. $[\text{NCS}^-]$ for the second reaction (k_3 step, Scheme 5.5) at different temperatures, $\mu = 1.0 \text{ M}$ (NaClO_4), $\lambda = 400 \text{ nm}$, $[\text{Co}(\text{nta})(\text{H}_2\text{O})_2] = 4 \times 10^{-3} \text{ M}$.

According to Scheme 5.5 the concentration of $[\text{Co}(\text{nta})(\text{H}_2\text{O})\text{OH}]^-$ will increase with an increase in pH. The results in Figure 5.7 clearly indicate an increase in substitution rate with an increase in pH. UVMIS spectra of $[\text{Co}(\text{nta})(\text{H}_2\text{O})\text{OH}]^-$ at $\text{pH} > 8.0$ indicated that the species in solution is not stable anymore, possibly due to dimer formation. In order to prevent further complication of the reaction scheme it was decided to investigate the reaction between Co(III)-nta and NCS^- ions between $\text{pH} 4 - 7.5$. This meant that the values of k_2 , k_{-2} and $\text{p}K_{\text{a}2}$ could only be determined from Equation 5.15 and that the influence of the k_1 and k_3 pathways as well as the dissociation constants $K_{\text{a}1}$ and $K_{\text{a}2}$ could not be ignored under these conditions.

The values for k_2 , k_{-2} and $\text{p}K_{\text{a}2}$ were calculated by fitting the data of a plot of k_{obs} vs $[\text{NCS}^-]$ at $\text{pH} 7.0$ (Figure 5.7) simultaneously with the data in Figure 5.8 into Equation 5.15. This was achieved by keeping the values of k_1 , k_{-1} , k_3 , k_{-3} and $\text{p}K_{\text{a}2}$, that was already determined in the previous paragraphs, constant. These results are also reported in Table 5.3.

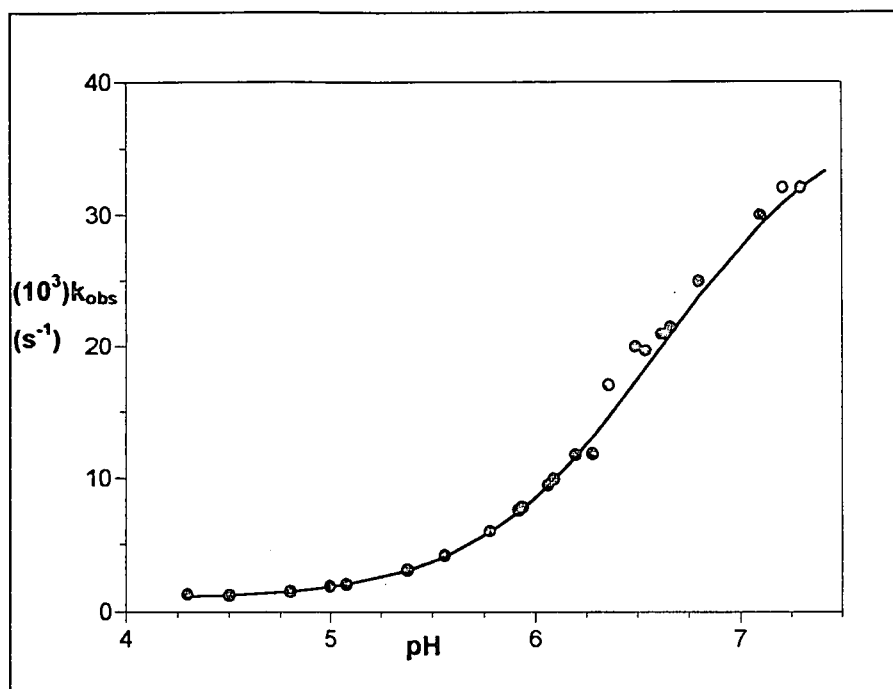


Figure 5.7. Plot of k_{obs} vs. pH at 25.0 °C for the first reaction between $[\text{Co}(\text{nta})(\text{H}_2\text{O})_2]$ and NCS^- ions. $\mu = 1.0 \text{ M (NaClO}_4\text{)}$, $\lambda = 400 \text{ nm}$, $[\text{NCS}^-] = 1.25 \times 10^{-2} \text{ M}$.

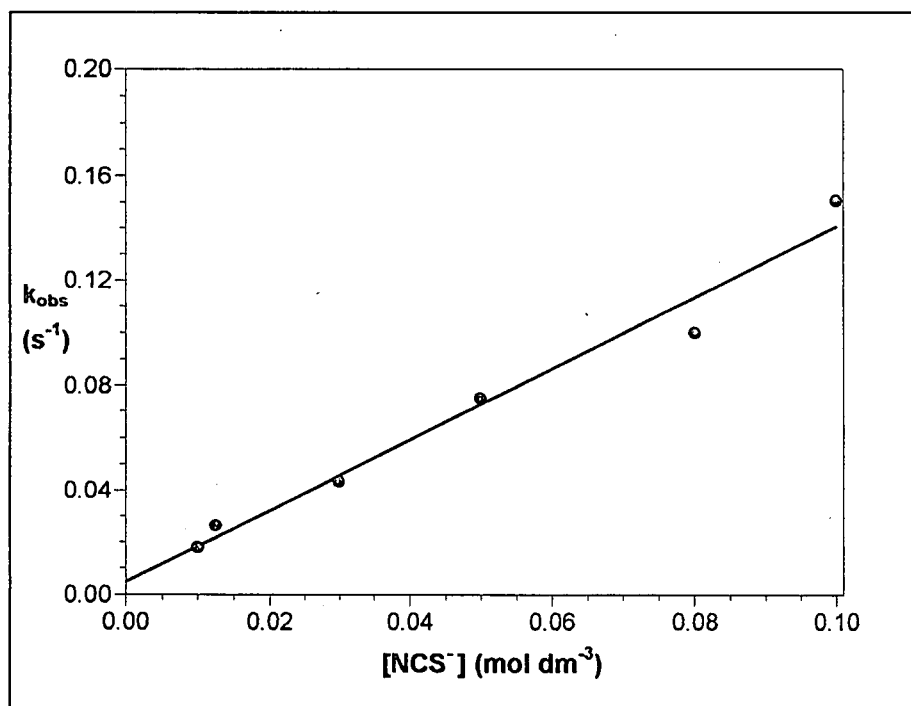


Figure 5.8. Plot of k_{obs} vs. $[\text{NCS}^-]$ for the first reaction at pH = 7.00, 25.0 °C, $\mu = 1.0 \text{ M (NaClO}_4\text{)}$, $\lambda = 400 \text{ nm}$.

Kinetic study of the reactions of *cis*-[Co(nta)(H₂O)₂]

Table 5.3. Summary of the rate constants and activation parameters for the reaction between [Co(nta)(H₂O)₂] and NCS⁻ ions.

Temperature (°C)	15.0	24.7	34.0	48.0
(10 ²)k ₁ (M ⁻¹ s ⁻¹)	1.25(2)	2.4(1)	3.9(1)	
(10 ⁴)k ₁ (s ⁻¹)	3.2(8)	6(1)	15(3)	
K ₁ (M ⁻¹) ^a	39(9)	40(7)	26(5)	
(10 ⁴)k ₃ (M ⁻¹ s ⁻¹)		1.98(6)	2.8(1)	6.0(4)
(10 ⁵)k ₃ (s ⁻¹)		2.1(4)	6.5(6)	14(2)
K ₃ (M ⁻¹) ^a		9(2)	4.3(4)	4.2(7)
k ₂ (M ⁻¹ s ⁻¹)		1.68(5)		
(10 ²)k ₂ (s ⁻¹)		1.7(4)		
K ₂ (M ⁻¹) ^a		98.8(3)		
pK _{a2}		6.7(3)		
ΔH [‡] (k ₁) (kJ mol ⁻¹)		157(2)		
ΔS [‡] (k ₁) (J mol ⁻¹ K ⁻¹)		-6.6(7)		

^a Determined as k_r/k_n

From Table 5.3 and the preceding figures it is clear that the experimental data fits well with the rate law (Equation 5.9) and we conclude that Scheme 5.5 is a fair representation of the mechanism of the substitution reactions between [Co(nta)(H₂O)₂] and NCS⁻ ions.

The stability constant, K₁, of [Co(nta)(H₂O)(NCS⁻)] at 24.7 °C was calculated as 40(7) M⁻¹. This is a factor of almost 70 orders of magnitude smaller than the similar value obtained for [Co(TPPS)(H₂O)(NCS⁻)]⁴⁻ and a factor of 160 orders of magnitude smaller than the value obtained for the formation of [Co(TMpyP)(H₂O)(NCS⁻)]⁴⁻ (Ashley & Leipoldt, 1981:2326). The increase in stability for the porphyrine complexes is probably due to the fact that the formal charge on these complexes is spread over a very large planar surface area, which does not exist for the nta complex. The mode of bonding of the thiocyanate ion is unknown, but one would anticipate that the ligand is sulfur bonded because of the apparent softness of cobalt(III).

The values obtained for K₁ are 2 – 3 orders of magnitude higher than that obtained for K₃ and 2 orders of magnitude lower than the value for K₂. This could be expected as the hydroxo ligand will be able to donate more electron density to the metal centre at higher pH, thereby slightly increasing the stability of the complexes at high pH.

The $[\text{Co}(\text{nta})(\text{H}_2\text{O})\text{OH}]^-$ complex reacts about 70 times faster at 24.7 °C with NCS^- than $[\text{Co}(\text{nta})(\text{H}_2\text{O})_2]$ with NCS^- ($k_2 = 1.68(5) \text{ M}^{-1} \text{ s}^{-1}$ vs. $2.4(1) \times 10^{-2} \text{ M}^{-1} \text{ s}^{-1}$ for k_1 at 24.7 °C). This clearly indicates that the hydroxo ligand labilises the *cis*-aqua bond so that an increase in rate is observed. This *cis*-labilising effect of the hydroxo ligand was also observed for the similar reaction of $[\text{Cr}(\text{nta})(\text{H}_2\text{O})\text{OH}]^-/[\text{Cr}(\text{nta})(\text{H}_2\text{O})_2]$ with NCS^- where an increase of about 8 times was observed (Visser *et al.*, 1994:1051).

The rate of substitution of the first aqua ligand ($k_1 = 2.4(1) \times 10^{-2} \text{ M}^{-1} \text{ s}^{-1}$ at 24.7 °C) at low pH is about 120 times faster than the rate of substitution of the second aqua ligand ($k_3 = 1.98(6) \times 10^{-4} \text{ M}^{-1} \text{ s}^{-1}$ at 24.7 °C). The reason for this is not well understood, but one would not expect the NCS^- ligand to have a high *cis*-labilising effect on the remaining aqua ligand. It is possible that additional $d \rightarrow \pi^*$ backbonding for strengthening the Co-NCS bond will enhance the σ -donation of H_2O to Co and thus strengthen this Co- H_2O bond in the ground state. More information e.g. crystallographic data is required in order to explain this decrease in rate successfully.

The value of k_1 at 24.7 °C is in the same order of magnitude as the value calculated for the reaction of $[\text{Co}(\text{TPPS})(\text{H}_2\text{O})_2]^{3+}$ with NCS^- ions ($k_1 = 3.24(2) \times 10^{-2} \text{ s}^{-1}$, Ashley & Leipoldt, 1981:2326) and about 10^5 orders of magnitude faster than the reactions of $[\text{Co}(\text{NH}_3)_5(\text{H}_2\text{O})]^{3+}$ with NCS^- ions (Van Eldik *et al.*, 1979:1520). This indicates that the nta ligand exerts a very high labilising effect on cobalt(III) complexes. This labilisation can be contributed to the fact that nta donates electron density to the central metal ion which in turn weakens the metal-aqua bond. This also indicates that the electron donating ability of the nta ligand is in the same order of magnitude of the porphine ligand. This trend was also observed for the similar Cr(III)-nta complexes (Visser *et al.*, 1994:1051).

The value of k_1 is a factor of 4 orders of magnitude higher than the value obtained for the similar reaction of $[\text{Cr}(\text{nta})(\text{H}_2\text{O})\text{OH}]^-/[\text{Co}(\text{nta})(\text{H}_2\text{O})_2]$ with NCS^- (k_1 was determined as $5.8 \times 10^{-3} \text{ M}^{-1} \text{ s}^{-1}$ for the chromium complex) (Visser *et al.*, 1994:1051). The value of k_2 at 24.7 °C ($1.68(5) \text{ M}^{-1} \text{ s}^{-1}$) is approximately 70 orders of magnitude faster than the value obtained for the similar reaction of $[\text{Cr}(\text{nta})(\text{H}_2\text{O})\text{OH}]^-/[\text{Co}(\text{nta})(\text{H}_2\text{O})_2]$ with NCS^- at 35.0 °C. This clearly indicates that Co(III) complexes are more labile than Cr(III) complexes. This was also observed for several M(III)-porphyrin ($M = \text{Co}/\text{Cr}$) complexes (Ashley *et al.*, 1980:1613).

Kinetic study of the reactions of *cis*-[Co(nta)(H₂O)₂]

The low positive value obtained for ΔS^\ddagger (k_1) suggests an I_d mechanism, especially as the activation parameters for several other Co(III)-porphyrine complexes also suggest an I_d activated mechanism (Ashley & Leipoldt, 1981:2330). However, additional information like high pressure kinetic studies are necessary in order to establish the intimate mechanism of substitution for Co(III)-nta complexes with certainty.

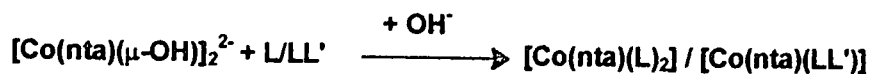
6 Kinetic study of the reactions of $[\text{Co}(\text{nta})(\mu\text{-OH})]_2^{2-}$

6.1 Introduction

It was reported earlier (Paragraph 3.4.1) that $[\text{Co}(\text{nta})(\mu\text{-OH})]_2^{2-}$ can successfully be used as starting material for the synthesis of monomeric Co(III)-nta complexes like $[\text{Co}(\text{nta})(\text{L})_2]$ or $[\text{Co}(\text{nta})(\text{LL}')]$ ($\text{L} = \text{dmap/py}$, $\text{LL}' = \text{en}/\text{N,N-Et}_2\text{en}$) at higher pH. Another observation was made that $[\text{Co}(\text{nta})(\mu\text{-OH})]_2^{2-}$ reacts with these different ligands at high pH to give similar products to that isolated for the reactions of $[\text{Co}(\text{nta})(\text{CO}_3)]^{2-}$ with the same ligands (Scheme 3.1).

The mechanism of the bridge cleavage reactions between $[\text{Co}(\text{nta})(\mu\text{-OH})]_2^{2-}$ and various ligands at $\text{pH} > 7.0$ has not yet been investigated up to this stage. Only a few reports on the cleavage of μ -hydroxo bridges by CO_2 in weakly basic media to form dimeric Co(III) complexes where CO_3^{2-} is the bridging ligand (Sadler & Dasgupta, 1987:185) or to form monomeric complexes with CO_3^{2-} acting as a bidentate ligand (Koshy & Dasgupta, 1984:2781) are available in the literature.

This chapter deals with the reactions of $[\text{Co}(\text{nta})(\mu\text{-OH})]_2^{2-}$ with py, dmap, en and N,N-Et₂en in basic medium (Scheme 6.1).



Scheme 6.1. Reactions of $[\text{Co}(\text{nta})(\mu\text{-OH})]_2^{2-}$ ($\text{L} = \text{dmap, py}$; $\text{LL}' = \text{en, N,N-Et}_2\text{en}$).

6.2 Experimental Procedures

All reagents and chemicals were of analytical grade and double distilled water was used in all experiments. All pH measurements were performed on a Hannah model 8519 pH meter using standard buffer solutions for calibration. Kinetic measurements were done on a GBC 916 spectrophotometer. Temperature control of the reaction solutions was maintained to within ± 0.1 °C by means of a circulating water bath system. The Scientist (Micromath, 1990) program was used to fit the data to selected functions. All the kinetic runs were performed under pseudo first-order conditions with the ligand in excess in each case. Linear plots of $\ln(A_\infty - A_t)$ vs. time were obtained for at least two half-lives under all conditions. The solid lines in the figures represent computer least squares fits of the data, while the experimentally determined values are represented by dots. Detailed tables of the experimental values are given in Appendix A.

6.3 Results and Discussion

6.3.1 Reactions between $[\text{Co}(\text{nta})(\mu\text{-OH})]_2^{2-}$ and monodentate ligands in basic medium

6.3.1.1 Reaction between $[\text{Co}(\text{nta})(\mu\text{-OH})]_2^{2-}$ and dimethylaminopyridine (dmap)

The synthesis of $[\text{Co}(\text{nta})(\text{dmap})_2]$ from $[\text{Co}(\text{nta})(\mu\text{-OH})]_2^{2-}$ at high pH and subsequent characterisation have been reported earlier (Paragraphs 3.3.8 and 3.4.2). Initial UV/VIS spectroscopic studies revealed that the dimer is stable up to $\text{pH} \approx 11.5$. At $\text{pH} 12 - 14$ a completely different change in spectrum compared to that of the substitution reactions of $[\text{Co}(\text{nta})(\mu\text{-OH})]_2^{2-}$ with the various ligands was observed. The quick formation of yellow-green precipitates in the reaction mixture at $\text{pH} > 11.5$ prevented the investigation of these reactions in detail. Initial tests also indicated that the rates of the substitution reactions between $[\text{Co}(\text{nta})(\mu\text{-OH})]_2^{2-}$ and the various ligands are influenced by $[\text{OH}^-]$. An increase in k_{obs} was observed with increase in $[\text{OH}^-]$ for all the reactions.

From the above evidence it was concluded that $[\text{Co}(\text{nta})(\mu\text{-OH})]_2^{2-}$ forms an intermediate species at $\text{pH} \sim 10$ which also reacts with the incoming ligands. At

CHAPTER 6

pH > 11.5 it seems as if a totally different intermediate species is formed which results in a discontinuity of the kinetics at pH 9 – 11.5. Therefore it was decided to follow the kinetics only up to pH 11.5.

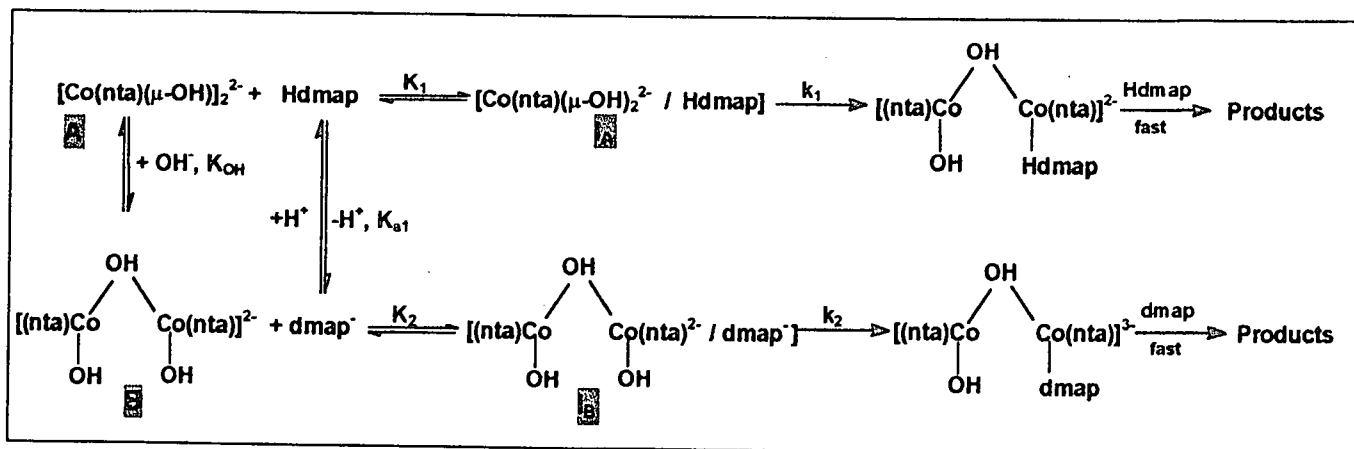
The insolubility of the above mentioned yellow-green precipitates prevented identification by ^1H NMR. IR spectra of these precipitates also did not give sufficient information for identification purposes. We believe that hydroxide ions act as incoming ligands at these pH values to form more polymeric products and that nta is completely dissociated from the metal centre at this pH. Confirmation of this is found in ^1H NMR results obtained for the reaction between $[\text{Co}(\text{nta})(\mu\text{-OH})_2]^{2-}$ and another strong nucleophile, CN^- . ^1H NMR spectra of the final product indicated the absence of nta from the final product. The IR spectrum of this product showed strong CN^- peaks at 2143 and 2130 cm^{-1} which is in good agreement to the 2149 and 2137 cm^{-1} found for $\text{K}_3[\text{Co}(\text{CN})_6]$ (Nakamoto, 1963). Because of the evidence above, it was decided to investigate the reaction between $[\text{Co}(\text{nta})(\mu\text{-OH})_2]^{2-}$ and dmap at pH 9.0 – 11.5.

As mentioned earlier the initial tests showed that the rate of the reaction between $[\text{Co}(\text{nta})(\mu\text{-OH})_2]^{2-}$ and the ligands under investigation (dmap in this case) increased with increase in pH, especially after pH 10. The final UV/VIS spectra of the reaction solutions were in agreement to that found for $[\text{Co}(\text{nta})(\text{dmap})_2]$ (Paragraph 3.3.8), indicating that the observed reactions were the formation of the final product and not an intermediate species.

Initial tests also revealed that only one reaction was observed spectrophotometrically under the experimental conditions. On the basis of these results and the fact that dmap exists as two species, Hdmap and dmap^- , ($\text{pK}_{\text{a}2} = 9.8$) between pH 9 – 11.5, three possible mechanisms can be constructed for these reactions.

Mechanism I

The first possibility (Scheme 6.2) proposes that $[\text{Co}(\text{nta})(\mu\text{-OH})]_2^{2-}$ equilibrates rapidly in aqueous basic solutions with a mono- μ -hydroxo bridged species similar to the one illustrated in Figure 6.1 and that both these species react with the incoming ligand to form ion pairs (rapid) which dissociates in the rate determining step to the products.



Scheme 6.2. Reaction scheme for the reaction between $[\text{Co}(\text{nta})(\mu\text{-OH})]_2^{2-}$ and dmap.

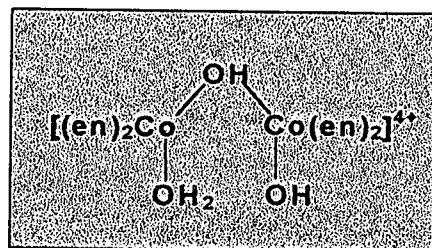


Figure 6.1. Intermediate formed during reaction between $[\text{Co}(\text{en})_2(\mu\text{-OH})]_2^{4+}$ and CO_2 (Koshy and Dasgupta, 1984:2781).

Scheme 6.2 further proposes that the rate determining steps for this reaction are the incoming of the first dmap ligand and that the second step is too fast to be observed spectrophotometrically under these reaction conditions.

Support for the existence of intermediate μ -hydroxo bridged species exist in the literature (Sadler & Dasgupta, 1987:185 and Koshy & Dasgupta, 1984:2781). The cleavage of μ -hydroxo bridges by CO_2 in weakly basic media suggested intermediates with at least one of the hydroxo bridges opened.

CHAPTER 6

It is suggested in this study that under these experimental conditions the intermediate mono- μ -hydroxo species in Scheme 6.2 only contain hydroxo ligands and not an aqua ligand (refer to Figure 6.1) as in the study of Koshy and Dasgupta (1984:2781).

According to Scheme 6.2, considering the above-mentioned arguments, the total rate can be described by Equation 6.1.

$$R = k_1[I_A] + k_2[I_B] \quad (6.1)$$

$[I_A]$ and $[I_B]$ represent the concentration of intermediates I_A and I_B in Scheme 6.2. The total Co(III) concentration, $[Co]_{tot}$, is indicated by Equation 6.2.

$$[Co]_{tot} = [A] + [B] + [I_A] + [I_B] \quad (6.2)$$

In Equation 6.2 $[A]$ represents the concentration of $[Co(nta)(\mu-OH)]_2^{2-}$ and $[B]$ represents the concentration of the mono- μ -hydroxo bridged Co(III)-nta species (Scheme 6.2). The total concentration of the incoming ligand, $[dmap]_{tot}$, is illustrated by Equation 6.3.

$$[dmap]_{tot} = [Hdmap] + [dmap^-] \quad (6.3)$$

The acid dissociation constant, K_{a1} , is given in Equation 6.4.

$$K_{a1} = \frac{[dmap^-][H^+]}{[Hdmap]} \quad (6.4)$$

The expression describing K_{OH} in Scheme 6.2 is given by Equation 6.5.

$$K_{OH} = \frac{[B]}{[A][OH^-]} \quad (6.5)$$

The expressions describing K_1 and K_2 in Scheme 6.2 is illustrated by Equations 6.6 and 6.7 respectively.

$$K_1 = \frac{[I_A]}{[Hdmap][A]} \quad (6.6)$$

$$K_2 = \frac{[\text{B}]}{[\text{dmap}][\text{B}]} \quad (6.7)$$

The observed rate, k_{obs} , can be derived from Equations 6.1 – 6.7.

$$k_{\text{obs}} = \frac{(k_1 K_1 [\text{H}^+] / K_{a1} + k_2 K_2 K_{\text{OH}} [\text{OH}^-]) [\text{dmap}]_{\text{tot}}}{(1 + [\text{H}^+] / K_{a1} + K_{\text{OH}} [\text{OH}^-]) [\text{H}^+] / K_{a1} + K_{\text{OH}} [\text{OH}^-] + (K_1 [\text{H}^+] / K_{a1} + K_2 K_{\text{OH}} [\text{OH}^-]) [\text{dmap}]_{\text{tot}}} \quad (6.8)$$

From Equation 6.8, $K_{a1} = 9.8$ (Meites, 1963) and the experimental conditions between $\text{pH} = 9 - 11.5$, it follows that $K_{\text{OH}} [\text{OH}^-] [\text{H}^+] / K_{a1} \ll 1$, so that Equation 6.8 can be simplified to Equation 6.9.

$$k_{\text{obs}} = \frac{(k_1 K_1 [\text{H}^+] / K_{a1} + k_2 K_2 K_{\text{OH}} [\text{OH}^-]) [\text{dmap}]_{\text{tot}}}{(1 + [\text{H}^+] / K_{a1} + K_{\text{OH}} [\text{OH}^-]) + (K_1 [\text{H}^+] / K_{a1} + K_2 K_{\text{OH}} [\text{OH}^-]) [\text{dmap}]_{\text{tot}}} \quad (6.9)$$

A simpler representation of Equation 6.9 is illustrated in Equation 6.10.

$$k_{\text{obs}} = \frac{C_1 [\text{dmap}]_{\text{tot}}}{C_2 + C_3 [\text{dmap}]_{\text{tot}}} \quad (6.10)$$

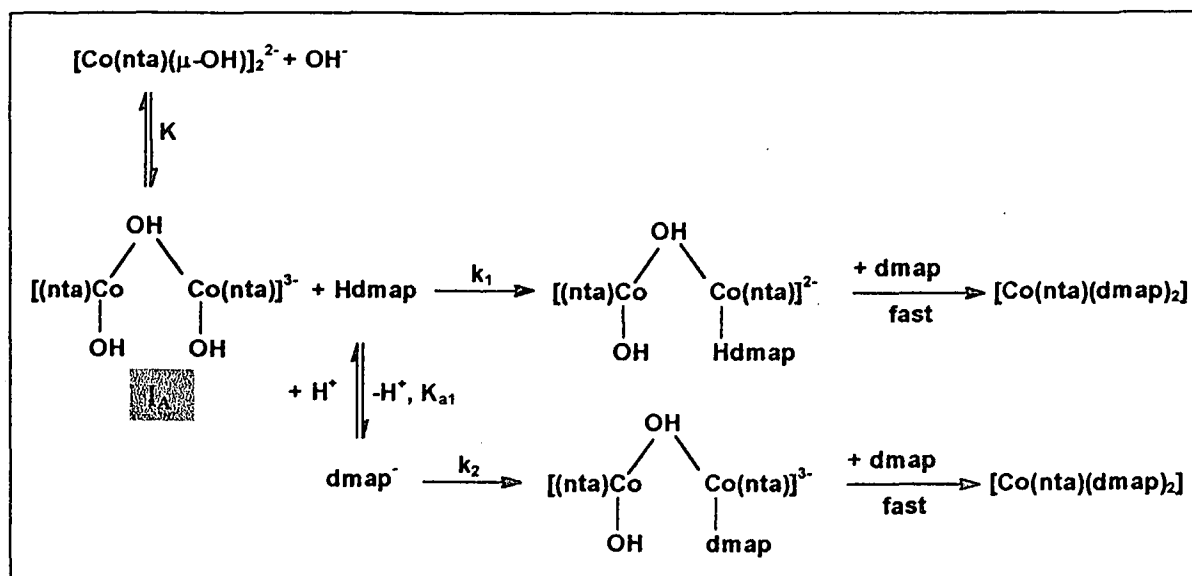
In Equation 6.10 $C_1 = (k_1 K_1 [\text{H}^+] / K_{a1} + k_2 K_2 K_{\text{OH}} [\text{OH}^-])$, $C_2 = (1 + [\text{H}^+] / K_{a1} + K_{\text{OH}} [\text{OH}^-])$ and $C_3 = (K_1 [\text{H}^+] / K_{a1} + K_2 K_{\text{OH}} [\text{OH}^-])$. According to Equation 6.10 a plot of k_{obs} vs $[\text{dmap}]_{\text{tot}}$ will be non-linear at any pH and will flatten out at high $[\text{dmap}]$.

Mechanism II

This mechanism (Scheme 6.3) proposes that $[\text{Co}(\text{nta})(\mu\text{-OH})]_2^{2-}$ equilibrates rapidly in aqueous basic solutions with a mono- μ -hydroxo bridged species similar to the one described by Scheme 6.2, but that only this species further reacts with the incoming ligand to form the product. Once again it is proposed that the second substitution step is too fast to be observed spectrophotometrically under these experimental conditions.

CHAPTER 6

This mechanism is similar to the studies on the cleavage of μ -hydroxo bridges by CO_2 in weakly basic media (Sadler & Dasgupta, 1987:185 and Koshy & Dasgupta, 1984:2781).



Scheme 6.3. Mechanism II for the reaction between $[\text{Co}(\text{nta})(\mu\text{-OH})]_2^{2-}$ and dmap.

The total rate according to Scheme 6.3 can be described by Equation 6.11.

$$R = (k_1[\text{Hdmap}] + k_2[\text{dmap}^-])[I_A] \quad (6.11)$$

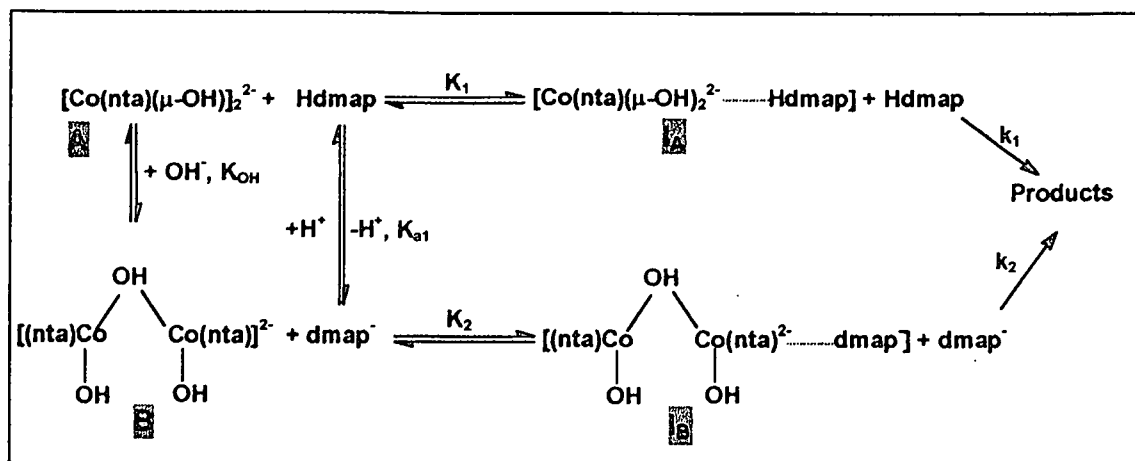
The observed rate, k_{obs} in Equation 6.12, can be derived from Equation 6.11 and by using similar arguments as set out before for the derivation of Equation 6.10.

$$k_{\text{obs}} = \frac{B_1[\text{OH}^-][\text{dmap}]_{\text{tot}}}{B_2(1 + K[\text{OH}^-])} \quad (6.12)$$

In Equation 6.12 $B_1 = k_1[\text{H}^+]/K_{a1} + k_2$ and $B_2 = 1 + [\text{H}^+]/K_{a1}$. According to Equation 6.12 a plot of k_{obs} vs. $[\text{dmap}]$ at constant pH should be linear, passing through the origin.

Mechanism III

The third possible mechanism (Scheme 6.4) is very similar to the first mechanism (Scheme 6.2). $[\text{Co}(\text{nta})(\mu\text{-OH})]_2^{2-}$ equilibrates rapidly in aqueous basic solutions with a mono- μ -hydroxo bridged species. Both these species react with the incoming ligands to form different ion pairs (rapid) which further react with the second incoming ligand in the rate determining steps to form the products.



Scheme 6.4. Mechanism III for the reaction between $[\text{Co}(\text{nta})(\mu\text{-OH})]_2^{2-}$ and dmap.

The only difference between the mechanism proposed here and the one proposed in Scheme 6.2 is that the rate determining step involves the second substitution step in this case whereas it was proposed in Scheme 6.2 that this step is too fast to be observed spectrophotometrically.

According to Scheme 6.4 the total rate can be described by Equation 6.13.

$$R = k_1[I_A][\text{Hdmap}]_{\text{tot}} + k_2[I_B][\text{dmap}^+]_{\text{tot}} \quad (6.13)$$

By using Equation 6.13 and similar arguments as before the observed rate, k_{obs} , can be derived.

$$k_{\text{obs}} = \frac{A_1[\text{dmap}]^2}{A_2 + A_3[\text{dmap}]} \quad (6.14)$$

In Equation 6.14 $A_1 = \{k_1K_1([\text{H}^+])^2/(K_{a1})^2 + k_2K_2\text{KOH}[\text{OH}^-]\}$, $A_2 = \{([\text{H}^+])^2/(K_{a1})^2 + 2[\text{H}^+]/K_{a1} + 2\text{KOH}[\text{OH}^-][\text{H}^+]/K_{a1} + \text{KOH}[\text{OH}^-][([\text{H}^+])^2/(K_{a1})^2 + \text{KOH}[\text{OH}^-])\}$ and $A_3 = \{K_1([\text{H}^+])^2/(K_{a1})^2 + K_2\text{KOH}[\text{OH}^-][\text{H}^+]/K_{a1} + K_1[\text{H}^+]/K_{a1} + K_2\text{KOH}[\text{OH}^-]\}$.

According to Equation 6.14 a plot of k_{obs} vs. $[\text{dmap}]$ will be an exponential curve.

Discussion of mechanism and kinetics

It is clear from the previous discussions that the three suggested mechanisms (Schemes 6.2, 6.3 and 6.4) exhibit vastly different relations between k_{obs} and $[\text{dmap}]$. The reaction between $[\text{Co}(\text{nta})(\mu\text{-OH})_2]^{2-}$ and dmap were investigated by performing two separate experiments. Firstly k_{obs} was measured as a function of $[\text{dmap}]$ at constant pH (Figure 6.2) and secondly k_{obs} was measured as a function of pOH and constant $[\text{dmap}]$ (Figure 6.3). The results in Figure 6.2 clearly indicate a non-linear relation between k_{obs} and $[\text{dmap}]$ that seems to flatten out at high $[\text{dmap}]$.

The k_{obs} vs. $[\text{dmap}]$ data and the k_{obs} vs. pOH data were fitted separately to Equations 6.9 (Scheme 6.2), 6.12 (Scheme 6.3) and 6.14 (Scheme 6.4). Only Equation 6.9 produced satisfactory fits for the experimental data, indicating that the preferred mechanism is Mechanism I.

The values for k_1 , k_2 , K_1 , K_2 and K_{OH} in Equation 6.9 were calculated by fitting the data represented in Figures 6.2 and 6.3 simultaneously into Equation 6.9 and by keeping the value of K_{a1} constant at 9.8. These results are reported in Table 6.1 (refer to page 116).

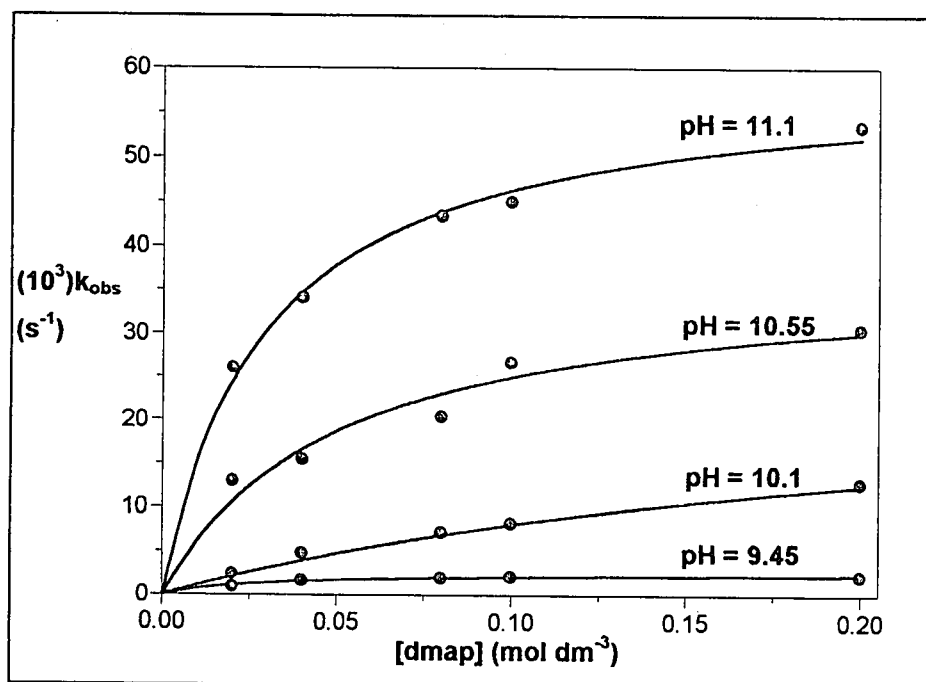


Figure 6.2. Plot of k_{obs} vs. $[\text{dmap}]$ for the reaction between $[\text{Co}(\text{nta})(\mu\text{-OH})_2]^{2-}$ and dmap at different pH levels, $25.0\text{ }^\circ\text{C}$, $\mu = 1.0\text{ M}$ (NaClO_4), $\lambda = 390\text{ nm}$, $[\text{dimer}] = 1.5 \times 10^{-3}\text{ M}$.

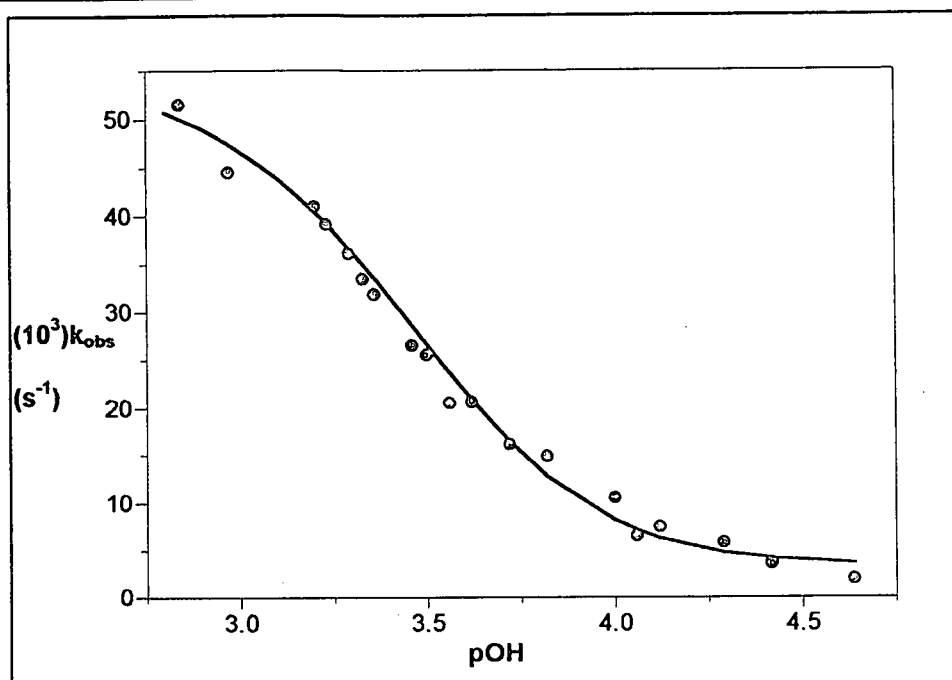


Figure 6.3. Plot of k_{obs} vs. pOH for the reaction between $[\text{Co}(\text{nta})(\mu\text{-OH})_2]^{2-}$ and dmap at 25.0 °C, $\mu = 1.0 \text{ M}$ (NaClO_4), $\lambda = 390 \text{ nm}$, $[\text{dimer}] = 1.5 \times 10^{-3} \text{ M}$.

From Table 6.1 and the preceding figures it is clear that the experimental data fits well into the rate law (Equation 6.9). We therefore conclude that Scheme 6.2 is the best representation of the mechanism of the bridge cleavage reactions between $[\text{Co}(\text{nta})(\mu\text{-OH})_2]^{2-}$ and dmap at high pH.

According to Scheme 6.2 $[\text{Co}(\text{nta})(\mu\text{-OH})_2]^{2-}$ equilibrates rapidly in aqueous basic solutions with a mono- μ -hydroxo bridged species. Both these species react with the incoming ligand to form an ion associated species (rapid) which dissociates in the rate-determining step to the products. The rate-determining steps for this reaction are the incoming of the first dmap ligand and the second substitution step is too fast to be observed spectrophotometrically under the reaction conditions.

The formation of the previously mentioned yellow-green residues in solutions of $[\text{Co}(\text{nta})(\mu\text{-OH})_2]^{2-}$ at $\text{pH} > 11.5$ prevented the determination of the values of k_2 and K_2 where the influence of the k_1 pathway could be ignored (at $\text{pH} > 11.7$, $[\text{OH}^-] \gg K_{\text{OH}}$). In order to verify the values of k_2 and K_2 determined from the data in Figures 6.2 and 6.3 and to get an idea of the mode of activation of these reactions and taking the above mentioned restrictions into consideration, the reaction between $[\text{Co}(\text{nta})(\mu\text{-OH})_2]^{2-}$ and

dmap were studied at pH = 10.50 and different temperatures. These results are illustrated in Figure 6.4.

The data at 25.0 °C were fitted into Equation 6.9 and k_2 and K_2 were calculated by keeping the values obtained for k_1 , K_1 , K_{OH} , K_{a1} (Table 6.1) constant. K_2 was determined as $1.4(2) \times 10^4 \text{ M}^{-1}$ and k_2 as $5.0(4) \times 10^{-2} \text{ s}^{-1}$. These results agree very well within experimental error with those in Table 6.1. The decision to keep k_1 and K_1 constant in these calculations is justified by the fact that it was possible to follow these reactions at pH levels where the k_2 pathway does not contribute to the total rate (pH = 9.45, Figure 6.2). Therefore k_1 and K_1 could be determined with confidence in the previous calculations (Table 6.1).

The data in Figure 6.4 were also used to determine an overall value for ΔH^\ddagger and ΔS^\ddagger by fitting the values obtained from the intercepts of plots of $1/k_{\text{obs}}$ vs. $1/[\text{dmap}]$ to the Eyring-Polyani equation. The value obtained for ΔH^\ddagger is $173(5) \text{ kJ mol}^{-1}$ and ΔS^\ddagger is $26(9) \text{ J mol}^{-1} \text{ K}^{-1}$. The fact that these results indicate a value of $\Delta S^\ddagger \approx 0$ might indicate that the overall reaction is I activated. However more information is required in order to offer predictions regarding the mechanism with confidence.

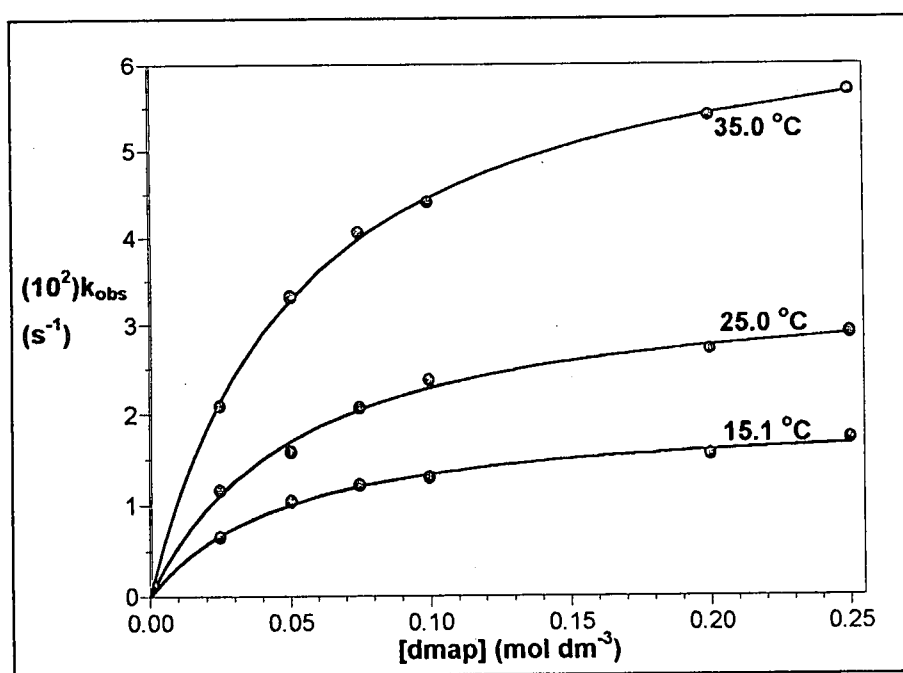


Figure 6.4. Plot of k_{obs} vs. $[\text{dmap}]$ for the reaction between $[\text{Co}(\text{nta})(\mu\text{-OH})]_2^{2-}$ and dmap at different temperatures, pH = 10.5, $\mu = 1.0 \text{ M}$ (NaClO_4), $\lambda = 390 \text{ nm}$, $[\text{dimer}] = 1.5 \times 10^{-3} \text{ M}$.

Kinetic study of the reactions of $[\text{Co}(\text{nta})(\mu\text{-OH})_2]^{2-}$

From Table 6.1 and the preceding figures it is clear that the experimental data fits well into the rate law (Equation 6.9) and that Scheme 6.2 is a fair representation of the mechanism of the bridge cleavage reactions of $[\text{Co}(\text{nta})(\mu\text{-OH})_2]^{2-}$ and dmap at high pH.

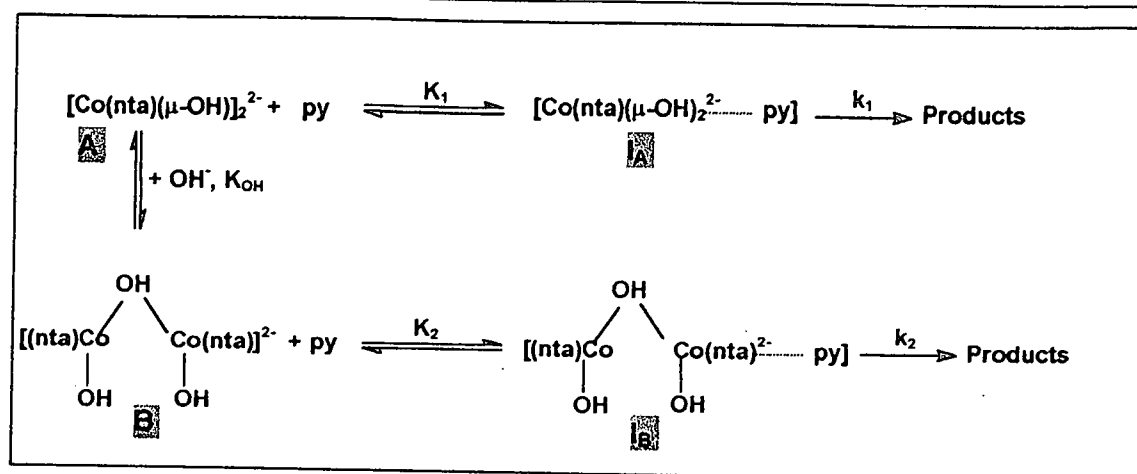
The ability of nta to labilise normally inert metal centres is once again evident in these reactions as can be seen by the relatively high values for the first order rate constants. The value obtained for k_1 is $3.3(7) \times 10^{-3} \text{ s}^{-1}$, almost a factor 20 orders of magnitude smaller than k_2 ($5.7(2) \times 10^{-2} \text{ s}^{-1}$). The stability constant K_1 ($37(3) \text{ M}^{-1}$) is a factor 280 orders of magnitude smaller than K_2 which was determined as $1.04(9) \times 10^4 \text{ M}^{-1}$.

Some very important observations can be made from this evidence. Firstly, it seems that the bridge cleavage reactions of $[\text{Co}(\text{nta})(\mu\text{-OH})_2]^{2-}$ at high pH is greatly influenced by the presence of OH^- ions. The existence of another species, supposedly a mono-bridged complex, at pH 10 and higher was proven kinetically. Both the dimer and the mono-bridged complex react with dmap under the current experimental conditions.

Secondly, it seems that the mono-bridged species (B in Scheme 6.2) labilises the Co(III)-hydroxo bond to such an extent that the k_2 pathway seems to be the preferred pathway for product formation. This seems to be highly likely as the one extra OH^- ligand would further increase the electron density on the mono- μ -hydroxo bridged Co(III) complex, thereby making it react more like a labile Co(II) species.

6.3.1.2. Reaction between $[\text{Co}(\text{nta})(\mu\text{-OH})_2]^{2-}$ and pyridine (py)

The reactions between $[\text{Co}(\text{nta})(\mu\text{-OH})_2]^{2-}$ and py were investigated in order to compare it with the work in the previous paragraphs and to further verify the mechanism of these bridge cleavage reactions. Initial test showed that the reaction between the dimer and py behaved in a similar manner to the reactions with dmap (Paragraph 6.3.1.1). On the basis of these results, together with the fact that py is fully deprotonated at pH 9 – 11 ($\text{p}K_a = 5.21$), a mechanism similar to the one proposed in Paragraph 6.3.1.1 is outlined in Scheme 6.5.



Scheme 6.5. Reaction scheme for the reaction between $[\text{Co}(\text{nta})(\mu\text{-OH})]_2^{2-}$ and py.

The total rate of the reaction described by Scheme 6.5 is similar to Equation 6.1.

$$R = k_1[\text{I}_A] + k_2[\text{I}_B] \quad (6.15)$$

$[\text{I}_A]$ and $[\text{I}_B]$ represent the concentration of intermediates I_A and I_B in Scheme 6.5. The total Co(III) concentration, $[\text{Co}]_{\text{tot}}$, is indicated by Equation 6.16.

$$[\text{Co}]_{\text{tot}} = [\text{A}] + [\text{B}] + [\text{I}_A] + [\text{I}_B] \quad (6.16)$$

The observed rate, k_{obs} , can be derived in the same manner as in Paragraph 6.3.1.1, but with the extra benefit of not having to accommodate the acid dissociation of the incoming ligand in this case.

$$k_{\text{obs}} = \frac{(k_1 K_1 + k_2 K_2 K_{\text{OH}} [\text{OH}^-]) [\text{py}]_{\text{tot}}}{1 + K_{\text{OH}} [\text{OH}^-] + (K_1 + K_2 K_{\text{OH}} [\text{OH}^-]) [\text{py}]_{\text{tot}}} \quad (6.17)$$

The results in Figure 6.5 clearly indicate an increase in substitution rate with an increase in pH, as was observed for the similar reactions with dmap.

According to Equation 6.17 a plot of k_{obs} vs. $[\text{py}]$ should be non-linear. Figure 6.6 represents plots of k_{obs} vs. $[\text{py}]$ at different pH levels. The values for k_1 , k_2 , K_1 , K_2 and K_{OH} were calculated by fitting the data represented in Figures 6.5 and 6.6 simultaneously into Equation 6.17. These results are reported in Table 6.1.

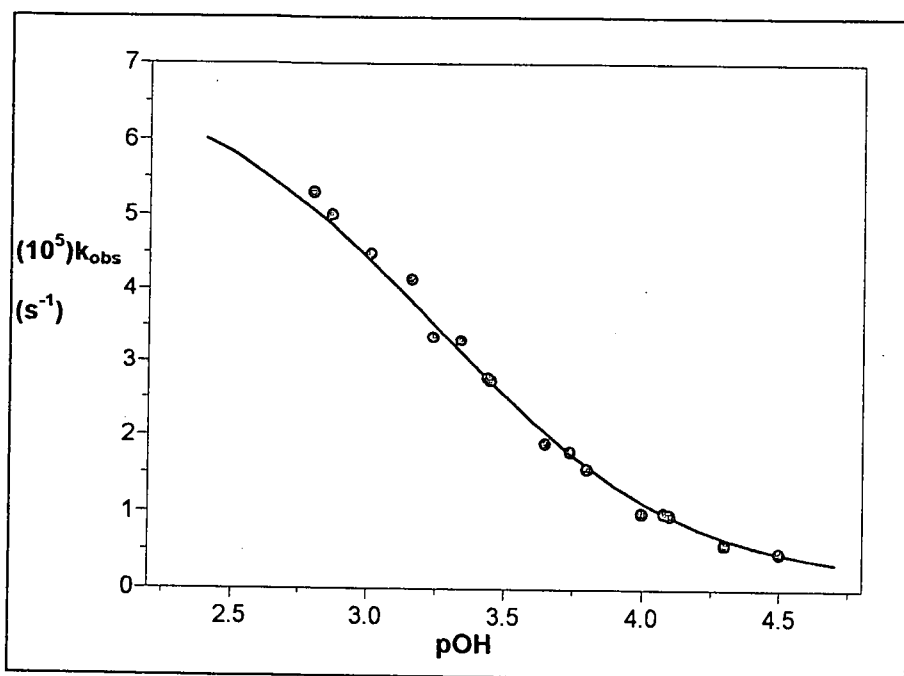


Figure 6.5. Plot of k_{obs} vs pOH for the reaction between $[\text{Co}(\text{nta})(\mu\text{-OH})]_2^{2-}$ and py, $\mu = 0.5 \text{ M}$ (NaClO_4), $\lambda = 410 \text{ nm}$, $[\text{dimer}] = 1.5 \times 10^{-3} \text{ M}$ and $25.0 \text{ }^\circ\text{C}$.

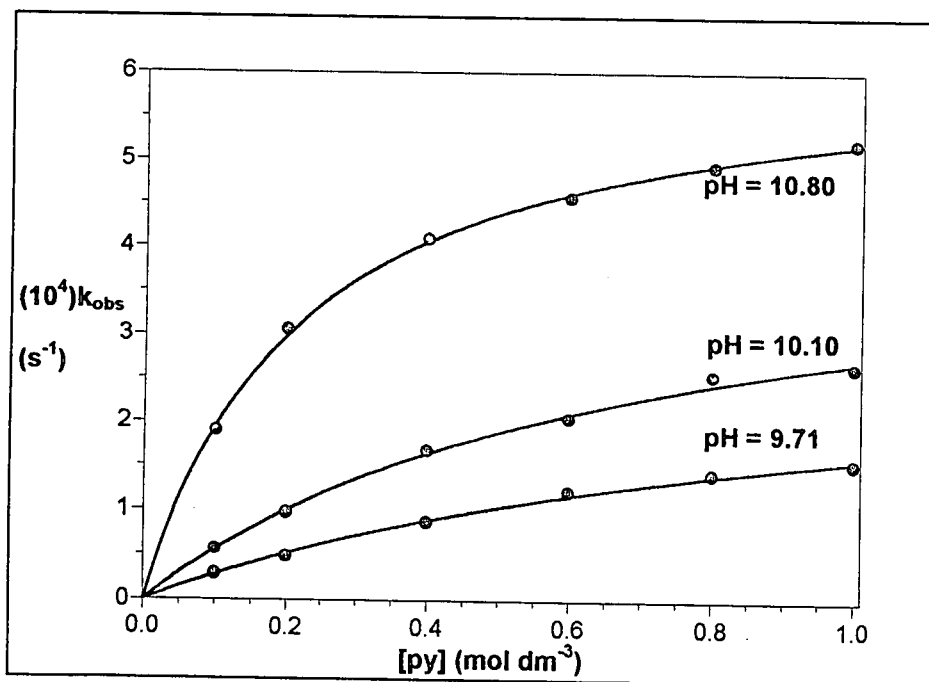


Figure 6.6. Plot of k_{obs} vs. $[\text{py}]$ for the reaction between $[\text{Co}(\text{nta})(\mu\text{-OH})]_2^{2-}$ and py at different pH levels, $\mu = 0.5 \text{ M}$ (NaClO_4), $\lambda = 410 \text{ nm}$, $[\text{dimer}] = 1.5 \times 10^{-3} \text{ M}$ and $25.0 \text{ }^\circ\text{C}$.

CHAPTER 6

Table 6.1 Summary of the rate constants for the reaction between $[\text{Co}(\text{nta})(\mu\text{-OH})_2]^{2-}$ and different monodentate ligands (dmap and py) at 25.0 °C.

	py	dmap
$(10^4)k_1 \text{ (s}^{-1}\text{)}$	1.0(3)	33(7)
$K_1 \text{ (M}^{-1}\text{)}$	0.5(1)	37(3)
$(10^4)k_2 \text{ (s}^{-1}\text{)}$	6.8(2)	570(20)
$(10^3)K_2 \text{ (M}^{-1}\text{)}$	2.1(2)	10.4(9)
$(10^4)k_2 \text{ (s}^{-1}\text{)}^*$		500(40)
$(10^3)K_2 \text{ (M}^{-1}\text{)}^*$		14(2)
pK_{OH}	3.30(2)	3.29(2)

* Calculated from data in Figure 6.4

From Table 6.1 and the preceding figures it is clear that the experimental data fits well into the rate law (Equation 6.17). Therefore we conclude that Scheme 6.5 is a fair representation of the mechanism of the bridge cleavage reactions between $[\text{Co}(\text{nta})(\mu\text{-OH})_2]^{2-}$ and py at high pH. This is similar to the mechanism of the bridge cleavage reactions between $[\text{Co}(\text{nta})(\mu\text{-OH})_2]^{2-}$ and dmap at high pH

Comparison of the rate data

The stability constant K_1 ($0.5(1) \text{ M}^{-1}$) is a factor 4200 orders of magnitude smaller than K_2 ($2.1(2) \times 10^3 \text{ M}^{-1}$). Also, the first order rate constant, k_1 , which was determined as $1.0(3) \times 10^{-4} \text{ s}^{-1}$ is a factor 5 orders of magnitude smaller than k_2 ($5.7(2) \times 10^{-4} \text{ s}^{-1}$). This evidence indicates that the mono-bridged species (B in Scheme 6.3) labilises the Co(III)-hydroxo bond to such an extent that the k_2 pathway seems to be the preferred pathway for product formation, as was found for the similar reactions with dmap (Paragraph 6.3.1.1).

A comparison of the data in Table 6.1 with the corresponding data for the reaction between $[\text{Co}(\text{nta})(\mu\text{-OH})_2]^{2-}$ and dmap (Table 6.1) illustrates that these reactions occur *via* the same mechanism. The rate of the reactions for both ligands increase with increase in $[\text{OH}^-]$, the k_{obs} vs. [ligand] data is non-linear at all pH levels studied and both reactions seem to prefer the k_2 pathway for product formation.

The reactions between dmap and $[\text{Co}(\text{nta})(\mu\text{-OH})_2]^{2-}$ is much faster than the similar reactions with py. The first order rate constants for the reaction with dmap are factors

Kinetic study of the reactions of $[\text{Co}(\text{nta})(\mu\text{-OH})]_2^{2-}$

30 and 80 orders of magnitude higher than what was found for the respective constants for py. This is to be expected as dmap should be a better nucleophile than py ($\text{pK}_a(\text{dmap}) = 9.8$ vs. $\text{pK}_a(\text{py}) = 5.21$). Smit *et al.* (1995) postulated that the rate of the substitution reactions between $[\text{MoO}(\text{H}_2\text{O})(\text{CN})_4]^{2-}$ and py would be faster than the same reaction with dmap as incoming ligand. Unfortunately these reactions were not studied due to the high lability of the aqua ligand.

In the light of the preceding evidence we postulate an I_A type mechanism for the bridge cleavage reactions between $[\text{Co}(\text{nta})(\mu\text{-OH})]_2^{2-}$ and various monodentate ligands. The value obtained for ΔS^\ddagger together with the fact that the rate-determining step is dependant on the nature of the incoming ligand supports this observation. More evidence e.g. high-pressure kinetic studies is required in order to verify the intimate mechanism of these reactions with more confidence.

6.3.2 Reactions between $[\text{Co}(\text{nta})(\mu\text{-OH})]_2^{2-}$ and bidentate ligands (LL') in basic medium

6.3.2.1 Reaction between $[\text{Co}(\text{nta})(\mu\text{-OH})]_2^{2-}$ and bidentate ligands (ethylenediamine (en) and *N,N*-diethyl-ethylenediamine (*N,N*-Et₂en))

The study of the bridge cleavage reactions of $[\text{Co}(\text{nta})(\mu\text{-OH})]_2^{2-}$ with bidentate ligands like en and *N,N*-Et₂en at high pH were undertaken to further verify the work in the previous paragraphs and to see what the effect of the two ethyl groups on *N,N*-Et₂en would have on the rate of the reaction. Both these ligands have more or less the same nucleophilicity ($\text{pK}_{a2}(\text{en}) = 9.96$ vs. $\text{pK}_{a2}(\text{N,N-Et}_2\text{en}) = 10.46$) so that any major difference in rate could be ascribed to the bulkiness of *N,N*-Et₂en.

The synthesis and characterisation of $[\text{Co}(\text{nta})(\text{en})]$ and $[\text{Co}(\text{nta})(\text{N,N-Et}_2\text{en})]$ from $[\text{Co}(\text{nta})(\mu\text{-OH})]_2^{2-}$ at high pH have been reported earlier (Gladkikh *et al.*, 1992:1231, Visser *et al.*, 2000a and Paragraph 4.4.3). It was decided to study the reactions between $[\text{Co}(\text{nta})(\mu\text{-OH})]_2^{2-}$ and the bidentate ligands (LL') between pH 9.5 and 11.5 due to the same reasons indicated in the study of the reactions with monodentate ligands (Paragraphs 6.3.1.1. and 6.3.1.2)

30 and 80 orders of magnitude higher than what was found for the respective constants for py. This is to be expected as dmap should be a better nucleophile than py ($\text{pK}_a(\text{dmap}) = 9.8$ vs. $\text{pK}_a(\text{py}) = 5.21$). Smit *et al.* (1995) postulated that the rate of the substitution reactions between $[\text{MoO}(\text{H}_2\text{O})(\text{CN})_4]^{2-}$ and py would be faster than the same reaction with dmap as incoming ligand. Unfortunately these reactions were not studied due to the high lability of the aqua ligand.

In the light of the preceding evidence we postulate an I_A type mechanism for the bridge cleavage reactions between $[\text{Co}(\text{nta})(\mu\text{-OH})]_2^{2-}$ and various monodentate ligands. The value obtained for ΔS^\ddagger together with the fact that the rate-determining step is dependant on the nature of the incoming ligand supports this observation. More evidence e.g. high-pressure kinetic studies is required in order to verify the intimate mechanism of these reactions with more confidence.

6.3.2 Reactions between $[\text{Co}(\text{nta})(\mu\text{-OH})]_2^{2-}$ and bidentate ligands (LL') in basic medium

6.3.2.1 Reaction between $[\text{Co}(\text{nta})(\mu\text{-OH})]_2^{2-}$ and bidentate ligands (ethylenediamine (en) and *N,N*-diethyl-ethylenediamine (*N,N*-Et₂en))

The study of the bridge cleavage reactions of $[\text{Co}(\text{nta})(\mu\text{-OH})]_2^{2-}$ with bidentate ligands like en and *N,N*-Et₂en at high pH were undertaken to further verify the work in the previous paragraphs and to see what the effect of the two ethyl groups on *N,N*-Et₂en would have on the rate of the reaction. Both these ligands have more or less the same nucleophilicity ($\text{pK}_{a2}(\text{en}) = 9.96$ vs. $\text{pK}_{a2}(\text{N,N-Et}_2\text{en}) = 10.46$) so that any major difference in rate could be ascribed to the bulkiness of *N,N*-Et₂en.

The synthesis and characterisation of $[\text{Co}(\text{nta})(\text{en})]$ and $[\text{Co}(\text{nta})(\text{N,N-Et}_2\text{en})]$ from $[\text{Co}(\text{nta})(\mu\text{-OH})]_2^{2-}$ at high pH have been reported earlier (Gladkikh *et al.*, 1992:1231, Visser *et al.*, 2000a and Paragraph 4.4.3). It was decided to study the reactions between $[\text{Co}(\text{nta})(\mu\text{-OH})]_2^{2-}$ and the bidentate ligands (LL') between pH 9.5 and 11.5 due to the same reasons indicated in the study of the reactions with monodentate ligands (Paragraphs 6.3.1.1. and 6.3.1.2)

Kinetic study of the reactions of $[\text{Co}(\text{nta})(\mu\text{-OH})_2]^{2-}$

By using the same arguments as for the reaction between $[\text{Co}(\text{nta})(\mu\text{-OH})_2]^{2-}$ and dmap (Paragraph 6.3.1.1) the following rate law can be derived.

$$k_{\text{obs}} = \frac{(k_1 K_1 [\text{H}^+] / K_{a1} + k_2 K_2 K_{\text{OH}} [\text{OH}^-]) [\text{LL}']_{\text{tot}}}{(1 + [\text{H}^+] / K_{a1} + K_{\text{OH}} [\text{OH}^-]) [\text{H}^+] / K_{a1} + K_{\text{OH}} [\text{OH}^-] + (K_1 [\text{H}^+] / K_{a1} + K_2 K_{\text{OH}} [\text{OH}^-]) [\text{LL}']_{\text{tot}}} \quad (6.19)$$

It was mentioned earlier that yellow-green residues formed when the pH of solutions containing $[\text{Co}(\text{nta})(\mu\text{-OH})_2]^{2-}$ was increased to > 11.5 . In order to prevent further complication of the reaction scheme it was decided to investigate the reaction between $[\text{Co}(\text{nta})(\mu\text{-OH})_2]^{2-}$ and LL' at pH 9.0 – 11.5. From Equation 6.14, $K_{a1} = 9.96/10.46$ respectively and the experimental conditions between pH = 9 – 11.5 it follows that $K_{\text{OH}} [\text{OH}^-] [\text{H}^+] / K_{a1} \ll 1$, so that Equation 6.19 can be simplified to Equation 6.20.

$$k_{\text{obs}} = \frac{(k_1 K_1 [\text{H}^+] / K_{a1} + k_2 K_2 K_{\text{OH}} [\text{OH}^-]) [\text{LL}']_{\text{tot}}}{(1 + [\text{H}^+] / K_{a1} + K_{\text{OH}} [\text{OH}^-]) + (K_1 [\text{H}^+] / K_{a1} + K_2 K_{\text{OH}} [\text{OH}^-]) [\text{LL}']_{\text{tot}}} \quad (6.20)$$

According to Scheme 6.6 [LL'] will increase with an increase in pH. The results in Figures 6.7 and 6.8 clearly indicate an increase in substitution rate with an increase in pH.

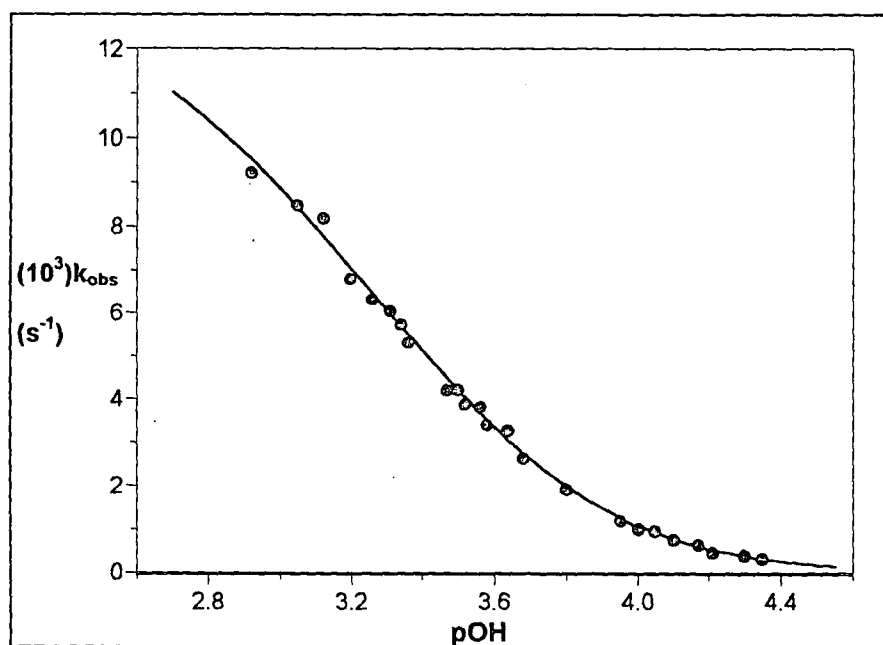


Figure 6.7. Plot of k_{obs} vs. pOH for the reaction between $[\text{Co}(\text{nta})(\mu\text{-OH})_2]^{2-}$ and en at 25.0 °C, $\mu = 0.2 \text{ M (NaClO}_4\text{)}$, $\lambda = 325 \text{ nm}$, $[\text{dimer}] = 1.5 \times 10^{-4} \text{ M}$.

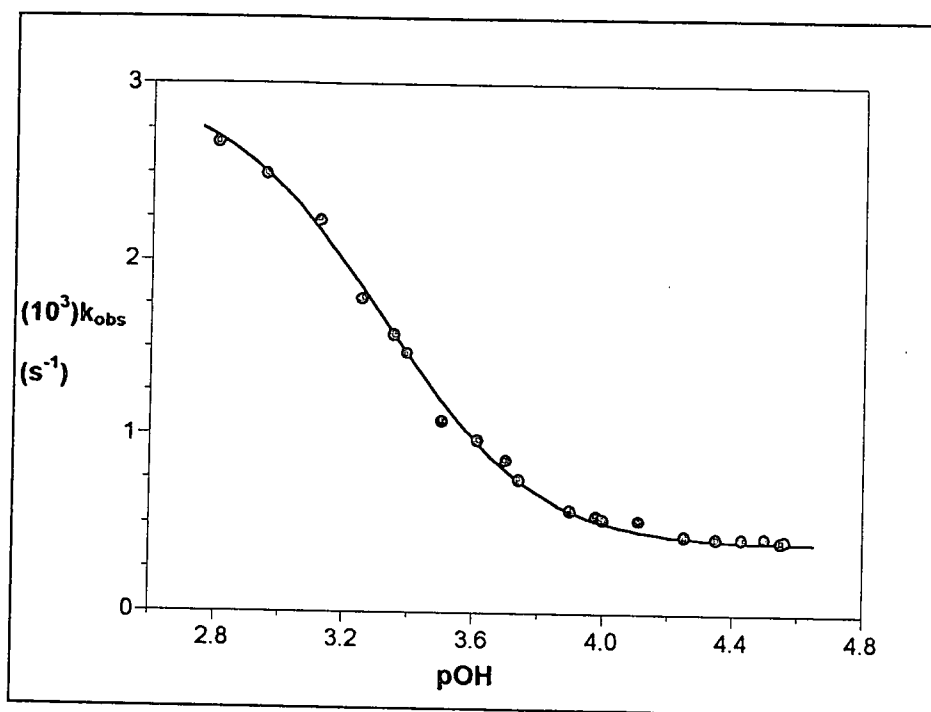


Figure 6.8. Plot of k_{obs} vs. pOH for the reaction between $[\text{Co}(\text{nta})(\mu\text{-OH})]_2^{2-}$ and $N,N\text{-Et}_2\text{en}$ at $25.0\text{ }^\circ\text{C}$, $\mu = 0.2\text{ M}$ (NaClO_4), $\lambda = 325\text{ nm}$, $[\text{dimer}] = 1.5 \times 10^{-4}\text{ M}$.

According to Equation 6.20 plots of k_{obs} vs. $[\text{LL}']$ should be non-linear at any pH . Figures 6.9 and 6.10 represent plots of k_{obs} vs. $[\text{LL}']$ at different pH levels.

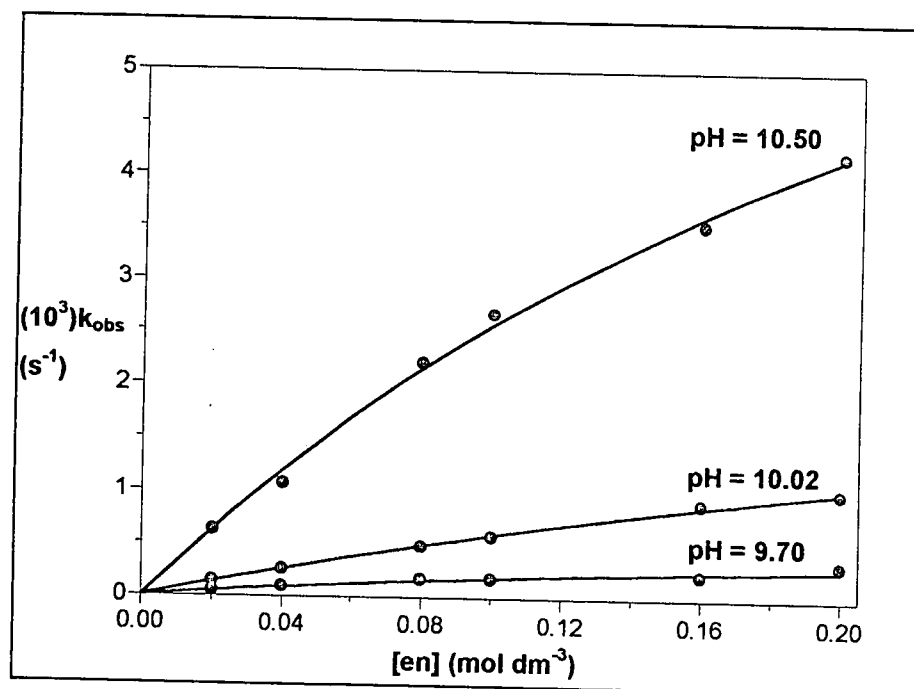


Figure 6.9. Plot of k_{obs} vs. $[\text{en}]$ for the reaction between $[\text{Co}(\text{nta})(\mu\text{-OH})]_2^{2-}$ and en at different pH levels, $25.0\text{ }^\circ\text{C}$, $\mu = 0.2\text{ M}$ (NaClO_4), $\lambda = 325\text{ nm}$, $[\text{dimer}] = 1.5 \times 10^{-4}\text{ M}$.

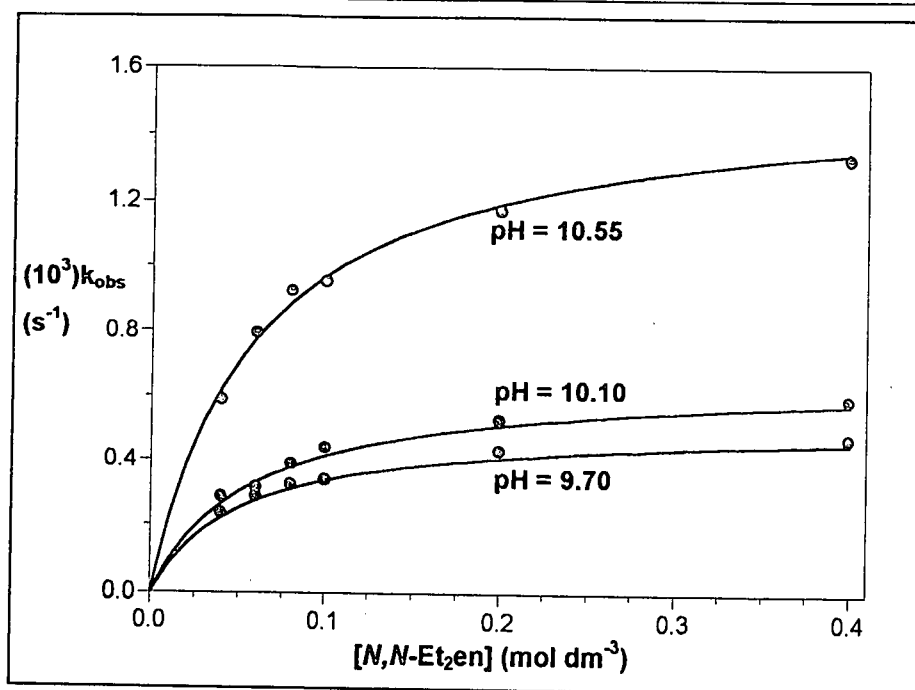


Figure 6.10. Plot of k_{obs} vs. $[\text{N,N-Et}_2\text{en}]$ for the reaction between $[\text{Co}(\text{nta})(\mu\text{-OH})]_2^{2-}$ and $\text{N,N-Et}_2\text{en}$ at different pH levels, $25.0\text{ }^\circ\text{C}$, $\mu = 0.2\text{ M}$ (NaClO_4), $\lambda = 325\text{ nm}$, $[\text{dimer}] = 1.5 \times 10^{-4}\text{ M}$.

The values for k_1 , k_2 , K_1 and K_2 for both LL' ligands were calculated by fitting the respective k_{obs} vs. pOH and k_{obs} vs. $[\text{LL}']$ data represented in Figures 6.7 - 6.10 simultaneously into Equation 6.20 and by keeping the value of $\text{p}K_{\text{a}2}$ constant at 9.96 (for en) or 10.46 (for $\text{N,N-Et}_2\text{en}$). These results are reported in Table 6.2.

Table 6.2. Summary of the rate constants for the reaction between $[\text{Co}(\text{nta})(\mu\text{-OH})]_2^{2-}$ and LL' (LL' = en / $\text{N,N-Et}_2\text{en}$) at $25.0\text{ }^\circ\text{C}$.

	en	$\text{N,N-Et}_2\text{en}$
$(10^5)k_1\text{ (s}^{-1}\text{)}$	8.7(7)	72(7)
$K_1\text{ (M}^{-1}\text{)}$	2.5(3)	15(3)
$(10^2)k_2\text{ (s}^{-1}\text{)}$	1.42(4)	0.32(1)
$(10^{-3})K_2\text{ (M}^{-1}\text{)}$	2.9(2)	4.6(6)
$\text{p}K_{\text{OH}}$	3.3(1)	3.3(1)

From Table 6.2 and the preceding figures it is clear that the experimental data fits well into the rate law (Equation 6.20), therefore we conclude that Scheme 6.6 is a fair representation of the mechanism of the bridge cleavage reactions of $[\text{Co}(\text{nta})(\mu\text{-OH})]_2^{2-}$ and bidentate ligands like en and $\text{N,N-Et}_2\text{en}$ at high pH.

CHAPTER 6

The k_2 pathway seems once again to be the dominant reaction route for these reactions. The value obtained for $k_1(en)$ is $8.7(7) \times 10^{-5} \text{ s}^{-1}$, is a factor 160 orders of magnitude smaller than $k_2(en)$ ($1.42(4) \times 10^{-2} \text{ s}^{-1}$). The stability constant $K_1(en)$ ($2.5(3) \text{ M}^{-1}$) is a factor 1200 orders of magnitude smaller than $K_2(en)$ which was determined as $2.9(2) \times 10^3 \text{ M}^{-1}$. This evidence indicates as with the reactions between the dimer and monodentate ligands that the mono-bridged species (B in Scheme 6.4) labilises the Co(III)-hydroxo bond to such an extent that the k_2 pathway is the preferred pathway for product formation.

The rate constants for the reaction between $[\text{Co}(\text{nta})(\mu\text{-OH})]_2^{2-}$ and LL' show similar trends. The value obtained for $k_1(N,N\text{-Et}_2en)$ is $7.2(7) \times 10^{-4} \text{ s}^{-1}$, a factor 4 orders of magnitude smaller than $k_2(N,N\text{-Et}_2en)$ ($3.2(1) \times 10^{-3} \text{ s}^{-1}$). The stability constant $K_1(N,N\text{-Et}_2en)$ ($15(3) \text{ M}^{-1}$) is a factor 300 orders of magnitude smaller than $K_2(en)$ which was determined as $4.6(6) \times 10^3 \text{ M}^{-1}$.

From the above data it is evident that the nature of the bidentate ethylene diamine ligand does not influence the rate of the reaction substantially. The fact that $k_1(N,N\text{-Et}_2en)$ is a factor 8 orders of magnitude higher than $k_1(en)$, while the value obtained for $k_2(N,N\text{-Et}_2en)$ is a factor 4 orders of magnitude smaller than the same value obtained for $k_2(en)$, indicates that steric hindrance is not the only factor that influences the rate of these reactions. This can be explained by examining the proposed mechanism.

It is possible that $N,N\text{-Et}_2en$ first associates with the unsubstituted nitrogen in the rate determining step, after which the fast, ring-closure step takes place. The rate-determining step would then be basically the same for both ligands as observed. The ring-closure step is so fast that it could not be detected spectrophotometrically, in spite of the substituents on the closing arm of the bidentate ligand in the case of $N,N\text{-Et}_2en$, that are supposed to hamper this reaction step.

6.4 Conclusion

The mechanism of the bridge cleavage reactions between $[\text{Co}(\text{nta})(\mu\text{-OH})_2]^{2-}$ and monodentate and bidentate ligands like dmap, py, en and *N,N*-Et₂en at high pH follow the same mechanism at pH 9 – 11.5. All the results are reported in Table 6.3.

Table 6.3. Summary of the rate constants for the reaction between $[\text{Co}(\text{nta})(\mu\text{-OH})_2]^{2-}$ and L/LL' (L = dmap, py and LL' = en and *N,N*-Et₂en) at 25.0 °C.

	en	<i>N,N</i> -Et ₂ en	py	dmap
$(10^3)k_1 (\text{s}^{-1})$	0.087(7)	0.72(7)	0.10(3)	3.3(7)
$K_1 (\text{M}^{-1})$	2.5(3)	15(3)	0.5(1)	37(3)
$(10^2)k_2 (\text{s}^{-1})$	1.42(4)	0.32(1)	0.068(2)	5.7(2)
$(10^3)K_2 (\text{M}^{-1})$	2.9(2)	4.6(6)	2.1(2)	10.4(9)
pK_{OH}	3.3(1)	3.3(1)	3.30(2)	3.29(2)

The following deductions can be made from this study:

- (1) nta labilise the Co(III) metal centre substantially, possibly by donating electron density to the metal, making it react more like a Co(II) species. This is evident from the high values obtained for the first order rate constants in Table 6.4.
- (2) The existence of an intermediate species (possibly a mono- μ -hydroxo bridged species) at high pH has been proven by the fact that pK_{OH} is the same for all four kinetic studies.
- (3) This mono- μ -hydroxo species is more labile towards substitution than the dimer itself, making the k_2 pathway the reaction route of choice. In the case of en as incoming ligand the difference between k_1 and k_2 was 160 orders of magnitude, illustrating this point. This seems to be highly likely as the one extra OH⁻ ligand would further increase the electron density on the mono- μ -hydroxo bridged Co(III) complex, thereby making it react more like a labile Co(II) species.
- (4) The formation of ion associated species were confirmed by the kinetic study and corresponding fits to the rate equations.
- (5) It seems that the rate of these reactions are affected by the nature of the incoming ligand (refer to Table 6.3).

- (6) The values obtained for K_2 are much higher than that obtained for K_1 , also indicating that the k_2 pathway is the reaction route of choice for these reactions.

It can therefore be concluded that $[\text{Co}(\text{nta})(\mu\text{-OH})_2]^{2-}$ equilibrates rapidly in aqueous basic solutions with a mono- μ -hydroxo bridged Co(III) species and that both these species react with the incoming ligand to form an ion associated species, after which ring-closure (bidentate ligands) or another substitution step (monodentate ligands) occurs rapidly to form the products. The last step is too fast to be observed spectrophotometrically under the experimental conditions of this study.

7

Critical evaluation

All the initial aims of this study have to a large extent successfully been met. The synthesis and characterisation of $[\text{Co}(\text{nta})(\mu\text{-OH})_2]^{2-}$ and $[\text{Cr}(\text{nta})(\mu\text{-OH})_2]^{2-}$ by way of X-ray crystallography, ^1H NMR etc. have removed all doubt on the identity of the respective species first prepared by Mori *et al.* (1958:940) and Uehara *et al.* (1967:2317). The various Co(III)- and Cr(III)-nta complexes that were isolated and characterised (Chapters 3 and 4) can successfully be used as biological model complexes in future studies. These complexes could for example be used to simulate the bonding of metal ions to functional groups of wool fibre or might have uses as models in pharmacology.

The high solubility of Co(III)-nta complexes with monodentate ligands in the two available *cis* positions unfortunately prevented X-ray crystallographical studies of these complexes. The only complex of this kind that was isolated in crystalline form up to now namely, $[\text{Co}(\text{nta})(\text{dmap})_2]$, was unfortunately multiply twinned.

The available information on ^1H NMR spectra of Co(III)-nta complexes have also been increased tremendously and should be of assistance in future studies.

The synthesis of $[\text{Co}(\text{nta})(\text{CO}_3)]^{2-}$ as an alternative to $[\text{Co}(\text{nta})(\mu\text{-OH})_2]^{2-}$ as starting material in the preparation of different Co(III)-nta complexes have also proven to be successful. New Co(III)-nta complexes can be successfully synthesised from the carbonato complex without having the additional burden of polymeric/other residues in the reaction mixture as was reported previously when $[\text{Co}(\text{nta})(\mu\text{-OH})_2]^{2-}$ was used (Mori *et al.*, 1958).

Mononuclear Co(III)-nta complexes with monodentate ligands in the two available *cis* positions could not be characterised with single-crystal X-ray crystallography.

Chapter 7

The strain experienced by the glycinato rings of coordinated nta have been investigated in detail. Comparisons with other studies have been attempted for the first time.

The study of the substitution reactions of $[\text{Co}(\text{nta})(\text{H}_2\text{O})_2]$ and $[\text{Co}(\text{nta})(\mu\text{-OH})_2]^{2-}$ with various ligands at different pH values in order to determine the mechanism was successful. The formation of $[\text{Co}(\text{nta})(\text{H}_2\text{O})_2]$ by acidifying the dimer could be investigated in more detail in the future, especially if multi-probe stopped-flow spectrophotometers can be applied.

The bridge cleavage reactions at high pH between $[\text{Co}(\text{nta})(\mu\text{-OH})_2]^{2-}$ and various ligands like dmap and en seems to have opened an interesting new field for kinetic study. According to our knowledge these reactions have not yet been investigated in such detail up to now. Unfortunately this study was hampered by the formation of precipitates at $\text{pH} > 11.5$. The isolation and characterisation of some of the final products in these reactions have helped tremendously in verifying the mechanism. High-pressure kinetic studies will provide more information on the intimate mechanism of these substitution reactions in future.

Supplementary data

Section I Crystal data

A Crystal data for $\text{Cs}_2[\text{Cr}(\text{nta})(\mu\text{-OH})]_2 \cdot 4\text{H}_2\text{O}$ (I)

Table A.1

Atomic coordinates ($\times 10^4$) and equivalent isotropic displacement parameters ($\text{\AA}^2 \times 10^3$) for I. $U(\text{eq})$ is defined as one third of the trace of the orthogonalized U_{ij} tensor.

Atom	x	y	z	U(eq)
Cs(1)	3544(1)	2993(1)	3510(1)	84(1)
Cr	4358(1)	2192(1)	929(1)	32(1)
O(1)	4685(3)	3025(3)	1539(6)	34(2)
O(6)	3411(3)	2454(3)	927(7)	43(2)
O(2)	4233(4)	1744(4)	2332(6)	43(2)
O(4)	4464(4)	2384(4)	-624(7)	46(2)
N(1)	4018(4)	1297(4)	335(8)	37(2)
C(5)	3291(5)	1379(5)	99(10)	40(3)
C(6)	2992(5)	2021(6)	548(9)	38(3)
C(4)	4540(7)	1860(8)	-1193(12)	60(4)
C(1)	4168(5)	788(6)	1200(11)	52(3)
C(3)	4402(6)	1183(6)	-673(11)	56(3)
O(22)	3025(13)	4381(8)	2370(24)	261(16)
O(11)	4103(14)	4525(11)	3640(32)	335(23)
O(7)	2388(3)	2094(4)	527(7)	46(2)
O(3)	4157(4)	754(5)	3118(8)	61(3)
O(5)	4737(7)	1874(6)	-2140(9)	100(4)

Supplementary Data

Table A.2 Bond angles [°] for I.

O(7)#1-Cs(1)-O(7)#2	64.87(11)	O(6)-C(6)-C(5)	116.3(9)
O(7)#1-Cs(1)-O(22)#1	116.8(4)	O(7)-C(6)-Cs(1)#4	51.1(6)
O(7)#2-Cs(1)-O(22)#1	81.6(4)	O(6)-C(6)-Cs(1)#4	74.7(6)
O(7)#1-Cs(1)-O(2)	97.2(2)	C(5)-C(6)-Cs(1)#4	165.3(7)
O(7)#2-Cs(1)-O(2)	125.3(2)	O(5)-C(4)-O(4)	122.9(14)
O(22)#1-Cs(1)-O(2)	60.4(6)	O(5)-C(4)-C(3)	118.5(14)
O(7)#1-Cs(1)-O(11)	124.6(5)	O(4)-C(4)-C(3)	118.5(12)
O(7)#2-Cs(1)-O(11)	102.6(6)	O(5)-C(4)-Cs(1)#3	74.7(9)
O(22)#1-Cs(1)-O(11)	80.0(4)	O(4)-C(4)-Cs(1)#3	91.4(8)
O(7)#2-Cs(1)-O(22)	101.6(6)	C(3)-C(4)-Cs(1)#3	102.9(8)
O(22)#1-Cs(1)-O(22)	162.0(6)	O(3)-C(1)-O(2)	123.4(12)
O(2)-Cs(1)-O(22)	126.9(6)	O(3)-C(1)-C(2)	119.7(10)
O(11)-Cs(1)-O(22)	48.4(7)	O(2)-C(1)-C(2)	116.8(10)
O(7)#1-Cs(1)-O(1)	120.7(2)	N(1)-C(2)-C(1)	111.2(9)
O(7)#2-Cs(1)-O(1)	173.3(2)	N(1)-C(3)-C(4)	108.2(10)
O(22)#1-Cs(1)-O(1)	92.2(4)	Cs(1)#4-O(22)-Cs(1)	89.1(4)
O(2)-Cs(1)-O(1)	52.3(2)	C(6)-O(7)-Cs(1)#4	110.8(7)
O(11)-Cs(1)-O(1)	77.5(5)	C(6)-O(7)-Cs(1)#5	127.2(7)
O(22)-Cs(1)-O(1)	83.5(6)	Cs(1)#4-O(7)-Cs(1)#5	93.4(2)
O(7)#1-Cs(1)-O(6)	70.2(2)	C(4)-O(5)-Cs(1)#3	86.6(9)
O(7)#2-Cs(1)-O(6)	133.7(2)	O(1)-Cs(1)-O(6)#1	114.4(2)
O(22)#1-Cs(1)-O(6)	110.0(6)	O(6)-Cs(1)-O(6)#1	70.90(14)
O(2)-Cs(1)-O(6)	49.9(2)	O(7)#1-Cs(1)-C(6)#1	8.1(2)
O(11)-Cs(1)-O(6)	111.9(7)	O(7)#2-Cs(1)-C(6)#1	66.3(2)
O(22)-Cs(1)-O(6)	80.7(5)	O(22)#1-Cs(1)-C(6)#1	100.3(5)
O(1)-Cs(1)-O(6)	51.0(2)	O(2)-Cs(1)-C(6)#1	82.4(2)
O(7)#1-Cs(1)-O(6)#1	38.4(2)	O(11)-Cs(1)-C(6)#1	142.7(5)
O(7)#2-Cs(1)-O(6)#1	67.2(2)	O(22)-Cs(1)-C(6)#1	97.2(4)
O(22)#1-Cs(1)-O(6)#1	80.2(5)	O(1)-Cs(1)-C(6)#1	117.6(2)
O(2)-Cs(1)-O(6)#1	68.6(2)	O(6)-Cs(1)-C(6)#1	67.5(2)
O(11)-Cs(1)-O(6)#1	162.2(4)	O(6)#1-Cs(1)-C(6)#1	20.5(2)
O(22)-Cs(1)-O(6)#1	117.5(4)	O(7)#1-Cs(1)-O(5)#3	165.4(2)
O(7)#2-Cs(1)-O(5)#3	104.8(2)	O(11)-Cs(1)-C(4)#3	65.5(5)
O(22)#1-Cs(1)-O(5)#3	49.4(5)	O(22)-Cs(1)-C(4)#3	106.0(5)
O(2)-Cs(1)-O(5)#3	80.2(2)	O(1)-Cs(1)-C(4)#3	50.3(2)
O(11)-Cs(1)-O(5)#3	66.3(6)	O(6)-Cs(1)-C(4)#3	99.1(3)
O(22)-Cs(1)-O(5)#3	69.0(2)	O(6)#1-Cs(1)-C(4)#3	132.2(3)

Supplementary data

Table A.2 continued

O(6)-Cs(1)-O(5)#3	116.8(2)	C(6)#1-Cs(1)-C(4)#3	151.1(3)
O(6)#1-Cs(1)-O(5)#3	129.3(2)	O(5)#3-Cs(1)-C(4)#3	18.7(2)
C(6)#1-Cs(1)-O(5)#3	149.6(3)	O(1)-Cr-O(6)	95.5(3)
O(7)#1-Cs(1)-C(4)#3	167.1(3)	O(1)-Cr-O(2)	95.2(3)
O(7)#2-Cs(1)-C(4)#3	123.5(3)	O(6)-Cr-O(2)	90.0(3)
O(22)#1-Cs(1)-C(4)#3	59.0(4)	O(1)-Cr-O(1)#3	81.5(3)
O(2)-Cs(1)-C(4)#3	70.0(3)	O(6)-Cr-O(1)#3	177.0(3)
O(2)-Cr-O(1)#3	90.4(3)	O(4)-Cr-Cs(1)	139.2(3)
O(1)-Cr-O(4)	100.1(3)	N(1)-Cr-Cs(1)	120.7(3)
O(6)-Cr-O(4)	92.9(3)	Cr#3-Cr-Cs(1)	88.37(7)
O(2)-Cr-O(4)	164.1(3)	Cr-O(1)-Cr#3	98.5(3)
O(1)#3-Cr-O(4)	87.6(3)	Cr-O(1)-Cs(1)	92.1(2)
O(1)-Cr-N(1)	178.1(3)	Cr#3-O(1)-Cs(1)	130.4(3)
O(6)-Cr-N(1)	85.0(3)	C(6)-O(6)-Cr	116.5(7)
O(2)-Cr-N(1)	82.9(3)	C(6)-O(6)-Cs(1)	127.4(7)
O(1)#3-Cr-N(1)	98.0(3)	Cr-O(6)-Cs(1)	90.4(3)
O(4)-Cr-N(1)	81.7(4)	C(6)-O(6)-Cs(1)#4	84.8(6)
O(1)-Cr-Cr#3	41.0(2)	Cr-O(6)-Cs(1)#4	157.6(3)
O(6)-Cr-Cr#3	136.5(2)	Cs(1)-O(6)-Cs(1)#4	80.8(2)
O(2)-Cr-Cr#3	93.7(2)	C(1)-O(2)-Cr	116.1(8)
O(1)#3-Cr-Cr#3	40.5(2)	C(1)-O(2)-Cs(1)	138.1(7)
O(4)-Cr-Cr#3	95.0(2)	Cr-O(2)-Cs(1)	95.8(3)
N(1)-Cr-Cr#3	138.5(2)	C(4)-O(4)-Cr	113.0(8)
O(1)-Cr-Cs(1)	58.2(2)	C(3)-N(1)-C(2)	114.2(9)
O(6)-Cr-Cs(1)	59.5(2)	C(3)-N(1)-C(5)	110.9(9)
O(2)-Cr-Cs(1)	54.3(2)	C(2)-N(1)-C(5)	112.1(8)
O(1)#3-Cr-Cs(1)	118.6(2)	C(3)-N(1)-Cr	105.3(7)
C(2)-N(1)-Cr	106.4(7)	O(7)-C(6)-O(6)	124.8(10)
C(5)-N(1)-Cr	107.3(6)	O(7)-C(6)-C(5)	118.8(10)
N(1)-C(5)-C(6)	113.8(9)		

Symmetry transformations used to generate equivalent atoms:

#1 $y, -x+1/2, z+1/4$

#2 $-x+1/2, -y+1/2, z+1/2$

#3 $-x+1, -y+1/2, -z+1/4$

#4 $-y+1/2, x+1-1, z-1/4$

#5 $-x+1/2, -y+1/2, z-1/2$

Supplementary Data

Table A.3 Bond lengths [Å] for I.

Cs(1)-O(7)#1	3.057(8)	Cr-O(2)	1.966(8)
Cs(1)-O(7)#2	3.116(8)	Cr-O(1)#3	1.961(6)
Cs(1)-O(22)#1	3.12(2)	Cr-O(4)	1.970(8)
Cs(1)-O(2)	3.201(8)	Cr-N(1)	2.048(9)
Cs(1)-O(11)	3.26(2)	Cr-Cr#3	2.955(3)
Cs(1)-O(22)	3.28(2)	O(1)-Cr#3	1.961(6)
Cs(1)-O(1)	3.337(7)	O(6)-C(6)	1.292(13)
Cs(1)-O(6)	3.379(8)	O(6)-Cs(1)#4	3.554(7)
Cs(1)-O(6)#1	3.554(7)	O(2)-C(1)	1.279(13)
Cs(1)-C(6)#1	3.670(11)	O(4)-C(4)	1.27(2)
Cs(1)-O(5)#3	3.718(14)	N(1)-C(3)	1.48(2)
Cs(1)-C(4)#3	3.847(14)	N(1)-C(2)	1.497(14)
Cr-O(1)	1.942(7)	N(1)-C(5)	1.492(12)
Cr-O(6)	1.965(7)	C(5)-C(6)	1.52(2)
C(6)-O(7)	1.217(12)	C(1)-C(2)	1.51(2)
C(6)-Cs(1)#4	3.670(11)	O(22)-Cs(1)#4	3.12(2)
C(4)-O(5)	1.24(2)	O(7)-Cs(1)#4	3.057(8)
C(4)-C(3)	1.52(2)	O(7)-Cs(1)#5	3.116(8)
C(4)-Cs(1)#3	3.847(14)	O(5)-Cs(1)#3	3.718(14)
C(1)-O(3)	1.231(13)		

Supplementary data

Table A.4 Anisotropic displacement parameters ($\text{\AA}^2 \times 10^3$) for I.

Atom	U11	U22	U33	U23	U13	U12
Cs(1)	61(1)	112(1)	79(1)	-20(1)	29(1)	-23(1)
Cr	26(1)	28(1)	41(1)	11(1)	0(1)	-1(1)
O(1)	32(4)	27(3)	43(4)	3(3)	1(3)	-1(3)
O(6)	35(4)	34(4)	61(5)	1(4)	-3(4)	3(3)
O(2)	40(4)	40(4)	49(5)	14(4)	7(4)	-6(3)
O(4)	41(4)	52(5)	43(5)	18(4)	-8(4)	1(4)
N(1)	29(4)	34(5)	49(6)	8(4)	-4(4)	2(4)
C(5)	30(5)	43(6)	46(7)	8(5)	-1(5)	2(5)
C(6)	29(6)	50(6)	35(6)	12(5)	2(5)	-1(5)
C(4)	62(8)	70(9)	49(9)	18(7)	8(7)	0(7)
C(1)	22(5)	43(7)	61(8)	23(6)	-6(5)	-1(5)
C(2)	48(7)	42(7)	66(10)	25(6)	-18(6)	-6(5)
C(3)	49(7)	61(8)	58(9)	-4(7)	19(6)	6(6)
O(22)	312(29)	94(12)	378(39)	73(17)	-203(28)	-65(15)
O(11)	233(25)	135(17)	636(67)	102(27)	181(34)	48(17)
O(7)	26(4)	64(5)	47(5)	10(4)	-3(3)	2(4)
O(3)	37(4)	74(6)	73(6)	46(5)	3(4)	-5(4)
O(5)	141(11)	103(9)	55(7)	14(6)	42(7)	21(8)

The anisotropic displacement factor exponent takes the form: $-2\pi^2[h2a^*2U11+\dots+2hka^*b^*U12]$

Table A.5 Hydrogen coordinates ($\times 10^4$) and isotropic displacement parameters ($\text{\AA}^2 \times 10^3$) for I.

	x	y	z	U(eq)
H(1)	4458(3)	3409(3)	1751(6)	70(16)
H(5A)	3050(5)	1002(5)	401(10)	70(16)
H(5B)	3226(5)	1372(5)	-679(10)	70(16)
H(2A)	4562(6)	562(6)	1059(11)	70(16)
H(2B)	3788(6)	456(6)	1186(11)	70(16)
H(3A)	4146(6)	904(6)	-1165(11)	70(16)
H(3B)	4820(6)	958(6)	-511(11)	70(16)

Supplementary Data

B Crystal data for Cs₂[Cr(nta)(μ-OH)]₂·4H₂O (II)

Table B.1 Atomic coordinates ($\times 10^4$) and equivalent isotropic displacement parameters ($\text{\AA}^2 \times 10^3$) for II. U(eq) is defined as one third of the trace of the orthogonalized U_{ij} tensor.

Atom	x	y	z	U(eq)
Cs(1)	3139(1)	2111(1)	1199(1)	36(1)
Cr(1)	1135(1)	5726(1)	-8(1)	15(1)
O(1)	279(2)	5274(2)	1287(2)	18(1)
O(2)	2599(3)	4621(2)	355(3)	23(1)
O(6)	2507(3)	6664(2)	1343(3)	24(1)
N(1)	1950(3)	6296(2)	-1368(3)	17(1)
C(3)	744(4)	6755(3)	-2534(4)	23(1)
C(6)	2984(4)	7154(3)	-634(4)	24(1)
C(2)	2596(4)	5361(3)	-1757(4)	23(1)
O(4)	-135(3)	6968(2)	-775(3)	24(1)
C(1)	3135(4)	4552(3)	-561(4)	23(1)
C(4)	-144(4)	7356(3)	-1926(4)	26(1)
O(3)	3978(3)	3869(2)	-549(3)	33(1)
O(7)	4054(3)	7950(2)	1605(3)	38(1)
O(5)	-847(4)	8134(3)	-2546(4)	47(1)
C(5)	3217(4)	7283(3)	881(4)	23(1)
OW1	5189(4)	48(3)	1692(4)	55(1)
OW2	2380(5)	305(6)	-1064(6)	109(2)

Supplementary data

Table B.2 Bond angles [°] for II.

O(7)#1-Cs(1)-OW2	132.85(11)	O(3)#3-Cs(1)-C(2)#3	37.26(7)
O(7)#1-Cs(1)-O(3)	78.24(8)	C(1)-Cs(1)-C(2)#3	169.96(8)
OW2-Cs(1)-O(3)	95.72(17)	C(4)#2-Cs(1)-C(2)#3	72.26(8)
O(7)#1-Cs(1)-O(2)	83.77(7)	C(6)#1-Cs(1)-C(2)#3	85.75(8)
OW2-Cs(1)-O(2)	121.33(15)	O(6)-Cr(1)-O(2)	88.69(11)
O(3)-Cs(1)-O(2)	40.69(6)	O(6)-Cr(1)-O(4)	90.96(11)
O(7)#1-Cs(1)-O(4)#2	125.08(8)	O(2)-Cr(1)-O(4)	163.63(10)
OW2-Cs(1)-O(4)#2	102.06(11)	O(6)-Cr(1)-O(1)	94.62(10)
O(3)-Cs(1)-O(4)#2	99.23(6)	O(2)-Cr(1)-O(1)	101.80(10)
O(2)-Cs(1)-O(4)#2	64.16(6)	O(4)-Cr(1)-O(1)	94.54(10)
O(7)#1-Cs(1)-OW	176.70(8)	O(6)-Cr(1)-O(1)#2	176.52(10)
OW2-Cs(1)-OW1	60.67(13)	O(2)-Cr(1)-O(1)#2	90.87(10)
O(3)-Cs(1)-OW1	108.04(9)	O(4)-Cr(1)-O(1)#2	90.43(10)
O(2)-Cs(1)-OW1	146.69(8)	O(1)-Cr(1)-O(1)#2	82.08(10)
O(4)#2-Cs(1)-OW1	148.60(8)	O(6)-Cr(1)-N(1)	84.50(11)
O(7)#1-Cs(1)-O(5)#2	111.17(10)	O(2)-Cr(1)-N(1)	82.09(10)
OW2-Cs(1)-O(5)#2	104.60(15)	O(4)-Cr(1)-N(1)	81.59(11)
O(3)-Cs(1)-O(5)#2	137.26(7)	O(1)-Cr(1)-N(1)	176.01(11)
O(2)-Cs(1)-O(5)#2	97.37(7)	O(1)#2-Cr(1)-N(1)	98.87(10)
O(4)#2-Cs(1)-O(5)#2	40.26(7)	Cr(1)-O(1)-Cr(1)#2	97.92(10)
OW1-Cs(1)-O(5)#2	114.70(9)	C(1)-O(2)-Cr(1)	116.0(2)
O(7)#1-Cs(1)-O(3)#3	65.58(7)	C(1)-O(2)-Cs(1)	93.3(2)
OW2-Cs(1)-O(3)#3	113.06(16)	Cr(1)-O(2)-Cs(1)	139.28(11)
O(3)-Cs(1)-O(3)#3	143.28(9)	C(6)-O(6)-Cr(1)	117.0(2)
O(2)-Cs(1)-O(3)#3	124.69(7)	C(3)-N(1)-C(2)	114.3(3)
O(4)#2-Cs(1)-O(3)#3	96.57(7)	C(3)-N(1)-C(5)	111.1(3)
OW1-Cs(1)-O(3)#3	70.57(9)	C(2)-N(1)-C(5)	112.1(3)
O(5)#2-Cs(1)-O(3)#3	58.20(8)	C(3)-N(1)-Cr(1)	104.17(19)
O(7)#1-Cs(1)-C(1)	84.40(8)	C(2)-N(1)-Cr(1)	106.6(2)
OW2-Cs(1)-C(1)	105.69(16)	C(5)-N(1)-Cr(1)	107.9(2)
O(3)-Cs(1)-C(1)	20.07(7)	N(1)-C(3)-C(4)	108.2(3)
O(2)-Cs(1)-C(1)	21.41(7)	N(1)-C(5)-C(6)	113.2(3)
O(4)#2-Cs(1)-C(1)	80.12(7)	N(1)-C(2)-C(1)	110.5(3)
OW1-Cs(1)-C(1)	128.09(9)	N(1)-C(2)-Cs(1)#4	161.4(2)
O(5)#2-Cs(1)-C(1)	117.21(8)	C(1)-C(2)-Cs(1)#4	81.17(18)
O(3)#3-Cs(1)-C(1)	140.87(7)	C(4)-O(4)-Cr(1)	114.7(2)
O(7)#1-Cs(1)-C(4)#2	116.00(9)	C(4)-O(4)-Cs(1)#2	95.6(2)
OW2-Cs(1)-C(4)#2	108.20(13)	Cr(1)-O(4)-Cs(1)#2	142.73(11)

Supplementary Data

Table B.2 continued

O(3)-Cs(1)-C(4)#2	117.65(7)	O(3)-C(1)-O(2)	124.5(3)
O(2)-Cs(1)-C(4)#2	78.85(7)	O(3)-C(1)-C(2)	119.6(3)
O(4)#2-Cs(1)-C(4)#2	21.04(7)	O(2)-C(1)-C(2)	115.8(3)
OW1-Cs(1)-C(4)#2	134.05(9)	O(3)-C(1)-Cs(1)	63.5(2)
O(5)#2-Cs(1)-C(4)#2	19.97(8)	O(2)-C(1)-Cs(1)	65.25(18)
O(3)#3-Cs(1)-C(4)#2	75.64(8)	C(2)-C(1)-Cs(1)	155.6(2)
C(1)-Cs(1)-C(4)#2	97.72(8)	O(5)-C(4)-O(4)	124.2(4)
O(7)#1-Cs(1)-C(6)#1	16.36(7)	O(5)-C(4)-C(3)	120.3(3)
OW2-Cs(1)-C(6)#1	121.04(11)	O(4)-C(4)-C(3)	115.5(3)
O(3)-Cs(1)-C(6)#1	90.03(8)	O(5)-C(4)-Cs(1)#2	64.7(2)
O(2)-Cs(1)-C(6)#1	100.10(7)	O(4)-C(4)-Cs(1)#2	63.38(18)
O(4)#2-Cs(1)-C(6)#1	134.78(8)	C(3)-C(4)-Cs(1)#2	156.8(3)
OW1-Cs(1)-C(6)#1	61.82(8)	C(1)-O(3)-Cs(1)	96.5(2)
O(5)#2-Cs(1)-C(6)#1	109.79(9)	C(1)-O(3)-Cs(1)#4	109.9(2)
O(3)#3-Cs(1)-C(6)#1	56.09(7)	Cs(1)-O(3)-Cs(1)#4	108.12(9)
C(1)-Cs(1)-C(6)#1	99.19(8)	C(6)-O(7)-Cs(1)#5	117.9(3)
C(4)#2-Cs(1)-C(6)#1	120.32(9)	C(4)-O(5)-Cs(1)#2	95.3(2)
O(7)#1-Cs(1)-C(2)#3	99.25(8)	O(7)-C(5)-O(6)	123.4(4)
OW2-Cs(1)-C(2)#3	78.75(17)	O(7)-C(5)-C(6)	119.7(3)
O(3)-Cs(1)-C(2)#3	169.94(7)	O(6)-C(6)-C(5)	117.0(3)
O(2)-Cs(1)-C(2)#3	149.19(7)	O(7)-C(6)-Cs(1)#5	45.7(2)
O(4)#2-Cs(1)-C(2)#3	90.19(7)	O(6)-C(6)-Cs(1)#5	102.3(2)
OW1-Cs(1)-C(2)#3	61.95(9)	C(6)-C(6)-Cs(1)#5	121.4(2)
O(5)#2-Cs(1)-C(2)#3	52.76(7)		

Supplementary data

Table B.3 Bond lengths [Å] for II.

Cs(1)-O(7)#1	3.117(3)	Cr(1)-O(1)#2	1.991(2)
Cs(1)-OW2	3.125(5)	Cr(1)-N(1)	2.061(3)
Cs(1)-O(3)	3.192(3)	N(1)-C(3)	1.481(4)
Cs(1)-O(2)	3.225(2)	N(1)-C(2)	1.482(4)
Cs(1)-O(4)#2	3.226(2)	N(1)-C(5)	1.498(4)
Cs(1)-OW1	3.254(4)	C(3)-C(4)	1.521(5)
Cs(1)-O(5)#2	3.262(3)	O(6)-C(6)	1.293(4)
Cs(1)-O(3)#3	3.386(3)	O(2)-C(1)	1.296(4)
Cs(1)-C(1)	3.545(4)	O(6)-C(6)	1.293(4)
Cs(1)-C(4)#2	3.592(4)	C(6)-C(5)	1.515(5)
Cs(1)-C(6)#1	3.847(4)	C(2)-C(1)	1.527(5)
Cs(1)-C(2)#3	3.910(3)	C(2)-Cs(1)#4	3.910(3)
Cr(1)-O(6)	1.954(2)	O(4)-C(4)	1.295(4)
Cr(1)-O(2)	1.985(2)	O(4)-Cs(1)#2	3.226(2)
Cr(1)-O(4)	1.988(2)	C(1)-O(3)	1.224(4)
Cr(1)-O(1)	1.987(2)	C(4)-O(5)	1.232(5)
C(4)-Cs(1)#2	3.592(4)	O(7)-Cs(1)#5	3.117(3)
O(3)-Cs(1)#4	3.386(3)	O(5)-Cs(1)#2	3.262(3)
O(7)-C(5)	1.227(5)	C(6)-Cs(1)#5	3.847(4)

Symmetry transformations used to generate equivalent atoms:

- #1 $-x+1, y-1/2, -z+1/2$
- #2 $-x, -y+1, -z$
- #3 $x, -y+1/2, z+1/2$
- #4 $x, -y+1/2, z-1/2$
- #5 $-x+1, y+1/2, -z+1/2$

Supplementary Data

Table B.4 Anisotropic displacement parameters ($\text{\AA}^2 \times 10^3$) for II.

Atom	U11	U22	U33	U23	U13	U12
Cs(1)	32(1)	33(1)	45(1)	7(1)	17(1)	1(1)
Cr(1)	15(1)	15(1)	17(1)	2(1)	8(1)	1(1)
O(1)	19(1)	22(1)	15(1)	0(1)	9(1)	-3(1)
O(2)	22(1)	23(1)	26(1)	5(1)	12(1)	5(1)
O(6)	24(1)	27(1)	25(1)	-6(1)	12(1)	-6(1)
N(1)	16(1)	17(1)	20(1)	2(1)	10(1)	2(1)
C(3)	20(2)	29(2)	22(2)	10(1)	9(1)	5(1)
C(6)	21(2)	24(2)	30(2)	-1(1)	14(1)	-6(1)
C(2)	29(2)	20(2)	26(2)	2(1)	18(1)	6(1)
O(4)	24(1)	22(1)	30(1)	7(1)	16(1)	6(1)
C(1)	20(2)	19(2)	29(2)	-3(1)	10(1)	0(1)
C(4)	20(2)	28(2)	32(2)	12(2)	13(1)	4(1)
O(3)	32(1)	28(1)	45(2)	5(1)	21(1)	14(1)
O(7)	36(2)	36(2)	40(2)	-14(1)	14(1)	-16(1)
O(5)	44(2)	46(2)	65(2)	38(2)	36(2)	27(2)
C(5)	19(2)	19(2)	30(2)	-5(1)	10(1)	-1(1)
OW1	52(2)	52(2)	51(2)	-2(2)	11(2)	-8(2)
OW2	58(3)	162(6)	79(4)	-68(4)	-1(2)	19(3)

Table B.5 Hydrogen coordinates ($\times 10^4$) and isotropic displacement parameters ($\text{\AA}^2 \times 10^3$) for II.

	x	y	z	U(eq)
H(1)	476	5468	2204	46(6)
H(3A)	212	6183	-3143	46(6)
H(3B)	1054	7245	-3072	46(6)
H(6A)	2668	7836	-1109	46(6)
H(6B)	3858	6979	-689	46(6)
H(2A)	3355	5608	-1983	46(6)
H(2B)	1921	5013	-2574	46(6)

Supplementary data

C Crystal data for $\text{Cs}_2[\text{Co}(\text{nta})(\mu\text{-OH})_2]\cdot 4\text{H}_2\text{O}$

Table C.1 Atomic coordinates ($\times 10^4$) and equivalent isotropic displacement parameters ($\text{\AA}^2 \times 10^3$) for $\text{Cs}_2[\text{Co}_2(\mu\text{-nta})_2(\text{OH})_2]\cdot 4\text{H}_2\text{O}$. $U_{(\text{eq})}$ is defined as one third of the trace of the orthogonalized U_{ij} tensor.

Atom	x	y	z	$U_{(\text{eq})}$
Cs(1)	3560(1)	2968(1)	3538(1)	53(1)
Co	4366(1)	2188(1)	963(1)	21(1)
O(1)	4689(2)	3012(2)	1571(4)	22(1)
O(6)	3437(2)	2461(3)	1009(5)	30(1)
O(2)	4267(3)	1781(3)	2317(4)	28(1)
O(4)	4454(3)	2470(3)	-469(4)	30(1)
N(1)	4071(3)	1335(3)	374(5)	24(1)
C(5)	3327(4)	1407(4)	113(7)	30(2)
C(6)	3019(4)	2036(4)	606(7)	26(2)
C(4)	4574(4)	1977(4)	-1075(7)	35(2)
C(1)	4198(4)	1132(4)	2281(7)	27(2)
C(2)	4197(4)	809(4)	1202(7)	32(2)
C(3)	4475(4)	1266(4)	-611(7)	33(2)
O(22)	3223(6)	4355(5)	2307(8)	103(3)
O(11)	4087(8)	4594(7)	4042(11)	146(5)
O(7)	2400(3)	2101(3)	591(5)	36(1)
O(3)	4168(3)	780(3)	3089(5)	36(1)
O(5)	4792(4)	2033(4)	-2005(6)	61(2)

Supplementary Data

Table C.2

Bond lengths [Å] for Cs₂[Co₂(nta)₂(μ-OH)₂].4H₂O.

Cs(1)-O(7)#1	3.008(6)	O(2)-C(1)	1.283(9)
Cs(1)-O(2)	3.117(5)	O(4)-C(4)	1.256(10)
Cs(1)-O(7)#2	3.201(6)	N(1)-C(3)	1.478(10)
Cs(1)-O(22)	3.203(10)	N(1)-C(2)	1.488(9)
Cs(1)-O(22)#1	3.234(11)	N(1)-C(5)	1.503(9)
Cs(1)-O(1)	3.324(5)	C(5)-C(6)	1.509(11)
Cs(1)-O(6)	3.342(6)	C(6)-O(7)	1.221(9)
Cs(1)-O(11)	3.418(14)	C(6)-Cs(1)#4	3.607(8)
Cs(1)-O(5)#3	3.458(8)	C(4)-O(5)	1.250(11)
Cs(1)-O(6)#1	3.504(5)	C(4)-C(3)	1.526(12)
Cs(1)-C(6)#1	3.607(8)	C(4)-Cs(1)#3	3.666(8)
Cs(1)-C(4)#3	3.666(8)	C(1)-O(3)	1.231(9)
Co-O(2)	1.892(5)	C(1)-C(2)	1.498(12)
Co-O(4)	1.893(6)	O(22)-Cs(1)#4	3.234(11)
Co-O(6)	1.902(5)	O(7)-Cs(1)#4	3.008(6)
Co-O(1)#3	1.897(4)	O(7)-Cs(1)#5	3.201(6)
Co-O(1)	1.899(5)	O(5)-Cs(1)#3	3.458(8)
Co-N(1)	1.922(6)	O(1)-Co#3	1.897(4)
Co-Co#3	2.868(2)	O(6)-Cs(1)#4	3.504(5)
O(6)-C(6)	1.276(9)		

Supplementary data

Table C.3 Bond angles [°] for Cs₂[Co₂(nta)₂(μ-OH)₂].4H₂O.

O(7)#1-Cs(1)-O(2)	98.80(14)	O(7)#1-Cs(1)-O(7)#2	65.13(8)
O(2)-Cs(1)-O(7)#2	128.95(14)	O(7)#1-Cs(1)-O(22)	85.3(2)
O(2)-Cs(1)-O(22)	119.3(2)	O(7)#2-Cs(1)-O(22)	107.7(2)
O(7)#1-Cs(1)-O(22)#1	112.2(2)	O(2)-Cs(1)-O(22)#1	59.2(2)
O(7)#2-Cs(1)-O(22)#1	81.7(2)	O(22)-Cs(1)-O(22)#1	162.5(2)
O(7)#1-Cs(1)-O(1)	120.2(2)	O(2)-Cs(1)-O(1)	49.87(12)
O(7)#2-Cs(1)-O(1)	174.19(13)	O(22)-Cs(1)-O(1)	75.9(2)
O(22)#1-Cs(1)-O(1)	93.7(2)	O(7)#1-Cs(1)-O(6)	71.45(14)
O(2)-Cs(1)-O(6)	48.74(13)	O(7)#2-Cs(1)-O(6)	135.49(13)
O(22)-Cs(1)-O(6)	77.2(2)	O(22)#1-Cs(1)-O(6)	106.8(2)
O(1)-Cs(1)-O(6)	49.25(12)	O(7)#1-Cs(1)-O(11)	123.2(3)
O(2)-Cs(1)-O(11)	130.9(3)	O(7)#2-Cs(1)-O(11)	93.9(2)
O(22)-Cs(1)-O(11)	50.0(3)	O(22)#1-Cs(1)-O(11)	116.0(3)
O(1)-Cs(1)-O(11)	84.9(2)	O(6)-Cs(1)-O(11)	118.5(3)
O(7)#1-Cs(1)-O(5)#3	163.2(2)	O(2)-Cs(1)-O(5)#3	75.9(2)
O(7)#2-Cs(1)-O(5)#3	105.5(2)	O(22)-Cs(1)-O(5)#3	111.3(2)
O(22)#1-Cs(1)-O(5)#3	51.3(2)	O(1)-Cs(1)-O(5)#3	68.74(14)
O(6)-Cs(1)-O(5)#3	113.73(14)	O(11)-Cs(1)-O(5)#3	69.6(3)
O(7)#1-Cs(1)-O(6)#1	38.92(13)	O(2)-Cs(1)-O(6)#1	71.39(12)
O(7)#2-Cs(1)-O(6)#1	67.18(13)	O(22)-Cs(1)-O(6)#1	122.5(2)
O(22)#1-Cs(1)-O(6)#1	74.5(2)	O(1)-Cs(1)-O(6)#1	115.09(12)
O(6)-Cs(1)-O(6)#1	73.21(10)	O(11)-Cs(1)-O(6)#1	157.6(3)
O(5)#3-Cs(1)-O(6)#1	125.5(2)	O(7)#1-Cs(1)-C(6)#1	18.6(2)
O(2)-Cs(1)-C(6)#1	83.9(2)	O(7)#2-Cs(1)-C(6)#1	67.0(2)
O(22)-Cs(1)-C(6)#1	102.3(2)	O(22)#1-Cs(1)-C(6)#1	95.0(2)
O(1)-Cs(1)-C(6)#1	117.1(2)	O(6)-Cs(1)-C(6)#1	68.7(2)
O(11)-Cs(1)-C(6)#1	141.4(3)	O(5)#3-Cs(1)-C(6)#1	146.1(2)
O(6)#1-Cs(1)-C(6)#1	20.62(14)	O(7)#1-Cs(1)-C(4)#3	164.1(2)
O(2)-Cs(1)-C(4)#3	65.4(2)	O(7)#2-Cs(1)-C(4)#3	125.4(2)
O(22)-Cs(1)-C(4)#3	100.8(2)	O(22)#1-Cs(1)-C(4)#3	62.1(2)
O(1)-Cs(1)-C(4)#3	48.9(2)	O(6)-Cs(1)-C(4)#3	95.4(2)
O(11)-Cs(1)-C(4)#3	70.5(3)	O(5)#3-Cs(1)-C(4)#3	19.9(2)
O(6)#1-Cs(1)-C(4)#3	129.8(2)	C(6)#1-Cs(1)-C(4)#3	147.9(2)
O(2)-Co-O(4)	172.0(2)	O(2)-Co-O(6)	89.6(2)
O(4)-Co-O(6)	91.9(2)	O(2)-Co-O(1)#3	91.9(2)
O(4)-Co-O(1)#3	87.2(2)	O(6)-Co-O(1)#3	175.6(2)
O(2)-Co-O(1)	91.8(2)	O(4)-Co-O(1)	95.9(2)

Supplementary Data

Table C.3 continued

O(6)-Co-O(1)	93.9(2)	O(1)#3-Co-O(1)	81.8(2)
O(2)-Co-N(1)	87.0(2)	O(4)-Co-N(1)	85.2(2)
O(6)-Co-N(1)	88.1(2)	O(1)#3-Co-N(1)	96.1(2)
O(1)-Co-N(1)	177.6(2)	O(2)-Co-Co#3	92.4(2)
O(4)-Co-Co#3	92.1(2)	O(6)-Co-Co#3	134.8(2)
O(1)#3-Co-Co#3	40.94(14)	O(1)-Co-Co#3	40.90(13)
O(2)-Co-Cs(1)	51.6(2)	O(4)-Co-Cs(1)	135.2(2)
O(6)-Co-Cs(1)	58.5(2)	O(1)#3-Co-Cs(1)	119.6(2)
O(1)-Co-Cs(1)	57.93(14)	N(1)-Co-Cs(1)	122.5(2)
Co#3-Co-Cs(1)	88.60(4)	Co#3-O(1)-Co	98.2(2)
Co#3-O(1)-Cs(1)	131.6(2)	Co-O(1)-Cs(1)	93.1(2)
C(6)-O(6)-Co	114.9(5)	C(6)-O(6)-Cs(1)	128.3(5)
Co-O(6)-Cs(1)	92.5(2)	C(6)-O(6)-Cs(1)#4	84.2(4)
Co-O(6)-Cs(1)#4	158.3(2)	Cs(1)-O(6)-Cs(1)#4	82.15(12)
C(1)-O(2)-Co	113.5(5)	C(1)-O(2)-Cs(1)	135.5(5)
Co-O(2)-Cs(1)	100.0(2)	C(4)-O(4)-Co	111.7(5)
C(3)-N(1)-C(2)	115.7(6)	C(3)-N(1)-C(5)	110.3(6)
C(2)-N(1)-C(5)	112.3(6)	C(3)-N(1)-Co	103.9(4)
C(2)-N(1)-Co	106.6(5)	C(5)-N(1)-Co	107.2(4)
N(1)-C(5)-C(6)	112.1(6)	O(7)-C(6)-O(6)	125.4(7)
O(7)-C(6)-C(5)	118.6(7)	O(6)-C(6)-C(5)	116.1(6)
O(7)-C(6)-Cs(1)#4	51.8(4)	O(6)-C(6)-Cs(1)#4	75.2(4)
C(5)-C(6)-Cs(1)#4	163.1(5)	O(5)-C(4)-O(4)	124.4(8)
O(5)-C(4)-C(3)	118.9(8)	O(4)-C(4)-C(3)	116.7(7)
O(5)-C(4)-Cs(1)#3	70.6(5)	O(4)-C(4)-Cs(1)#3	99.1(5)
C(3)-C(4)-Cs(1)#3	98.7(4)	O(3)-C(1)-O(2)	122.2(8)
O(3)-C(1)-C(2)	120.7(7)	O(2)-C(1)-C(2)	117.0(7)
N(1)-C(2)-C(1)	109.9(6)	N(1)-C(3)-C(4)	107.8(6)
Cs(1)-O(22)-Cs(1)#4	88.7(2)	C(6)-O(7)-Cs(1)#4	109.6(5)
C(6)-O(7)-Cs(1)#5	126.4(5)	Cs(1)#4-O(7)-Cs(1)#5	92.8(2)
C(4)-O(5)-Cs(1)#3	89.5(5)	N(1)-Co-Co#3	137.0(2)

Symmetry transformations used to generate equivalent atoms:

#1: $y, -x+1/2, z+1/4$, #2: $-x+1/2, -y+1/2, z+1/2$, #3: $-x+1, -y+1/2, -z+1/4$, #4: $-y+1/2, x+1-1, z-1/4$, #5: $-x+1/2, -y+1/2, z-1/2$

Supplementary data

Table C.4 Anisotropic displacement parameters ($\text{\AA}^2 \times 10^3$) for $\text{Cs}_2[\text{Co}_2(\text{nta})_2(\mu\text{-OH})_2] \cdot 4\text{H}_2\text{O}$.

Atom	U_{11}	U_{22}	U_{33}	U_{23}	U_{13}	U_{12}
Cs(1)	39(1)	65(1)	56(1)	-7(1)	13(1)	-6(1)
Co	19(1)	18(1)	25(1)	5(1)	-1(1)	-1(1)
O(1)	19(2)	18(2)	29(3)	0(2)	2(2)	1(2)
O(6)	23(3)	29(3)	37(3)	-1(3)	-2(3)	2(2)
O(2)	28(3)	26(3)	30(3)	7(2)	2(2)	-6(2)
O(4)	33(3)	28(3)	29(3)	10(3)	-4(2)	0(2)
N(1)	21(3)	24(3)	25(4)	2(3)	0(3)	1(2)
C(5)	20(4)	34(4)	38(5)	-1(4)	-7(4)	0(3)
C(6)	24(4)	30(4)	25(4)	6(3)	0(3)	-2(3)
C(4)	27(4)	47(5)	32(5)	9(4)	-3(4)	2(4)
C(1)	16(3)	32(4)	34(5)	9(4)	1(3)	-7(3)
C(2)	33(4)	25(4)	38(5)	8(3)	-6(4)	-1(3)
C(3)	30(4)	29(4)	39(5)	-7(4)	1(4)	2(3)
O(22)	138(9)	86(7)	84(7)	11(6)	-5(7)	-18(6)
O(11)	155(11)	138(11)	146(12)	-2(9)	25(10)	-15(9)
O(7)	20(3)	47(3)	42(4)	4(3)	0(2)	-1(2)
O(3)	29(3)	37(3)	42(4)	22(3)	3(3)	-4(2)
O(5)	73(5)	71(5)	40(4)	10(4)	15(4)	10(4)

Supplementary Data

Table C.5Hydrogen coordinates ($\times 10^4$) and isotropic displacement parameters ($\text{\AA}^2 \times 10^3$) for $\text{Cs}_2[\text{Co}_2(\text{nta})_2(\mu\text{-OH})_2]\cdot 4\text{H}_2\text{O}$.

	x	y	z	$U_{(\text{eq})}$
H(1)	4457(2)	3395(2)	1810(4)	26
H(5A)	3085(4)	1008(4)	368(7)	37(9)
H(5B)	3272(4)	1428(4)	-652(7)	37(9)
H(2A)	4632(4)	591(4)	1073(7)	37(9)
H(2B)	3845(4)	463(4)	1168(7)	37(9)
H(3A)	4237(4)	978(4)	-1116(7)	37(9)
H(3B)	4913(4)	1061(4)	-455(7)	37(9)

Supplementary data

D Crystal data for $\text{Cs}_2[\text{Co}(\text{nta})\text{CO}_3]\cdot\text{H}_2\text{O}$

Table D.1 Atomic coordinates ($\times 10^4$) and equivalent isotropic displacement parameters ($\text{\AA}^2 \times 10^3$) for $\text{Cs}_2[\text{Co}(\text{nta})\text{CO}_3]\cdot\text{H}_2\text{O}$.

Atom	x	y	z	U(eq)
Cs(1)	2398(1)	2082(1)	1960(1)	25(1)
Cs(2)	4557(1)	1055(1)	-1456(1)	35(1)
Co(1)	2378(1)	-2137(1)	672(1)	17(1)
O(1)	1330(2)	-1444(3)	1937(2)	25(1)
O(2)	3377(2)	-1755(3)	1257(2)	26(1)
O(3)	2347(2)	31(3)	42(2)	24(1)
O(4)	2571(2)	-4128(3)	1368(2)	27(1)
O(5)	3325(2)	-3006(3)	-618(2)	27(1)
N(1)	1385(2)	-2920(3)	147(2)	19(1)
O(7)	3473(2)	-5312(3)	-1639(2)	37(1)
O(8)	3799(2)	-4061(3)	2015(2)	41(1)
O(9)	1520(2)	1461(3)	-793(2)	40(1)
O(10)	-252(2)	-2099(3)	2856(2)	42(1)
C(1)	3279(2)	-3357(4)	1587(2)	26(1)
C(2)	1712(2)	138(4)	-419(2)	25(1)
C(3)	497(2)	-2185(4)	2050(3)	25(1)
C(4)	2968(2)	-4281(4)	-983(2)	25(1)
OW1	4663(2)	2931(4)	809(3)	55(1)
C(5)	495(2)	-3276(4)	1114(2)	26(1)
C(6)	1835(2)	-4469(4)	-495(3)	29(1)
C(7)	1216(3)	-1525(4)	-520(3)	31(1)

U(eq) is defined as one third of the trace of the orthogonalized U_{ij} tensor.

Supplementary Data

Table D.2 Bond lengths [Å] for Cs₂[Co(nta)CO₃].H₂O.

Cs(1)-O(9) ^{#1}	3.046(2)	Cs(1)-C(6) ^{#4}	3.817(3)
Cs(1)-O(4) ^{#2}	3.048(2)	Cs(2)-O(8) ^{#5}	3.091(2)
Cs(1)-O(3)	3.068(2)	Cs(2)-O(2) ^{#6}	3.145(2)
Cs(1)-O(10) ^{#3}	3.089(3)	Cs(2)-O(3)	3.193(2)
Cs(1)-OW1	3.137(3)	Cs(2)-O(8) ^{#6}	3.225(3)
Cs(1)-O(1)	3.160(2)	Cs(2)-O(7) ^{#7}	3.237(3)
Cs(1)-O(7) ^{#4}	3.173(2)	Cs(2)-O(7) ^{#2}	3.292(3)
Cs(1)-O(2)	3.298(2)	Cs(2)-OW1	3.443(4)
Cs(1)-O(8) ^{#2}	3.643(3)	Cs(2)-OW1 ^{#6}	3.525(4)
Cs(1)-Co(1)	3.7265(4)	Cs(2)-C(1) ^{#6}	3.556(3)
Cs(1)-C(1) ^{#2}	3.750(3)	Cs(2)-O(5)	3.606(2)
Cs(2)-C(2)	3.895(3)	Cs(2)-OW1 ^{#8}	3.725(4)
Co(1)-O(4)	1.889(2)	O(3)-C(2)	1.288(4)
Co(1)-O(1)	1.897(2)	O(4)-C(1)	1.312(4)
Co(1)-O(3)	1.901(2)	O(4)-Cs(1) ^{#9}	3.048(2)
Co(1)-O(5)	1.902(2)	O(5)-C(4)	1.298(4)
Co(1)-O(2)	1.908(2)	N(1)-C(5)	1.485(4)
Co(1)-N(1)	1.920(2)	N(1)-C(7)	1.489(4)
Co(1)-C(1)	2.306(3)	N(1)-C(6)	1.490(4)
O(1)-C(3)	1.294(4)	O(7)-C(4)	1.221(4)
O(2)-C(1)	1.316(4)	O(7)-Cs(1) ^{#5}	3.173(2)
O(2)-Cs(2) ^{#6}	3.145(2)	O(7)-Cs(2) ^{#10}	3.237(3)
O(7)-Cs(2) ^{#9}	3.292(3)	C(1)-Cs(2) ^{#6}	3.556(3)
O(8)-C(1)	1.233(4)	C(1)-Cs(1) ^{#9}	3.750(3)
O(8)-Cs(2) ^{#4}	3.091(2)	C(2)-C(7)	1.513(4)
O(8)-Cs(2) ^{#6}	3.225(3)	C(3)-C(5)	1.524(4)
O(8)-Cs(1) ^{#9}	3.643(3)	C(4)-C(6)	1.532(4)
O(9)-C(2)	1.225(4)	C(4)-Cs(1) ^{#5}	3.855(3)
O(9)-Cs(1) ^{#8}	3.046(2)	OW1-Cs(2) ^{#6}	3.525(4)
O(10)-C(3)	1.223(4)	OW1-Cs(2) ^{#1}	3.725(4)
O(10)-Cs(1) ^{#11}	3.089(3)	C(6)-Cs(1) ^{#5}	3.817(3)

Supplementary data

Table D.3 Bond angles [°] for Cs₂[Co(nta)CO₃].H₂O.

O(9) ^{#1} -Cs(1)-O(4) ^{#2}	82.14(7)	O(1)-Cs(1)-O(7) ^{#4}	88.60(6)
O(9) ^{#1} -Cs(1)-O(3)	154.81(6)	O(9) ^{#1} -Cs(1)-O(2)	127.07(7)
O(4) ^{#2} -Cs(1)-O(3)	108.03(6)	O(4) ^{#2} -Cs(1)-O(2)	145.05(6)
O(9) ^{#1} -Cs(1)-O(10) ^{#3}	78.71(8)	O(3)-Cs(1)-O(2)	54.91(5)
O(4) ^{#2} -Cs(1)-O(10) ^{#3}	78.67(6)	O(10) ^{#3} -Cs(1)-O(2)	121.56(6)
O(3)-Cs(1)-O(10) ^{#3}	80.81(7)	OW1-Cs(1)-O(2)	77.83(7)
O(9) ^{#1} -Cs(1)-OW1	113.06(9)	O(1)-Cs(1)-O(2)	50.72(5)
O(4) ^{#2} -Cs(1)-OW1	72.28(7)	O(7) ^{#4} -Cs(1)-O(2)	61.57(6)
O(3)-Cs(1)-OW1	92.10(8)	O(9) ^{#1} -Cs(1)-O(8) ^{#2}	72.71(7)
O(10) ^{#3} -Cs(1)-OW1	146.29(8)	O(4) ^{#2} -Cs(1)-O(8) ^{#2}	38.00(5)
O(9) ^{#1} -Cs(1)-O(1)	107.96(6)	O(3)-Cs(1)-O(8) ^{#2}	129.34(6)
O(4) ^{#2} -Cs(1)-O(1)	146.59(6)	O(10) ^{#3} -Cs(1)-O(8) ^{#2}	112.19(6)
O(3)-Cs(1)-O(1)	51.27(5)	OW1-Cs(1)-O(8) ^{#2}	49.35(7)
O(10) ^{#3} -Cs(1)-O(1)	72.57(6)	O(1)-Cs(1)-O(8) ^{#2}	175.14(5)
OW1-Cs(1)-O(1)	127.15(7)	O(7) ^{#4} -Cs(1)-O(8) ^{#2}	87.07(6)
O(9) ^{#1} -Cs(1)-O(7) ^{#4}	71.61(7)	O(2)-Cs(1)-O(8) ^{#2}	124.90(5)
O(4) ^{#2} -Cs(1)-O(7) ^{#4}	124.56(6)	O(9) ^{#1} -Cs(1)-Co(1)	136.25(5)
O(3)-Cs(1)-O(7) ^{#4}	116.47(6)	O(4) ^{#2} -Cs(1)-Co(1)	138.41(4)
O(10) ^{#3} -Cs(1)-O(7) ^{#4}	137.77(6)	O(3)-Cs(1)-Co(1)	30.58(4)
OW1-Cs(1)-O(7) ^{#4}	74.68(8)	O(10) ^{#3} -Cs(1)-Co(1)	92.29(5)
OW1-Cs(1)-Co(1)	98.11(6)	O(1)-Cs(1)-C(6) ^{#4}	66.49(6)
O(1)-Cs(1)-Co(1)	30.60(4)	O(7) ^{#4} -Cs(1)-C(6) ^{#4}	38.72(6)
O(7) ^{#4} -Cs(1)-Co(1)	89.07(5)	O(2)-Cs(1)-C(6) ^{#4}	72.62(6)
O(2)-Cs(1)-Co(1)	30.76(4)	O(8) ^{#2} -Cs(1)-C(6) ^{#4}	111.01(6)
O(8) ^{#2} -Cs(1)-Co(1)	146.98(5)	Co(1)-Cs(1)-C(6) ^{#4}	85.01(5)
O(9) ^{#1} -Cs(1)-C(1) ^{#2}	77.07(7)	C(1) ^{#2} -Cs(1)-C(6) ^{#4}	125.22(7)
O(4) ^{#2} -Cs(1)-C(1) ^{#2}	18.87(6)	O(8) ^{#5} -Cs(2)-O(2) ^{#6}	136.58(7)
O(3)-Cs(1)-C(1) ^{#2}	119.59(6)	O(8) ^{#5} -Cs(2)-O(3)	77.21(7)
O(10) ^{#3} -Cs(1)-C(1) ^{#2}	95.54(7)	O(2) ^{#6} -Cs(2)-O(3)	138.67(6)
OW1-Cs(1)-C(1) ^{#2}	59.46(7)	O(8) ^{#5} -Cs(2)-O(8) ^{#6}	128.46(3)
O(1)-Cs(1)-C(1) ^{#2}	165.38(6)	O(2) ^{#6} -Cs(2)-O(8) ^{#6}	41.56(6)
O(7) ^{#4} -Cs(1)-C(1) ^{#2}	106.02(6)	O(3)-Cs(2)-O(8) ^{#6}	144.13(6)
O(2)-Cs(1)-C(1) ^{#2}	137.19(6)	O(8) ^{#5} -Cs(2)-O(7) ^{#7}	74.24(7)
O(8) ^{#2} -Cs(1)-C(1) ^{#2}	19.13(6)	O(2) ^{#6} -Cs(2)-O(7) ^{#7}	62.53(6)
Co(1)-Cs(1)-C(1) ^{#2}	146.68(5)	O(3)-Cs(2)-O(7) ^{#7}	143.58(6)
O(9) ^{#1} -Cs(1)-C(6) ^{#4}	55.21(7)	O(8) ^{#6} -Cs(2)-O(7) ^{#7}	72.29(7)
O(4) ^{#2} -Cs(1)-C(6) ^{#4}	136.34(7)	O(8) ^{#5} -Cs(2)-O(7) ^{#2}	95.00(7)
O(3)-Cs(1)-C(6) ^{#4}	114.74(6)	O(2) ^{#6} -Cs(2)-O(7) ^{#2}	110.53(6)

Supplementary Data

Table D.3 continued

O(10) ^{#3} -Cs(1)-C(6) ^{#4}	99.36(6)	O(3)-Cs(2)-O(7) ^{#2}	82.48(6)
OW1-Cs(1)-C(6) ^{#4}	113.38(9)	O(8) ^{#6} -Cs(2)-O(7) ^{#2}	71.77(6)
O(7) ^{#7} -Cs(2)-O(7) ^{#2}	121.88(6)	O(8) ^{#6} -Cs(2)-OW1 ^{#6}	115.05(7)
O(8) ^{#5} -Cs(2)-OW1	161.74(8)	O(7) ^{#7} -Cs(2)-OW1 ^{#6}	68.79(7)
O(2) ^{#6} -Cs(2)-OW1	59.77(7)	O(7) ^{#2} -Cs(2)-OW1 ^{#6}	169.28(7)
O(3)-Cs(2)-OW1	84.54(6)	OW1-Cs(2)-OW1 ^{#6}	91.81(8)
O(8) ^{#6} -Cs(2)-OW1	68.24(7)	O(8) ^{#5} -Cs(2)-C(1) ^{#6}	137.99(7)
O(7) ^{#7} -Cs(2)-OW1	122.14(7)	O(2) ^{#6} -Cs(2)-C(1) ^{#6}	21.55(6)
O(7) ^{#2} -Cs(2)-OW1	83.04(7)	O(3)-Cs(2)-C(1) ^{#6}	144.67(6)
O(8) ^{#5} -Cs(2)-OW1 ^{#6}	86.93(8)	O(8) ^{#6} -Cs(2)-C(1) ^{#6}	20.20(6)
O(2) ^{#6} -Cs(2)-OW1 ^{#6}	74.40(6)	O(7) ^{#7} -Cs(2)-C(1) ^{#6}	68.00(7)
O(3)-Cs(2)-OW1 ^{#6}	87.69(6)	O(7) ^{#2} -Cs(2)-C(1) ^{#6}	89.80(7)
OW1-Cs(2)-C(1) ^{#6}	60.26(7)	O(7) ^{#2} -Cs(2)-OW1 ^{#8}	65.78(6)
OW1 ^{#6} -Cs(2)-C(1) ^{#6}	95.82(7)	OW1-Cs(2)-OW1 ^{#8}	142.30(2)
O(8) ^{#5} -Cs(2)-O(5)	60.77(6)	OW1 ^{#6} -Cs(2)-OW1 ^{#8}	122.21(8)
O(2) ^{#6} -Cs(2)-O(5)	120.08(5)	C(1) ^{#6} -Cs(2)-OW1	109.44(6)
O(3)-Cs(2)-O(5)	46.96(5)	O(8) ^{#5} -Cs(2)-C(2)	63.90(7)
O(8) ^{#6} -Cs(2)-O(5)	161.56(5)	O(2) ^{#6} -Cs(2)-C(2)	155.88(6)
O(7) ^{#7} -Cs(2)-O(5)	98.57(6)	O(3)-Cs(2)-C(2)	17.60(5)
O(7) ^{#2} -Cs(2)-O(5)	125.84(6)	O(8) ^{#6} -Cs(2)-C(2)	143.93(7)
OW1-Cs(2)-O(5)	105.83(7)	O(7) ^{#7} -Cs(2)-C(2)	136.89(6)
OW1 ^{#6} -Cs(2)-O(5)	46.69(6)	O(7) ^{#2} -Cs(2)-C(2)	73.47(6)
C(1) ^{#6} -Cs(2)-O(5)	141.58(6)	OW1-Cs(2)-C(2)	98.32(7)
O(8) ^{#5} -Cs(2)-OW1 ^{#8}	48.67(7)	OW1 ^{#6} -Cs(2)-C(2)	98.11(7)
O(2) ^{#6} -Cs(2)-OW1 ^{#8}	110.74(6)	C(1) ^{#6} -Cs(2)-C(2)	154.82(7)
O(3)-Cs(2)-OW1 ^{#8}	110.34(6)	O(5)-Cs(2)-C(2)	52.48(6)
O(8) ^{#6} -Cs(2)-OW1 ^{#8}	81.71(7)	OW1 ^{#8} -Cs(2)-C(2)	92.75(6)
O(7) ^{#7} -Cs(2)-OW1 ^{#8}	65.10(6)	O(4)-Co(1)-O(1)	90.08(10)
O(4)-Co(1)-O(3)	170.57(9)	O(3)-Co(1)-O(5)	91.99(9)
O(1)-Co(1)-O(3)	90.42(9)	O(4)-Co(1)-O(2)	69.46(9)
O(4)-Co(1)-O(5)	88.52(10)	O(1)-Co(1)-O(2)	93.36(9)
O(1)-Co(1)-O(5)	173.62(9)	O(3)-Co(1)-O(2)	101.11(9)
O(5)-Co(1)-O(2)	91.98(9)	C(2)-O(3)-Cs(2)	113.8(2)
O(4)-Co(1)-N(1)	100.91(9)	Co(1)-O(3)-Cs(2)	108.86(8)
O(1)-Co(1)-N(1)	87.99(10)	Cs(1)-O(3)-Cs(2)	94.30(5)
O(3)-Co(1)-N(1)	88.52(9)	C(1)-O(4)-Co(1)	90.3(2)
O(5)-Co(1)-N(1)	86.17(10)	C(1)-O(4)-Cs(1) ^{#9}	112.4(2)
O(2)-Co(1)-N(1)	170.26(9)	Co(1)-O(4)-Cs(1) ^{#9}	156.22(10)
O(4)-Co(1)-C(1)	34.69(10)	C(4)-O(5)-Co(1)	111.5(2)

Supplementary data

Table D.3 continued

O(1)-Co(1)-C(1)	93.26(10)	C(4)-O(5)-Cs(2)	140.7(2)
O(3)-Co(1)-C(1)	135.89(10)	Co(1)-O(5)-Cs(2)	94.63(7)
O(5)-Co(1)-C(1)	89.13(10)	C(5)-N(1)-C(7)	112.7(2)
O(2)-Co(1)-C(1)	34.81(10)	C(5)-N(1)-C(6)	114.3(2)
N(1)-Co(1)-C(1)	135.51(10)	C(7)-N(1)-C(6)	112.0(3)
O(4)-Co(1)-Cs(1)	117.78(7)	C(5)-N(1)-Co(1)	105.0(2)
O(1)-Co(1)-Cs(1)	57.96(6)	C(7)-N(1)-Co(1)	107.6(2)
O(3)-Co(1)-Cs(1)	55.18(6)	C(6)-N(1)-Co(1)	104.3(2)
O(5)-Co(1)-Cs(1)	127.99(6)	C(4)-O(7)-Cs(1) ^{#5}	115.2(2)
O(2)-Co(1)-Cs(1)	62.10(7)	C(4)-O(7)-Cs(2) ^{#10}	118.5(2)
N(1)-Co(1)-Cs(1)	90.66(8)	Cs(1) ^{#5} -O(7)-Cs(2) ^{#10}	98.66(6)
O(4)-Co(1)-Cs(2)	127.97(7)	C(4)-O(7)-Cs(2) ^{#9}	133.4(2)
O(1)-Co(1)-Cs(2)	126.55(7)	Cs(1) ^{#5} -O(7)-Cs(2) ^{#9}	91.24(6)
O(3)-Co(1)-Cs(2)	45.85(6)	Cs(2) ^{#10} -O(7)-Cs(2) ^{#9}	92.22(6)
O(5)-Co(1)-Cs(2)	58.61(6)	C(1)-O(8)-Cs(2) ^{#4}	164.7(2)
O(2)-Co(1)-Cs(2)	72.51(7)	C(1)-O(8)-Cs(2) ^{#6}	95.2(2)
N(1)-Co(1)-Cs(2)	114.22(7)	Cs(2) ^{#4} -O(8)-Cs(2) ^{#6}	96.30(7)
C(1)-Co(1)-Cs(2)	100.41(8)	C(1)-O(8)-Cs(1) ^{#9}	85.3(2)
Cs(1)-Co(1)-Cs(2)	70.369(8)	Cs(2) ^{#4} -O(8)-Cs(1) ^{#9}	86.26(6)
C(3)-O(1)-Co(1)	112.3(2)	Cs(2) ^{#6} -O(8)-Cs(1) ^{#9}	164.43(10)
C(3)-O(1)-Cs(1)	145.6(2)	C(2)-O(9)-Cs(1) ^{#8}	130.6(2)
Co(1)-O(1)-Cs(1)	91.45(7)	C(3)-O(10)-Cs(1) ^{#11}	126.5(2)
C(1)-O(2)-Co(1)	89.3(2)	O(8)-C(1)-O(4)	124.2(3)
C(1)-O(2)-Cs(2) ^{#6}	97.1(2)	O(8)-C(1)-O(2)	125.0(3)
Co(1)-O(2)-Cs(2) ^{#6}	161.90(11)	O(4)-C(1)-O(2)	110.8(2)
C(1)-O(2)-Cs(1)	141.5(2)	O(8)-C(1)-Co(1)	175.8(3)
Co(1)-O(2)-Cs(1)	87.14(7)	O(4)-C(1)-Co(1)	55.00(14)
Cs(2) ^{#6} -O(2)-Cs(1)	97.98(6)	O(2)-C(1)-Co(1)	55.85(14)
C(2)-O(3)-Co(1)	114.3(2)	O(8)-C(1)-Cs(2) ^{#6}	64.6(2)
C(2)-O(3)-Cs(1)	128.1(2)	O(4)-C(1)-Cs(2) ^{#6}	165.1(2)
Co(1)-O(3)-Cs(1)	94.25(7)	O(2)-C(1)-Cs(2) ^{#6}	61.4(2)
Co(1)-C(1)-Cs(2) ^{#6}	115.20(11)	O(4)-C(1)-Cs(1) ^{#9}	48.72(14)
O(8)-C(1)-Cs(1) ^{#9}	75.5(2)	O(2)-C(1)-Cs(1) ^{#9}	159.2(2)
Co(1)-C(1)-Cs(1) ^{#9}	103.43(10)	O(1)-C(3)-C(5)	115.9(3)
Cs(2) ^{#6} -C(1)-Cs(1) ^{#9}	137.32(9)	O(7)-C(4)-O(5)	124.3(3)
O(9)-C(2)-O(3)	124.3(3)	O(7)-C(4)-C(6)	120.6(3)
O(9)-C(2)-C(7)	119.9(3)	O(5)-C(4)-C(6)	115.0(2)
O(3)-C(2)-C(7)	115.8(2)	O(7)-C(4)-Cs(1) ^{#5}	48.2(2)
O(9)-C(2)-Cs(2)	93.8(2)	O(5)-C(4)-Cs(1) ^{#5}	158.1(2)

Supplementary Data

Table D.3 continued

O(3)-C(2)-Cs(2)	48.57(14)	C(6)-C(4)-Cs(1) ^{#5}	77.1(2)
C(7)-C(2)-Cs(2)	126.8(2)	Cs(1)-OW1-Cs(2)	88.34(8)
O(10)-C(3)-O(1)	124.2(3)	Cs(1)-OW1-Cs(2) ^{#6}	93.57(9)
O(10)-C(3)-C(5)	119.8(3)	Cs(2)-OW1-Cs(2) ^{#6}	88.19(8)
Cs(1)-OW1-Cs(2) ^{#1}	84.21(9)	N(1)-C(6)-C(4)	110.0(2)
Cs(2)-OW1-Cs(2) ^{#1}	166.34(11)	N(1)-C(6)-Cs(1) ^{#5}	149.3(2)
Cs(2) ^{#6} -OW1-Cs(2) ^{#1}	80.88(8)	C(4)-C(6)-Cs(1) ^{#5}	79.9(2)
N(1)-C(5)-C(3)	111.1(2)	N(1)-C(7)-C(2)	112.5(2)

Symmetry transformations used to generate equivalent atoms:

#1	$x, -y+1/2, z+1/2$	#2	$x, y+1, z$	#3	$-x, y+1/2, -z+1/2$
#4	$x, -y-1/2, z+1/2$	#5	$x, -y-1/2, z-1/2$	#6	$-x+1, -y, -z$
#7	$-x+1, y+1/2, -z-1/2$	#8	$x, -y+1/2, z-1/2$	#9	$x, y-1, z+$
#10	$-x+1, y-1/2, -z-1/2$	#11	$-x, y-1/2, -z+1/2$		

Supplementary data

Table D.4 Anisotropic displacement parameters ($\text{\AA}^2 \times 10^3$) for $\text{Cs}_2[\text{Co}(\text{nta})\text{CO}_3] \cdot \text{H}_2\text{O}$.

Atom	U11	U22	U33	U23	U13	U12
Cs(1)	25(1)	20(1)	29(1)	-1(1)	-10(1)	0(1)
Cs(2)	26(1)	41(1)	39(1)	-5(1)	-13(1)	-3(1)
Co(1)	15(1)	15(1)	24(1)	0(1)	-9(1)	-1(1)
O(1)	23(1)	24(1)	27(1)	-5(1)	-8(1)	-2(1)
O(2)	23(1)	24(1)	37(1)	-2(1)	-17(1)	-2(1)
O(3)	25(1)	18(1)	31(1)	4(1)	-12(1)	-4(1)
O(4)	30(1)	19(1)	38(1)	5(1)	-19(1)	-2(1)
O(5)	19(1)	31(1)	31(1)	-5(1)	-9(1)	-1(1)
N(1)	17(1)	16(1)	26(1)	-2(1)	-10(1)	0(1)
O(7)	31(1)	39(1)	37(1)	-15(1)	-10(1)	9(1)
O(8)	43(1)	44(1)	48(1)	5(1)	-32(1)	6(1)
O(9)	48(2)	29(1)	45(1)	14(1)	-20(1)	3(1)
O(10)	26(1)	49(2)	40(1)	-12(1)	1(1)	-5(1)
C(1)	24(1)	28(1)	28(1)	-1(1)	-13(1)	4(1)
C(2)	25(1)	24(1)	23(1)	4(1)	-6(1)	2(1)
C(3)	20(1)	22(1)	31(2)	-1(1)	-7(1)	0(1)
C(4)	24(1)	27(1)	26(1)	-3(1)	-12(1)	4(1)
OW1	24(1)	48(2)	84(2)	-13(2)	-11(2)	1(1)
C(5)	16(1)	29(1)	31(2)	-1(1)	-6(1)	-7(1)
C(6)	23(2)	25(2)	40(2)	-14(1)	-13(1)	2(1)
C(7)	33(2)	29(2)	40(2)	7(1)	-26(1)	-2(1)

The anisotropic displacement factor exponent take the form:

$$-2\pi^2[h^2a^*U11 + \dots + 2hka^* b^*U12]$$

Table D.5 Hydrogen coordinates ($\times 10^4$) and isotropic displacement parameters ($\text{\AA}^2 \times 10^3$) for $\text{Cs}_2[\text{Co}(\text{nta})\text{CO}_3] \cdot \text{H}_2\text{O}$.

	x	y	z	U(eq)
H(5A)	485(2)	-4480(4)	1298(2)	49(5)
H(5B)	-101(2)	-3035(4)	969(2)	49(5)
H(6A)	1575(2)	-4613(4)	-1057(3)	49(5)
H(6B)	1662(2)	-5479(4)	-44(3)	49(5)
H(7A)	506(3)	-1334(4)	-310(3)	49(5)
H(7B)	1471(3)	-1884(4)	-1260(3)	49(5)
HW1	4385(56)	3869(101)	1158(59)	110(24)
HW2	5277(53)	3007(79)	644(52)	82(20)

Supplementary Data

E Crystal data for [Co(NTA)(N,N-Et₂en)].

Table E.1 Atomic coordinates ($\times 10^4$) and equivalent isotropic displacement parameters ($\text{\AA}^2 \times 10^3$) for [Co(NTA)(N,N-Et₂en)].

Atom	x	y	z	U(eq)
Co	2374(1)	1307(1)	2500	22(1)
O(1)	2527(2)	1304(2)	854(2)	30(1)
N(3)	2745(5)	2770(3)	2500	26(1)
O(3)	1923(4)	-87(3)	2500	37(1)
N(1)	4213(4)	893(3)	2500	24(1)
C(3)	2887(6)	-718(4)	2500	39(2)
C(2)	4772(3)	1291(3)	1411(3)	32(1)
N(2)	470(5)	1711(4)	2500	41(1)
O(4)	2789(5)	-1652(3)	2500	81(2)
C(4)	4226(5)	-256(4)	2500	33(1)
C(1)	3723(4)	1292(3)	486(3)	32(1)
C(5)	1522(6)	3368(4)	2500	43(2)
O(2)	4031(3)	1312(2)	-541(2)	50(1)
C(6)	518(7)	2773(5)	1903(7)	42(2)
C(71)	-198(9)	1036(8)	1505(9)	38(2)
C(81)	-1636(8)	1303(9)	1210(10)	66(3)
C(82)	-533(12)	768(8)	967(10)	58(3)
C(72)	-237(8)	1757(8)	1514(8)	39(2)

U(eq) is defined as one third of the trace of the orthogonalized U_{ij} tensor.

Supplementary data

Table E.2 Bond lengths [Å] for [Co(nta)(*N,N*-Et₂en)].

Co-O(3)	1.884(4)	N(1)-C(4)	1.505(6)
Co-O(1)	1.905(2)	C(3)-O(4)	1.228(7)
Co-O(1) ^{#1}	1.905(2)	C(3)-C(4)	1.492(8)
Co-N(1)	1.950(4)	C(2)-C(1)	1.511(5)
Co-N(3)	1.953(4)	N(2)-C(72) ^{#1}	1.348(9)
Co-N(2)	2.011(5)	N(2)-C(72)	1.348(9)
O(1)-C(1)	1.290(4)	N(2)-C(6) ^{#1}	1.553(8)
N(3)-C(5) ^{#1}	1.472(7)	N(2)-C(6)	1.553(8)
N(3)-C(5)	1.472(7)	N(2)-C(71)	1.601(10)
O(3)-C(3)	1.284(7)	N(2)-C(71) ^{#1}	1.601(10)
N(1)-C(2) ^{#1}	1.475(4)	C(1)-O(2)	1.226(4)
N(1)-C(2)	1.475(4)	C(5)-C(6)	1.459(9)
C(71)-C(81)	1.543(11)	C(82)-C(72)	1.472(14)

Supplementary Data

Table E.3 Bond angles [°] for [Co(nta)(*N,N*-Et₂en)].

O(3)-Co-O(1)	91.03(8)	C(2) ^{#1} -N(1)-C(2)	116.8(4)
O(3)-Co-O(1) ^{#1}	91.03(8)	C(2) ^{#1} -N(1)-C(4)	110.5(2)
O(1)-Co-O(1) ^{#1}	170.6(2)	C(2)-N(1)-C(4)	110.5(2)
O(3)-Co-N(1)	87.9(2)	C(2) ^{#1} -N(1)-Co	105.8(2)
O(1)-Co-N(1)	85.46(7)	C(2)-N(1)-Co	105.8(2)
O(1) ^{#1} -Co-N(1)	85.46(7)	C(4)-N(1)-Co	106.7(3)
O(3)-Co-N(3)	177.0(2)	O(4)-C(3)-O(3)	125.5(6)
O(1)-Co-N(3)	89.21(8)	O(4)-C(3)-C(4)	118.6(6)
O(1) ^{#1} -Co-N(3)	89.21(8)	O(3)-C(3)-C(4)	115.9(5)
N(1)-Co-N(3)	95.0(2)	N(1)-C(2)-C(1)	109.2(3)
O(3)-Co-N(2)	91.1(2)	C(72) ^{#1} -N(2)-C(72)	115.1(8)
O(1)-Co-N(2)	94.56(7)	C(72) ^{#1} -N(2)-C(6) ^{#1}	66.6(5)
O(1) ^{#1} -Co-N(2)	94.56(7)	C(72)-N(2)-C(6) ^{#1}	110.6(6)
N(1)-Co-N(2)	179.1(2)	C(72) ^{#1} -N(2)-C(6)	110.6(6)
N(3)-Co-N(2)	85.9(2)	C(72)-N(2)-C(6)	66.6(5)
C(1)-O(1)-Co	114.0(2)	C(6) ^{#1} -N(2)-C(6)	52.6(7)
C(5) ^{#1} -N(3)-C(5)	0.0(5)	C(72) ^{#1} -N(2)-C(71)	113.7(6)
C(5) ^{#1} -N(3)-Co	111.0(4)	C(72)-N(2)-C(71)	36.1(5)
C(5)-N(3)-Co	111.0(4)	C(6) ^{#1} -N(2)-C(71)	145.7(6)
C(3)-O(3)-Co	116.0(4)	C(6)-N(2)-C(71)	101.0(5)
C(72) ^{#1} -N(2)-C(71) ^{#1}	36.1(5)	C(71) ^{#1} -N(2)-Co	105.3(4)
C(72)-N(2)-C(71) ^{#1}	113.7(6)	C(3)-C(4)-N(1)	113.4(4)
C(6) ^{#1} -N(2)-C(71) ^{#1}	101.0(5)	O(2)-C(1)-O(1)	124.1(4)
C(6)-N(2)-C(71) ^{#1}	145.7(6)	O(2)-C(1)-C(2)	120.1(4)
C(71)-N(2)-C(71) ^{#1}	91.6(8)	O(1)-C(1)-C(2)	115.8(3)
C(72) ^{#1} -N(2)-Co	121.8(4)	C(6)-C(5)-N(3)	107.9(5)
C(72)-N(2)-Co	121.8(4)	C(5)-C(6)-N(2)	107.0(5)
C(6) ^{#1} -N(2)-Co	101.8(4)	C(81)-C(71)-N(2)	115.9(8)
C(6)-N(2)-Co	101.8(4)	N(2)-C(72)-C(82)	115.6(9)
C(71)-N(2)-Co	105.3(4)		

Symmetry transformations used to generate equivalent atoms:

^{#1} $x, y, -z+1/2$

Supplementary data

Table E.4 Anisotropic displacement parameters ($\text{Å}^2 \times 10^3$) for $[\text{Co}(\text{nta})(N,N\text{-Et}_2\text{en})]$.

Atom	U11	U22	U33	U23	U13	U12
Co	23(1)	22(1)	20(1)	0	0	3(1)
O(1)	33(1)	35(1)	21(1)	-3(1)	-2(1)	7(1)
N(3)	38(3)	21(2)	20(2)	0	0	2(2)
O(3)	30(2)	24(2)	56(3)	0	0	-1(2)
N(1)	23(2)	24(2)	23(2)	0	0	6(2)
C(3)	44(4)	28(3)	46(4)	0	0	-1(2)
C(2)	27(2)	39(2)	30(2)	4(2)	8(2)	8(2)
N(2)	25(2)	32(3)	65(4)	0	0	7(2)
O(4)	59(3)	24(2)	159(6)	0	0	-4(2)
C(4)	40(3)	26(3)	33(3)	0	0	7(2)
C(1)	43(2)	29(2)	23(2)	1(2)	5(2)	14(2)
C(5)	43(4)	26(3)	60(4)	0	0	11(3)
O(2)	68(2)	60(2)	22(1)	8(2)	13(1)	31(2)
C(6)	40(4)	37(5)	50(5)	6(4)	-4(4)	17(4)
C(71)	28(5)	44(6)	41(6)	-16(5)	-15(4)	8(4)
C(81)	31(4)	84(7)	81(7)	-27(7)	-24(5)	14(5)
C(82)	62(8)	54(7)	57(7)	2(6)	-11(6)	-11(6)
C(72)	32(4)	47(5)	39(6)	5(5)	2(4)	9(4)

The anisotropic displacement factor exponent takes the form:

$$-2\pi^2[h^2a^2U_{11} + \dots + 2hka^*b^*U_{12}]$$

Supplementary Data

Table E.5 Hydrogen coordinates ($\times 10^4$) and isotropic displacement parameters ($\text{\AA}^2 \times 10^3$) for [Co(NTA)(N,N-Et₂en)].

	x	y	z	U(eq)
H(3)	3113(35)	2922(27)	1872(32)	31(11)
H(2A)	5502(3)	866(3)	1168(3)	51(5)
H(2B)	5096(3)	1979(3)	1530(3)	51(5)
H(4A)	4698(5)	-492(4)	1821	51(5)
H(4B)	4698(5)	-492(4)	3179	51(5)
H(5A)	1249(6)	3509(4)	3289	51(5)
H(5B)	1658(6)	4013(4)	2105	51(5)
H(6A)	739(7)	2699(5)	1090(7)	51(5)
H(6B)	-328(7)	3109(5)	1962(7)	51(5)
H(71A)	322(9)	1103(8)	806(9)	51(5)
H(71B)	-163(9)	326(8)	1740(9)	51(5)
H(81A)	-2000(18)	780(22)	724(38)	51(5)
H(81B)	-1664(9)	1945(21)	809(39)	51(5)
H(81C)	-2137(13)	1351(37)	1912(11)	51(5)
H(82A)	-854(50)	880(8)	196(20)	51(5)
H(82B)	-1188(39)	418(19)	1414(28)	51(5)
H(82C)	251(16)	363(18)	936(42)	51(5)
H(72A)	237(8)	2174(8)	960(8)	51(5)
H(72B)	-1060(8)	2099(8)	1681(8)	51(5)

Section II Kinetic data

The tables in this section give the observed first-order rate constant for the reactions described in Chapters 5 and 6. The number of the figure representing a specific data set is included in brackets after the table number.

A Kinetic data for Chapter 5

Table A.1 (Figure 5.1) Plot of Abs ($\lambda = 320$ nm) vs. pH for the $[\text{Co}(\text{nta})(\mu\text{-OH})]_2^{2-}$ system. 25.0°C , $\mu = 1$ M (NaClO_4), $[\text{dimer}] = 2 \times 10^{-3}$ M.

pH	A	pH	A
2.2	0.1784	3.55	0.533
2.33	0.159	3.7	0.526
2.6	0.227	3.79	0.544
2.7	0.252	3.87	0.568
2.79	0.256	3.95	0.566
2.86	0.314	4.33	0.585
2.94	0.323	4.52	0.594
2.99	0.36	4.56	0.596
3.25	0.438	5.75	0.59
3.38	0.4803		

Supplementary Data

Table A.2 (Figure 5.2) Plot of Abs ($\lambda = 400$ nm) vs pH for $[\text{Co}(\text{nta})(\text{H}_2\text{O})_2]$ (0.002 M), 25.0 °C, $\mu = 1$ M (NaClO_4).

pH	A	pH	A
3.53	0.638	6.11	0.574
4.23	0.636	6.22	0.561
4.48	0.641	6.33	0.546
4.70	0.636	6.43	0.527
5.05	0.634	6.52	0.509
5.25	0.629	6.62	0.494
5.44	0.621	6.75	0.473
5.64	0.615	6.0	0.450
5.74	0.608	7.02	0.435
5.84	0.603	7.17	0.418
5.92	0.593	7.55	0.402
6.02	0.581		

Table A.3 (Figure 5.3) Plot of k_{obs} vs $[\text{H}^+]$ at different temperatures, $\mu = 1.0$ M (NaClO_4), $\lambda = 550$ nm, $[\text{dimer}] = 1 \times 10^{-2}$ M.

$[\text{H}^+]$ (mol dm^{-3})	$(10^3) k_{\text{obs}}$ (s^{-1})		
	15.9 °C	25.9 °C	35.1 °C
0.1	2.25(1)	5.26(1)	13.7(2)
0.2	4.41(1)	9.85(3)	26.0(1)
0.3	6.4(2)	15.2(3)	33.9(3)
0.5	10.4(4)	23(1)	50.4(3)
0.7	14(1)	31(2)	62(1)
1.0	18.1(4)	39.1(5)	82(1)

Supplementary data

Table A.4 (Figure 5.5) Plot of k_{obs} vs $[\text{NCS}^-]$ for first reaction at different temperatures, $\mu = 1.0 \text{ M}$ (NaClO_4), $\lambda = 400 \text{ nm}$, $[\text{Co}(\text{nta})(\text{H}_2\text{O})_2] = 4 \times 10^{-3} \text{ M}$.

$[\text{NCS}^-]$ (mol dm^{-3})	$(10^4) k_{\text{obs}}$ (s^{-1})		
	15.0 °C	25.7 °C	34.0 °C
0.1	1.61(3)	3.2(2)	5.5(1)
0.2	2.87(3)	5.7(2)	8.9(2)
0.3	4.1(1)	7.9(3)	13(1)
0.5	6.5(2)	12(3)	22(1)
0.8	10.2(4)	20(2)	33.1(9)
1.0	13(2)	25(1)	40.5(9)

Table A.5 (Figure 5.6) Plot of k_{obs} vs $[\text{NCS}^-]$ for second reaction at different temperatures, $\mu = 1.0 \text{ M}$ (NaClO_4), $\lambda = 400 \text{ nm}$, $[\text{Co}(\text{nta})(\text{H}_2\text{O})_2] = 4 \times 10^{-3} \text{ M}$.

$[\text{NCS}^-]$ (mol dm^{-3})	$(10^5) k_{\text{obs}}$ (s^{-1})		
	26.9 °C	34.0 °C	48.0 °C
0.1	3.5(1)	9.(1)	19.5(5)
0.2	6.4(2)	11(1)	27.5(1)
0.3	8.1(3)	16(2)	36(2)
0.5	12.4(3)	21(2)	42(2)
0.8	17.3(7)	29(3)	59(3)
1.0	22(3)	34(3)	78(3)

Supplementary Data

Table A.6 (Figure 5.7)

Plot of k_{obs} vs pH at 25.0 °C for the first reaction between $[\text{Co}(\text{nta})(\text{H}_2\text{O})_2]$ and NCS^- ions. $\mu = 1.0 \text{ M}$ (NaClO_4), $\lambda = 400 \text{ nm}$, $[\text{NCS}^-] = 1.25 \times 10^{-2} \text{ M}$.

pH	$(10^3) k_{\text{obs}}$ (s^{-1})	pH	$(10^3) k_{\text{obs}}$ (s^{-1})
4.30	1.335(5)	6.28	11.8(4)
4.50	1.233(4)	6.36	17(2)
4.80	1.522(2)	6.39	11.6(3)
5.0	1.88(2)	6.49	20(1)
5.08	2.066(4)	6.54	19.7(2)
5.38	3.133(5)	6.62	21(3)
5.56	4.165(4)	6.66	25.1(5)
5.78	5.998(4)	6.80	27.5(3)
5.92	7.569(4)	7.10	30(2)
5.94	7.822(2)	7.21	32(3)
6.06	9.492(3)	7.30	34(3)
6.09	9.95(2)	7.42	37(3)
6.20	11.8(3)		

Table A.7 (Figure 5.8)

Plot of k_{obs} vs $[\text{NCS}^-]$ for the first reaction at pH = 7.00, 25.0 °C, $\mu = 1.0 \text{ M}$ (NaClO_4), $\lambda = 400 \text{ nm}$.

$[\text{NCS}^-]$ (mol dm^{-3})	$(10^3) k_{\text{obs}}$ (s^{-1})
0.0100	1.8(2)
0.0125	2.6(2)
0.0300	4.3(1)
0.0500	7.5(3)
0.0800	10(1)
0.1000	15.1(5)

Supplementary data

B Kinetic data for Chapter 6

Table B.1 (Figure 6.2) Plot of k_{obs} vs [dmap] for the reaction between $[\text{Co}(\text{nta})(\mu\text{-OH})_2]^{2-}$ and dmap at different pH levels, 25.0 °C, $\mu = 1.0 \text{ M}$ (NaClO_4), $\lambda = 390 \text{ nm}$, [dimer] = $1.5 \times 10^{-3} \text{ M}$.

[dmap] (mol dm^{-3})	$(10^2) k_{\text{obs}}$ (s^{-1})			
	pH = 9.45	pH = 10.1	pH = 10.55	pH = 11.1
0.02	0.96(2)	2.46(3)	12.9	26(2)
0.04	1.63(2)	4.83(3)	15.5	34(3)
0.08	1.98(2)	7.2(2)	20.3	43.3(4)
0.10	2.07(1)	8.2(2)	26.7	45(3)
0.20	2.2(2)	12.74(4)	30.5	53.5(4)

Table B.2 (Figure 6.3) Plot of k_{obs} vs pOH for the reaction between $[\text{Co}(\text{nta})(\mu\text{-OH})_2]^{2-}$ and dmap at 25.0 °C, $\mu = 1.0 \text{ M}$ (NaClO_4), $\lambda = 390 \text{ nm}$, [dimer] = $1.5 \times 10^{-3} \text{ M}$.

pOH	$(10^3) k_{\text{obs}}$ (s^{-1})	pOH	$(10^3) k_{\text{obs}}$ (s^{-1})
4.64	1.94(2)	3.50	25.5(3)
4.42	3.61(2)	3.46	26.5(3)
4.29	5.7(1)	3.36	31.8(2)
4.12	7.4(2)	3.33	33.4(2)
4.06	6.51(3)	3.29	36.1(3)
4.00	10.5(3)	3.23	39.1(3)
3.82	14.9(4)	3.20	41(1)
3.72	16.1(3)	2.97	44.5(3)
3.62	20.6(4)	2.84	51.5(5)
3.56	20.5(3)		

Supplementary Data

Table B.3 (Figure 6.4) Plot of k_{obs} vs [dmap] for the reaction between $[\text{Co}(\text{nta})(\mu\text{-OH})_2]^{2-}$ and dmap at different temperatures, $\text{pH} = 10.5$, $\mu = 1.0 \text{ M}$ (NaClO_4), $\lambda = 390 \text{ nm}$, $[\text{dimer}] = 1.5 \times 10^{-3} \text{ M}$.

[dmap] (mol dm^{-3})	$(10^2) k_{\text{obs}}$ (s^{-1})		
	15.1 °C	25.0 °C	35.0 °C
0.025	0.65(2)	1.16(3)	2.09(1)
0.050	1.04(3)	1.58(2)	3.32(2)
0.075	1.29(2)	2.07(2)	4.05(2)
0.100	1.32(3)	2.37(3)	4.4(2)
0.200	1.55(2)	2.71(2)	5.4(1)
0.250	1.71(2)	2.9(3)	5.7(2)

Table B.4 (Figure 6.5) Plot of k_{obs} vs pOH for the reaction between $[\text{Co}(\text{nta})(\mu\text{-OH})_2]^{2-}$ and py, $\mu = 0.5 \text{ M}$ (NaClO_4), $\lambda = 410 \text{ nm}$, $[\text{dimer}] = 1.5 \times 10^{-3} \text{ M}$ and 25.0 °C .

pOH	$(10^5) k_{\text{obs}}$ (s^{-1})	pOH	$(10^5) k_{\text{obs}}$ (s^{-1})
4.50	0.485(2)	3.45	2.74(2)
4.30	0.585(2)	3.44	2.78(2)
4.10	0.968(3)	3.34	3.3(2)
4.08	0.99(2)	3.24	3.34(3)
4.00	1.0(2)	3.16	4.13(3)
3.80	1.56(3)	3.01	4.48(3)
3.74	1.79(3)	2.87	5.01(2)
3.65	1.9(3)	2.80	5.3(3)

Supplementary data

Table B.5 (Figure 6.6)

Plot of k_{obs} vs $[\text{py}]$ for the reaction between $[\text{Co}(\text{nta})(\mu\text{-OH})_2]^{2-}$ and py at different pH levels, $\mu = 0.5 \text{ M}$ (NaClO_4), $\lambda = 410 \text{ nm}$, $[\text{dimer}] = 1.5 \times 10^{-3} \text{ M}$ and $25.0 \text{ }^\circ\text{C}$.

[py] (mol dm ⁻³)	(10 ⁴) k_{obs} (s ⁻¹)		
	pH = 9.71	pH = 10.10	pH = 10.80
0.1	0.553(2)	0.287(3)	1.9(1)
0.2	0.97(3)	0.48(2)	3.05(2)
0.4	1.67(2)	0.865(4)	4.09(3)
0.6	2.04(3)	1.21(2)	4.56(3)
0.8	2.53(2)	1.41(3)	4.93(3)
1.0	2.63(2)	1.52(2)	5.2(2)

Table B.6 (Figure 6.7)

Plot of k_{obs} vs pOH for the reaction between $[\text{Co}(\text{nta})(\mu\text{-OH})_2]^{2-}$ and en at $25.0 \text{ }^\circ\text{C}$, $\mu = 0.2 \text{ M}$ (NaClO_4), $\lambda = 325 \text{ nm}$, $[\text{dimer}] = 1.5 \times 10^{-4} \text{ M}$.

pOH	(10 ³) k_{obs} (s ⁻¹)	pOH	(10 ³) k_{obs} (s ⁻¹)
2.92	9.2(2)	3.58	3.4(1)
3.05	8.47(2)	3.64	3.25(3)
3.12	8.18(3)	3.68	2.62(1)
3.20	6.77(3)	3.80	1.90(2)
3.26	6.3(1)	3.95	1.17(1)
3.31	6.02(3)	4.00	0.987(6)
3.34	5.7(2)	4.05	0.935(5)
3.36	5.3(1)	4.10	0.73(2)
3.47	4.18(2)	4.17	0.62(1)
3.50	4.2(1)	4.21	0.45(1)
3.52	3.87(2)	4.30	0.385(3)
3.56	3.8(1)	4.35	0.31(3)

Supplementary Data

Table B.7 (Figure 6.8)

Plot of k_{obs} vs pOH for the reaction between $[\text{Co}(\text{nta})(\mu\text{-OH})_2]^{2-}$ and $\text{N,N-Et}_2\text{en}$ at $25.0\text{ }^\circ\text{C}$, $\mu = 0.2\text{ M}$ (NaClO_4), $\lambda = 325\text{ nm}$, $[\text{dimer}] = 1.5 \times 10^{-4}\text{ M}$.

pOH	$(10^3) k_{\text{obs}}$ (s^{-1})	pOH	$(10^3) k_{\text{obs}}$ (s^{-1})
2.80	2.67(2)	3.98	0.544(4)
2.95	2.49(3)	4.00	0.527(2)
3.12	2.23(2)	4.11	0.524(4)
3.25	1.78(3)	4.25	0.437(5)
3.35	1.58(2)	4.35	0.429(6)
3.50	1.079(4)	4.43	0.425(3)
3.61	0.97(2)	4.50	0.43(1)
3.70	0.86(1)	4.55	0.41(1)
3.74	0.75(2)	4.56	0.414(2)
3.90	0.579(3)		

Table B.8 (Figure 6.9)

Plot of k_{obs} vs $[\text{en}]$ for the reaction between $[\text{Co}(\text{nta})(\mu\text{-OH})_2]^{2-}$ and en at different pH levels, $25.0\text{ }^\circ\text{C}$, $\mu = 0.2\text{ M}$ (NaClO_4), $\lambda = 325\text{ nm}$, $[\text{dimer}] = 1.5 \times 10^{-4}\text{ M}$.

$[\text{en}]$ (mol dm^{-3})	$(10^3)k_{\text{obs}}$ (s^{-1})		
	pH = 9.70	pH = 10.02	pH = 10.50
0.02	0.049(2)	0.143(3)	0.63(2)
0.04	0.093(2)	0.259(3)	1.07(2)
0.08	0.168(2)	0.48(2)	2.2(2)
0.10	0.18(2)	0.58(2)	2.67(3)
0.16	0.22(2)	0.89(3)	3.53(2)
0.20	0.32(2)	1.0(2)	4.2(2)

Supplementary data

Table B.9 (Figure 6.10) Plot of k_{obs} vs $[\text{N,N-Et}_2\text{en}]$ for the reaction between $[\text{Co}(\text{nta})(\mu\text{-OH})]_2^{2-}$ and $\text{N,N-Et}_2\text{en}$ at different pH levels, 25.0 °C, $\mu = 0.2 \text{ M}$ (NaClO_4), $\lambda = 325 \text{ nm}$, $[\text{dimer}] = 1.5 \times 10^{-4} \text{ M}$.

$[\text{N,N-Et}_2\text{en}]$ (mol dm^{-3})	$(10^3)k_{\text{obs}}$ (s^{-1})		
	pH = 9.70	pH = 10.10	pH = 10.55
0.04	0.235(2)	0.286	0.588(2)
0.06	0.289(2)	0.315	0.793(2)
0.08	0.325(1)	0.387	0.924(3)
0.10	0.339(2)	0.44	0.952(2)
0.20	0.43(3)	0.527	1.17(2)
0.40	0.47(3)	0.591	1.33(2)

Bibliography

- ALMAZÁN, F, GARCÍA-ESPAÑA, E., MOLLAR, M., LLORET, F., JULVE, M., FAUS, J., SOLANS, X. & ALINS, N., 1990. *J. Chem. Soc. Dalton Trans.*, p. 2565.
- ASHLEY, K.R., LEIPOLDT, J.G. & JOSHI, V.K., 1980. *Inorg. Chem.*, 19:1608.
- ASHLEY, R.A. & LEIPOLDT, J.G., 1981. *Inorg. Chem.*, 20:2326.
- ATWOOD, J.D. & BROWN, T.L., 1976. *J. Am. Chem. Soc.*, 98:3160.
- BARNES, J.A., HODGSON, D.J. & HATFIELD, W.E., 1972. *Inorg. Chem.*, 11:144.
- BATTAGLIA, L.P., CORRADI, A.B. & TANI, M.E.V., 1975. *Acta Cryst.*, B31:1160.
- BESWICK, C.L., SHALDERS, R.D. & SWADDLE, T.W., 1996. *Inorg. Chem.*, 35:991.
- BHATTACHARYYA, S.K. & BANERJEE, R., 1997. *Polyhedron*, 16:849.
- BHATTACHARYYA, S.K. & BANERJEE, R., 1997. *Polyhedron*, 16:4217.
- BIGOLI, F., LANFRANCHINI, M., LEPORATI, E. & PELLINGELLI, M.A., 1980. *Cryst. Struct. Comm.*, 9:1261.
- BOCARSLEY, J.R. & BARTON, J.K., 1992. *Inorg. Chem.*, 31:2827.
- BOCARSLEY, J.R., CHIANG, M.Y., BRYANT, L. & BARTON, J.K., 1990. *Inorg. Chem.*, 29:4898.
- BRANDENBURG, K. & BERNDT, M., 1998. Visual Crystal Structure Information System, Version 2.1, Germany.
- BUSH, D.H. & BAILAR, J.C., 1953. *J. Am. Chem. Soc.*, 75:4574.
- BUSH, D.H. & BAILAR, J.C., 1956. *J. Am. Chem. Soc.*, 78:716.
- CONNET, P.H. & WETTERHAHN, K.E., 1983. *Struct. Bonding (Berlin)*, 54:93.
- COOPER, J.A., BLACKWELL, L.F. and BUCKLEY, P.D., 1984. *Inorg. Chim. Acta*, 92:23.
- DASGUPTA, T.P. & HARRIS, G.M., 1971. *J. Am. Chem. Soc.*, 93:91.
- DASGUPTA, T.P. & HARRIS, G.M., 1974. *Inorg. Chem.*, 13:1275.
- DEMAINE, M.M. & HUNT, J.B., *Inorg. Chem.*, 10:2106, (1971).
- DOBOZY, O.K., 1973. *Am. Dyestuff Reporter*, 62:36.
- EDWARDS, J.D., WIEGHARDT, K. & SYKES, G., 1974. *J. Chem. Soc. Dalton Trans.*, 2198.
- EL-AWADY, A.A. & HUGUS, Z.Z., 1971. *Inorg. Chem*, 10, 1415, (1971).

Bibliography

- ELLIS, D., SCOTT, K.L., WHARTON & R.K., 1972. SYKES, A.G., *Inorg. Chem.*, 11:2565.
- FALLAB, S., 1967. *Angew. Chem. (Int. Ed.)*, 6:496.
- FUJIHARA, T., FUYUHIRO, A. & KAIZAKI, S., 1995. *J. Chem. Soc. Dalton Trans.*, p. 1813.
- GARNETT, P.J. & WATTS, D.W., 1974. *Inorg. Chim. Acta*, 8:307.
- GARNETT, P.J. & WATTS, D.W., 1974. *Inorg. Chim. Acta*, 8:313.
- GLADKIKH, O.P., POLYNOVA, T.N., PORAI-KOSHITS, M.A. & POZNYAK, A.L., 1992. *Koord. Khim.*, 18:1231.
- GLADKIKH, O.P., POLYNOVA, T.N., PORAI-KOSHITS, M.A. & POZNYAK, A.L., 1992. *Koord. Khim.*, 18:908.
- GORDON, P.F. & GREGORY, P., 1983. *Organic Chemistry in Colour*. Berlin: Springer-Verlag.
- GRANT, D.M. & HAMM, R.E., 1958. *J. Am. Chem. Soc.*, 80:4166.
- GREEN, J.A., KOINE, N. & WILLET, D., 1990. *Inorg. Chim. Acta*, 176:87.
- HALLORAN, L.J., CAPUTO, R.E., WILLET, R.D. & LEGG, J.I., 1975. *Inorg. Chem.*, 14:1762.
- HARRIS, G.M. & HYDE, K.E., 1978. *Inorg. Chem.*, 17:1892.
- HARTFORD, W.H. (In GRAYSON, m., ed. Kirk-Othmer Encyclopedia of Chemical Technology. New York: John Wiley & Sons. p. 82-120.)
- HARTLEY, F.R., 1969. *J.S.D.C.*, 85:66.
- HAY, R.W., 1984. *Coord. Chem. Rev.*, 57:1.
- HAYLOCK, S.J., BUCKLEY, P.D. & BLACKWELL, L.F., 1983. *J. Inorg. Biochem.*, 19:105.
- HELIS, H.M., DE MEESTER, P. & HODGSON, D.J., 1977. *J. Am. Chem. Soc.*, 99:3309.
- HOFFMAN, A.B. & TAUBE, H., 1968. *Inorg. Chem.*, 7:903.
- HUALIN, Z. & XU, Z., 1990. *Polyhedron*, 9:137.
- JITSUKAWA, K., MORIOKA, T., MASUDA, H., OGOSHI, H. & EINAGA, H., 1994. *Inorg. Chim. Acta*, 216:249.
- JITSUKAWA, K., MORIOKA, T., MASUDA, H., OGOSHI, H. & EINAGA, H., 1994. *Inorg. Chim. Acta*, 216:249.
- KOINE, N., BIANCHINI, J. & LEGG, I., 1986. *Inorg. Chem.*, 25:2835.
- KOINE, N., SAKOTA, N, HIDAKA, J & SHIMURA, Y., 1969. *Bull. Chem. Soc. Japan*, 42:1583.

Bibliography

- KOSHY, K. & DASGUPTA, T.P., 1984. *J. Chem. Soc. Dalton Trans.*, 2781.
- LEE HIN-FAT & HIGGINSON, W.C.E., 1971. *J. Chem. Soc. A*, 2589, (1971).
- LEIPOLDT, J.G. & MEYER, H., 1987. *Polyhedron*, 6:1361.
- LEIPOLDT, J.G., BASSON, S.S. & ROODT, A., 1993. Octacyano and oxo- and nitridotetracyano complexes of second and third series early transition metals. (*In Advances in inorganic chemistry*, vol. 40, p241 – 322).
- LEIPOLDT, J.G., PURCELL, W. & MEYER, H., 1991. *Polyhedron*, 10:1379.
- LEWIS, D.L., HATFIELD, W.E. & HODGSON, D.J., 1972. *Inorg. Chem.*, 11:2216.
- LEY, H. & FICKEN, K., 1912. *Chem. Ber.*, 45:377.
- LINHARDT, V.M. & SIEBERT, H., 1969. *Z. Anorg. Allg. Chem.*, 364:24.
- MEITES, L., 1963. *Handbook of Analytical Chemistry*, 1st. Edit., McGraw-Hill Book Company.
- MELOON, D.R. & HARRIS, G.M., 1977. *Inorg. Chem.*, 16:434.
- MERTZ, W. 1975. *Nutr. Revs.*, 33:129.
- MINSQ; Least-squares Parameter Estimation; Micromath; 1991.
- MOORE, P., 1984. (*In Twigg, M.V., ed. Mechanisms of Inorganic and Organometallic Reactions, Volume 2. New York: Plenum Press.*)
- MORI, M., SHIBATA, M., KYUNO, E. & OKUBO, Y., 1958. *Bull. Chem. Soc. Japan*, 31:940.
- MORRAL, F.R. 1979. Cobalt compounds. (*In GRAYSON, m., ed. Kirk-Othmer Encyclopedia of Chemical Technology. New York: John Wiley & Sons. p. 495-510.*)
- NAGAO, R., FUMIYUKI, M. & SAITO, Y., 1972. *Acta Cryst.*, B28:1852.
- NAKAMOTO, K., 1963. *Infrared Spectra of Inorganic and Coordination Compounds. New York: John Wiley & Sons.*
- OGINO, H., WATANABE, T. & TANAKA, N., 1975. *Inorganic Chemistry*, 14:2093.
- OKAMOTO, K., HIDAKA, J., FUKAGAWA, M. & KANAMORI, K., 1992. *Acta Cryst.*, C48:1025.
- PALMER, D.A. & HARRIS, G.M., 1974. *Inorg. Chem.*, 13:965.
- PLANINSEK, F & NEWKIRK, J.B., 1979. Cobalt and cobalt alloys. (*In GRAYSON, M., ed. Kirk-Othmer Encyclopedia of Chemical Technology. New York: John Wiley & Sons. p. 481-494.*)
- PUPER, H.C., 1962. *Tex.*, 21:322.
- PURCELL, F.P. & KOTZ, J.C., 1985. *Inorganic Chemistry*, Japan: W.B. Saunders Company. p. 710.
- RADANOVIC, D.J., 1984. *Coord. Chem. Rev.*, 54:159.

Bibliography

- SADLER, G.G. & DASGUPTA, T.P., 1987. *Inorg. Chim. Acta*, 130:185.
- SADLER, G.G. & DASGUPTA, T.P., 1987. *Inorg. Chem.*, 26:3254.
- SANTOS, T.M., DE JESUS, J.P. & O'BRIEN, P., 1992. *Polyhedron*, 11:1687.
- Scientist for Windows; Least Squares Parameter Estimation, Version 4.00, Micromath, 1990.
- SHANNON, R.D., 1976. *Acta Cryst.*, A 32:751.
- SHELXL93, SHELDRIK, G.M., 1993. Program for Crystal Structure Determination, University of Göttingen, Germany.
- SHELXL97, SHELDRIK, G.M., 1997. Program for Crystal Structure Determination, University of Göttingen, Germany.
- SHELXS86, SHELDRIK, G.M., 1986. Program for Crystal Structure Determination, University of Göttingen, Germany.
- SKRZYPCZAK-JANKUN, E. & SMITH, D.A., 1994. *Acta Cryst.*, Section C:1097.
- SMIT, J.P., 1995. Ph.D Thesis, University of the Orange Free State.
- SMITH, B.B. & SAWYER, D.T., 1968. *Inorg. Chem.*, 7:923.
- SMITH, G.S. & HOARD, J.L., 1959. *J. Am. Chem. Soc.*, 81:556.
- SRDANOV, G., HERAK, R., RADANOVIC, D.L. & VESSELINOVIC, D.S., 1980. *Inorg. Chim. Acta*, 38:37.
- SUDMEIER, J.L. & OCCUPATI, 1968. *Inorg. Chem.*, 7:2524.
- SULFAB, Y., TAYLOR, R.S. & SYKES, A.G., 1976. *Inorg. Chem.*, 15:2388.
- SWAMINATHAN, K. & SINHA, U.C., 1989. *Acta Cryst.*, C45:566.
- SYKES, A.G. & WEIL, J.A., 1970. (In Edwards, J.O. ed. *Inorganic Reaction Mechanisms*, Volume 13. New York: John Wiley and Sons).
- TERRIL, J.B. & REILLY, C.N., 1966. *Inorg. Chem.*, 5:1988.
- THACKER, M.A. & HIGGINSON, C.E., 1975. *J. Chem. Soc. Dalton Trans.*, p. 704.
- TOEPFER, E.W., MERTZ, W., POLANSKY, M.M., ROGINSKY, E.E. & WOLF, W.R., 1977. *J. Agric. Food Chem.*, 25:162.
- TOFTLUND, H. & SPRINGBORG, J., 1976. *J. Chem. Soc. Chem. Comm.*, p. 1017.
- TORIAMI, K. & SAITO, Y., 1975. *Acta Cryst.*, Sect. B, 31:1247.
- UEHARA, A., KYUNO, E. & TSUCHIYA, R., 1967. *Bull. Chem. Soc. Japan*, 40:2317.
- VAN ELDIK, R., DASGUPTA, T.P. & HARRIS, G.M., 1975. *Inorg. Chem.*, 14:2573.
- VAN ELDIK, R., PALMER, D.A. & KELM H., 1979. *Inorg. Chem.*, 18:1520.
- VAN ELDIK, R., SPITZER, U. & KELM, H., 1983. *Inorg. Chim. Acta*, 74:149.
- VEAL, J.T., HATFIELD, W.E., JETER, D.Y., HEMPEL, J.C. & HODGSON, D.J., 1973. *Inorg. Chem.*, 12:343.

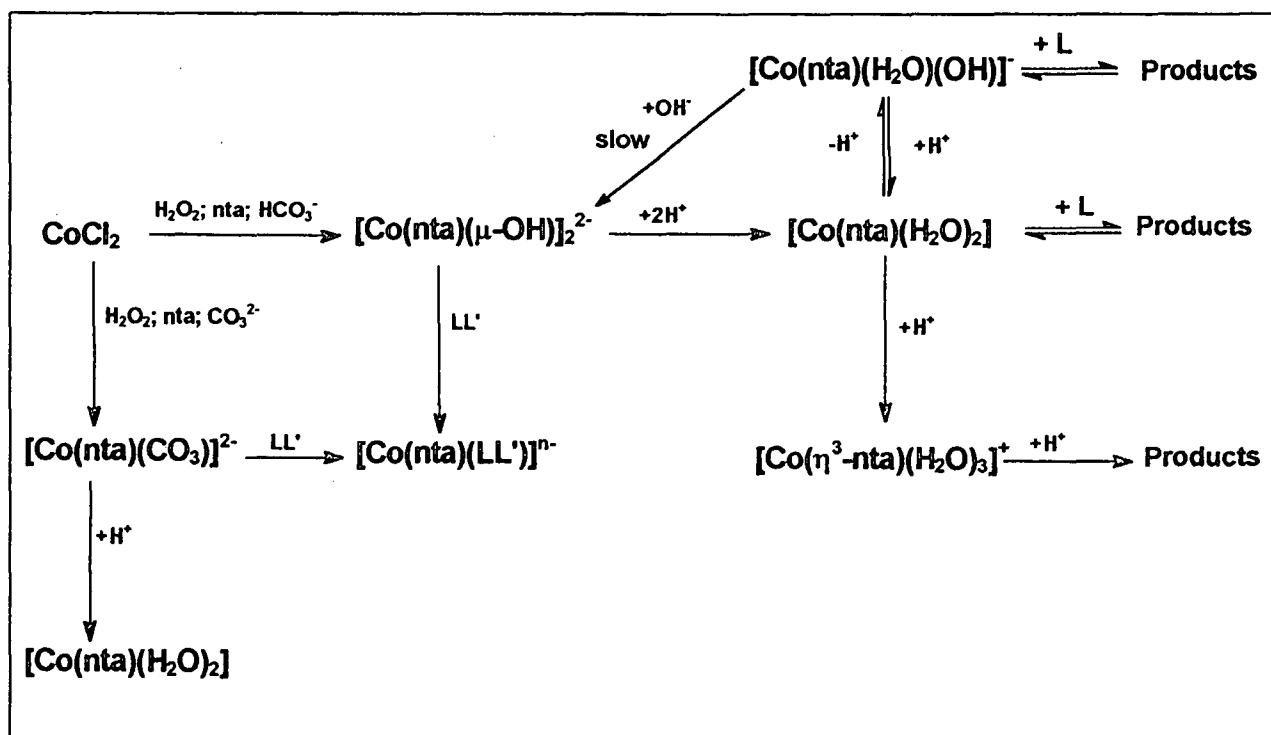
Bibliography

- VISSER, H.G. 1992. Fundamentele aspekte van die kleur van wol: kinetika van die substitusiereaksies van chroom(III) komplekse. Bloemfontein: UOVS. (Dissertation – M.Sc.)
- VISSER, H.G., LEIPOLDT, J.G., PURCELL, W. & MOSTERT, D., 1994. *Polyhedron*, 13:1051.
- VISSER, H.G., PURCELL W. & BASSON, S.S. 1999. *Polyhedron*, 18:2795.
- VISSER, H.G., PURCELL W. & BASSON, S.S. 2000a. *Transition Metal Chemistry*, submitted and accepted for publication.
- VISSER, H.G., PURCELL W. & BASSON, S.S. 2000b. *Polyhedron*, submitted and accepted for publication.
- VISSER, H.G., PURCELL, W., BASSON, S.S. & CLAASSEN, Q., 1997. *Polyhedron*, 16:2851.
- VOGEL, A.I. 1989. Vogel's Textbook of Quantitative Chemical Analysis, Fifth Edition. Essex: Longman. P. 317.
- WEAKLIEM, H.A. & HOARD, J.L., 1959. *J. Am. Chem. Soc.*, 81:549.
- WELHAM, A.C., 1986. *J.S.D.C.*, 102:126.
- WESTBROOK, J.H. Chromium and chromium alloys. (In GRAYSON, M., ed. Kirk-Othmer Encyclopedia of Chemical Technology. New York: John Wiley & Sons. p. 54-82.)
- WEYH, J.A., MAYNARD, R.B. & BAKER, T.J., 1976. *Inorg. Chem.*, 15:2298.
- WEYH, J.A., NEWLUN, A.K., BAKER, T.J. & SHIOYAMA, T.K., 1973 *Inorg. Chem.*, 12:2374.
- WHITE, L.S., NILSSON, P.V., PIGNOLET, L.H. & QUE, L., 1984. *J. Am. Chem. Soc.*, 106:8312.
- WHITLOW, S.H., 1972. *Acta Cryst.*, B28:1914.
- WOLCOTT, D. & HUNT, J.B., 1968. *Inorg. Chem.*, 7:755.

Abstract

The synthesis and reactions of Co(III) and Cr(III) complexes with nitrilotriacetic acid (nta) as tetradentate ligand have widespread interest, mainly because of the fact that these complexes can be used as biological model complexes and because nta labilises usually inert metal centres. Mori *et al* (1958:940) and Uehara *et al.* (1967:2317) were the first to prepare different Co(III)-nta and Cr(III)-nta complexes respectively. Since then these complexes have been used in several kinetic and synthetic studies (Visser *et al.* 1997:2581; Visser *et al.* 1994:1051 and Thacker & Higginson, 1975:704). However the identity and purity of these complexes were questionable and had not been solved up to the time of this study.

The question regarding the identity of the different Co(III)-nta species in solution at different pH levels have largely been accounted for in this study (refer to Scheme 1).



Scheme 1

Complexes and reactions of Co(III)-nta.

The identity of the complex first prepared by Mori *et al* (1958:940) was finally characterised with X-ray crystallography as being $[\text{Co}(\text{nta})(\mu\text{-OH})]_2^{2-}$. Crystals of

Abstract

$\text{Cs}_2[\text{Co}(\text{nta})(\mu\text{-OH})]_2 \cdot 4\text{H}_2\text{O}$ crystallises in the orthorhombic space group $I4_1/a$ ($R_1 = 0.0322$). The Co-N bonding distance was determined as 1.922(6) Å.

$[\text{Co}(\text{nta})(\mu\text{-OH})]_2^{2-}$ undergo bridge-cleavage upon acidification with H^+ ions to form $[\text{Co}(\text{nta})(\text{H}_2\text{O})_2]$. The pK_a of this reaction was determined as 3.09(3). Further acidification of $[\text{Co}(\text{nta})(\text{H}_2\text{O})_2]$ leads to the stepwise dissociation of nta. The formation of an ion associated species between $[\text{Co}(\text{nta})(\text{H}_2\text{O})_2]$ and H^+ ions upon addition of acid is postulated. This ion associated species dissociates in the rate determining step to form the tridentate nta complex, $[\text{Co}(\eta^3\text{-nta})(\text{H}_2\text{O})_3]^+$. The value of k_1 at 25.9 °C was determined as 0.13(1) s^{-1} .

Another acid-base equilibrium is observed when the pH of a $[\text{Co}(\text{nta})(\text{H}_2\text{O})_2]$ solution is increased. It was concluded that the newly formed species is not the dimer, but rather $[\text{Co}(\text{nta})(\text{H}_2\text{O})(\text{OH})]^-$ which reverts back to the dimer at pH 6 – 7 after several days. This second pK_a was determined as 6.52(2).

The substitution reactions between $[\text{Co}(\text{nta})(\text{H}_2\text{O})_2]$ and NCS^- ions have been investigated. At pH = 2.00 NCS^- ions substitute the aqua ligands in a stepwise fashion. The substitution of the first aqua ligand ($k_1 = 2.4(1) \times 10^{-2} \text{ M}^{-1} \text{ s}^{-1}$ at 24.7 °C) is about 120 orders of magnitude faster than the rate of substitution of the second aqua ligand ($k_3 = 1.98(6) \times 10^{-4} \text{ M}^{-1} \text{ s}^{-1}$ at 24.7 °C). The $[\text{Co}(\text{nta})(\text{H}_2\text{O})\text{OH}]^-$ complex reacts about 70 times faster at 24.7 °C with NCS^- than $[\text{Co}(\text{nta})(\text{H}_2\text{O})_2]$ with NCS^- ($k_2 = 1.68(5) \text{ M}^{-1} \text{ s}^{-1}$ vs. $2.4(1) \times 10^{-2} \text{ M}^{-1} \text{ s}^{-1}$ for k_1 at 24.7 °C). This clearly indicates that the hydroxo ligand labilises the *cis*-aqua bond so that an increase in rate is observed. Hydroxide is not substituted by NCS^- ions at higher pH so that only one reaction is observed spectrophotometrically.

$[\text{Co}(\text{nta})(\mu\text{-OH})]_2^{2-}$ undergo bridge cleavage at higher pH upon addition of various ligands like en, dmap or py. As a result of this several $[\text{Co}(\text{nta})(\text{LL}')]_2$ and $[\text{Co}(\text{nta})(\text{L})_2]$ ($\text{LL}' =$ various N,N and N,O donors and $\text{L} =$ dmap, py) complexes have been synthesised. The X-ray crystallographical structure determination of $[\text{Co}(\text{nta})(N,N\text{-Et}_2\text{en})]$ is a result of one of the synthetic studies. Crystals of $[\text{Co}(\text{nta})(N,N\text{-Et}_2\text{en})]$ crystallises in the orthorhombic space group Pbcm ($R_1 = 0.0309$). The Co-N bonding distance was determined as 1.950(4) Å.

Abstract

The bridge cleavage reactions of μ -hydroxo bridged Co(III)-complexes have not been studied to our knowledge. The substitution reactions between $[\text{Co}(\text{nta})(\mu\text{-OH})_2]^{2-}$ and various ligands like dmap, py, en and *N,N*-Et₂en have been investigated at pH 9 – 11.5. It is suggested that $[\text{Co}(\text{nta})(\mu\text{-OH})_2]^{2-}$ equilibrates rapidly in aqueous basic solutions with a mono- μ -hydroxo bridged species and that both these species react with the incoming ligand to form ion associated species (rapid) which dissociates in the rate determining step to the products.

The existence of the formed mono- μ -hydroxo bridged complex was confirmed by the fact that the value for the equilibrium constant, pK_{OH} , was determined as 3.3 for all the reactions studied. This mono- μ -hydroxo species is more labile towards substitution than the dimer itself as is illustrated by the fact that $k_1 < k_2$ for all the reactions studied. The values of k_1 varied between $8.7(7) \times 10^{-5} \text{ s}^{-1}$ and $3.3(7) \times 10^{-3} \text{ s}^{-1}$ and those of k_2 between $6.8(2) \times 10^{-4} \text{ s}^{-1}$ and $5.7(2) \times 10^{-2} \text{ s}^{-1}$.

The synthesis and characterisation of $\text{Cs}_2[\text{Co}(\text{nta})(\text{CO}_3)] \cdot \text{H}_2\text{O}$ was also undertaken. This complex crystallises in the monoclinic space group $\text{P}2_1/\text{c}$ ($R_1 = 0.0249$) and can be used as an alternative to $[\text{Co}(\text{nta})(\mu\text{-OH})_2]^{2-}$ for the synthesis of different Co(III)-nta complexes. The Co-N bonding distance was calculated as $1.920(2) \text{ \AA}$.

The uncertainty surrounding the identity of the Cr(III)-nta complexes first prepared by Uehara *et al.* (1967:2317) have been erased with the X-ray crystal structure determination of $\text{Cs}_2[\text{Cr}(\text{nta})(\mu\text{-OH})] \cdot 4\text{H}_2\text{O}$. $\text{Cs}_2[\text{Cr}(\text{nta})(\mu\text{-OH})] \cdot 4\text{H}_2\text{O}$ crystallise in two different space groups, tetragonal $\text{I}4_1/\text{a}$ ($R_1 = 0.0354$) and monoclinic $\text{P}2_1/\text{c}$ ($R_1 = 0.0354$). The Cr-N bonding distances were $2.048(9)$ and $2.061(3) \text{ \AA}$ respectively.

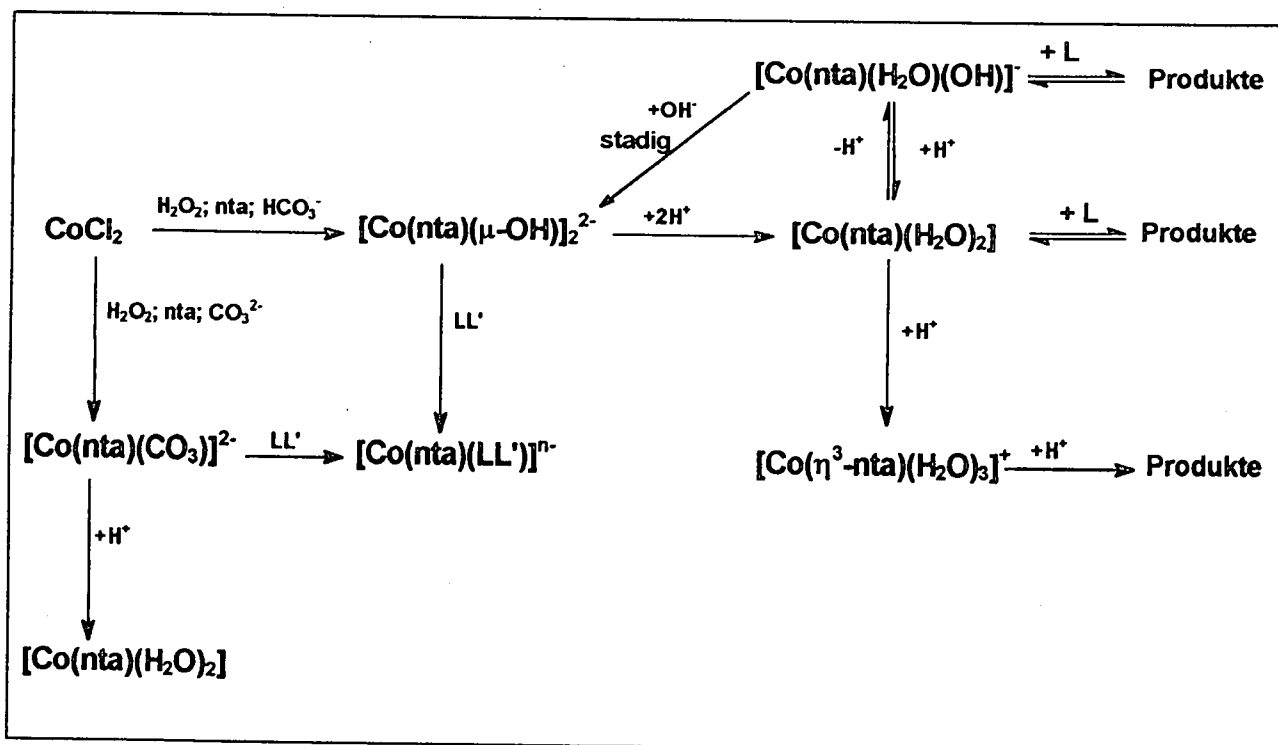
The strain experienced by the glycinato rings of coordinated nta decreases in the order $\text{G} > \text{R}$ for all the complexes studied. The R rings in all the complexes are almost perfectly planar in all cases, while the G rings are non-planar.

Keywords: cobalt(III), chromium(III), nitrilotriacetic acid, substitution and ring cleaving reactions, single crystal x-ray crystallography

Opsomming

Die sintese en reaksies van Co(III)- en Cr(III)-komplekse met nitrilotriasyne (nta) as tetradentate ligand lok wye belangstelling, veral omdat hierdie komplekse as biologiese modelkomplekse gebruik kan word en omdat die nta ligand metaalsentra wat gewoonlik inert is, labiliseer. Mori *et al.* (1958:940) en Uehara *et al.* (1967:2317) het aanvanklik verskillende Co(III)-nta en Cr(III)-nta komplekse respektiewelik berei. Sedertdien is hierdie komplekse in verskeie kinetiese en sintetiese studies as uitgangstof gebruik (Visser *et al.* 1997:2581; Visser *et al.* 1994:1051 en Thacker & Higginson, 1975:704). Tot en met tyde van hierdie studie was die struktuur van hierdie komplekse nog nie opgeklaar met sekerheid nie en die suiwerheid van die bereide komplekse was onder verdenking.

Die vraag rondom die identiteit van die verskillende Co(III)-nta spesies in oplossing (sien Skema 1) by verskillende pH's is grootliks in hierdie studie beantwoord.



Skema 1 Komplekse en reaksies van Co(III)-nta.

Opsomming

Die struktuur van die kompleks wat eerste deur Mori *et al* (1958:940) berei en karakteriseer was, is uiteindelik met behulp van X-straal kristallografie bepaal as $[\text{Co}(\text{nta})(\mu\text{-OH})]_2^{2-}$. Kristalle van $\text{Cs}_2[\text{Co}(\text{nta})(\mu\text{-OH})] \cdot 4\text{H}_2\text{O}$ kristalliseer in die ortorombiese ruimtgroep, $I4_1/a$ ($R_1 = 0.0322$). Die Co-N bindingsafstand is bereken as 1.922(6) Å.

Hierdie studie het bevind dat die hidrokso brûe van $[\text{Co}(\text{nta})(\mu\text{-OH})]_2^{2-}$ gesplyt word met byvoeging van H^+ ione om $[\text{Co}(\text{nta})(\text{H}_2\text{O})_2]$ te vorm. Die pK_a van hierdie reaksie is as 3.09(3) bepaal. Verdere byvoeging van suur lei tot die stapsgewyse dissosiasie van die nta ligand. Dit word gepostuleer dat 'n ioongeassosieerde spesie tydens die reaksie tussen $[\text{Co}(\text{nta})(\text{H}_2\text{O})_2]$ en H^+ ione met byvoeging van suur vorm. Hierdie ioongeassosieerde spesie dissosieer in die tempobepalende stap om 'n tridentate nta kompleks, $[\text{Co}(\eta^3\text{-nta})(\text{H}_2\text{O})_3]^+$, te vorm. Die waarde van k_1 by 25.9 °C is as 0.13(1) s^{-1} bepaal.

Nog 'n suur-basis ewewig is tydens die die pH-verhoging van 'n $[\text{Co}(\text{nta})(\text{H}_2\text{O})_2]$ oplossing waargeneem. Die gevolgtrekking is dat die nuutgevormde spesies nie die dimeer is nie, maar eerder $[\text{Co}(\text{nta})(\text{H}_2\text{O})(\text{OH})]$ wat terugkeer na die dimeer by pH 6 – 7 na verloop van 'n paar dae. Hierdie tweede pK_a is as 6.52(2) bepaal.

Die substitusioreaksies tussen $[\text{Co}(\text{nta})(\text{H}_2\text{O})_2]$ en NCS^- ione is ook ondersoek. NCS^- ione substitueer die akwaligande stapsgewys by pH = 2.0. Die substitusie van die eerste akwa ligand ($k_1 = 2.4(1) \times 10^{-2} \text{ M}^{-1} \text{ s}^{-1}$ by 24.7 °C) is omtrent 'n faktor 120 keer vinniger as die tempo van die tweede akwa-substitusie ($k_3 = 1.98(6) \times 10^{-4} \text{ M}^{-1} \text{ s}^{-1}$ by 24.7 °C). Die $[\text{Co}(\text{nta})(\text{H}_2\text{O})\text{OH}]^-$ kompleks reageer omtrent 70 keer vinniger by 24.7 °C met NCS^- as wat $[\text{Co}(\text{nta})(\text{H}_2\text{O})_2]$ met NCS^- reageer ($k_2 = 1.68(5) \text{ M}^{-1} \text{ s}^{-1}$ vs. $2.4(1) \times 10^{-2} \text{ M}^{-1} \text{ s}^{-1}$ vir k_1 by 24.7 °C). Hierdie resultate toon duidelik dat die hidrokso ligand die *cis*-akwa binding sodanig labiliseer dat 'n toename in tempo waargeneem word. Verder toon dit aan dat die hidroksiedligande nie deur NCS^- ione by hoër pH gesubstitueer word nie aangesien slegs een reaksie by hierdie pH waargeneem word.

Die hidrokso brûe van $[\text{Co}(\text{nta})(\mu\text{-OH})]_2^{2-}$ word ook by hoër pH's deur verskillende ligande soos en, dmap of py gesplyt. As gevolg hiervan is verskeie $[\text{Co}(\text{nta})(\text{LL}')]$ en $[\text{Co}(\text{nta})(\text{L})_2]$ ($\text{LL}' =$ verskillende N,N and N,O donors en $\text{L} =$ dmap, py) komplekse berei. Die X-straal kristalstruktuurbeplating van $[\text{Co}(\text{nta})(\text{N},\text{N}\text{-Et}_2\text{en})]$ is 'n resultaat van een van

Opsomming

die bogenoemde reaksies. Kristalle van $[\text{Co}(\text{nta})(\text{N},\text{N}\text{-Et}_2\text{en})]$ kristalliseer in die ororombiese ruimtegroep, Pbcm ($R_1 = 0.0309$). Die Co-N bindingsafstand is bepaal as $1.950(4) \text{ \AA}$.

Die brugsplytingsreaksies van μ -hidrokso gebrugde Co(III)-komplekse is nog nie voorheen ondersoek nie. Die substitusiereaksies tussen $[\text{Co}(\text{nta})(\mu\text{-OH})]_2^{2-}$ en verskillende ligande soos dmap , py , en and $\text{N},\text{N}\text{-Et}_2\text{en}$ is by pH 9 – 11.5 ondersoek. Dit word gepostuleer dat $[\text{Co}(\text{nta})(\mu\text{-OH})]_2^{2-}$ 'n ewewig met 'n mono- μ -hidrokso gebrugde spesie in waterige, basiese oplossings vorm en dat beide spesies met die inkomende ligande reageer. Hierdie reaksies lei tot die vorming van ioongeassosieerde spesies wat in die tempobepalende stap dissosieer om die produkte te vorm.

Die bestaan van die gevormde mono- μ -hidrokso gebrugde kompleks is ook bevestig aangesien die ewewigskonstante, pK_{OH} , as 3.3 bepaal is vir al die reaksies wat bestudeer is. Die resultate toon ook dat die mono- μ -hidrokso spesie meer labiel ten opsigte van substitusie as die dimeer self is. Laasgenoemde word geïllustreer deur die feit dat $k_1 < k_2$ is vir al die reaksies wat ondersoek is. Die waardes van k_1 wissel tussen $8.7(7) \times 10^{-5} \text{ s}^{-1}$ en $3.3(7) \times 10^{-3} \text{ s}^{-1}$ en k_2 tussen $6.8(2) \times 10^{-4} \text{ s}^{-1}$ en $5.7(2) \times 10^{-2} \text{ s}^{-1}$.

Die sintese en karakterisering van $\text{Cs}_2[\text{Co}(\text{nta})(\text{CO}_3)] \cdot \text{H}_2\text{O}$ is ook onderneem. Hierdie kompleks kristalliseer in die monokliniese ruimtegroep $\text{P2}_1/\text{c}$ ($R_1 = 0.0249$) en kan as 'n alternatiewe uitgangstof in die sintese van verskillende Co(III)-nta komplekse gebruik word. Die Co-N bindingsafstand is as $1.920(2) \text{ \AA}$ bereken.

Die onsekerheid aangaande die identiteit van Cr(III)-nta komplekse wat aanvanklik deur Uehara *et al.* (1967:2317) berei is, is uit die weg geruim met die X-straal kristalstruktuurbeplanning van $\text{Cs}_2[\text{Cr}(\text{nta})(\mu\text{-OH})] \cdot 4\text{H}_2\text{O}$. $\text{Cs}_2[\text{Cr}(\text{nta})(\mu\text{-OH})] \cdot 4\text{H}_2\text{O}$ kristalliseer in twee verskillende ruimtegroepe, tetragonaal $\text{I4}_1/\text{a}$ ($R_1 = 0.0354$) en monoklinies $\text{P2}_1/\text{c}$ ($R_1 = 0.0354$). Die Cr-N bindingsafstande is respektiewelik as $2.048(9)$ en $2.061(3) \text{ \AA}$ bepaal.

Die vervorming van die glisinato ringe van gekoördineerde nta neem af in die volgorde $\text{G} > \text{R}$ vir al die komplekse wat ondersoek is. Die R ringe is amper ten volle planêr vir al die gevalle, terwyl die G ringe almal nie-planêr is.